Characterization of the mechanisms leading to tumour phagocytes pathogenic reprogramming

Kevin Mulder

université PARIS-SACLAY

Characterization of the mechanisms leading to tumour phagocytes pathogenic reprogramming

Caractérisation des mécanismes responsables de la reprogrammation pathogénique des phagocytes tumoraux

Thèse de doctorat de l'université Paris-Saclay

École doctorale n° 582, Cancérologie : Biologie, Médecine, Santé (CBMS)
Spécialité de doctorat : Sciences du cancer
Graduate School : Life Science and Health. Référent : Faculté de Médecine

Thèse préparée dans l'unité de recherche Immunologie anti-Tumorale et Immunothérapie du Cancer (INSERM, Université Paris-Saclay), sous la direction de **Florent GINHOUX,** Professeur Associé, la co-direction de **Charles-Antoine DUTERTRE,** CRCN Chargé de recherche.

Thèse soutenue à Paris-Saclay, le 24 octobre 2024, par

Kevin Mulder

Composition du Jury

Florence APPARAILLY Research director, INSERM U1183	Présidente
Martin GUILLIAMS Professor, Gent University	Rapporteur & Examinateur
Matthew COLLIN Professor, Newcastle University	Rapporteur & Examinateur
Ruth FRANKLIN Assistant Professor, Harvard University	Examinatrice

THESE DE DOCTORAT

NNT : 2024UPASL076

université PARIS-SACLAY
ÉCOLE DOCTORALE
Cancérologie : biologie - médecine - santé (CBMS)

Titre : Caractérisation des mécanismes responsables de la reprogrammation pathogénique des phagocytes tumoraux

Mots clés : Macrophages, Monocytes, Cellules dendritiques, Analyses en cellules uniques, Biologie spatiale

Résumé : Les phagocytes mononucléaires (MNP), notamment les cellules dendritiques, les monocytes et les macrophages, sont essentiels à la défense immunitaire et au maintien de l'équilibre dans l'organisme. Cependant, la compréhension de ces cellules a été difficile en raison de leur complexité et de leur dénomination variée selon les tissus et les maladies. Pour simplifier cela, nous avons créé le MNP-VERSE, un outil complet qui cartographie les MNP de 13 tissus, offrant une vue unifiée de ces cellules.

Nous avons développé MoMac-VERSE, en nous concentrant sur les macrophages, en particulier sur leurs rôles dans le cancer et l'inflammation. Nous avons découvert des macrophages immunosuppresseurs associés aux tumeurs, qui pourraient avoir un impact sur la façon dont les patients répondent au traitement.

En parallèle, nous avons créé DC-VERSE, un atlas détaillé des cellules dendritiques, mettant en évidence la relation entre certaines cellules et le pronostic des patients atteints de cancer.

Enfin, nous avons présenté Sopa, un outil d'analyse de données spatiales complexes, aidant les chercheurs à mieux comprendre comment les cellules interagissent au sein des tissus. Ces ressources offrent de nouvelles perspectives sur la fonction immunitaire et les thérapies potentielles pour des maladies comme le cancer.

Title : Characterization of the mechanisms leading to tumour phagocytes pathogenic reprogramming

Keywords : Macrophages, Monocytes, Dendritic cells, Single cell, Spatial

Résumé : Mononuclear phagocytes (MNPs), including dendritic cells, monocytes, and macrophages, are crucial for immune defence and maintaining balance in the body. However, understanding these cells has been challenging due to their complexity and varied naming across tissues and diseases. To simplify this, we created the MNP-VERSE, a tool that maps MNPs from 13 tissues, offering a unified view of these cells.

We further developed the MoMac-VERSE, focusing on macrophages, especially their roles in cancer and inflammation. We discovered immune-suppressive tumour-associated macrophages, which could impact how patients respond to therapy.

In parallel, we created DC-VERSE, an atlas of dendritic cells, highlighting how certain cells relate to better or worse outcomes in cancer.

Finally, we introduced Sopa, a tool to analyse spatial data, helping to understand better how cells interact within tissues. These resources offer new insights into functions and potential therapies for diseases like cancer.

Acknowledgements

I would like to thank my supervisor, Florent Ginhoux, for all the guidance, advice, and support throughout my PhD studies. I would have never believed that one simple email would bring me across the world, from Singapore to finishing my PhD here.

Secondly, I would like to thank my second supervisor, Charles Antoine Dutertre. Thank you for teaching me more things than I can write down. You have been an important part of this journey.

I would like to thank the jury for accepting my invitation for this defence. As much I would like to thank the monitoring committee for the guidance and insight over the PhD.

I would like to thank Laurence Zitvogel and the unit of U1015 for their support and collaborative environment and extend this to all the collaborators that I have worked with.

This journey has been something that I could have never imagined, and there are so many people who have contributed to this, from high school with Vincent to university with Stijn and Amy, as well as all my friends that I grew up with in Berkel en Rodenrijs. Thank you all for shaping me and making this journey possible.

Pap en mam, bedankt voor jullie steun. Ik had nooit gedacht, na het zakken van VWO, dat ik ooit hier zou zijn. Jullie hebben altijd in me geloofd en ik kan jullie niet genoeg bedanken hiervoor. En dit geldt natuurlijk ook voor mijn grote broer Jeroen. Bedankt voor je steun en gezelligheid die je altijd bracht wanneer ik je zag.

Dear Rosalind, you entered my life just as I started my PhD. You have been a support that I did not imagine I could have. Thank you for your love and presence during this whole journey.

I would like to thank the whole lab for their kindness and wisdom. Many people have joined and gone, but it always felt like a group I looked forward to seeing and working with. Some people who have had an impact on this were Amit, Grégoire, Jeanne, Elisa, Sindija, Ahmed, Leticia, Leslie, Aline, Clemence, Camille, and Aymeric.

Garett (Garryberry), from a random Zoom call during COVID, when I was in Singapore and you were in Paris, you have become one of my best friends. Thank you for sharing this PhD journey with me.

Mathilde (Mathouu), the normal girl. Thank you for all your help in so many ways. From the first nights we met when the drinks spilled to all the fun we've had, your kindness will always stay with me.

Marco (insert turtle eeeee), thank you for your positivity and the fun. The walking Vivino app, thank you for all the amazing wines.

Claudia (Clau Clau), thank you for your kindness and positivity that you unconditionally brought. Also, for fixing my thumb :)

Wan Ting (*****), it is crazy to think that you have been on the whole journey from Singapore to Paris. We have seen a lot together, from crying to laughing. When I think of you, I always think of the truffle fries in Bodacious and maybe a few drinks.

Margaux, I think I have never seen anybody cry for so many different reasons. Luckily, almost always, there was a smile attached to it. You joined halfway through the PhD, but you have left me with a full set of memories. Thank you for all your help.

Benoit (Beu Beu), HabbaBaba? Thanks for the discussions and all the fun times.

Javi, thank you for the pisco and parties. Carlito, thank you for singing everybody's name during lunch. Gerry, Alleeeeee. Quentin, thank you for teaching me many things and the collaborative fun we had.

Thank you all

CONTENT

Abbreviations

MNP : Mononuclear phagocytes

APCs : antigen-presenting cells

MHC : Major Histocompatibility Complex

TCRs : T cell receptors

DC : Dendritic cell

PAMPs : pattern-associated molecular patterns

LPS : lipopolysaccharide

TLR : Toll-like receptors

PRRs : pattern recognition receptors

RLRs : RIG-I-like receptors

RNA : Ribosomal Nucleic acid

BCG : Bacillus Calmette-Guérin

GFP : Green Fluorescents protein

HSCs : hematopoietic stem cells

MPPs : multipotent progenitors

CMPs : common myeloid progenitors

CLPs : common lymphoid progenitors

GMPs : granulocyte and macrophage progenitors

cDCs : conventional dendritic cells

moDCs : monocyte-derived dendritic cells

TRMs : tissue-resident macrophages

CCR : CC-chemokine receptor

GM-CSF : granulocyte-macrophage colony-stimulating factor

KCs : Kupffer cells

LCMs : liver capsular macrophages

CNS : central nervous system

IL : Interleukin

CSF1R : colony-stimulating factor 1 receptor

pDCs : plasmacytoid dendritic cells

TNF : tumour necrosis factor

PBMC : peripheral blood mononuclear cells

dsRNA : double-stranded RNA

ssRNA : single-stranded RNA

IFN-λ : type III interferon

TME : tumour microenvironment

TAMs Tumor-associated macrophages

PDAC : pancreatic ductal adenocarcinoma

NSCLC : non-small-cell lung cancer

FOLR2 : folate receptor-β

HCC : hepatocellular carcinoma

Tregs : regulatory T cells

EMT : epithelial-mesenchymal transition

STAT : signal transducer and activator of transcription

IRF : IFN regulatory factor

CAFs : cancer-associated fibroblasts

mAb : monoclonal antibody

PGE2 : prostaglandin E2

infDCs : inflammatory DCs

SLE : systemic lupus erythematosus

CD : clusters of differentiation

PCA : principal component analysis

UMAP : uniform manifold approximation and projection

BMDC : bone marrow-derived dendritic cells

scRNA-seq : single-cell RNA sequencing

CITE-seq : Cellular Indexing of Transcriptomics and Epitopes by Sequencing

H&E : Hematoxylin and eosin

IL-1β : interleukin-1β

ICB : immune checkpoint blockade

transf.matrix : transformed matrix

DEG : Differential expressed gene

TLS : tertiary lymphoid structure

TNBC : triple-negative breast cancer

FFPE : formalin-fixed paraffin-embedded

IHF : immunohistofluorescence

1 INTRODUCTION

1.1 IMMUNOLOGY ON MONONUCLEAR PHAGOCYTES

Immunology, the scientific study of the immune system, explores a comprehensive network composed of cells, tissues, and molecular mechanisms that collaborate to protect the body against infectious agents and diseases. The immune system is broadly classified into two primary types: innate immunity and adaptive immunity, each playing a unique and critical role in body defence mechanisms.

Adaptive immunity is characterised by its specificity and memory, enabling a tailored and long-lasting response to pathogens. This branch involves lymphocytes, specifically B cells and T cells. B cells are responsible for a humoral immunity through the production of antibodies, whereas T cells mediate cellular immunity. Examples are helper T cells ($CD4^+$) activating other immune cells, while cytotoxic T cells ($CD8^+$) directly eliminate infected cells (Janeway et al., 2001).

A fundamental concept in adaptive immunity is antigen recognition. B cells recognise antigens via their B cell receptors (BCRs), which are membrane-bound antibodies, while T cells recognise processed antigen fragments presented by Major Histocompatibility Complex (MHC) molecules on antigen-presenting cells (APCs) through their T cell receptors (TCRs). This specific interaction is crucial for initiating a precise immune response (Chaplin, 2010).

The clonal selection explains the adaptive immune system's ability to generate diverse antigen-specific lymphocytes. Upon encountering an antigen, lymphocytes undergo clonal expansion and differentiation into effector and memory cells, ensuring a rapid and robust response upon subsequent exposures to the same antigen. Effector mechanisms include antibody production by plasma cells, the direct killing of infected cells by cytotoxic T lymphocytes, and the activation of other immune cells through cytokine secretion by helper T cells, establishing immunological memory and forming the basis for vaccination (Chaplin, 2010; Janeway et al., 2001).

In contrast, innate immunity represents the body's first line of defence, providing a rapid, albeit non-specific, response to invaders through barriers like the skin and mucous membranes and through various immune cells such as macrophages, neutrophils, and natural killer cells. This layer of defence also involves soluble factors such as cytokines and complement proteins that aid in orchestrating the overall immune response.

Within the innate immunity, the mononuclear phagocyte system plays a vital role. It includes monocytes, macrophages, and dendritic cells, each contributing to host defence, tissue remodelling, and regulation of immune responses. The historical discovery and role of these cells were significantly advanced by the pioneering studies of Ilya Metchnikoff in the late 19th and early 20th centuries (Metchnikoff, 1892). Metchnikoff's discovery of phagocytic cells, which ingest and destroy pathogens—a process he named phagocytosis—earned him a Nobel Prize and laid the groundwork for our current understanding of cellular immunity.

Monocytes, primarily circulating in the bloodstream, can differentiate into macrophages upon entering tissues, where they adapt to the local environment. Macrophages are highly versatile and tasked with detecting, engulfing, and destroying pathogens. They also have the capacity to play a role in orchestrating immune responses by presenting antigens to T cells and secreting cytokines that regulate inflammation and immunity (Medzhitov and Janeway, 2000).

Dendritic cells (DC), another integral component of the mononuclear phagocyte system, are adept at capturing and processing antigens. They are considered the most potent antigen-presenting cells, bridging innate and adaptive immunity. After encountering pathogens, they migrate to lymphoid tissues, present antigens to T cells, and initiate adaptive immune responses—a significant advancement in our understanding brought forth by Ralph Steinman in the 1970s (Steinman and Cohn, 1973).

The innate immune system recognises pathogens through pattern-associated molecular patterns (PAMPs). These molecular structures, which include bacterial peptidoglycan and lipopolysaccharide (LPS), are foreign to the host organisms, allowing the immune system to differentiate between self and non-self. This discrimination is crucial for proper immune functioning (Janeway, 1989).

Initially overshadowed by the complexities of adaptive immunity, the innate immune system's role has been recognised as equally vital to the body. It encompasses various mechanisms beyond lymphocytes, such as skin and mucosal barriers, mucus secretion, and chemical agents like lysozyme and stomach acidity. Recognising the complement system's classical, alternative, and lectin pathways highlights its sophisticated involvement in pathogen detection, inflammation activation, and clearance (Al et al., 2023; Netea et al., 2020).

Recent studies have showcased the complement system's regulatory properties, with components like C5a enhancing phagocyte survival and effector functions and C3 playing a crucial role in maintaining gut health by balancing microbial populations (Desai et al., 2023; Sherwood et al., 2022; Trouw and Daha, 2011; West et al., 2018). The discovery of pattern recognition receptors (PRRs) and their role in detecting PAMPs marks a significant leap in our understanding of innate immune mechanisms (Kopp and Medzhitov, 1999; West and Kemper, 2023).

Pattern Recognition Receptors (PRRs), such as Toll-like receptors (TLRs), NOD-like receptors (NLRs), and RIG-I-like receptors (RLRs), each play specific roles in pathogen recognition and the initiation of immune responses. TLRs, for instance, recognise conserved components of microbes, such as LPS from gram-negative bacteria or double-stranded RNA from viruses, triggering immune activation and the production of cytokines that help coordinate further immune reactions (Medvedev et al., 2006; Medzhitov et al., 1997).

Additionally, the concept of "trained immunity," a form of innate memory facilitated primarily through epigenetic changes in myeloid cells, has revolutionised our understanding of how certain vaccines,

like Bacillus Calmette-Guérin (BCG), provide broad protection against a range of diseases beyond their specific targets (Sherwood et al., 2022). The interaction of cytokines in regulating inflammation and linking innate to adaptive immunity further emphasises the interconnected and dynamic nature of the immune system.

1.2 MONOCYTES AND MACROPHAGES

1.2.1 Monocytes

Monocytes originate from bone marrow hematopoietic stem cells and circulate in the bloodstream. These cells are conserved across all vertebrates and are characterised by specific locations, phenotypic features, morphological attributes, and distinct gene expression signatures (Ingersoll et al., 2010; Kapellos et al., 2019). In both mice and humans, monocytes constitute about 4% to 10% of nucleated cells in the the blood, respectively, with significant reserves located in the spleen and lungs that can be mobilised when needed (Swirski et al., 2009; van Furth and Cohn, 1968).

Monocytes play several crucial roles in the immune system. They can differentiate into tissue macrophages to maintain homeostatic functions under normal conditions (Ginhoux and Jung, 2014). Additionally, monocytes can become inflammatory macrophages during acute inflammatory responses and anti-microbial immunity.

The identification of distinct monocyte populations marked a significant advancement in the understanding of their biology. Initially, these populations were distinguished in humans based on morphology and the differential expression of CD14 and CD16 markers (Passlick et al., 1989). This differentiation led to the classification of monocytes into three principal subsets: $CD14^{+}CD16^{-}$ monocytes or "classical" monocytes, which represent 80–90% of the monocyte pool, and the remaining 10–20% comprised of $CD14^{+}CD16^{+}$ "intermediate" and $CD14^{Low}CD16^{+}$ "non-classical" monocytes (Guilliams et al., 2018; Kapellos et al., 2019).

In mice, a significant development occurred with the creation of a mouse strain with a reporter protein engineered into the *Cx3cr1* gene (CX3CR1-GFP mice), facilitating the identification of two distinct $CD11b^{+}CD115^{+}$ monocyte subsets (Geissmann et al., 2003; Jung et al., 2000). The "classical" monocytes in mice are identified as $Ly6C^{Hi}CX3CR1^{int}CCR2^{+}CD62L^{+}CD43^{Low}$ cells, whereas "non-classical" monocytes, also known as patrolling monocytes, have a $Ly6C^{Low}CX3CR1^{Hi}CCR2^{Low}CD62L^{-}CD43^{+}$ phenotype (Geissmann et al., 2003; Jakubzick et al., 2013; Jung et al., 2000; Palframan et al., 2001). Comparative transcriptional analyses between mouse and human monocytes have correlated $Ly6C^{Hi}$ monocytes with 'classical' $CD14^{+}CD16^{-}$ monocytes and $Ly6C^{Low}$ monocytes with 'non-classical' $CD14^{Low}CD16^{+}$ monocytes, highlighting some differences in gene expression and surface markers between the species (Guilliams et al., 2018; Kapellos et al., 2019).

In addition, less well-defined transitional states have been reported, the prevalence of which could have substantial clinical implications. The expression of 6-sulfo LacNac sugar antigen linked to the cell surface protein PSGL-1 is termed SLAN. SLAN expression defines non-classical $CD16^{+}$ in humans and provides a practical way to distinguish them from the "intermediate" $CD14^{+}CD16^{+}$ monocytes (Hofer et al., 2015).

The developmental pathways by which monocytes arise from hematopoietic stem cells are commonly understood through a model that conceptualises it as a hierarchical, tree-like structure based on canonical progression. This paradigm assumes that progenitor cells, ranging from oligopotent to unipotent, gradually become more specialised through a series of branching decisions, culminating in forming all types of circulating blood cells. At the foundation of this model, a subset of active hematopoietic stem cells (HSCs) (Busch et al., 2015) exhibit the capacity for self-renewal and give rise to a varied population of multipotent progenitors (MPPs) (Pietras et al., 2015). These progenitors then differentiate into two primary lineages: common myeloid progenitors (CMPs) (Akashi et al., 2000) and common lymphoid progenitors (CLPs) (Kondo et al., 1997).

CLPs are precursors to lymphoid cells such as T cells, B cells, and natural killer cells, but they are incapable of differentiating into the myeloerythroid lineage. Conversely, CMPs, which no longer retain the potential to develop into lymphoid cells, can differentiate into megakaryocyte and erythrocyte progenitors (MEPs) and granulocyte and macrophage progenitors (GMPs) (Akashi et al., 2000). It is within this GMP category that a monocyte/dendritic cell progenitor (MDP) has been identified. This progenitor is suggested to predominantly produce monocytes and conventional dendritic cells (cDCs), but not neutrophils, in both mice (Fogg et al., 2006; Olsson et al., 2016) and humans (Lee et al., 2015). Notably, in murine models, MDPs have also been detected in mice within the CMP population and might emerge directly from CMPs expressing Flt3 rather than exclusively from GMPs (Yáñez et al., 2017). Recent studies have further suggested that Ly6C^{Hi} monocytes can originate from both the GMP and MDP populations (Trzebanski et al., 2024; Yáñez et al., 2017).

GMP-dependent monocytes coexist alongside MDP-derived monocytes, with each playing a crucial role in immune responses (Trzebanski et al., 2024; Wolf et al., 2019). MDP-derived monocytes, in particular, possess the capacity to generate monocyte-derived dendritic cells (moDCs). Through the use of fate mapping studies in mice involving Ms4a3 cre/*Ms4a3* CreERT2 driver lines, the contributions of GMP-dependent monocytes to the tissue-resident macrophages (TRMs) pool have been accurately assessed (Liu et al., 2019).

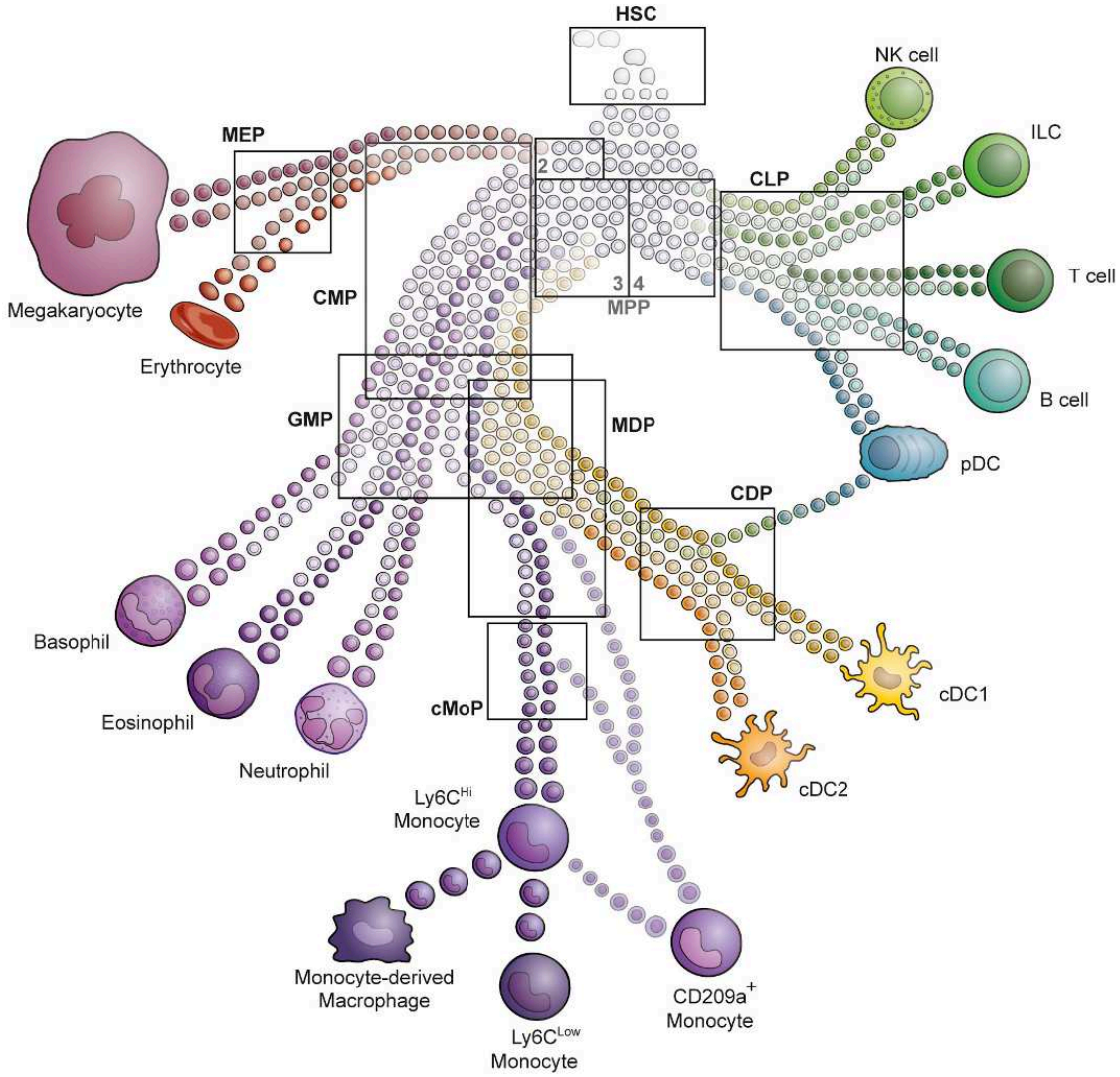

Figure 1: *Schematic representation of hematopoietic system development based on single-cell analysis. Hematopoietic development initiates with a small number of active hematopoietic stem cells (HSCs), which populate a pool of multipotent progenitors (MPPs). Within this pool, distinct subsets of MPPs (indicated by numbers 2–4, as described by Pietras et al., 2015) are already primed toward specific cell lineages or exhibit characteristics similar to terminally differentiated cells (depicted by light-coloured circles). The further differentiated precursor populations comprise a heterogeneous mixture of these primed cells, represented within the rectangles, which often share overlapping surface marker profiles. Adapted from Guilliams et al., 2018.*

The transformation of monocytes into cells with dendritic cell-like features, initially demonstrated in vitro, has been supported by numerous lines of evidence underscoring its physiological importance. moDCs are particularly significant in pathophysiological conditions, impacting the exacerbation or regulation of inflammation (Coillard and Segura, 2019). The development of these cells is intricately regulated by transcription factors, further emphasising the complexity of monocyte differentiation (Villar et al., 2023).

Monocyte migration from the bone marrow is predominantly driven in mice by CC-chemokine receptor 2 (CCR2), which binds to chemokine ligands such as CCL2 and CCL7 (Tsou et al., 2007). Under mild inflammatory conditions, mesenchymal stem cells and their progeny, including CXCL12-abundant reticular cells, serve as primary sources of CCL2 production in the BM of mice (Shi and Pamer, 2011), although this may vary under healthy conditions. The role of CCR2 in human monocyte egression remains to be fully understood, as it is shown in human CCR2 knockout patients with normal levels of monocytes in the blood (Neehus et al., 2024).

Classical monocytes, a transient population, display diverse differentiation potentials and are known for their ability to migrate into tissues under normal conditions. Once released from the bone marrow during healthy homeostasis, they circulate for about a day before either repopulating tissue-resident macrophages or converting into non-classical monocytes (Patel et al., 2017; Yona et al., 2013). Non-classical monocytes patrol the vasculature, clear dying endothelial cells, and play a role in maintaining vascular health (Auffray et al., 2007).

It is important to recognise that the production of monocyte subsets during homeostasis is influenced by a dynamic interplay of environmental and genetic factors, suggesting that homeostatic conditions are far from uniform (Kapellos et al., 2019; Patel and Yona, 2019). For instance, in the intestine, while macrophages are generally short-lived and continuously replenished by monocytes, $TIM4^{+}CD4^{+}$ macrophages in mice are self-sustaining for months and are essential for maintaining intestinal homeostasis. Disruption of these cells leads to various intestinal issues, including reduced enteric neurons, vascular

leakage, and delayed motility (De Schepper et al., 2018).

1.2.2 Macrophages

Macrophages are highly plastic and adaptable cells, capable of performing a wide range of functions depending on their environment. Since their early identification as mononuclear phagocytes in both invertebrates and vertebrates, macrophages have become increasingly important in understanding human health and disease. Their fundamental role involves "cleaning" their surroundings by phagocytosing cellular debris and regulating tissue repair and maintenance, making them key sentinel cells present across various organs (Wynn et al., 2013). Remarkably, these tissue-resident macrophages (TRMs) participate in a variety of complex processes, reflecting their ability to adapt to specific tissue environments while retaining core functions as phagocytes (Lavin and Merad, 2013; Lavin et al., 2014; Gosselin et al., 2014; Amit et al., 2016; Cohen et al., 2018). Their identity is further shaped by tissue-specific signals that can remodel their phenotype, gene expression, and chromatin architecture, leading to significant heterogeneity. While macrophages are essential to all organs in the body, here are some of the more well-known specific examples of tissue functionality in mice.

Lung

The lungs, constantly exposed to the external environment through inhaled air, contain three distinct populations of macrophages: alveolar macrophages, which reside in the alveoli and are directly exposed to air, and two populations of interstitial macrophages (Aegerter et al., 2022). Alveolar macrophages play a critical role in clearing the alveolar space of cellular and pathogenic debris, as well as mucus. Their development and maintenance are dependent on granulocyte-macrophage colony-stimulating factor (GM-CSF), which is produced by type II airway epithelial cells (Guilliams et al., 2013). In mouse models, the absence of GM-CSF or mutations in its receptor leads to pulmonary alveolar proteinosis, underscoring the importance of these cells (Guilliams et al., 2013) (Suzuki et al., 2008).

Liver

The liver hosts a diverse population of macrophages, including the well-known Kupffer cells (KCs) and liver capsular macrophages (LCMs), along with central vein macrophages and lipid-associated macrophages (Guilliams and Scott, 2022). Kupffer cells, residing in the sinusoidal areas exposed to the constant blood flow from the portal vein, are involved in the phagocytosis of senescent erythrocytes and play critical roles in systemic iron and cholesterol metabolism (Wen et al., 2021). They also contribute to microbial defence, cell debris clearance, and immune tolerance. In mouse models, Clec4f has been identified as a specific marker for targeting Kupffer cells in mice, highlighting the role of transcription factors like *Zeb2* and *LXRα* induced by *DLL4* in their development and function (Sakai et al., 2019; Scott et al., 2018).

Central nervous system

Macrophages in the central nervous system (CNS), particularly microglia, are among the most well-studied macrophages. Microglia, which reside in the CNS parenchyma, and other macrophage populations that occupy CNS interfaces, maintain themselves via cell-autonomous proliferation once they are established in the CNS (Goldmann et al., 2013; Hashimoto et al., 2013). These long-lived cells rarely proliferate throughout their lifespan but rely on specific niche factors released by local tissue cells to mature and perform their specialised functions during CNS development and homeostasis. The two colony-stimulating factor 1 receptor (CSF1R) ligands, CSF1 and IL-34, released by neurons and astrocytes (Erblich et al., 2011; Greter et al., 2012; Wang et al., 2012), are essential for maintaining mature microglia in the adult CNS in a regionally defined manner.

Gut

The gut represents a complex system with multiple anatomical layers, including the epithelial region, lamina propria, submucosa, and muscularis externa, each with different macrophage functions (Delfini et al., 2022). Lamina propria macrophages are crucial for maintaining intestinal barrier homeostasis, as evidenced by the fact that mutations in the IL-10 receptor pathway can cause severe pediatric inflammatory bowel disease (Hoffmann et al., 2021; Ye et al., 2021). Intestinal macrophages interact with the neuronal components of the gut, supporting their survival and development (Gabanyi et al., 2016; Muller et al., 2014). In the deeper layers of the intestine, such as the submucosa and muscularis externa, long-lived macrophages reside within specific tissue niches (Delfini et al., 2022). In the large intestine, muscularis macrophages have been shown to play a key role in maintaining intestinal motility (De Schepper et al., 2018).

These examples underscore macrophages' remarkable plasticity and adaptability, allowing them to perform essential roles in various tissues throughout the body. Their ability to respond to tissue-specific signals while carrying out fundamental functions as phagocytes is crucial for maintaining health and responding to disease.

Ontogeny

Beyond the residency of macrophages, another aspect that contributes to their heterogeneity is time, specifically their ontogeny, which defines their origin. The understanding that macrophages are not solely derived from monocytes began to take shape in the early 2000s. Langerhans cells, the epidermal macrophages in the skin, were found to resist high radiation levels. Remarkably, after bone marrow transplantation, Langerhans cells were repopulated by cells originating from the host, while the monocytes were derived from the donor. Similar findings were observed for microglia, indicating that these macrophage populations can maintain themselves independently of bone marrow-derived circulating precursors, even after exposure to lethal irradiation (Ajami et al., 2007; F. Ginhoux et al., 2010).

Further evidence supporting the independence of certain adult

macrophage populations from bone marrow or monocyte-derived precursors comes from studies using parabiotic mice, which share the same blood circulation, leading to a significant mixing of circulating precursors. These studies demonstrated that while monocytes mixed freely between the paired animals, certain macrophage populations, such as Langerhans cells (Merad et al., 2002), microglia and alveolar macrophages (Guilliams et al., 2013; Hashimoto et al., 2013; Jakubzick et al., 2013), remained distinct and did not mix. In contrast, macrophages in the gut, dermis, and heart did show some degree of mixing, suggesting that these tissues may receive contributions from bone marrow or monocyte-derived cells (Bain et al., 2014; Epelman et al., 2014; Molawi et al., 2014; Tamoutounour et al., 2013).

With the advent of advanced fate-mapping techniques, such as the Ms4a3cre system (Liu et al., 2019), tracking macrophages more precisely and confirming their origins has become possible. These technological developments continue to refine our understanding of macrophage biology, revealing the complex and diverse origins of macrophage populations across different tissues.

The recognition that macrophages are not exclusively derived from monocytes began to emerge in the early 2000s, challenging traditional views of macrophage development. This shift in understanding was sparked by observations in Langerhans cells, the epidermal macrophages in the skin. These cells were found to withstand high radiation levels, and, notably, even after bone marrow transplantation, Langerhans cells were repopulated by cells from the original host, while monocytes originated from the donor (Merad et al., 2002). Similar patterns were later observed in microglia, suggesting that these macrophage populations maintain themselves independently of bone marrow-derived precursors, even under extreme conditions like lethal irradiation (Ajami et al., 2007; Florent Ginhoux et al., 2010).

Further insights into macrophage origin came from studies using parabiotic mice, which share blood circulation and thus experience a mixing of circulating precursors. These experiments revealed that, while monocytes readily mixed between the animals, certain macrophage populations, such as Langerhans cells (Merad et al., 2002, p. 200), microglia (Ajami et al., 2007; Florent Ginhoux et al., 2010), and

alveolar macrophages (Guilliams et al., 2013; Hashimoto et al., 2013; Jakubzick et al., 2013), remained distinct and did not blend. This contrasted with macrophages in the gut, dermis, and heart, which showed some degree of mixing, indicating possible contributions from bone marrow or monocyte-derived cells in these tissues (Bain et al., 2014; Epelman et al., 2014; Tamoutounour et al., 2013).

The development of advanced fate-mapping techniques, such as the Ms4a3-cre system (Liu et al., 2019), has provided new tools to trace the origins of macrophages more accurately. These advancements are reshaping our understanding of how macrophage populations develop and are maintained across different tissues, revealing a complex and varied landscape of macrophage biology.

Understanding the development and specialisation of macrophages is crucial for comprehending their diverse roles in the immune system. The monocytes that are the circulating macrophage precursors are known to carry a fundamental core macrophage signature even before they integrate into tissues (Gautier et al., 2012; Gosselin et al., 2014; Guilliams et al., 2020; Hagemeyer et al., 2016; Lavin et al., 2014; Mass et al., 2016). This signature includes genes essential for macrophage survival and function, such as *Csf1r* and Maf, which support basic survival, as well as genes involved in key macrophage activities like efferocytosis (*Timd4, Mertk, and Sirpa*), non-opsonic phagocytosis (*Cd14, Cd36, Clec7a, and Mrc1*), opsonic receptor-dependent phagocytosis (*Fcgr1, Fcgr3, Fcgr*4, and *Itgam*), and complement-mediated immunity (*C1qb*, *C1qc*, and *C3ar1*).

As fetal macrophages migrate into developing tissues, they acquire specific characteristics finely tuned to their new environments (Stremmel et al., 2018). This process of tissue-specific programming intensifies during late gestation, resulting in the emergence of diverse macrophage subtypes in adult tissues (Gautier et al., 2012; Gosselin et al., 2014; Mass et al., 2016). The combined influence of intrinsic macrophage programming and external tissue signals is important in shaping tissue-resident macrophages' unique identities and functions. This dynamic relationship highlights macrophage differentiation's complexity and the tissue environment's importance in defining their specialised roles.

Subtissular Macrophage Niches

Subtissular niches, the specialised microenvironments within tissues, play a crucial role in macrophages' survival and functional specialisation. These microanatomical neighbourhoods, identified across various tissues, exhibit remarkable complexity and adaptability, responding to both healthy and diseased states (Mass et al., 2023). Originally described as the 'fibroblast–macrophage circuit' (Zhou et al., 2018), it is now recognised that macrophage niches are far more intricate and can dynamically adjust to different physiological conditions.

For example, in the liver, Kupffer cells are sustained by a subtissular niche formed through the interaction between hepatic stellate cells and liver sinusoidal endothelial cells, fibroblasts or lymphocytes (Bonnardel et al., 2019; Martinek et al., 2022; Sakai et al., 2019). These interactions are essential for maintaining Kupffer cell identity and function, and they contribute to restoring homeostasis and supporting organ regeneration. In the lungs, alveolar macrophages rely on their close proximity to airway epithelial cells to receive GM-CSF, which is vital for their maintenance (Gschwend et al., 2021). Similarly, in the synovium of joints, macrophages work alongside synovial fibroblasts to preserve fibroblast integrity (Knab et al., 2022).

Macrophages also form specific associations with various tissue structures according to their roles. LYVE1^{hi} macrophages, for instance, are linked to blood vessels, facilitating growth and branching. In contrast, MHCII^{hi} macrophages are commonly found near nerve endings and bundles, as seen in the lung, intestinal muscularis, and brown adipose tissue (Chakarov et al., 2019; De Schepper et al., 2018; Wolf et al., 2017). Additionally, interactions between macrophages and other cell types, such as cardiomyocytes or adipocytes, are essential for maintaining tissue health, particularly through processes like mitochondrial recycling (Brestoff et al., 2021; Nicolás-Ávila et al., 2020). This exchange of metabolites and mitochondrial components is a key function of resident macrophages, enabling them to effectively regulate tissue function throughout the organism's lifespan (Scheiblich et al., 2021; van der Vlist et al., 2022).

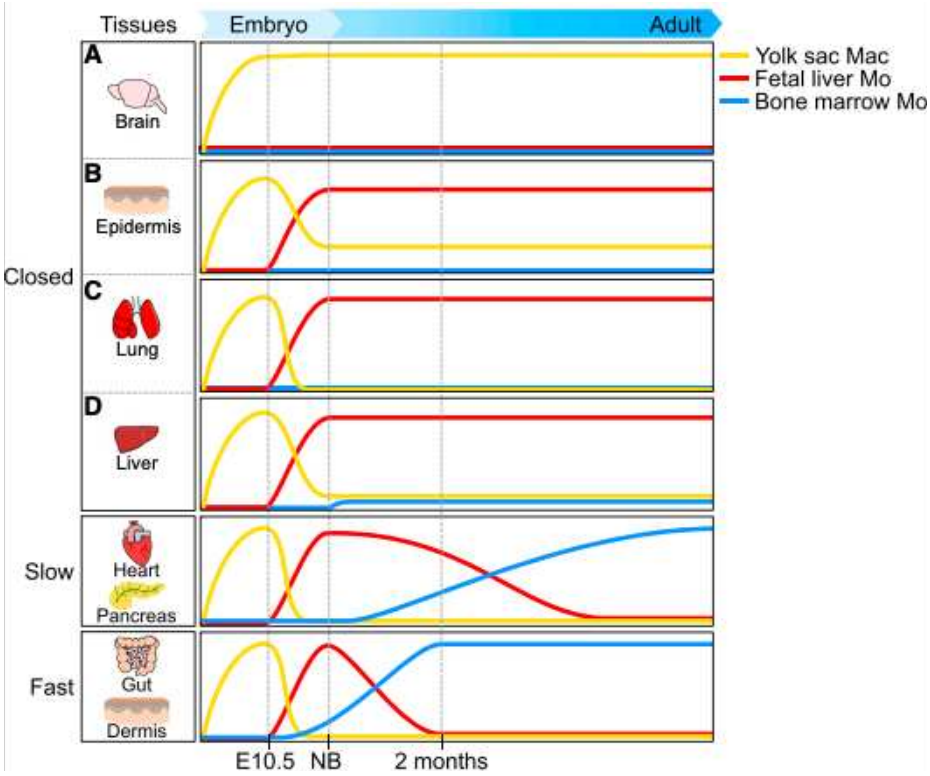

Figure 2: *Origin and differentiation of tissue-resident macrophages across different tissues. In closed tissues, macrophages may arise solely from embryonic-derived sources(Yolk sac Mac & Fetal liver Mo): (A) Yolk sac-derived macrophages (e.g., microglia), from a combination of yolk sac (YS) macrophages and fetal liver (FL) monocytes (B, Langerhans cells—approximately 20% from YS macrophages and 80% from FL monocytes), or primarily from FL monocytes (C, alveolar macrophages and D, Kupffer cells). In open tissues, bone marrow-derived monocytes are recruited and differentiated into macrophages with tissue-specific kinetics, showing slower replacement in tissues such as the heart and pancreas and faster replacement in tissues like the gut and dermis. Adapted from Ginhoux & Guilliams 2016*

1.3 DENDRITIC CELLS

Dendritic cells (DCs) are essential players in the immune system, serving as key communicators between the body's adaptive and innate immune responses. They achieve this by monitoring their surroundings and conveying critical information to leukocytes. However, dendritic cells are not uniform; they differ based on their location within the body, the danger signals they detect, and the specific molecules they produce.

Human dendritic cells are recognised as antigen-presenting cells (APCs), characterised by their consistent expression of MHCII (including HLA-DR) and the absence of certain lineage-specific markers such as CD3, CD15, CD19, CD20, and CD56. Initially identified in peripheral blood due to its accessibility, human dendritic cells share similarities with their mouse counterparts.

Dendritic cells in humans are categorised into two primary subsets: plasmacytoid dendritic cells (pDCs) and conventional dendritic cells (cDCs) (Guilliams et al., 2014; Merad et al., 2013). Early research identified progenitors with the potential to develop into dendritic cells, known as "common" DC progenitors (CDPs), **see Figure 1**, as these progenitors were thought to give rise to both cDCs and pDCs (Naik et al., 2007; Onai et al., 2007). However, subsequent studies revealed that pDC precursors are distinct from those that develop into cDCs, leading to a more precise definition of CDPs as progenitors specifically for conventional DCs (Cabeza-Cabrerizo et al., 2021; Dress et al., 2019; Rodrigues et al., 2018).

CDPs eventually develop into pre-cDCs, a stage marked by the upregulation of CD11c. Pre-cDCs were initially discovered in lymphoid tissues (Diao et al., 2006; Naik et al., 2006), and it was later established that these cells leave the bone marrow through the bloodstream to populate lymphoid and non-lymphoid tissues, where they further differentiate into cDCs (Liu et al., 2009).

Human pDCs are defined as MHCII^{low}CD45RA^{+}CD123(IL-3Rα)$^{+}$CD303(BDCA2)$^{+}$ performing similar functions as in mice; human pDCs produce large amounts of IFN-α in response to viruses (Colonna et al., 2004). Regarding cDCs, there are considerable differences between human and mouse subsets. In mice, circulating pre-cDCs mature in the two cDC subsets once they reach the peripheral tissues, whereas, in humans, the two subsets are present in peripheral blood. The first is the CD141 (BDCA3) expressing cDC1, which corresponds to murine CD8α^{+} /CD103^{+} cDCs (Ginhoux et al., 2009), and the other is CD1c (BDCA1) expressing cDC2, the human counterpart for mouse CD11b^{+} cDCs (Haniffa et al., 2012; Robbins et al., 2008; Watchmaker et al., 2014). Although there are phenotypic differences, the two cDC subsets were shown to be transcriptionally conserved between species, with some markers being shared among mice and humans, such as XCR1, CADM1 and CLEC9A in cDC1 and CD2, FcεR1a, CD172a and CLEC10A in cDC2 (Brown et al., 2019; Haniffa et al., 2012; Robbins et al., 2008; Watchmaker et al., 2014).

1.3.1 Migration/Activation of DC

Dendritic cells (DCs) play a crucial role in the immune system by detecting danger signals, such as pathogen-associated molecular patterns (PAMPs) or damage-associated molecular patterns (DAMPs). These signals are recognised through pattern recognition receptors (PRRs) binding, which are expressed differently across various DC subsets. The specific PRRs present on a DC determine its ability to respond to particular danger signals and produce a variety of cytokines and interferons.

When dendritic cells (DCs) capture and process antigens, they detect associated danger signals that contribute to their activation. This leads to increased expression of MHC-II molecules, costimulatory molecules, and the production of cytokines and chemokines. The activated DCs then migrate to lymph nodes, where they present the processed antigens to CD8 and CD4 T cells. This maturation process transforms immature DCs, which have a low capacity to stimulate T cells, into highly effective stimulators of T-cell responses.

As DCs mature, they migrate from peripheral tissues to secondary lymphoid organs. This migration is driven by the expression of CCR7, a receptor that makes activated DCs responsive to the chemokines CCL19 and CCL21 produced by lymphoid tissues (Förster et al., 2008; Iwasaki and Medzhitov, 2015). These chemokines guide the DCs through the lymphatic system to the local lymphoid tissues. Upon arriving in the lymphoid tissues, DCs lose their ability to engulf antigens but instead express high levels of MHC -I and -II molecules, which are loaded with processed peptides.

Additionally, mature DCs upregulate the expression of costimulatory molecules such as CD80 (B7.1) and CD86 (B7.2), which interact with the CD28 receptor on T cells (McLellan et al., 1995). This interaction is essential for T cell activation, proliferation, and cytokine production. The B7 family of molecules also has an immunoregulatory role, as they can bind to CTLA-4 on T cells, inhibiting T cell effector functions (Tekguc et al., 2021).

Another key molecule in DCs is CD40, a transmembrane glycoprotein that belongs to the tumour necrosis factor (TNF) superfamily. CD40 binds to its ligand, CD40L (CD154), which is typically expressed by activated CD4 and CD8 T cells (O'Sullivan and Thomas, 2003). This interaction further enhances the expression of CD80 and CD86 and stimulates the production of IL-12, which drives the differentiation of naïve T cells into Th1 cells (Balan et al., 2019). Finally, CD83 is highly expressed on DC, which has an effect on $CD4^+$ T cell development in the thymus and is upregulated on DCs MHC II and CD86(Fujimoto et al., 2002; Tze et al., 2011). Through these mechanisms, DCs effectively stimulate and direct specific T-cell responses, playing a vital role in the immune system's ability to fight infections and other threats.

1.3.2 cDC1

Human myeloid cDC1s are the rarest subset of conventional dendritic cells, comprising only about one-tenth the frequency of cDC2s in steady-state conditions, which equates to approximately 0.03% of total peripheral blood mononuclear cells (PBMCs) (Collin and Bigley, 2018).

Initially, cDC1s were identified based on the expression of thrombomodulin (CD141/BDCA3) (Dzionek et al., 2000), but it was later discovered that CD141 alone is not a definitive marker, as it can also be moderately expressed by monocytes and cDC2s in vitro (Collin and Bigley, 2018; Haniffa et al., 2012). To more accurately identify cDC1s, additional markers are used, including the C-type lectin receptor CLEC9A (also known as DNGR1) (Poulin et al., 2012), the cell adhesion molecule CADM1, the chemokine receptor XCR1, which is conserved across many species (Crozat et al., 2010), and the antigen BTLA (CD272) (Collin and Bigley, 2018). While BTLA is also expressed by a subset of human peripheral blood cDC2s, it is typically at lower levels, and using a combination of at least two of these markers significantly enhances the accuracy of identifying cDC1s in both blood and tissues (Guilliams et al., 2016a).

The development of cDC1s is tightly regulated by specific transcription factors, similar to their mouse counterparts. Human cDC1s express FLT3 (CD135) and depend on FLT3 ligand (FLT3L) for their development, both in vitro (Poulin et al., 2012; Proietto et al., 2008) and in vivo (Ding et al., 2004). Additionally, like mouse cDC1s, human cDC1s require the transcription factors IRF8 and BATF3 to develop. IRF8 plays a crucial role in developing all dendritic cell subsets and monocytes, as evidenced by the significantly reduced numbers of these cells in patients with mutations in the IRF8 gene (Hambleton et al., 2011). The role of BATF3 in humans, however, is less clear. Although BATF3 is essential for cDC1 expansion in vitro, it seems to be less critical in vivo (Poulin et al., 2012).

Functional differences between mouse and human cDC1s are also notable. While murine cDC1s are highly efficient at cross-presenting antigens via MHCI to $CD8^+$ T cells (den Haan et al., 2000), this ability is less pronounced in human cDC1s, as indicated by lower levels of gene transcripts associated with MHCI presentation in human $CD141^+$ DCs compared to their mouse counterparts (Ardouin et al., 2016; Balan and Dalod, 2016). Despite this, human cDC1s have a range of other important functions. They express high levels of TLR3, which senses double-stranded RNA (dsRNA), and TLR8, which senses single-stranded RNA (ssRNA), enabling them to detect viral nucleic acids (Collin et al., 2013). When TLR3 is activated by viral hepatitis C virus

antigens or synthetic dsRNA (Poly I:C), cDC1s produce significant amounts of type III interferon (IFN-λ), aiding in viral clearance (Luber et al., 2010; Yoshio et al., 2013). Additionally, human cDC1s secrete tumour necrosis factor α (TNF-α) and CXCL10, though they produce relatively low levels of IL-12, which is a key difference from their mouse counterparts (Haniffa et al., 2012; Jongbloed et al., 2010; Poulin et al., 2010). Furthermore, cDC1s are particularly adept at sensing dead or necrotic cells through their unique marker, CLEC9A (Sancho et al., 2009).

1.3.3 cDC2

cDC2s represent the largest population of conventional dendritic cells in human blood, tissues, and lymphoid organs, accounting for about 0.3% of total PBMCs. Human cDC2s are typically identified by the expression of markers such as CD1c, FcεR1a, CD172a (SIRPα), and myeloid antigens like CD11b, CD11c, and CD33 (Dutertre et al., 2019; Heger et al., 2018). CD1c is a commonly used marker for identifying cDC2s across various tissues, leading to their frequent designation as $CD1c^+$ DCs. However, CD1c is not exclusive to cDC2s; it is also strongly expressed by nearly all B cells (Allan et al., 2011). Therefore, when using CD1c as a marker for cDC2s, it is essential to exclude $CD19^+CD20^+$ B cells and include markers specific to cDC1s for accurate identification. Additional markers such as CLEC10A (CD301) and FcεR1α have proven to be more reliable for distinguishing cDC2s in blood, thymus, and spleen (Brown et al., 2019; Dutertre et al., 2019; Heger et al., 2018).

Blood cDC2s can be further divided into two subpopulations based on CD5 expression. $CD5^+CD1c^+$ cells are more characteristic of cDC2s, while $CD5^-CD1c^+$ cells share transcriptional similarities with monocytes (Yin et al., 2017). Beyond blood, skin is another valuable source of human tissue for studying cDC2 variability. Dermal cDC2s, for example, express the marker CD1a and are migratory, capable of exiting in vitro dermis explants (Kissenpfennig et al., 2005; Lenz et al., 1993). Although Langerhans cells (LCs) also express CD1a, they can be distinguished from dermal cDC2s by lower levels of EpCAM, Langerin (CD207), and CD1a itself (Bigley et al., 2015; De Monte et al., 2016).

The transcriptional regulation of cDC2s is not fully understood, as no single transcription factor has been identified as exclusively controlling their development. Similar to their mouse counterparts, human cDC2s depend on FLT3 ligand (FLT3L) for their development, both in vitro and in vivo (Breton et al., 2016; Ding et al., 2014; Jefford et al., 2003; Maraskovsky et al., 2000), while patients with FTL3L mutations showed almost no presence of cDC2 and cDC1 (Momenilandi et al., 2024). The preferential expression of IRF4 suggests its potential role in their development (Suzuki et al., 2004), though this has yet to be definitively proven. Patients with *GATA2* mutations are deficient in cDC2s, indicating that this transcription factor is also crucial for their development (Bigley et al., 2019).

1.3.4 DC3

Recent high-dimensional single-cell studies have revealed significant cellular diversity in the MNPs, leading to the identification of a new dendritic cell subpopulation known as DC3 or DC2b (Brown et al., 2019; Dutertre et al., 2019; Villani et al., 2017). This DC3 population is present in the blood, bone marrow, spleen, and dermis, and its numbers increase under pathological or inflammatory conditions. Unlike traditional monocytes, DC3 cells express the CD14 marker but can be distinguished from monocytes by using the CD88 marker. Within the HLADR^{+} CD1c^{+} population, DC3s are identified alongside cDC2 cells through the differential expression of CD5 and CD14 (Dutertre et al., 2019; Villani et al., 2017). A more refined nomenclature was established after observing that DC3 expressed a continuum of expression of CD163 and CD14 markers depending on the inflammatory state (Bourdely et al., 2020; Cytlak et al., 2020). In non-inflammatory conditions, DC3s are typically CD1c^{+} CD5^{-} CD163low CD14^{low}, while under inflammatory conditions, they become CD1c^{+} CD5^{-} CD163^{high} CD14^{high} (Dutertre et al., 2019).

The origins and differentiation pathways of the DC3 is complex, particularly when comparing human and mouse models. In mice, distinct populations such as cDC2a and cDC2b arise from a cDC lineage (Minutti et al., 2024; Rodrigues et al., 2024), while DC3 has been traced

back to an MDP progenitor (Bourdely et al., 2020; Liu et al., 2023; Rodrigues et al., 2024). Transcriptomic comparisons suggest some overlap between mouse and human DC3 cells, though further research is needed to fully confirm these findings (Bourdely et al., 2020).

1.3.5 Pre DC

Despite years of research into dendritic cells (DCs), a more precise understanding of their various subpopulations and origins became possible only with the advent of high-dimensional single-cell analysis technologies. These advanced techniques have allowed for a more detailed characterisation and refinement of DC nomenclature. Before 2017, the "pDC" population was recognized as heterogeneous, with a subpopulation of cells expressing CD2, CD81, and AXL, capable of producing IL-12p70 and stimulating $CD4^+$ T cells (Matsui et al., 2009).

Single-cell transcriptomic studies in humans, supported by mass cytometry, identified a distinct population of cDC precursor cells in peripheral blood and various tissues. These cells, known as pre-DCs or ASDCs depending on the source (Alcántara-Hernández et al., 2017; See et al., 2017; Villani et al., 2017), differ significantly from pDCs. Human pre-DCs, which comprise 2 to 3% of total DCs, are characterised by the expression of AXL and SIGLEC-6 receptors, earning them the alternative name "ASDC." These studies revealed that pre-DCs share features with both pDCs and cDCs (See et al., 2017; Villani et al., 2017). Phenotypically, pre-DCs display both CD45RA and CD123 receptors, typical of pDCs, as well as CD11c and CD33, aligning with cDCs. Additional markers identified on pre-DCs include Siglec-1 (CD169) and CD5 (Dutertre et al., 2019). Functionally, pre-DCs produce IL-12p70 and stimulate T cells, and when cultured in vitro on stromal cells with FLT3L, they preferentially differentiate into a cDC2 phenotype (See et al., 2017; Villani et al., 2017) with later more investigation highlighting both a DC2a and DC2b predetermined fate in the blood of mice (Minutti et al., 2024). These findings suggest that pre-DCs are precursors of cDCs, originating from the bone marrow and found in the blood and secondary lymphoid organs (See et al., 2017; Villani et al., 2017).

Interestingly, a similar population of DC precursors had been identified in mice years earlier, though without a specific name. It was noted that DCs are replenished by progenitors present in tissues, with cDC precursors found in mice's bone marrow, blood, and spleen (Liu et al., 2007, p. 2; Naik et al., 2006). These cDC precursors are thought to be produced in the bone marrow and pre-committed to either a cDC1 or cDC2 fate before migrating to organs where they mature into cDCs (Schlitzer et al., 2015). Around the same time, studies demonstrated the existence of a comparable population of pre-cDCs in human blood and tissues (Breton et al., 2015; Lee et al., 2015). These cells, marked by the expression of CD34, are considered progenitors of cDCs, possibly at an earlier stage than the previously identified pre-DCs (See et al., 2017; Villani et al., 2017).

1.4 MACROPHAGES IN THE TUMOUR MICROENVIRONMENT

Cancer is a complex group of diseases characterised by the uncontrolled growth and spread of abnormal cells. These malignant cells can invade surrounding tissues and form tumours, disrupting the normal functioning of organs. While the causes of cancer are multifaceted, involving genetic mutations, environmental factors, and lifestyle choices, a key aspect of cancer progression is how it interacts with the body's immune system.

One of the major challenges in cancer treatment is resistance, which can be inherent to the tumour cells themselves or influenced by the surrounding non-malignant cells within the tumour microenvironment (TME). The TME includes both tissue-resident and recruited immune cells, which, in certain cancers like breast cancer, can constitute up to 50% of the TME. Within this environment, mononuclear phagocytes are evidently present. However, the role is less evident.

Initially, it was believed that immune cells within the TME were primarily involved in the body's attempt to reject tumours. It is still thought that in the earliest stages of cancer development, the immune system responds by activating T cells and macrophages to clear the tumour, thereby reducing cancer incidence (Dunn et al., 2004) However, as the tumour progresses past its initial stage, the immune environment tends to shift, becoming more supportive of tumour growth and suppressing immune-mediated cell death (Gajewski et al., 2013). In this process, there is clinical and experimental evidence that macrophages are highly abundant in most tumour types and have, in the majority, a tumour-promoting role (Noy and Pollard, 2014), see **Figure 3**. However, recent studies suggest a more nuanced understanding, indicating that certain types of macrophages can also exhibit antitumor activity (Pittet et al., 2022).

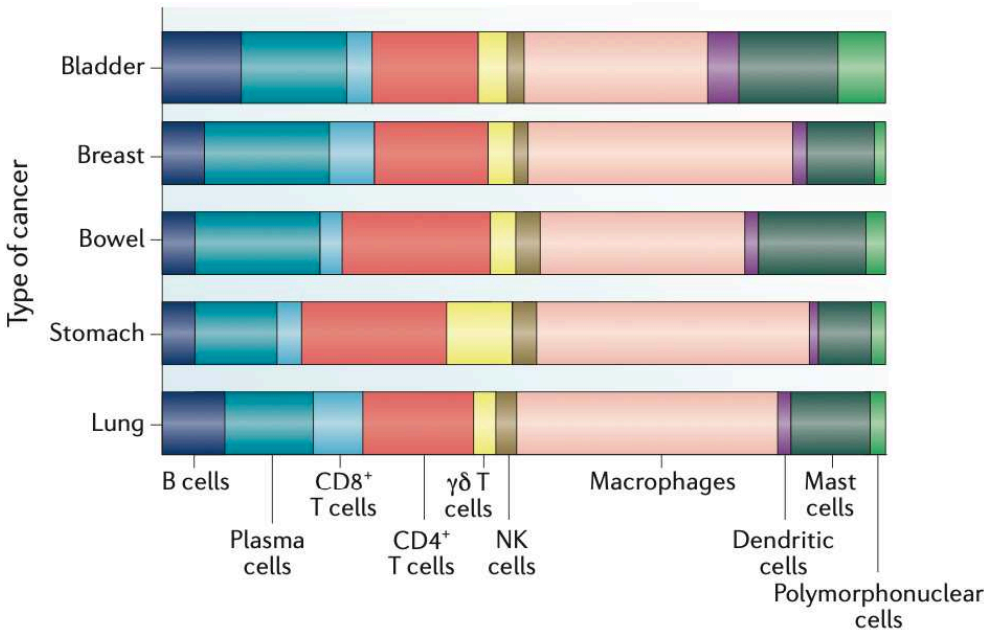

***Figure 3**: Partitions of immune compartments across various tumours. CIBERSORT analysis of tissue microarray data sets from solid human tumours, illustrating the average immune cell composition across bladder, breast, bowel, stomach, and lung cancers. The data are presented as estimated fractions of leukocyte RNA, highlighting that immune infiltrates vary by cancer type. Notably, macrophages emerge as the predominant population infiltrating most human cancers. Adapted from Cassetta and Pollard, 2018.*

Macrophages have historically been classified into two distinct polarization states: M1, pro-inflammatory, and M2, anti-inflammatory (Charles D. Mills et al., 2000; Stein et al., 1992). This binary classification has been useful for describing macrophage behaviour in vitro, particularly in response to various stimuli. Bacterial products like lipopolysaccharides and pro-inflammatory cytokines such as interferons and TNFα typically induce M1 macrophages. These macrophages are known to produce factors like IL-12 and CXCL10, which are associated with antitumor immunity. On the other hand, M2 macrophages are driven by immunoregulatory cytokines like IL-4, IL-

10, and TGF-β, leading to the secretion of tissue-remodelling and pro-angiogenic factors such as matrix metalloproteinases and VEGF, which are associated to tumour promotion. However, Tumor-associated macrophages (TAMs), rarely fit neatly into the M1 or M2 categories (Cheng et al., 2021; Locati et al., 2020; Szulzewsky et al., 2015; Yang et al., 2018).

The simple M1/M2 dichotomy has proven inadequate to capture the true complexity of macrophage behaviour in vivo, particularly within different anatomical sites, tissue niches, and disease contexts (9,29,30). To better reflect their diversity, some researchers have proposed additional subcategories, such as M2a, M2b, and M2c, or more flexible terms like M1-like and M2-like (Mantovani et al., 2017, 2004; Murray et al., 2014).

Despite these efforts, the full complexity of TAMs remains difficult to encapsulate within these classifications. For instance, M2-like TAMs are often found in hypoxic tumour areas, where they exhibit strong pro-angiogenic activity, and their numbers tend to increase as tumours progress. Yet, TAMs can co-express both M1 and M2 gene signatures, and tumour-promoting macrophages may express genes not traditionally associated with the M2 phenotype (Cassetta et al., 2019; Cheng et al., 2021; Pombo Antunes et al., 2021; Wu et al., 2021; Zilionis et al., 2019). This highlights the need for a more nuanced understanding of macrophage diversity, especially in the context of cancer, where their roles can be multifaceted and context-dependent.

In cancer, just as in healthy tissues, the origins and local environment significantly influence the diverse populations of macrophages found within tumours. It was believed that tumour-associated macrophages (TAMs) originated primarily from circulating monocytes continuously recruited to the tumour site in response to inflammation (van Furth et al., 1972). While it has been confirmed that monocyte-derived cells often make up the majority of TAMs (Cortez-Retamozo et al., 2012; Ruth A. Franklin et al., 2014; Qian et al., 2011), these cells coexist within the tumour microenvironment (TME) alongside macrophages that were already present in the tissue before the tumour developed. Notably, macrophages derived from embryonic origins (RTMs) and those derived from adult monocytes perform different roles. For example, in

murine models of pancreatitis and pancreatic cancer, embryonic RTMs are key drivers of fibrotic responses (Baer et al., 2023), whereas monocyte-derived TAMs are more involved in regulating adaptive immune responses (Zhu et al., 2017).

However, neither the origins of these macrophages nor their specific location within the tumour fully explain when and how they become TAMs. Interestingly, monocyte-derived macrophages with TAM-like tumour-promoting characteristics can be recruited to tissues even before the development of tumours, as seen in cases of injury-induced pancreatic metaplasia (Liou et al., 2023).

When monocytes enter the tumour environment, they encounter various signals that shape their behaviour as they become TAMs. A time-stamping fate-mapping study, which allows for information on the timed arrival of monocytes in pancreatic ductal adenocarcinoma (PDAC), revealed that monocytes first differentiate into a transient intermediate population of TAMs. This population then gives rise to longer-lived, terminally differentiated TAMs with distinct gene expression profiles, phenotypes, and specific locations within the tumour (Dunsmore et al., 2024). This highlights how the tumour environment influences the characteristics and functions of TAMs within the tumour.

There is still no clear answer as to which cells are primarily responsible for TAMs. Ontology seems to play a role, as RTMs are potent promoters of fibrotic responses (Baer et al., 2023). However, overall, the majority of TAMs have been shown to be of monocyte-derived origin (Ruth A. Franklin et al., 2014).

The classification of tumour-associated macrophages (TAMs) remains an unresolved and ongoing area of debate. Currently, the most widely accepted approach to categorising TAMs relies on identifying specific gene and protein signatures associated with their functions within the tumour microenvironment. In the following sections, we will highlight some of the more commonly observed TAM populations found in tumours.

1.4.1 TREM2 TAMs

TREM2 is a gene associated with lipid metabolism and is found in various cell types, including microglia in the brain, osteoclasts in bone, and specific subsets of macrophages in tissues such as the liver, adipose tissue, skin, gut, and tumours (Colonna, 2023). TREM2-expressing TAMs have been frequently identified in single-cell immune cell analyses of both early and late-stage metastatic non-small-cell lung cancer (NSCLC) (Lavin et al., 2017; Leader, 2021; Maynard et al., 2020; Zhang et al., 2022). In these tumours, $TREM2^+$ TAMs primarily originate from blood monocytes and are characterized by the expression of genes associated with lipid metabolism, immunosuppression, and complement activation. A high infiltration of $TREM2^+$ TAMs has been linked to disease progression (Zhang et al., 2022). Similar findings have been observed in human breast cancer (Azizi et al., 2018; Ramos et al., 2022; Timperi et al., 2022; Wu et al., 2021; Y. Zhang et al., 2021), where $TREM2^+$ TAMs display a transcriptome profile akin to that in lung cancer, also deriving mainly from blood monocytes and associated with immunosuppression and poor prognosis. Interestingly, TREM2 expression was found to be mutually exclusive with folate receptor-β (FOLR2), distinguishing immunosuppressive TAMs from immunostimulatory ones (Ramos et al., 2022). Histological analysis revealed distinct spatial distributions for these subsets: $FOLR2^+$ TAMs were predominantly located in the tumour stroma, while $TREM2^+$ TAMs were present in both the stroma and tumour nests, particularly along the invasive margin, suggesting direct influence by tumour cells.

In colorectal carcinoma and its liver metastases, a heterogeneous population of TAMs has been identified, including a subset expressing both TREM2 and the complement component C1QC (Liu et al., 2022). $TREM2^+$ TAMs have also been found in melanoma (Xiong et al., 2020), clear-cell renal carcinoma (Obradovic et al., 2021), and pancreatic ductal adenocarcinoma (Kemp et al., 2021), where they are associated with immunosuppression and disease recurrence. Single-cell transcriptomics of 15 human parenchymal brain metastases revealed the presence of metastasis-associated macrophages expressing TREM2, APOE, and C1QB (Gonzalez et al., 2022).

The role of TREM2$^+$ TAMs in hepatocellular carcinoma is less clear. One study found that these immunosuppressive macrophages were associated with decreased survival (Zhou et al., 2022). However, another study reported that mice deficient in TREM2 developed more diethylnitrosamine-induced liver tumours and increased liver damage, inflammation, and oxidative stress (Esparza-Baquer et al., 2021). Overall, TREM2$^+$ TAMs typically promote immunosuppression and tumour growth, although their impact may vary depending on the type and underlying pathology of the tumour.

1.4.2 RTM-TAMs

RTM-TAMs Macrophages in the tumour are often linked to macrophages that resemble normal resident tissue macrophages, though their signature can vary. Key genes in this signature include LYVE1, HES1, and FOLR2 (Cheng et al., 2021; Li et al., 2024; Sharma et al., 2020; Zilionis et al., 2019). RTM-TAMs are characterised by their similarity to normal RTMs, showing high expression of embryonic precursor genes (Casanova-Acebes et al., 2021; Sharma et al., 2020) and often being enriched in tissues adjacent to the tumour (Cheng et al., 2021; Ramos et al., 2022).

In various cancer types and organ sites, RTM-TAMs express gene signatures that closely resemble those of their normal counterparts. For instance, in lung cancer (Cheng et al., 2021; Kim et al., 2020; Zilionis et al., 2019) and lung metastasis of osteosarcoma (Yan Zhou et al., 2020), RTM-TAMs exhibit high levels of MARCO, scavenger receptors, and *FABP4*, akin to alveolar macrophages. Similarly, in hepatocellular carcinoma (HCC) (Massalha et al., 2020; Sharma et al., 2020) and colorectal cancer liver metastasis (Che et al., 2021), RTM-TAMs express *MARCO*, *VSIG4*, and *FOLR2*, similar to Kupffer cells in the liver.

While RTM-TAMs are often found in tissues adjacent to tumours, studies have shown that they can promote tumour invasiveness by inducing epithelial-mesenchymal transition (EMT) in tumour cells and recruiting regulatory T cells (Tregs) in lung cancer models (Casanova-Acebes et al., 2021) and glioblastoma models (Hara et al., 2021).

However, in breast cancer, these macrophages can enhance the infiltration of $CD8^+$ T cells, contributing to an anti-tumor response (Ramos et al., 2022).

Over time, RTMs adapt to their environment, developing a form of "memory" that potentially influences their function within the tumour microenvironment (TME). Recently, the concept of "PreTAMs" was introduced to highlight macrophages that were present in tissues before tumour development, regardless of their specific origin. "Pre" signifies their prior existence, while "TAM" underscores their role as key cellular contributors to tumour progression (Blériot et al., 2024). PreTAMs are thought to connect pre-existing inflammation to cancer development, while TAMs, recruited from circulating monocytes after tumour formation, work together with PreTAMs in promoting tumour-related inflammation as they become reprogrammed within the TME.

Although RTMs may exhibit an embryonic gene signature, it is important to note that they can also originate from bone marrow monocytes in various organs (Blériot et al., 2020). Thus, the gene signature of RTM-TAMs may reflect not only their origin but also the influence of the surrounding tissue environment, distinct from the tumour microenvironment.

1.4.3 IFN-TAMs

IFN-TAMs are characterised by high expression of interferon-regulated genes, such as *CXCL9*, *CXCL10*, *PDL1* and *ISG15*, along with M1-like markers, including CD86 and MHCII (Bill et al., 2023; Cheng et al., 2021; Zilionis et al., 2019). These TAMs have been identified across various tumour types, such as breast cancer (BRCA), colorectal cancer (CRC), hepatocellular carcinoma (HCC), head and neck cancer (HNC), lymphoma, melanoma, nasopharyngeal carcinoma (NPC), nonsmall cell lung cancer (NSCLC), ovarian cancer (OVC), pancreatic ductal adenocarcinoma (PDAC), thyroid carcinoma (THCA), and uterine corpus endometrial carcinoma (UCEC) (Che et al., 2021; Cheng et al., 2021; L. Zhang et al., 2020), as well as multiple myeloma, osteosarcoma, glioblastoma, and spinal ependymomas (Zavidij et al., 2020; Q. Zhang

et al., 2021; Yan Zhou et al., 2020).

IFN-TAMs bear the closest resemblance to M1-like macrophages among the different TAM subsets (Bill et al., 2023). However, unlike the typical anti-tumor role associated with M1-like macrophages, IFN-TAMs have been linked to immunosuppressive functions. They can suppress immune responses through mechanisms like tryptophan degradation and the recruitment of regulatory T cells (Tregs) (Sadik et al., 2020). However, in lung cancer, *CXCL10*$^{+}$ TAMs are organised around stem-immunity hubs, which benefit treatment (Chen et al., 2024).

The high expression of immune checkpoint molecules, such as *PD-L1* and *IDO1*, in IFN-TAMs is regulated by factors including signal transducer and activator of transcription 1 (*STAT1*), *STAT2*, ETS variant transcription factor 7 (*ETV7*), and IFN regulatory factor 1 (*IRF1*). This regulation is closely linked to the location of these TAMs within the tumour. The possibility that IFN-TAMs may exhibit antitumor functions in certain contexts remains an area for further research.

1.4.4 Macrophage crosstalk

The interaction/crosstalk between macrophages and fibroblasts is widely acknowledged as a crucial node/nexus in both tissue homeostasis and pathological conditions. These two cell types coexist in various tissues under steady-state conditions (Uderhardt et al., 2019), with a mutual exchange of growth factor signals between them. This dynamic has been described as a stable two-cell circuit reliant on the exchange of growth factors, characterised by resilience and regulatory mechanisms to prevent unchecked proliferation of either cell type (Zhou et al., 2018).

The interplay between macrophages and fibroblasts is even more relevant in the context of cancer. In the cancer microenvironment, macrophages and stromal cells inherently support tumour growth, even when their clients are cancer cells (Okabe and Medzhitov, 2016). Tumours have been likened to "wounds that do not heal" (Dvorak, 1986), where fibroblasts, also known as cancer-associated fibroblasts

(CAFs), and macrophages, also known as tumour-associated macrophages (TAMs), are recognised as key cellular components. TAMs exhibit high heterogeneity in the tumour microenvironment (Sharma et al., 2022). When translating these populations into a fibrosis context, programs can be found in both fibrosis and cancer settings, such as the TREM2 TAMs (Ramachandran et al., 2019).

Additionally, the macrophage-fibroblast interaction within this unique ecosystem varies in functional specialisation depending on the cancer type. In colorectal cancer, the interplay between *FAP*$^{+}$ fibroblasts and *SPP1*$^{+}$ macrophages is associated with poor patient survival, suggesting a regulatory role in the maintenance and function of both cell types through extracellular matrix remodelling (Qi et al., 2022).

Similarly, in HCC, a cooperative relationship between *POSTN*$^{+}$ CAFs and *FOLR2*$^{+}$ TAMs within the tumour microenvironment emphasises the importance of cell-cell communication and immunomodulatory functions, with the IL34-CSF1R axis playing a crucial role in macrophage differentiation (Li et al., 2024). This paper highlights the oncofetal reprogramming, which is on the premise that tumours show a fetal-like reprogramming in the tumour microenvironment at a level of cellular heterogeneity and plasticity (Sharma et al., 2022). Similar to the tumour environment, wound healing, such as epithelial regeneration, is driven not only by inflammation but also by the crosstalk of the microenvironment (Deyell et al., 2021). This highlights how similarity can be found within a disease context, but a complex heterogeneity can be found within these environments.

1.4.5 Therapeutic potential

TAMs are an essential and profound presence in the TME with multiple roles, such as orchestration of angiogenesis, extracellular matrix remodelling, cancer cell proliferation, metastasis and immunosuppression, as well as in resistance to chemotherapeutic agents and checkpoint blockade immunotherapy. With the knowledge of how heterogeneous the macrophage population is in the tumour with a pro or anti-tumour effect, it is essential to have a precise target

or approach. Macrophage-centred therapeutic strategies have the potential to complement and synergise with currently available tools in the oncology armamentarium.

TAMs play a crucial and multifaceted role in the tumour microenvironment. They orchestrate processes like angiogenesis, extracellular matrix remodelling, cancer cell proliferation, metastasis, and immunosuppression. Given the diverse nature of macrophages in tumours, which can have either pro-tumour or anti-tumour effects, it's important to develop precise targeting strategies. Focusing on macrophage-centered therapies could effectively complement and enhance existing cancer treatments (Cassetta and Pollard, 2018; Mantovani et al., 2022).

Recent studies have shown that blocking TREM2, a receptor expressed by macrophages in several tissues, including tumours, can significantly inhibit tumour growth. For instance, TREM2 deficiency and anti-TREM2 monoclonal antibody (mAb) treatment have both effectively curbed tumour growth in mice (Molgora et al., 2020). When combined with an NK cell-activating agent, TREM2 blockade further enhances the inhibition of tumour growth (Park et al., 2023). A humanised mAb targeting $TREM2^{+}$ macrophages, known as PY314 (Binnewies et al., 2021), is currently being tested in a phase I clinical trial for advanced solid tumours that have been resistant to previous treatments.

Inhibition of the CSF1R has shown significant clinical benefits in patients with a rare tumour type, diffuse-type tenosynovial giant cells, where CSF1 is overexpressed, leading to positive outcomes in 71% of patients studied (Bissinger et al., 2021). However, CSF1R inhibitors have shown limited effectiveness as single agents in other solid tumours. Several clinical trials are ongoing, exploring combinations of CSF1R inhibition with chemotherapy, radiotherapy, or immune checkpoint blockade (ICB) (Lin et al., 2020; Manji et al., 2021). While durable clinical responses have not yet been reported, some patients have experienced disease stabilization or partial responses, and the potential benefits of this approach are still under investigation (Mantovani et al., 2022).

Additionally, IL-4, derived from bone marrow basophils and

eosinophils, has been shown to influence the development of immunosuppressive, tumour-promoting myeloid cells (LaMarche et al., 2024). A clinical trial of the IL-4Rα blocking antibody dupilumab, administered in conjunction with PD-1/PD-L1 checkpoint blockade, demonstrated promising results in patients with relapsed or refractory non-small cell lung cancer (NSCLC) who had previously progressed on PD-1/PD-L1 therapy alone ("Study Details | Dupilumab_Metastatic NSCLC | ClinicalTrials.gov," n.d.). The treatment reduced circulating monocytes expanded tumour-infiltrating $CD8^+$ T cells and led to a near-complete clinical response in one patient within two months.

Efforts to target monocyte attractants, such as CCL2 and its receptor CCR2, have included the use of monoclonal antibodies and receptor antagonists in solid tumours and haematological malignancies. Preclinical studies in murine tumour models have demonstrated that CCR2 antagonism, in combination with anti-PD-1 therapy, can enhance tumour response beyond that achieved with anti-PD-1 monotherapy alone (Nywening et al., 2016; Tu et al., 2020). Although these preclinical models showed promise, these strategies have not yet yielded positive clinical results and have been discontinued in some cases (Mantovani et al., 2022).

1.5 DENDRITIC CELLS IN THE TUMOUR MICROENVIRONMENT

Dendritic cells are specialised antigen-presenting cells that play a key role in the link between innate and adaptive immune responses. Despite being a relatively rare population within the immune system, DCs are critical in generating specific T-cell-mediated antitumor responses by cross-presenting tumour-associated antigens to naïve T cells. This function is essential for controlling tumour growth and preventing the spread of cancer cells. However, the antitumor activity of DCs can be significantly compromised within the immunosuppressive environment of tumours. While much of what we know about DC subsets and their functions comes from studies in mouse models, there is a growing focus on understanding the biology of human DCs to improve our insights into their role in cancer.

1.5.1 cDC1

The presence and function of cDC1 cells in the tumour microenvironment are closely linked to better survival rates and enhanced responsiveness to treatment in various human cancers (Barry et al., 2018; Böttcher et al., 2018; Böttcher and Reis e Sousa, 2018; Michea et al., 2018; Spranger et al., 2017). These cells are essential for antitumor immunity, primarily due to their ability to cross-present tumour antigens to cytotoxic $CD8^+$ T cells (Böttcher and Reis e Sousa, 2018; Broz et al., 2014). In addition, studies have shown that cDC1 cells can also present tumour-derived antigens to $CD4^+$ T cells in animal models (Ferris et al., 2020). Furthermore, cDC1 cells are unique among antigen-presenting cells in their ability to transport intact antigens to lymph nodes and prime tumour-specific $CD8^+$ T cells (Salmon et al., 2016).

An example of protection, in a mouse melanoma model, systemic injections of FLT3L and intratumoral poly I:C expanded and activated cDC1 cells, offering protection against tumour rechallenge and enhancing responses to BRAF and PD-L1 blockade therapies (Salmon et al., 2016). Another study showed that human cDC1 cells increase DNA uptake and express T cell–recruiting chemokines like CXCL9 and

CXCL11 via a TIM-3-dependent mechanism (de Mingo Pulido et al., 2021).

During tumour progression, cDC1 function can be impaired. In a lung tumour model, tumour progression inhibited the capability to capture antigen by lung cDC1 cells. This was linked to downregulation of the TIM4 receptor, impairing cDC1 phagocytic ability and promoting tumour growth (Caronni et al., 2021). This was further explored in humans, and it was shown that when TIM4 expression was enhanced, the prognostic value of the cDC1 signature predicted PD-1 therapy response (Caronni et al., 2021). Additionally, tumour-derived G-CSF inhibited DC development by suppressing IRF8, correlating with reduced DC progenitor levels and lower $CD141^+$ cDC1 frequencies in breast and pancreatic cancer patients (Meyer et al., 2018; Roth et al., 2000).

The ability of cDC1 cells to coordinate immune responses depends on their migration and infiltration into tumours. A study showed that transgenic expression of FLT3L and XCL1 by tumour cells enhanced cDC1-mediated T-cell cross-priming (Sánchez-Paulete et al., 2018). XCL1 is a chemotactic ligand for the XCR1 receptor on human cDC1, which in turn is a specific receptor on cDC1. NK cells play a key role in this recruitment process (Barry et al., 2018; Böttcher et al., 2018). In human cancers, cDC1 and NK cell signatures often correlate within tumours, predicting better survival in melanoma, head and neck squamous cell carcinoma, and lung adenocarcinoma patients (Böttcher et al., 2018). In mouse models, cDC1 recruitment depended on NK cell-derived chemokines, while tumour-derived prostaglandin E2 (PGE2) impaired NK and cDC1 function, aiding immune evasion (Böttcher et al., 2018). Coexpression of CCL5 and FLT3L in metastatic cancers correlated with cDC1 signatures and better survival (Cueto et al., 2021). Tumor-secreted gelsolin was found to inhibit CLEC9A binding in cDC1 cells, reducing their ability to cross-present antigens, a process linked to worse outcomes in hepatocellular carcinoma and other cancers (Giampazolias et al., 2021).cDC1 cells are an important factor in orchestrating antitumor responses at tumour sites and lymph nodes.

Their effectiveness is influenced by interactions within the tumour microenvironment, which sometimes can be inhibited or enhanced with, for example, NK cells.

1.5.2 DC2/3

cDC2 cells are recognised as key inducers of $CD4^+$ T helper cells (Binnewies et al., 2019). However, recent findings suggest that cDC1 cells also contribute to $CD4^+$ T cell priming (Ferris et al., 2020). Notably, human cDC2 cells, unlike their mouse counterparts, secrete high levels of interleukin-12 (IL-12), which has the potential to prime cytotoxic T cells for antitumour responses (Mittag et al., 2011; Nizzoli et al., 2013).

As mentioned before, circulating cDC2 cells are now understood to be a heterogeneous group, including both true cDC2 and DC3 cells, also known as inflammatory DCs (infDCs) due to their inflammatory signature (Dutertre et al., 2019; Villani et al., 2017). DC3 cells expand during immune diseases like systemic lupus erythematosus (SLE) (Dutertre et al., 2019) and rely on the proinflammatory cytokine GM-CSF for their development (Bourdely et al., 2020; Liu et al., 2023). Similar inflammatory DCs have been observed in tumour ascites from ovarian and breast cancer patients before treatment (Segura et al., 2013), initially thought to arise from monocytes. These cells share molecular signatures with both DCs and monocytes, expressing markers such as CD1c, FceRI, CD206, and lower levels of CD14 compared to monocytes/macrophages (Segura et al., 2013). They also induce autologous naïve $CD4^+$ T cell responses and IL-17 production but are absent in cancer-free lymph nodes from breast cancer patients or healthy controls (Segura et al., 2013)

The extent to which DC3 and cDC2 cells contribute to T cell activation in humans, potentially influencing outcomes ranging from tolerance to antitumour immunity, remains unclear and likely varies depending on the tumour niche and type. For instance, in breast cancer, a higher cDC1 signature is associated with better outcomes in both luminal and triple-negative breast cancer, while a cDC2 signature is only linked to better outcomes in the luminal type (Michea et al., 2018). Inversely, a

higher monocyte/macrophage signature is associated with lower survival in both cancer types. In head and neck squamous cell carcinoma, higher levels of cDC2 and lower levels of T regulatory cells (Tregs) correlate with better prognosis (Binnewies et al., 2019). Therefore, it is essential to explore the specific roles of DC3 cells, which share characteristics with both cDC2 and monocytes/macrophages, in inducing tolerance and/or antitumor responses at the tumour site.

In patients with melanoma and non-small cell lung cancer (NSCLC), the DC3 population was found to be increased, although they showed weak tumour antigen-specific CD8 T cell activation (Becker et al., 2024). In breast cancer, $CD5^+$ cDC2 and $CD14^+$ DC3 cells were present at similar frequencies within tumours. DC3 cells were capable of priming naïve $CD4^+$ and $CD8^+$ T cells, though less efficiently than cDC2 cells (Bourdely et al., 2020). Interestingly, DC3 cells were particularly effective at inducing a $CD103^+$ tissue residency phenotype in $CD4^+$ and $CD8^+$ T cells compared to cDC2 cells or monocytes. The presence of DC3 cells correlated with tissue-resident $CD8^+CD103^+CD69^+$ T cells within breast tumours (Bourdely et al., 2020), a T cell subtype associated with improved breast cancer prognosis (Savas et al., 2018). However, a DC3-like $CD1c^+CD14^+$ myeloid cell population with PD-L1–mediated $CD4^+$ T cell–suppressive capacity was found to expand in patients with melanoma (Becker et al., 2024).

Further investigation of the heterogeneous DC2/3 compartment is crucial as clear separation is needed from true cDC2 cells from DC3 and monocyte-derived cells.

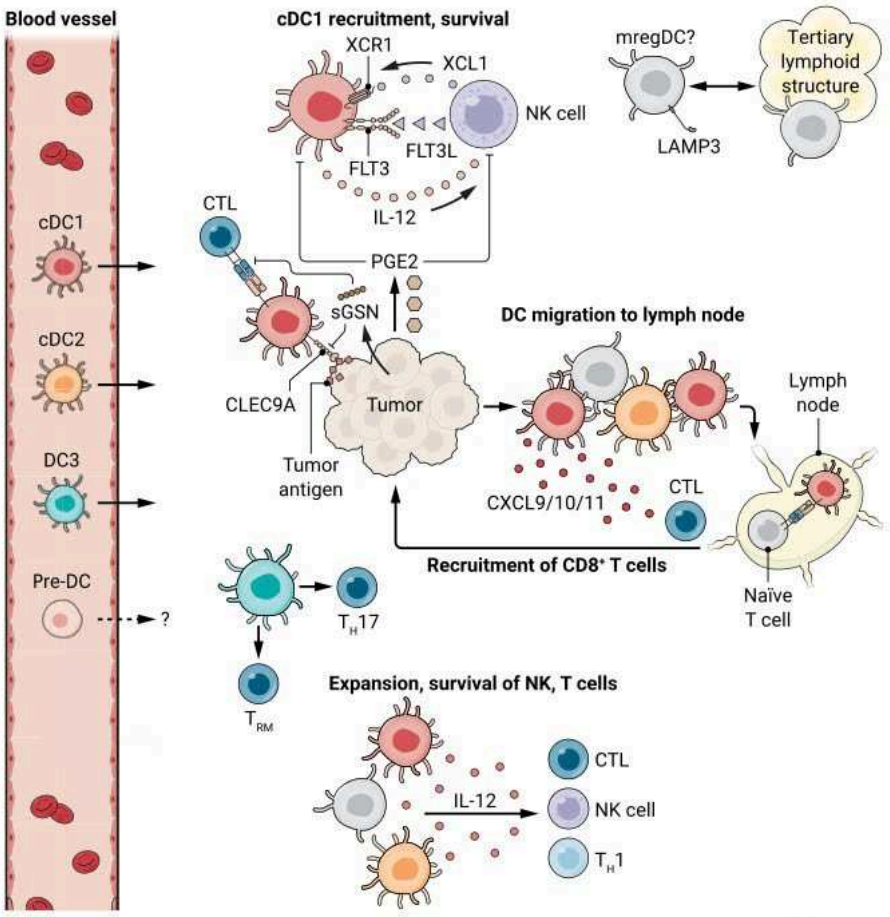

Figure 4: *The effect of human DC in the tumour microenvironment. Circulating cDC1, cDC2 and DC3 infiltrate tumours through the entry and effects. Once within the tumour, DCs contribute to antitumor immunity by inducing, priming, and activating T cells, either directly at the tumour site, within surrounding tertiary lymphoid structures, or in the lymph nodes. Key interactions include DC-derived IL-12, essential for NK and T cell expansion and survival, and DC3-mediated induction of tissue-resident memory (TRM) T cells and TH17 cells. Tumours can suppress cDC1 cross-presentation and block both cDC1 and NK cell functions, disrupting these antitumor responses. A feedback loop between cDC1 and NK cells is shown, along with the proximity of migratory DCs—potentially mregDCs—near tertiary lymphoid structures. DCs migrate to lymph nodes carrying tumour antigens, initiating T cell responses and recruiting tumour-specific cytotoxic T lymphocytes (CTLs) via cDC1. Adapted from Kvedaraite & Ginhoux, 2022.*

1.5.3 Migration of DC in the TME

While the earlier parts focused on lineage-specific responses of dendritic cells (DCs) within the tumour microenvironment (TME), it's important to note that the majority of all DCs share a conserved program despite these differences. Within the TME, it has been shown that there is a program that induces a state for the DC to have immunoregulation (PD-L1, PD-L2, and CD200) and migration/maturation (CD40, CCR7, and IL-12) combined with migration markers like LAMP3 and CCR7, as per such named mregDCs (Maier et al., 2020). In experimental models, both cDC1 and cDC2 have been shown to upregulate mregDC-related proteins upon encountering tumours, contributing to this cell state (Maier et al., 2020). These cells, often called mregDCs, $LAMP3^+$ DCs or $CCR7^+$ DCs, have been detected in various cancers (Cheng et al., 2021; Li et al., 2024; Zilionis et al., 2019). While the name and function have been associated with cancer, it has also been detected in healthy tissue, suggesting it is more to a maturation program (Kvedaraite and Ginhoux, 2022).

In human tumors, mregDCs include cells resembling both cDC1 and cDC2. Interestingly, mregDCs may not function identically across all tumours. For instance, *IL12B* expression is specific to cDC1-like mregDCs, which can induce a TH1-like response, highlighting the conserved functional traits of cDC1 in the mregDC state (Cheng et al., 2021). Within human tumours, better survival has been shown for primary tumour-draining lymph nodes (Lee et al., 2024; Movassagh et al., 2004). These megrDCs have been associated in location with tertiary lymphoid structures or cluster with T cells in the stroma (Dieu-Nosjean et al., 2008; Germain et al., 2014). While this shows a strategic and sometimes positive role as an antitumoural function, it has also been shown to have a negative effect on the patient with an accumulation of Tregs (You et al., 2024).

While the mregDC program appears to be a tissue-induced maturation state rather than a cancer-specific entity, further research is needed to explore its role across various human diseases and the possibility of modulation. Understanding the developmental relationship between mregDCs and other DC subsets, such as cDC1, cDC2, and DC3, will be critical for advancing our knowledge of DC functionality in cancer and other conditions.

1.5.4 DC therapy

Dendritic cells play a central role in antitumor immunity by conditioning the tumour microenvironment and priming antitumor T-cell responses. However, the tumour microenvironment can also impair DC functions through various mechanisms, such as inhibiting their recruitment, differentiation, and immunostimulatory capacity. Despite these challenges, manipulating DCs holds significant potential for inducing effective antitumor immunity.

Chemotherapeutic agents like anthracyclines can trigger immunogenic cell death, a process that depends on the presence of DCs to stimulate an immune response effectively (Ma et al., 2013). Additionally, small-molecule inhibitors targeting pathways such as STAT3, MAPK, and mTOR can modulate DC function, offering another strategy for therapeutic intervention (Nefedova et al., 2005; Oosterhoff et al., 2012; Ott and Adams, 2011). Antibodies targeting co-inhibitory receptors, such as those in the PD-1/PDL1 axis, or activating costimulatory receptors like CD137, have been shown to regulate antitumor immune responses (Sánchez-Paulete et al., 2016). Notably, combining pembrolizumab, an anti-PD-1 antibody, with TLR9 agonists has demonstrated clinical benefits in melanoma, highlighting the potential of such combination therapies in cancer treatment (Ribas et al., 2018).

Another important aspect of the role of dendritic cells (DCs) in cancer regulation is their involvement in cancer vaccinations. The primary objectives of anticancer vaccines are to induce tumour-specific effector T cell responses and to stimulate long-lived memory T cells. These goals are crucial for both overcoming tumour growth and controlling tumour relapse. Although developing these therapies is challenging and risks failure (Thomas et al., 2018), some trials have shown promising results. These studies highlight the potential of therapeutic vaccination to induce clinical remission, particularly in low-burden tumours and suggest that enhancing DC mobilisation could further improve outcomes (Harper et al., 2019; Trimble et al., 2015).

1.6 OMICS TO CAPTURE MONONUCLEAR PHAGOCYTES

Understanding the complexity of the immune system remains a significant challenge, requiring the continual development of new experimental techniques to better capture its intricacies. Collaborative initiatives like the ImmGen project aim to deepen our immunological understanding of gene expression and regulatory networks on a global scale (Heng et al., 2008). Additionally, many research groups have published atlases of various tissues and pathologies (Rozenblatt-Rosen et al., 2017). Together with these endeavours, technological advancements have emerged to facilitate discoveries and further enhance our understanding.

1.6.1 Fluorescence-based assays

In immunology, fluorescence-based assays are among the most commonly used techniques. Notable examples include immunofluorescence and flow cytometry, which enable the detection and localisation of various antigens in different tissue types and cell preparations (Fang et al., 2019). Immunofluorescence uses antibodies tagged with fluorescent dyes to detect specific antigens in cells or tissue sections, which are then examined under a fluorescence microscope. The presence and location of antigens are indicated by the fluorescent signal. In contrast, flow cytometry involves tagging antibodies with fluorescent markers that bind to specific antigens on or within cells. As these labelled cells pass through the flow cytometer, lasers excite the fluorescent markers, and the emitted light is detected and analysed.

Modern flow cytometry techniques have evolved to include panels of multiple fluorochrome-conjugated antibodies (conventional flow cytometry) or metal-conjugated antibodies (mass cytometry) to measure protein expression profiles of individual cells. This approach allows for high-throughput analysis, capturing both common and rare cell populations. However, despite these advancements, current fluorescence and mass cytometry are still limited to 50 or fewer parameters (Konecny et al., 2024). This limitation is stark when

considering that at least 371 clusters of differentiation (CD) markers are recognized (Engel et al., 2015), excluding other relevant surface proteins. To bridge this gap, machine-learning computational tools have been developed to target and analyze all available CD markers (Becht et al., 2021; Ferchen et al., 2023). In various studies, this approach has proven beneficial in uncovering the complexities of mononuclear phagocytes (Dunsmore et al., 2024; Dutertre et al., 2019; Liu et al., 2023).

As protocols and techniques continue to evolve, the complexity of data analysis is also increasing. Computational methods, such as principal component analysis (PCA) (Pearson, 1901) and uniform manifold approximation and projection (UMAP), are essential for interpreting this complex data (Becht et al., 2019). Traditionally, cell types have been annotated through manual gating, a process that is not only time-consuming but also prone to issues with reproducibility and batch effects. However, the advent of advanced cytometers, like spectral flow and mass cytometers, has produced increasingly rich and high-dimensional datasets, making manual gating even more impractical.

To address the challenges posed by high-dimensional analyses, new tools are being developed. One such tool is Scyan, a deep generative model designed to map protein expressions into a biologically meaningful latent space (Blampey et al., 2023). Scyan offers batch-effect correction, debarcoding, and population discovery capabilities, making it a valuable asset in modern cytometric analysis.

1.6.2 Single-cell

Toward the end of the 20th century, the development of technologies like flow cytometry, which allowed for measuring multiple proteins on individual cells, revolutionized immunology. These advancements enabled researchers to categorize immune cells into distinct phenotypic groups and lineages based on specific cell-surface antigens. Shortly after, the advent of next-generation genomic technologies further transformed the field. By 2003, the first complete

human genome was sequenced (Collins et al., 2003), marking the beginning of a new genomic era in immunology.

This era allowed scientists to combine marker-based sorting of specific cell populations with deep molecular analyses, including RNA, epigenetic, and DNA sequencing (Chaussabel et al., 2008; Heng et al., 2008; Wilson et al., 2009). These advancements have been instrumental in making significant discoveries and developing new treatments, such as cancer and autoimmune diseases (Smillie et al., 2019).

The first single-cell RNA sequencing (scRNA-seq) study, published in 2009, marked a significant milestone in cell biology by profiling an individual mouse blastomere from a four-cell stage embryo (Tang et al., 2009). The application of scRNA-seq to immune cells began in 2013 and early 2014, with researchers profiling in vitro bone marrow-derived dendritic cells (BMDC) (Shalek et al., 2013) and creating the first unbiased scRNA-seq map of immune cells from tissue (Jaitin et al., 2014). This study, facilitated by the development of MARS-seq, produced a combined transcriptional and protein surface marker atlas of over 4,000 splenic immune cells from a mouse. By integrating transcriptional signatures with canonical protein surface markers, distinct murine dendritic cell and monocyte subtypes were identified, prompting further research into these heterogeneous cell types.

Since then, the number of scRNA-seq studies in immunology has increased dramatically, as researchers used this technology to explore classical immunological models and questions, such as hematopoiesis. These studies have led to revisions in our understanding of immune cell generation and development (Paul et al., 2015) and have deepened our knowledge of complex processes (Pellin et al., 2019) and revise classifications (Ginhoux et al., 2022).

In 2016, scRNA-seq was applied to analyze the ecosystem of tumour, immune, and stromal cells from 19 patients with metastatic melanoma, revealing patient-specific heterogeneity and T-cell exhaustion signatures based on profiles from 4,600 cells (Tirosh et al., 2016). Subsequent studies advanced our understanding of the diverse immune subsets within the tumour environment and the mechanisms of immune regulation in cancer (Azizi et al., 2018; Cassetta et al., 2019;

Chen et al., 2024). Additionally, combining scRNA-seq with clinical metadata has enabled the identification of molecular features associated with the success or failure of immunotherapy (Cohen et al., 2021; Sade-Feldman et al., 2018). Following that, a multi-tissue analysis of more than 200 patients unifying modalities of cell types in one large analysis (Cheng et al., 2021).

An important advancement in single-cell analysis is the integration of mRNA and protein markers at the single-cell level. This integration has been made possible through techniques like index sorting (Dutertre et al., 2019; Paul et al., 2015) which relies on fluorophores, and the use of oligonucleotide-labeled antibodies, which are more commercially available. These methods allow the simultaneous measurement of dozens of protein markers on individual cells. Two technologies were introduced in the same year that pushed the boundaries of this approach. Cellular Indexing of Transcriptomics and Epitopes by Sequencing (CITE-seq) (Stoeckius et al., 2017) and RNA Expression and Protein Sequencing (REAP-seq) (Peterson et al., 2017) were developed to quantify over a hundred different surface proteins on single cells while also generating their transcriptional profiles.

Despite the challenges posed by high signal-to-noise ratios in surface protein measurements, these issues can be mitigated through analytical and experimental approaches (Buus et al., 2021). Recent advancements have extended these technologies to include intracellular protein detection (Katzenelenbogen et al., 2020) and the empirical measurement of differentiation trajectories (Kirschenbaum et al., 2024), offering more profound insights into cellular processes at the single-cell level.

1.6.3 Spatial-omics

One of the challenges with some of the techniques mentioned earlier is the potential loss of tissue context. The spatial context within tissues, particularly in subtissular niches, is crucial for understanding the intricate dynamics of cellular biology. For example, the tumour microenvironment is a highly complex ecosystem within the body, where its intricate organisation significantly influences cancer progression (Bressan et al., 2023). Recognising the spatial arrangement of these cells has become increasingly important in cancer research. Hematoxylin and eosin (H&E) staining has traditionally been the go-to method for analysing tissue architecture or a low plex staining of immunofluorescence. However, recent technological advancements have allowed for much deeper exploration.

These advancements fall under the umbrella of spatial-omics. Cutting-edge imaging technologies now enable the measurement of over 1,000 genes through Spatial Transcriptomics and analysis of more than 50 proteins via Multiplex Imaging (Vandereyken et al., 2023). Techniques like MerFISH (Chen et al., 2015), ISH (Jin and Lloyd, 1997), ISS (He et al., 2022), MICS (Kinkhabwala et al., 2022), PhenoCycler (Jhaveri et al., 2023), and IMC (Chang et al., 2017) offer single-cell resolution that surpasses the capabilities of earlier spot-based methods like 10X Visium or Nanostring GeoMX (Merritt et al., 2020). Notably, a recent update to 10X Visium has increased its spot density to achieve near single-cell resolution.

One of the current challenges in the field is effectively analyzing and interpreting the complex data generated by these advanced techniques. While significant efforts are being made to improve data analysis methods (Marconato et al., 2024), there is still much progress to be made. The potential for deeper insights is substantial, but unlocking this potential requires continued advancements in computational tools and methodologies. Despite the complexity of the data generated by these techniques, new discoveries are emerging rapidly. The next section will delve deeper into some of the significant observations and insights gained through spatial-omics.

1.7 SPATIAL DISTRIBUTION OF MONONUCLEAR PHAGOCYTES IN THE TUMOUR MICROENVIRONMENT

The role and location of mononuclear phagocytes in the tumour microenvironment have long been recognised, but the full complexity of their interactions is still being unravelled. As technological advancements continue, we are beginning to understand that these interactions are not singular but part of a broader ecosystem that drives shifts in the tumour environment.

Recent spatial omics studies in lung tumours have identified $CXCL10^+$ macrophages and $CCR7^+LAMP3^+$ dendritic cells within a "stem-immunity hub," where they interact with $CCL19^+$ fibroblasts and $TCF7^+PD\text{-}1^+CD8^+$ T cells, contributing to a favourable outcome for lung cancer patients (Chen et al., 2024). In human breast and colon cancers, distinct macrophage populations have been observed: IL4I1+ SPP1+ macrophages localise within necrotic tumour areas, while FOLR2 macrophages are found in peri-tumoral regions, often near FAP fibroblasts or within a lymphoid niche surrounded by CD4 and CD8 T cells. Additionally, LYVE1 macrophages are associated with the perivascular niche (Matusiak et al., 2024).

While in breast and colon cancers, the *IL4I1*$^+$ *SPP1*$^+$ macrophages localise within necrotic tumour areas. In pancreatic ductal adenocarcinoma (PDAC), a subset of tumour-associated macrophages (TAMs) expressing interleukin-1β (IL-1β) has been found within hypoxic areas, forming an inflammatory loop with tumour cells (Caronni et al., 2023). This interaction is driven by a local synergy between prostaglandin E2 (PGE2) and tumour necrosis factor (TNF).

The tumour microenvironment can also exhibit fetal-like reprogramming, highlighting these cells' remarkable plasticity and heterogeneity (Sharma et al., 2022). In hepatocellular carcinoma (HCC), *POSTN*$^+$ extracellular matrix cancer-associated fibroblasts (EM CAFs) play a key role as an oncofetal interacting hub, driving tumour progression. Spatial transcriptomics and cell-cell communication analyses have shown interactions and co-localization among oncofetal cells, including *POSTN*$^+$ CAFs, *FOLR2*$^+$ macrophages, and *PLVAP*$^+$ endothelial cells (Li et al., 2024).

In patients with HCC treated with PD-1 inhibitors, a positive response to immune checkpoint blockade (ICB) was associated with the clonal expansion of intratumoral *CXCL13*$^{+}$*CH25H*$^{+}$*IL-21*$^{+}$*PD-1*$^{+}$*CD4*$^{+}$ T helper cells ("*CXCL13*$^{+}$ TH") and Granzyme K^{+} PD-1^{+} effector-like CD8^{+} T cells (Magen et al., 2023). In contrast, non-responders exhibited a dominance of terminally exhausted *CD39*^{hi}*TOX*^{hi}*PD-1*^{hi}*CD8*$^{+}$ T cells. These Progenitor CD8^{+} T cells were found to interact with CXCL13^{+} TH cells within cellular triads around dendritic cells enriched in maturation and regulatory molecules, also termed "mregDC." This suggests that specific intratumoral niches, including mregDC and *CXCL13*$^{+}$ TH cells, play a potential role in differentiating tumour-specific exhausted CD8^{+} T cells following ICB treatment.

These observations underscore how the specific microenvironment, or subtissular niche, dictates or requires certain functions which are essential for maintenance processes.

1.8 OBJECTIVES

The mononuclear phagocyte system, particularly within the tumour microenvironment, is characterized by significant heterogeneity and diversity. This complexity presents challenges in unifying and accurately defining these diverse cell populations, especially in the context of rapidly advancing technologies.

My PhD focuses on addressing these challenges by gaining a deeper understanding of the heterogeneity among monocytes, macrophages, and dendritic cells, aiming to align nomenclature with current literature. By uncovering the intricacies of these cell populations, my research aims to contribute to a more standardized framework for their classification. While also uncovering new insight into their role within the tumour microenvironment.

Additionally, as technological advancements continue to evolve, another key objective of my research is to develop more effective approaches and pipelines for analyzing spatial data. With the proliferation of new techniques, establishing a unifying methodology will be essential for researchers to extract meaningful insights from their data, ultimately advancing our understanding of the tumour microenvironment and its impact on cancer progression.

2 RESULTS

2.1 CROSS-TISSUE SINGLE CELL LANDSCAPE OF HUMAN MONOCYTES AND MACROPHAGES IN HEALTH AND DISEASE

Kevin Mulder[1,2,**], Amit Ashok Patel[1,2,**], Wan Ting Kong[3,**], Cécile Piot[3,4,], Evelyn Halitzki[3,5], Garett Dunsmore[1,2], Shabnam Khalilnezhad[3], Sergio Erdal Irac[3], Agathe Dubuisson[1,2], Marion Chevrier[3], Xiao Meng Zhang[3], John Kit Chung Tam[6], Tony Kiat Hon Lim[7], Regina Men Men Wong[8], Rhea Pai[8], Ahmed Ibrahim Samir Khalil[9], Pierce Kah Hoe Chow[10], Suny Z. Wu[11,12], Ghamdan Al-Eryani[11,12], Daniel Roden[11,12], Alexander Swarbrick[11,12], Jerry Kok Yen Chan[13,14,15,16], Salvatore Albani[17], Lisa Derosa[1,18], Laurence Zitvogel[1,2,18,19,20],Ankur Sharma[8,21,22], Jinmiao Chen[3], Aymeric Silvin[1,2], Antonio Bertoletti[16], Camille Blériot[1,2], Charles-Antoine Dutertre[1,2,3,17,*,***] and Florent Ginhoux[3,17,23,*,***]

[1]Gustave Roussy Cancer Campus, Villejuif, France.
[2]Institut National de la Santé Et de la Recherche Médicale (INSERM) U1015, Equipe Labellisée—Ligue Nationale contre le Cancer, Villejuif, France.
[3]Singapore Immunology Network (SIgN), A*STAR, 8A Biomedical Grove, Immunos Building, Singapore 138648, Singapore
[4]Present address: Immunobiology Laboratory, The Francis Crick Institute, 1 Midland Road, London NW1 1AT, UK
[5]Life and Medical Sciences Institute, University of Bonn, Bonn, Germany
[6]Department of Surgery, Yong Loo Lin School of Medicine, National University of Singapore, 1E Kent Ridge Road, Singapore 119228, Singapore
[7]Department of Pathology, Singapore General Hospital, 20 College Road, Singapore 169856, Singapore.
[8]Genome Institute of Singapore, A*STAR, 60 Biopolis Street, Genome, #02-01, Singapore 138672, Singapore
[9]Nanyang Technological University, 50 Nanyang Ave, 639798, Singapore
[10]Division of Surgical Oncology, National Cancer Centre, Singapore 169610, Singapore
[11]The Kinghorn Cancer Centre and Cancer Research Division, Garvan Institute of Medical Research, Darlinghurst, NSW 2010, Australia
[12]St Vincent's Clinical School, Faculty of Medicine, UNSW Sydney, NSW 2052, Australia
[13]Department of Reproductive Medicine, KK Women's and Children's Hospital, 229899, Singapore
[14]Academic Clinical Program in Obstetrics and Gynaecology, Duke-NUS Medical School, Singapore 169857
[15]Experimental Fetal Medicine Group, Department of Obstetrics and Gynaecology, Yong Loo Lin School of Medicine, National University of Singapore, 1E Kent Ridge Road, Singapore 119228
[16]Program in Emerging Infectious Disease, Duke-NUS Medical School, 8 College Road, Singapore 169857, Singapore
[17]Translational Immunology Institute, SingHealth/Duke-NUS Academic Medical Centre, the Academia, 20 college road, Discovery tower level 8, Singapore 169856, Singapore
[18]Cancer Medicine Department, Gustave Roussy, Villejuif, France.
[19]Université Paris-Saclay, Ile-de-France, France.
[20]Center of Clinical Investigations in Biotherapies of Cancer (BIOTHERIS) 1428, Villejuif, France.
[21]Harry Perkins Institute of Medical Research, QEII Medical Centre and Centre for Medical Research, the University of Western Australia, PO Box 7214, 6 Verdun Street, Nedlands, Perth, WA 6009, Australia
[22]School of Pharmacy and Biomedical Sciences, Curtin Health Innovation Institute, Curtin University, Perth, WA 6102, Australia
[23]Shanghai Institute of Immunology, Shanghai Jiao Tong University School of Medicine, Shanghai 200025, China
* Correspondence: charles-antoine.dutertre@inserm.fr, Florent_Ginhoux@immunol.a-star.edu.sg
** Equal contribution
*** Equal contribution

SUMMARY

Mononuclear phagocytes (MNP) encompass dendritic cells, monocytes and macrophages (MoMac), which exhibit antimicrobial, homeostatic and immunoregulatory functions. MNP characterised across tissues and diseases using various nomenclature has overwhelmed the field. Here, we integrated 178,651 MNP from 13 tissues across 41 datasets to generate a MNP single-cell RNA compendium (MNP-VERSE), a publicly available tool to map MNPs (https://gustaveroussy.github.io/FG-Lab/), and defined universal gene signatures of MNP populations. Next, we generated a compendium (MoMac-VERSE) that revealed an array of specialised cell subsets widely distributed across multiple tissues and the expansion of specific pathological forms in cancer and inflammation. All neoplastic tissues contained conserved tumour-associated macrophage populations. Among them, we focused on IL4I1^{+}CD274(PD-L1)$^{+}$IDO1^{+} macrophages which display immune-suppressive macrophages through tryptophan degradation and promotion of regulatory T cell entry into tumours. This integrated analysis provides a robust online-available platform for the uniform annotation, ontological mapping and dissection of specific macrophage functions in healthy and pathological states.

Keywords: Macrophages, Monocytes, Heterogeneity, Single-cell, scRNAseq, Inflammatory diseases, Cancer, MNP-VERSE, MoMac-VERSE, IDO1, PD-L1, IL4I1, TREM2

Link to the online web site for MNP- and MoMac- VERSES exploration:

https://gustaveroussy.github.io/FG-Lab/

INTRODUCTION

The mononuclear phagocyte system (MPS) was introduced almost 50 years ago and proposed a new classification of macrophages, monocytes and their precursor cells (van Furth et al., 1972). These cells were included in the MPS based on similarities in morphology, function, origin and kinetics. Following this, the identification of stellate-like cells, now known as dendritic cells (DC) by Steinman & Cohn (Steinman and Cohn, 1973), led to a further addition to the MPS family. A considerable amount of work has since been done to characterize the cells of the MPS, providing an overview of their varied functions in development, homeostasis and inflammation, and their relationships to one another (Guilliams et al., 2014). Dichotomies have thus emerged with classical versus non-classical monocytes, plasmacytoid versus classical DC (this latter being subsequently divided into cDC1 versus cDC2) and pro-inflammatory M1 versus anti-inflammatory M2 macrophages (Geissmann et al., 2003; Merad et al., 2013; C. D. Mills et al., 2000; Passlick et al., 1989; Ziegler-Heitbrock et al., 2010a). These classifications have led to substantial conceptual advances and remain widely used. However, the application of high-dimensional approaches such as mass cytometry and single-cell RNA sequencing has revealed finer levels of heterogeneity, leading to the identification of subpopulations in both healthy and diseased states and across various tissues (Passlick et al., 1989; See et al., 2017; Villani et al., 2017; Ziegler-Heitbrock et al., 2010a).

In particular, single-cell transcriptomics have revolutionised our understanding of immune cell heterogeneity by providing snapshots of individual cell activity with increasing scale and resolution(Giladi and Amit, 2018; Stubbington et al., 2017). These technologies have been exploited to generate accessible atlases of the mouse (The Tabula Muris Consortium et al., 2018; Van Hove et al., 2019) and human (Regev et al., 2017; Rozenblatt-Rosen et al., 2017; Svensson et al., 2019) immune cells, in addition to organ-specific databases (Peters et al., 2020). Nevertheless, comparison between these different studies and extraction of granular detail is difficult owing to the distinct sequencing protocols and analytical pipelines employed. A unified analytical approach has the potential to reveal synergy between

published data sets and to avoid duplication of effort and irregularities of nomenclature.

This need for transcriptomic data unification is particularly clear for studies of MNP, especially in disease settings. MNP are critical for immune defence and homeostasis: patients who are deficient in these cell populations are highly susceptible to recurrent infections (Bigley et al., 2019); while in cancer, tumour-associated macrophages (TAM) are implicated in promoting tumour progression, angiogenesis and metastasis (Pollard, 2004), and DC are thought to prime anti-tumour T-cells (Wculek et al., 2019). Accordingly, many studies aim to elucidate the functions of MNP in various pathologies, generating a high volume of overlapping data. Multiple studies examining the same or different tissues have defined similar MNP subpopulations but designated various names for them, as seen in the past for the case of DC (Guilliams et al., 2014). In order to achieve clarity and to extract fundamental commonalities of potential therapeutic importance, there is a need to unify the multiple identities assigned to MNPs across healthy and pathological tissues.

Here we generated an integrated meta-analysis of multiple high-dimensional transcriptomic studies on MNP in an attempt to elucidate system-wide characteristics of the MPS in health and disease. To achieve this, we selected and integrated single-cell RNAseq datasets from 41 studies to build a comprehensive view of human MNP in health and disease states (the MNP-VERSE). All major previously defined MNP subsets we delineated, including classical and $CD16^{+}$ monocytes, conventional dendritic cells (cDC) subsets [cDC1, cDC2 (DC2+DC3)], as well as their progenitors (pre-DC) and terminally differentiated mature DCs enriched in immunoregulatory molecules (mregDC) (Dutertre et al., 2019; Maier et al., 2009; See et al., 2017; Ziegler-Heitbrock et al., 2010a). This organisation was validated using complementary analytical pipelines. To demonstrate the utility of this approach, we then focused on monocytes and macrophages and generated a "MoMac-VERSE". Using the recently developed Azimuth algorithm (Hao et al., 2020), we demonstrated that these VERSES can be used to do a *de novo* mapping of datasets that were not initially integrated, a process that can provide a robust annotation tool of MNP subsets for any other human scRNAseq dataset. The MoMac-VERSE

revealed subsets of TAM that were enriched in all cancers studied. Of particular interest was a population of macrophages expressing IL4I1 and IDO1; these cells appear to be programmed through interactions with $CD40L^+$ $CD4^+$ T cells and activated $IFN\gamma^+$ $CD8^+$ T cells. Additionally, $IL4I1^+$ macrophages could contribute to tryptophan degradation through the IL4I1-induced activation of aryl hydrocarbon receptor (AHR), leading to an accumulation of regulatory T cells (Treg), thereby establishing an immunosuppressive environment in tumours. This work provides a resource to explore MNPs and, more specifically, monocyte and macrophages across human healthy and diseased tissues and can be explored through an online platform (https://gustaveroussy.github.io/FG-Lab/).

RESULTS

The human MNP-VERSE defines universal gene signatures of major MNP subsets

To establish a universal atlas of human MNP across healthy and pathologic tissues, we selected 41 single-cell RNA sequencing (scRNAseq) datasets from studies that included MNP from healthy and pathological tissues (**Figure 1A** and **Table S1**). Datasets were initially integrated tissue-by-tissue using the Seurat V3 pipeline (Stuart et al., 2019) to generate sub-atlases where MNP were identified by the expression of canonical markers, including *S100A8* and *S100A9* for monocytes (Mo); *C1QA*, *C1QB* and *CD68* for macrophages (Mac); *CADM1*, *CLEC9A* and *XCR1* for classical DC1 (cDC1); *FCER1A*, *CD1C* and *CD1E* for cDC2, and the recently described mature DCs enriched in immunoregulatory molecules (mregDC) genes from Maier *et al.* (Maier et al., 2020) (**Figure 1A** and **Figure S1A**). Of note, we excluded plasmacytoid DC (pDC) from the MNP-VERSE as we and others have recently demonstrated the lymphoid origin of these cells (Dress et al., 2019; Rodrigues et al., 2018).

A total of 178,651 MNP were extracted from 13 tissues and integrated into a common universe - the MNP-VERSE (**Figure 1B**) - that was mapped in a Uniform Manifold Approximation and Projection (UMAP) space (Becht et al., 2018) (**Figure S1B**). Importantly, we included in-house indexed-SMARTseq2 scRNAseq data of 1,830 cells from 5 different tissues (spleen, lung, liver, skin and tonsil), which allowed us to broadly identify the major MNP populations based on surface protein expression, namely $CD88^{+}CD16^{+/-}CD14^{+}CD11b^{+}CD206^{+/-}$ Mo/Mac, $CD123^{+}CD5^{+}CD169^{+}$ pre-DC, $CD141^{+}$ classical cDC1 and $CD1c^{+}$ cDC2; encompassing both cDC2 and DC3 as recently reported (Bourdely et al., 2020; Dutertre et al., 2019) (**Figure 1C** and **Figure S1C**, **Table S2**). The populations were validated by independently analysing our in-house indexed-SMARTseq2 data that included 5 different tissues (tonsil, spleen, blood, lung and liver). We identified the major DC and monocyte/macrophage populations based on differentially expressed genes (DEGs) and indexed-data protein expression (**Figure S2A-B**) and back-mapped these populations onto the MNP-VERSE.

The annotation aligned with the MNP-VERSE annotations (**Figure S2C**), validating the approach of integrating SMARTseq2 datasets with 10X and other droplet-based scRNAseq datasets.

In order to analyse gene expression from all cells of the 41 integrated datasets, we generated a transformed matrix (transf.matrix) that included all the cells of the MNP-VERSE for which the gene expression values were transformed, as obtained with the Seurat V3 pipeline (**Figure 1D**). Of the 41 datasets, 6 datasets included relatively less genes and were consequently excluded from the transf.matrix (**Figure S1F**). To confirm the annotation of the major MNP populations at the gene expression level, we used the Phenograph algorithm (Levine et al., 2015) and calculated the differentially-expressed "transformed" genes (DEtGs) for all Phenograph clusters using the transf.matrix (**Figure 1E-F**, **Table S3**). This analysis allowed us to identify 6 major MNP subsets defined by uniquely-expressed DEtGs (UEtGs): cDC1, cDC2 (cDC2 & DC3), mregDC, classical monocytes (cMo), non-classical/intermediate monocytes ($CD16^+$ Mo) and macrophages; confirming the annotation obtained with our indexed-data **(Figure 1G-H**, **Figure S1D** and **Table S4**). In addition, a strong correlation between transf.matrix and original counts was observed in selected genes, validating the integrated approach (**Figure S1E**). Thus, these universal signatures allowed us to precisely define all the major MNP subsets from scRNAseq data across human tissues. Together, these compiled data define the "MNP-VERSE" and provide a platform to assemble findings from existing literature. In line with other reports, the MNP-VERSE showed that cDC1 and mregDC were separated from the main body of MNP and formed discrete populations, while monocytes and cDC2 were clustering more closely as well as the monocytes and macrophages. These results support and validate our pipeline, allowing further downstream analysis of monocyte and macrophage populations across healthy and diseased tissues.

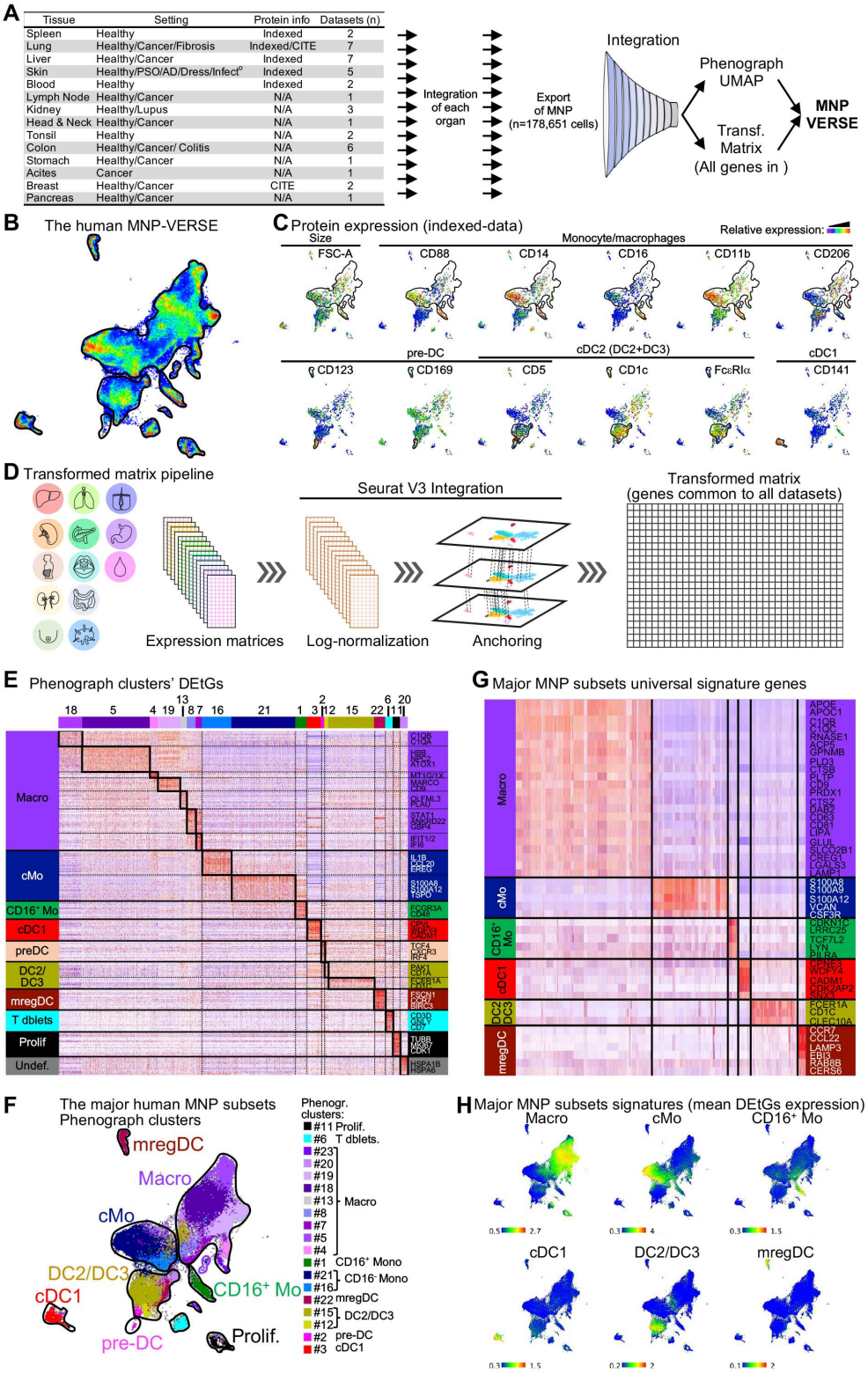

Figure 1: The MNP-VERSE reveals universal signatures of major

MNP subsets across human tissues. *(**A**) Summary of the data that was integrated and scheme of the meta-analysis. An integration was first performed at the organ level and MNPs were extracted. Organ-restricted MNPs were then integrated generating (**B**) the human MNP-VERSE. (**C**) Meaning plots of protein expression data from in-house indexed-SMARTseq2 scRNAseq data overlayed onto the MNP-VERSE. (**D**) Pipeline of the transformed matrix generation. (**E**) Heatmap of differentially expressed "transformed" genes (DEtGs, Log FC>0.25) in Phenograph clusters. Selected genes are highlighted. (**F**) Visualisation of Phenograph clusters on the MNP-VERSE UMAP space. (**G**) Heat map showing relative expression levels of MNP universal signature genes across human tissues and visualisation of (**H**) their mean expression overlayed onto the MNP-VERSE UMAP space.*

The human MoMac-VERSE establishes conserved monocyte and macrophage states and identifies patterns of tissue-specific imprinting in health and disease

Having established a broad overview of the integrated MNP data, we extracted data from macrophages and monocytes (from both healthy and pathologic tissues) and re-integrated them to establish the MoMac-VERSE (**Figure 2A**). As before, we mapped cells into a UMAP space and calculated DEtGs between the different Phenograph clusters using the transf.matrix (**Figure 2A**, **Figure S3A** and **Table S5**). We identified two distinct cell populations comprised of monocytes ($CD16^+$ Mo, clusters #1 and #5, and $CD16^-$ Mo, *$ISG15^+ISG20^+IFIT1^+IFIT2^+IFIT3^+$* "*ISG*" #4, #8, #12 and "IL1B" #15) and macrophages ("HES1" #2, "TREM2" #3, "IL4I1" #6, #7, #13, #16 and "FTL" #17), respectively. Mac #16 strongly expressed *C1QA/B/C* and MHCII transcripts and comprised lung alveolar macrophages (Alv. Mac; **Figure S3B-C**). Interestingly, Mo #4 (ISG_Mo) and IL4I1_Mac (#6) shared a similar gene expression signature (**Figure S3A** and **Table S5**), suggestive of a close relationship that we will explore later. Of note, DEtGs associated with TREM2_Mac (#3) shared similarities with signatures recently described in murine TREM2 macrophages (**Figure S3D**) (Katzenelenbogen et al., 2020; Yingyue Zhou et al., 2020), suggesting a potential for the MoMac-VERSE to generate cross-species comparisons. We were also able to identify the presence of

non-MoMac cells: cluster #14 corresponded to contaminating DC2, and cluster #9 represented MNP/T cell doublets. A third outlying population (#10) was identified as proliferating cells. As above for the MNP-VERSE, we confirmed the relationship between transf.matrix of the MoMac-VERSE and the TPM of the original datasets. 6 datasets (Kim et al., 2020; Lee et al., 2020; Sharma et al., 2020; Smillie et al., 2019; L. Zhang et al., 2020; Zheng et al., 2017) were chosen which adequately represented the UMAP space of the MoMac-VERSE. DEGs were selected across phenograph clusters from the 6 datasets using their original TPM. The DEGs identified in the 6 original datasets closely resembled to the DEtGs found between phenograph cluster within the transf.matrix [**Figure S3E** and **Table S6**].

Having generated a unified overview of monocytes and macrophages across tissues at the gene expression level, we next used the combined dataset to establish common and specific features of key subpopulations at the transcription factors' gene regulatory network level. Using SCENIC analysis (Aibar et al., 2017), we identified on three datasets the differentially-expressed regulons (DER; which are sets of transcription factors and genes predicted to be regulated by them) common to cells from the colon (L. Zhang et al., 2020), liver (Sharma et al., 2020) and lung (Kim et al., 2020) (**Figure 2B** and **Table S7**). As observed in the DEtGs analysis (**Figure 2A**, **Figure S3A** and **Table S5**), ISG_Mo (#4) and IL4I1_Mac (#6) shared a similar DER profile, while TREM2_Mac (#3) shared DER with macrophage clusters #6 and HES1_Mac (#2). The regulon analysis could also be used to refine subpopulation functions, as exemplified by the *NFKB1* and *NFKB2* DER of IL1B_Mo #15, which confirms their classification as inflammatory monocytes.

To address the commonly used M1/M2 classification of macrophages, we defined the number of M1- or M2- associated genes as published by Martinez *et al.* (Martinez et al., 2006) that were common to the DEtGs of each MoMac-VERSE cluster (**Figure 2C-D** and **Figure S3F**). ISG_Mo (#4), IL4I1_Mac (#6) and inflam _Mono (#15) were enriched in M1 genes, while the other macrophage subsets such as HES1_Mac (#2), Cluster_#17, $C1Q^{hi}$_mac (#16) and Trem2_Mac (#3) expressed mostly M2 genes. Other clusters, that included the other monocyte subsets as well as cDC2 (#14) had no more than 2 of their DEtGs being

classified as M1 or M2 (**Figure 2C-D**). Of note, although the IL4I1_Mac (#6) exhibited a strong M1 program, these cells did not appear to express genes such as *IL12B* (**Figure S3G),** which has been described as a prototypic M1 cytokine of *in vitro* monocyte-derived macrophages. Although, the M1/M2 macrophage classification can be useful in profiling human *in vivo* primary macrophages, discrepancies arise in comparison with the historical *in vitro* derived signatures.

We next evaluated their reprogramming in pathologic settings. The MoMac-VERSE incorporated cells from healthy tissues as well as different pathological disease states, containing matched cells from healthy individuals, cancer and various inflammatory disease patients, allowing for their comparison (**Figure S3H**).

Globally, we found that the proportion of monocyte-related cells increased in cancer and inflammatory diseases as compared to healthy tissues (**Figure S3I**). Using the transf.matrix, we generated DEtGs comparing total macrophages and total monocytes obtained from matched healthy tissues and six different cancers (lung, colon, liver, breast, stomach and pancreas) (**Figure 2E-F, Figure S3J** and **Table S8**). Pathway analysis revealed that macrophages in tumours specifically expressed genes involved in lipid metabolism and inflammation pathways, while monocytes expressed genes involved in pathways triggered by their stimulation by inflammatory cytokines (**Figure 2G**, **Table S9**). Monocytes and macrophages commonly expressed genes involved in shared pathways related to their maturation and their interaction with T cells.

We then conducted a similar analysis comparing inflamed tissues from colitis and lupus nephritis patients with matched healthy tissues (**Figure 2H-I**). Inflammatory disease monocytes expressed genes involved in pathways such as Th1 and Th2 activation and their stimulation by cytokines, whilst macrophage-specific pathways were related to oxidative phosphorylation, proliferation and cellular stress (**Figure 2J**). During inflammation, monocytes and macrophages also shared expression pathways involved in *IL-6* and TNF-mediated inflammation.

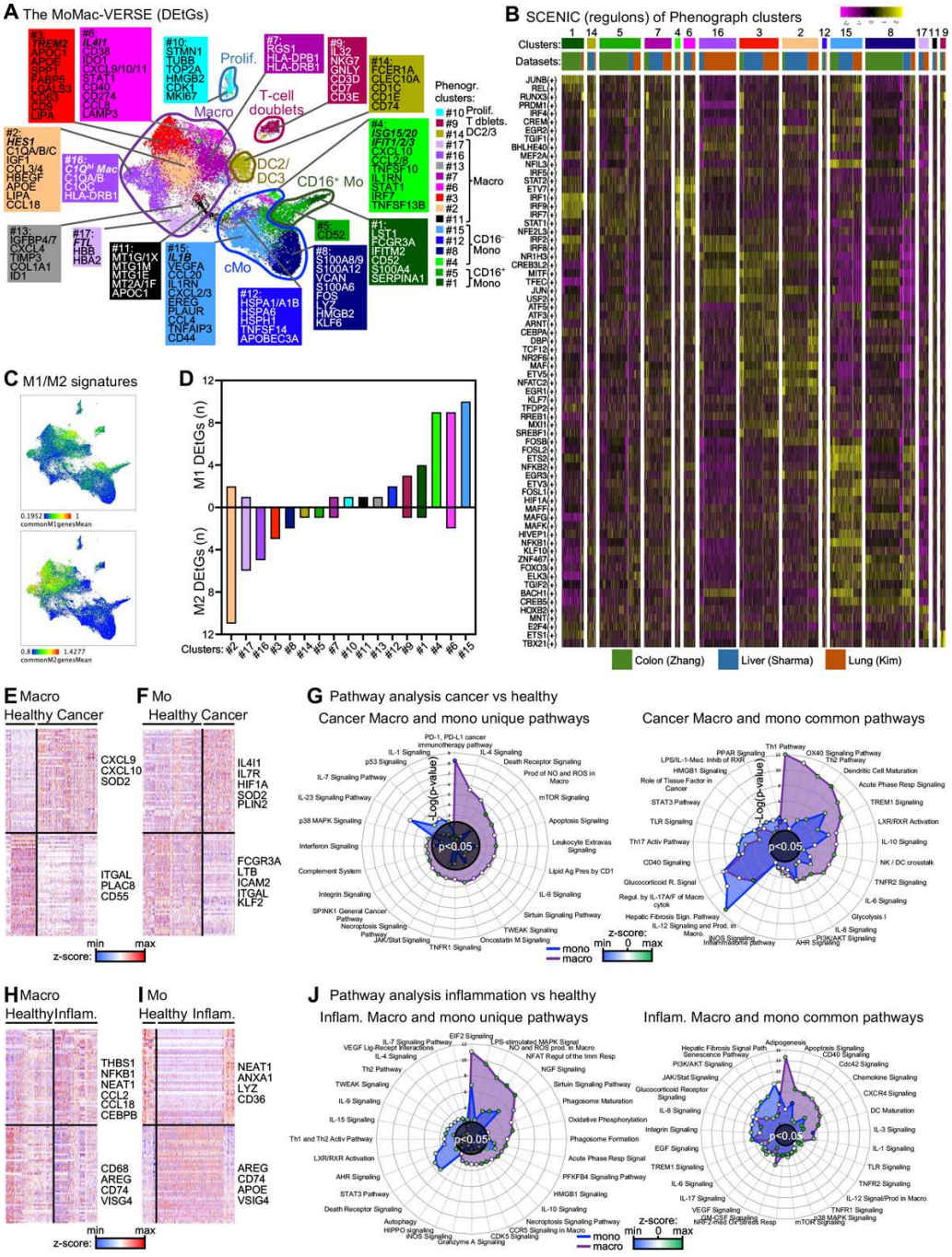

Figure 2. The MoMac-VERSE identifies conserved monocyte and macrophage states and global imprinting across human tissues. *Monocyte and macrophage clusters were extracted from the MNP-VERSE and reintegrated to generate a MoMac-VERSE. (**A**) Visualisation of MoMac-VERSE Phenograph clusters onto the MoMac-VERSE UMAP*

*space. Selected differentially expressed "transformed" genes DEtGs for each cluster are highlighted. (**B**) Heatmap showing relative expression levels of differentially expressed regulons (DER) in between Phenograph clusters common to colon (Zhang 10X), Liver (Sharma) and Lung (Kim) as revealed by a Scenic analysis. (**C**) Overlay of the expression of common M1 and M2 signature genes Martinez et al. (Martinez et al., 2006) in the MoMac-VERSE UMAP space. (**D**) Graphical representation of the number of M1 and M2 DEtGs expressed by each cluster. (**E-F**) Heatmap showing relative expression levels of DEtGs in the whole (**E**) macrophage or (**F**) monocyte populations comparing matched cancer and healthy tissues. (**G**) Radar plot showing pathways obtained from DEtGs in (**E-F**). (**H-I**) Heatmap showing relative expression levels of DEtGs in the whole (**H**) macrophage or (**I**) monocyte populations comparing matched inflamed and healthy tissues. (**J**) Radar plot showing pathways obtained from DEtGs in (**H-I**).*

MoMac-VERSE as a resource to study MNP across tissues and specific pathologies

The Azimuth algorithm developed by Rahul Satija's laboratory (Hao et al., 2020) proved to be robust when one of the pre-integrated datasets (Liver Sharma) was used as a "query" dataset to map onto the MoMac-VERSE as a reference atlas (**Figure 3A**), demonstrating high correlation of the initially integrated MoMac-VERSE and the *de novo* mapped UMAP coordinates (**Figure 3B**) and percentage phenograph clusters of Liver (Sharma) on the MoMac-VERSE (**Figure 3C**).

To further validate and extend the use of MoMac-VERSE as a resource, we employed Azimuth to map three new "query" datasets [Arthritic diseases synovial tissues, COVID-19 blood and Bronchoalveolar lavage (BAL)] on the MoMac-VERSE (Kuo et al., 2019; Liao et al., 2020; Silvin et al., 2020). This approach allowed unsupervised recapitulation of the major findings of these three studies in terms of macrophage heterogeneity by simply mapping their data onto the MoMac-VERSE. Of note, monocytes and macrophages were initially identified in these datasets using our defined signatures (**Figure 1G)**. This is necessary as cells that are neither macrophages nor monocytes will be forced to be mapped onto the MoMac-VERSE (data not shown) and can consequently be misinterpreted. *HBEGF*$^{+}$ (Kuo et al. cluster 1), MERTK^{+}

(Kuo et al. cluster 2), and IFN/STAT (Kuo et al. cluster 4) populations identified in the study of Kuo *et al.* in osteoarthritic and rheumatoid arthritis patients corresponded to HES1_Mac (#2), TREM2_Mac (#3) and IL4I1_Mac (#6) of the MoMac-VERSE, respectively (**Figure 3D-F**). In addition, we also identified cells that mapped to the FTL_Mac (#17) population, which were not pre-defined in Kuo et al., thus highlighting how further heterogeneity can be uncovered with the MoMac-VERSE.

Previous work by Silvin *et al*. has shown that monocyte populations in the blood of severe COVID-19 patients had decreased *HLA-DRB1* gene expression, and increased *NFKBIA* and *C5AR1* gene expression (Silvin et al., 2020). When this data was projected onto the MoMac-VERSE, the majority of cells fell within the $CD16^{+}$_Mono (#1, #5) and $CD16^{-}$_Mono (#8, #15) clusters of the MoMac-VERSE with expression of HLA-DRB1, NKFBIA and *C5AR1* following the observations of Silvin *et al*. (**Figure 3G-I**). We were also able to identify macrophages from the bronchoalveolar lavage (BAL) of COVID-19 patients in the MoMac-VERSE by mapping them with Azimuth. Cells from COVID-19 patients fell within the clusters of the TREM2_Mac (#3) ISG_Mono (#4) and IL4I1_Mac (#6). In mild COVID-19 samples, mapped macrophage fell within the TREM2_Mac (#3) cluster. In contrast, the BAL macrophages from severe COVID-19 patients mapped mostly to IL4I_Mac (#6), which were in association with stronger *CXCL10* and *ISG* gene expression. These results are in agreement with observations made by Zhang *et al.* and Liao *et al*. respectively and are reiterated within the MoMac-VERSE (Liao et al., 2020; F. Zhang et al., 2020). Note that the link between COVID-19 BAL ISG_Mo (#4) and IL4I1_Mac (#6) further strengthens the connection between these two cell subsets (**Figure 3J-M**). The results of mapping of COVID-19 patient BAL and blood with azimuth reveal the capacity of the MoMac-VERSE to recapitulate findings with increased specificity to well-conserved and identified macrophage/monocyte populations. Note also that blood monocytes mapped only to the MoMac-VERSE monocytes while BAL macrophages mapped to macrophages. Together, these results show that the MoMac-VERSE is capable of both recapitulating findings and adding increased depth to observations about cell phenotypes.

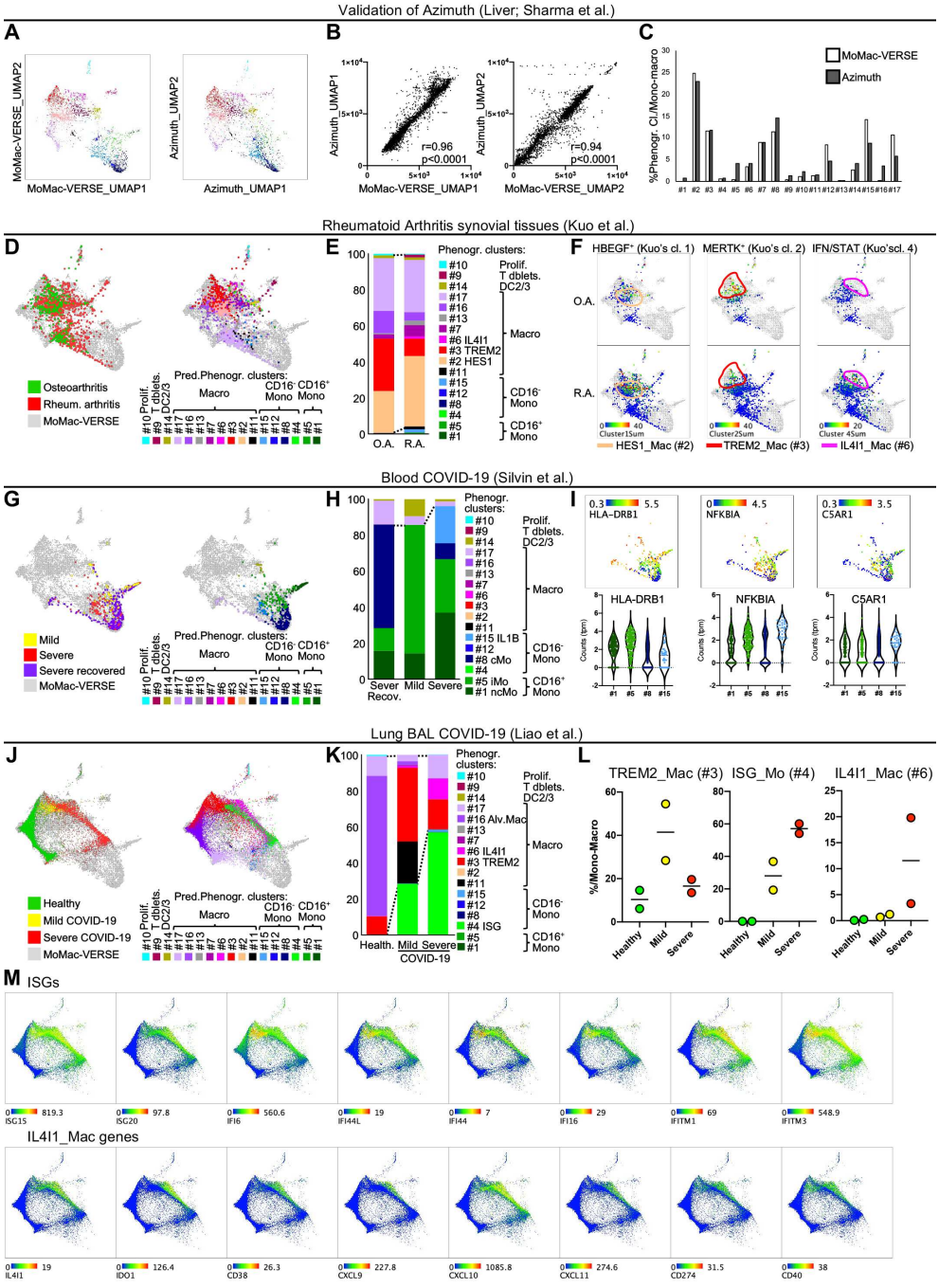

Figure 3. De novo mapping of rheumatoid arthritis synovial tissue and of COVID-19 lung macrophages on the MoMac-VERSE using Azimuth. *(**A**) Validation of the Azimuth "query dataset mapping" algorithm. Projection of (left panel) initially integrated and of (right panel) de novo "mapped query cells" (Liver, Sharma et al. dataset) onto*

*the MoMac-VERSE UMAP space using The Azimuth algorithm (Hao et al., 2020). (**B**) Correlation of the initially integrated MoMac-VERSE and the de novo mapped UMAP coordinates. The Pearson correlation co-efficient (r) was calculated alongside the p-value. (**C**) Percentage of phenograph clusters of Liver (Sharma) on the MoMac-VERSE. (**D-M**) Mapping of (**D-F**) Rheumatoid Arthritis (Kuo et al., 2019) and of COVID-19 patients' blood (Silvin et al., 2020) (**G-I**) and (**J-M**) bronchoalveolar lavage (BAL) (Liao et al., 2020) new datasets onto the MoMac-VERSE. (**D, G, J**) Mapping of cells from different patient groups and (**E, H, K**) their corresponding frequencies within the MoMac-VERSE Phenograph clusters are shown. (**F**) **Mapping of** HBEGF^{+}, MERTK^{+}, and IFN/STAT clusters identified in the study of Kuo et al. (Kuo et al., 2019) in osteoarthritic and rheumatoid arthritic patients that correspond to HES1_Mac (#2), TREM2_Mac (#3) and IL4I1_Mac (#6) of the MoMac-VERSE, respectively. (**I**) Mapping of HLA-DRB1^{hi} cells (increased in mild COVID-19 patients) and of NFKBIA^{hi} and C5AR1^{hi} (increased in severe COVID-19 patients) identified in the study of Silvin et al. (Silvin et al., 2020). (**L**) Frequency of the TREM2_Mac (#3), ISG_Mono (#4) and IL4I1_Mac (#6) in individual Healthy, Mild COVID-19 and Severe COVID-19 patients included in the COVID-19 BAL analysis. (**M**) Visualisation of the mean expression of cells for ISGs and IL4I1_Mac (#6) genes in the study of Liao et al. and overlaid on the MoMac-VERSE.*

The MoMac-VERSE identifies disease-specific monocyte and macrophage states

Next, we looked at cellular reprogramming events in individual pathologies (**Figure 4** and **Figure S4A-H**). Liver cirrhosis was associated with an accumulation of CD16^{+} monocytes (#1) when compared to healthy liver (**Figure 4A-B**). When deconvoluting data based on patients, including only healthy liver (excluding "normal adjacent" samples from cancer patients and including only patients for which at least 100 cells were sequenced), cells from cluster #1 also trended to increase. In the kidney of patients with lupus nephritis, cells with a monocyte-derived DC genotype (#7) and MNP/T cell doublets (#9) were increased (**Figure 4C-D**); while classical *S100A8/A9/A12*^{hi} monocytes accumulated in the inflamed colon of patients presenting with colitis (**Figure 4E-F**), this latter observation being also confirmed at the patient level (**Figure 4F**).

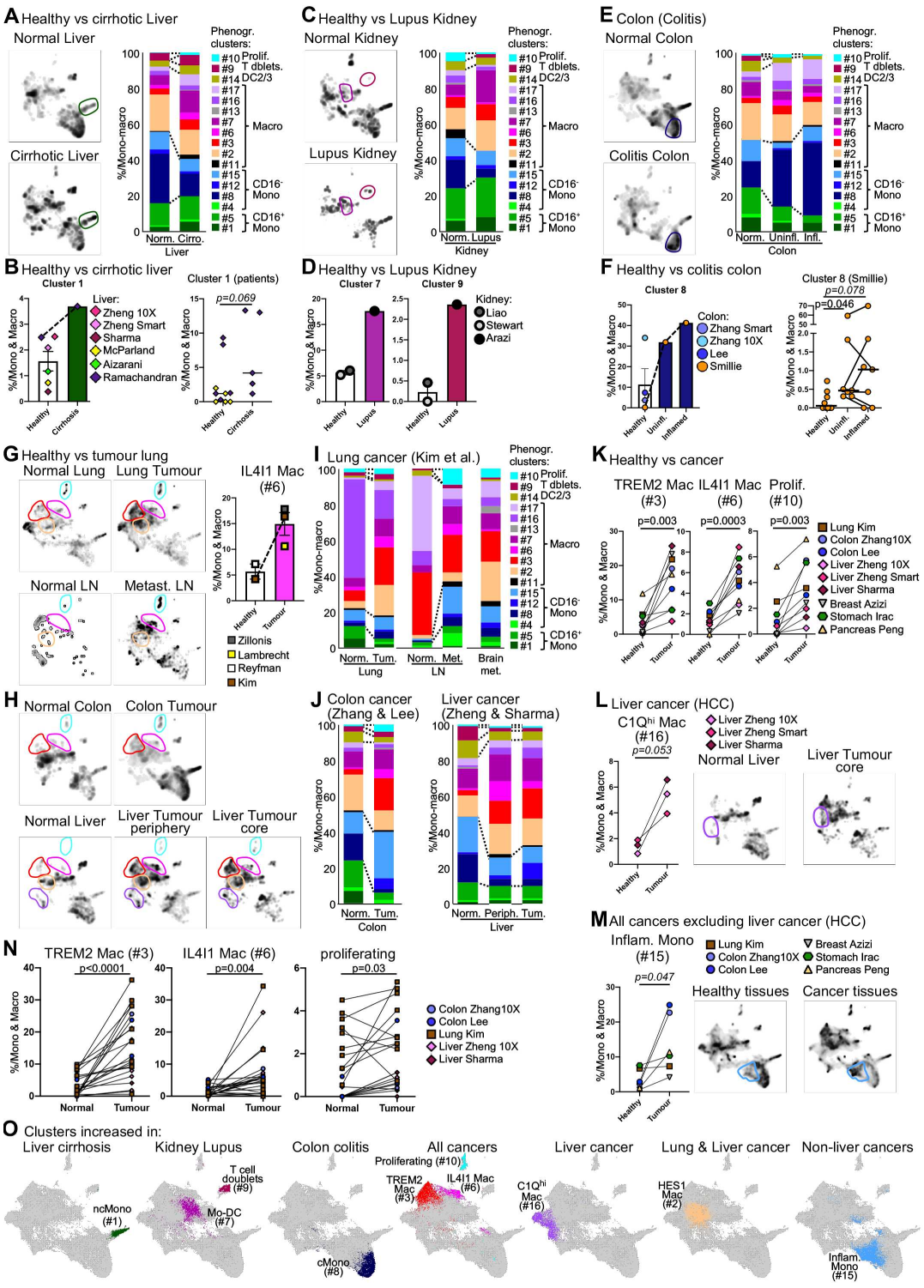

Figure 4. Definition of monocyte and macrophage states triggered in inflamed and cancerous tissue. *(**A-L**) Density plots and*

*quantification of the different clusters in different conditions: (**A-B**) cirrhosis, (**C-D**) lupus, (**E-F**) colitis and (**G-M**) cancer. For each condition, quantification of each cluster is provided across datasets and (**B,F**) for individual patients for which at least 100 cells per sample were sequenced. (**K-M**) Graphical representation of the relative proportion of clusters increased in (**K**) all cancer studies, (**L**) only in liver cancer or (**M**) in all cancers excluding liver cancer. (**N**) Quantification of TREM2_Mac (#3), IL4I1_Mac (#6) and proliferating cells (#10) in healthy tissues and corresponding tumours in each patient of liver, lung and colon datasets. Included patients had at least 35 cells in health or in tumour tissues. (**O**) Summary of clusters increased in the different diseased tissues. P values were calculated using a paired t-test.*

We also looked into individual cancers and observed an accumulation of HES1_Mac (#2), IL4I1_Mac (#6) and proliferating_Mac (#10) both in the tumour and metastatic lymph nodes (LN) of lung cancer patients, while TREM2_Mac (#3) also accumulated but only in the tumours (**Figure 4G-J**, **Figure S4I-J**). Colon and liver tumours also contained increased proportions of TREM2_Mac (#3), IL4I1_Mac (#6) and proliferating_Mac (#10). Alongside, liver tumours exhibited increased HES1_Mac (#2) and $C1Q^{hi}$_Mac (#16), as recently described (Sharma et al., 2020).

In summary, TREM2_Mac (#3), IL4I1_Mac (#6) and proliferating_Mac (#10) were accumulated in all tumours from the 6 cancer types included in this study (**Figure 4K**, **Figure S4K-L** and **Figure 4O**). Among these cancer types, liver tumours were unique in their accumulation of monocyte-like $C1Q^{hi}$_Mac (#16) and were the only tumours in which the inflammatory IL1B_Mo #15 were not accumulating (**Figure 4L-M**). In certain datasets where patient information was available, patients for which more than 35 cells were sequenced in both the normal adjacent and the tumour were selected for the analysis. At the patient level, TREM2_Mac (#3), IL4I1_Mac (#6) and proliferating_Mac (#10) were also significantly enriched in the tumour (**Figure 4N** and **Figure S4M-N**). Together, these results show that the MoMac-VERSE provides a platform to identify unique and conserved cell types and states across tissues and pathologies.

Identification of long-term resident and monocyte-derived-like macrophages across human tissues

A recent breakthrough in the field of monocyte and macrophage biology was the clarification of tissue-resident macrophage ontogeny (Blériot et al., 2020). Based on murine studies, it has been shown that in most healthy tissues, the majority of tissue-resident macrophages do not derive from adult circulating monocytes but directly from embryonic precursors seeded in tissues early during development and constitute a pool of "long-term resident" macrophages (Florent Ginhoux et al., 2010; Mass et al., 2016), while monocyte-derived macrophage accumulates notably during inflammation or carcinogenesis (R A Franklin et al., 2014; Zhu et al., 2017).

We next asked whether the MoMac-VERSE could be used to indicate the likely "long-term resident" versus recently differentiated adult monocytic source of distinct Mac populations from various tissues, based on similarities in gene expression profile. We overlayed cells expressing the mean universal $CD16^-$ monocyte signature derived from **Figure 1G** onto the MoMac-VERSE UMAP space (**Figure 5A** and **Figure S5A**). This revealed that monocyte-derived DC-like macrophages (#7), TREM2_Mac (#3) and IL4I1_Mac (#6) expressed monocyte signature genes, whereas HES1_Mac (#2) did not. We recently described that most murine tissues were populated by two phenotypically-distinct populations of interstitial macrophages that can be discriminated based on differential *LYVE1* expression (Chakarov et al., 2019). In mice, both these populations were initially derived from embryonic precursors and then replaced by monocytes at a tissue-specific pace. Here we also observed that differential LYVE1 expression separated the total human macrophage population, but interestingly, we noticed that *LYVE1*$^+$ cells strongly overlap with fetal liver macrophages included in the MoMac-VERSE (**Figure 5A**). This suggested either their common embryonic origin or that a full reprogramming of monocytes had occurred during the establishment of long-term tissue residency. In addition, these *LYVE1*$^+$ macrophages fell mostly within the HES1_Mac (#2) and the Ferritin Light Chain gene (FTL) expressing macrophages (FTL_Mac), in line with our recent description of the fetal-like reprogramming of $HES1^+FOLR2^+$ macrophages in liver tumours (Sharma et al., 2020) and the iron

metabolism-related program detected in human embryonic macrophages (Bian et al., 2020). Of note, similar to what has been reported in mouse studies (R A Franklin et al., 2014; Zhu et al., 2017), we observed that macrophages accumulating in cancer tissues had a more prominent monocyte signature (**Figure 5B**). Notably, apart from liver tumours, where the "long-term resident"-like HES1_Mac (#2) accumulated, all macrophage populations that were increased in cancer corresponded to the putative monocyte-derived macrophages characterised in **Figure 4**, highlighting the cancer type-specific imprinting on certain MNP populations with the recruitment of monocyte-derived TAM.

We were particularly interested in the IL4I1_Mac (TAM, #6) that accumulated in all tumour types, and noted that they exhibited a marked overlap in DEtGs (transformed genes) and DER (regulons) with ISG_Mo (#4) (**Figure 2B** and **Figure S3A**). This degree of both DEtG and DER overlap was higher than for the other Phenograph cluster comparisons, suggesting a close relationship between IL4I1_Mac (#6) and ISG_Mo (#4) and a potential differentiation path between the ISG_Mo (#4) to the IL4I1_Mac (#6) (**Figure 5C**). When we dissected the expression of genes that might directly regulate the functions of ISG_Mo (#4) and IL4I1_Mac (#6) DEtGs (defined in **Figure 2A** and **Figure S3A**), we identified common key transcription factors among DER of both cell types that could be responsible for their specific activation program (**Figure 5D**): *STAT1*, *STAT2*, *ETV7*, *IRF1* and *IRF7* could be involved in the regulation of IDO1 and IL4I1 genes. Although *IDO1* has been considered as a master regulator of the aryl hydrocarbon receptor (AHR) activation, a recent study demonstrated that IL4I1 was a more potent activator of AHR and thus acts as a metabolic immune checkpoint that can promote tumour progression through the catabolism of tryptophan (Sadik et al., 2020). Of note, we noticed that IL4I1_Mac (#6) had a higher expression of IDO1 and IL4I1 in tumours than in matched healthy adjacent tissues (**Figure S5D-E**). We also observed that many shared DEtGs between ISG_Mo (#4) and IL4I1_Mac (#6) or IL4I1_Mac (#6)-specific DEtGs have also recently been described as highly expressed by mature DC enriched in immunoregulatory molecules (mregDC), suggesting that similar events and interactions could drive both IL4I1_Mac (#6) and mregDC

programming in tumours (Maier et al., 2020) (**Figure 5E**).

We recently developed a new fate-mapping mouse model using the expression of *Ms4a3* gene to label monocyte-derived cells (Liu et al., 2019). To further validate the monocytic origin of the IL4I1_Mac (#6), we integrated in-house-generated liver data from Ms4a3cre-RosatdTomato mice with publicly available mouse liver scRNAseq data (Remmerie et al., 2020; Seidman et al., 2020) (**Figure 5F-H and Figure S5F**). We confirmed that mouse *Trem2*$^{+}$*Spp1*$^{+}$ macrophages were monocyte-derived, while *Hes1*$^{+}$*Folr2*$^{+}$ macrophages were mostly of non-monocytic origin (**Figure 5G**) (Sharma et al., 2020). Strikingly, a minor subset of cells that shared genes with the human IL4I1_Mac (#6) (see **Figure 5E**) could also be detected in the mouse liver (**Figure 5H**). Mouse *Il4i1*$^{+}$-like macrophages were all dTomato^{+} and thus, derived from monocytes. Altogether, human IL4I1_Mac (#6) expressed monocyte genes, shared DEtGs and DER with ISG_Mono (#4) and share similarities with a monocyte-derived murine orthologous population, which argues that the human IL4I1_Mac (#6) population is of monocytic origin.

Finally, we aimed to extend the ontogenical characterization of the various macrophage populations included in the MoMac-VERSE. We evaluated the commonalities between signatures of macrophage subsets from different studies and the top 5 DEtGs of the MoMac-VERSE Phenograph clusters that were either uniquely-expressed transformed genes (UEtGs) or DEtGs with at least a 2-fold increase of LogFC expression as compared to DEtGs from other clusters (**Figure S5G**). We grouped the MoMac-VERSE clusters into five main categories: monocytes (both classical CD16^{-} Mo and CD16^{+} Mo), monocyte-derived macrophages (moMac), macrophages (Mac), proliferating macrophages (Prolif) and cells with low viability (Dead). We then compared these 5 main groups with the published cluster annotations: monocyte (blue) or macrophage (green) and inflammatory (pink), anti-inflammatory (light green) or cycling (light blue) (**Figure 5I**). We observed that most populations reported as 'inflammatory macrophages' had commonalities with monocyte clusters of the MoMac-VERSE, arguing for their monocytic origin. In addition, the MoMac-VERSE wide integration allows the clarification of the annotation of MNP subpopulations. For example, whilst some

studies have used the term "macrophages" to annotate cells belonging to the *S100A8*$^{+}$*S100A9*$^{+}$*S100A12*$^{+}$ classical monocytes (cluster #8), others have called them monocytes. But within the MoMac-VERSE, all these differently annotated but highly similar populations belong to a common tissue monocyte subpopulation (**Figure 5I)**.

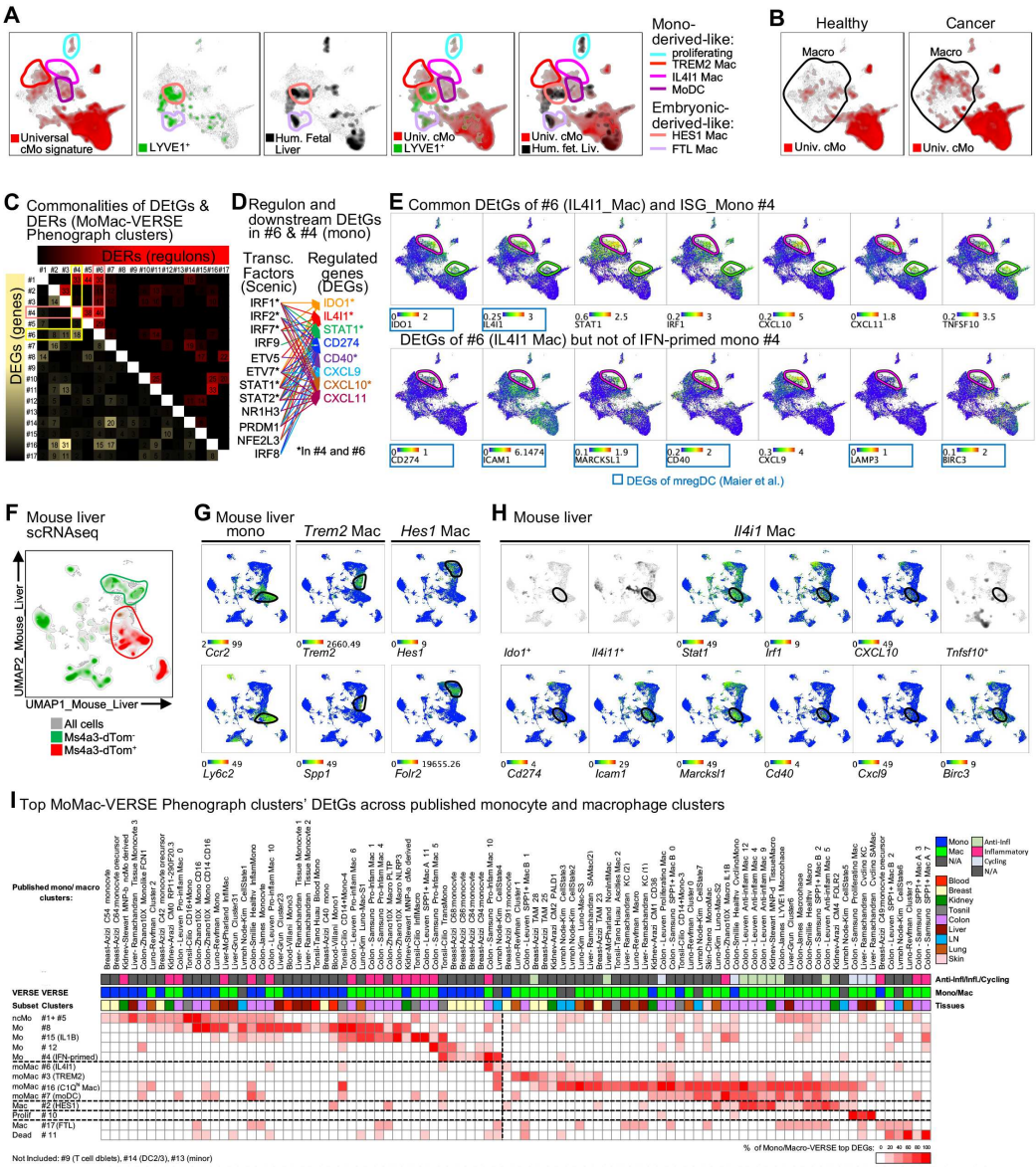

Figure 5. Characterisation of human long-term resident and of monocyte-derived macrophages. *(**A**) Overlay of the universal cMo mean signature from **Figure 1G-H**, of LYVE-expressing cells and of human fetal liver cells on the MoMac-VERSE UMAP. (**B**) Overlay of the universal cMo mean signature in healthy and cancer tissues. (**C**)*

*Heatmap showing relative expression levels of the number of common DEtGs and DER between Phenograph clusters of the MoMac-VERSE. (**D**) Visualisation of DEtGs predicted as regulated by transcription factors of IL4I1_Mac (#6) and ISG_Mo (#4) DER. (**E**) Overlay of the expression on indicated genes on the MoMac-VERSE. Representative common DEtGs between ISG_Mo (#4) and IL4I1_Mac (#6; up) and DEtGs specific for IL4I1_Mac (#6; down) are displayed. DEtGs identified as specific for mregDC (Maier et al., 2020) are indicated in blue frames. (**F**) UMAP space obtained following integration of in-house generated liver data originating from Ms4a3cre-RosatdTomato mice and publicly available data (Remmerie et al., 2020; Seidman et al., 2020). Briefly, two libraries have been generated separately on tdTomato$^-$ and tdTomato$^+$ cells and integrated with available data coming from healthy mice only. Ms4a3$^-$ and Ms4a3$^+$ cells are displayed in green and red, respectively. (**G-H**) Expression of genes to define (**G**) monocytes, Trem2 and Hes1 mouse macrophages, and (**H**) of genes to define mouse Il4i1 macrophages. (**I**) Re-assignment of published monocyte and macrophage clusters according to the MoMac-VERSE. The clusters as designed in the original studies are compared to the top 3 to 5 DEtGs (selected either as UEtG or DEtG with an at least 2-fold increase of LogFC expression as compared to DEtGs from other clusters) of the MoMac-VERSE Phenograph clusters.*

Exploring the MoMac-VERSE allows in-depth characterisation of IL4I1 tumour-associated macrophages

We next aimed at clarifying the functions of the different TAM subpopulations. Using DEtGs obtained with the transf.matrix (**Figure 2A** and **Figure S3A)**, we examined the pathways of the TAM populations that were increased in all included cancer studies (**Figure 6A** and **Table S10**) and the ISG_Mo (#4), as we hypothesized that they could give rise to IL4I1_Mac (#6). This analysis confirmed the inflammatory potential of IL1B_Mac (#15), and suggested that TREM2_Mac (#3) were involved in lipid metabolism (Jaitin et al., 2019), and that ISG_Mo (#4) were IFN-primed. IL4I1_Mac (#6) were associated with antigen presentation, interaction with both Th2 and Th1 T cells, T cell exhaustion and, importantly, tryptophan degradation, again linking this population to tumour progression through the catabolism of tryptophan (Sadik et al., 2020). IL4I1_Mac (#6) were the only macrophages that also expressed genes involved in phagosome

maturation. Therefore, similarly to the mregDC, with which they share a strong common specific gene expression profile (**Figure 5E**), the IL4I1_Mac (#6) could have their gene expression program modulated following phagocytosis (Maier et al., 2020). Next, we looked at the predicted upstream regulators of these cell subsets. We confirmed that IFN-I was the top predicted upstream regulators of ISG_Mo (#4) and also observed that *IFNG* was among the top predicted upstream regulators of both ISG_Mo (#4) and IL4I1_Mac (#6) (**Figure 6B**).

Next, we focused on three studies (two liver cancer and one colon cancer datasets) of the MoMac-VERSE containing cells isolated from three distinct anatomical sectors: the normal adjacent tissue, the tumour periphery and the tumour core. Contrary to the other subsets, ISG_Mo (#4) and IL4I1_Mac (#6) were detected in greater proportion in the tumour periphery (**Figure 6C**). This observation supported the hypothesis of a recruitment of monocytes which mature in TAM within the tissue microenvironment (TME). Given the strong IFNG imprinting in IL4I1_Mac (#6) and that IL4I1_Mac (#6) pathways revolved around antigen presentation and interaction with T cells, we hypothesized that ISG_Mo (#4) and IL4I1_Mac (#6) interact with IFNγ secreting T cells present in the tumour periphery.

We carried out a NicheNet analysis to predict putative T cells interactions with monocyte/macrophage subsets in cancer (**Figure 6D**, **Figure S6A** and **Table S11**). We chose the ISG_Mo (#4), and the MoMac subsets that were increased in all included cancer studies (#2, 3, 6, 15) as "target" populations, and asked which T cell-related molecules and T cell subsets would be predicted to act as "stimulators". We confirmed that *IFNG* was the top predicted stimulator of ISG_Mo (#4) and IL4I1_Mac (#6), but not for the other cell subsets. Importantly, CD40LG was also one of the top predicted stimulators of ISG_Mo (#4) and IL4I1_Mac (#6), but only in the tumour periphery where these subsets were detected most abundantly (**Figure 6C**). Furthermore, IFNG-expressing cytotoxic $CD8^+$ T cells and CD40LG-expressing $CD4^+$ T cells were also most abundant within the tumour periphery, where higher expression of *IFNGR1/2* and *CD40* in ISG_Mo (#4) and IL4I1_Mac (#6) was evident (**Figure 6E-F** and **Figure S6B-C**). This is in agreement with a previous study demonstrating that activated $CD69^+CD8^+$ T cells can induce *IDO1* expression in monocyte-derived

macrophages in an IFNγ-dependent manner (Zhao et al., 2012). In addition, several studies have demonstrated that *IDO1* expression can be induced *in vitro* in monocyte-derived macrophages through their stimulation by CD40-ligand (CD40LG) and IFNγ (IFNG) (Munn et al., 1999; Zhao et al., 2012). Furthermore, CXCL9, CXCL10 and CXCL11 were among the top DEtGs of IL4I1_Mac (#6) (**Figure 2A**, **Figure S3A** and **Table S5**). *CXCR3*, the receptor for these 3 chemokines, was strongly expressed by regulatory T cells (Tregs) within the tumour periphery and core, the two tissue regions where Tregs were also the most abundant (**Figure 6F-G**). Therefore, our observations suggest a potential interaction of CD40L-expressing $CD4^+$ T cells and IFNγ-producing $CD69^+$ activated $CD8^+$ T cells with ISG_Mo #4, contributing to their reprogramming into immunosuppressive IDO1/IL4I_Mac. These macrophages, through their specific chemokine production, their expression of *PD-L1* and *PD-L2* and their *IL4I1/AHR* tryptophan degradation function might in turn suppress T cells and attract Tregs into the tumour (**Figure 6H**).

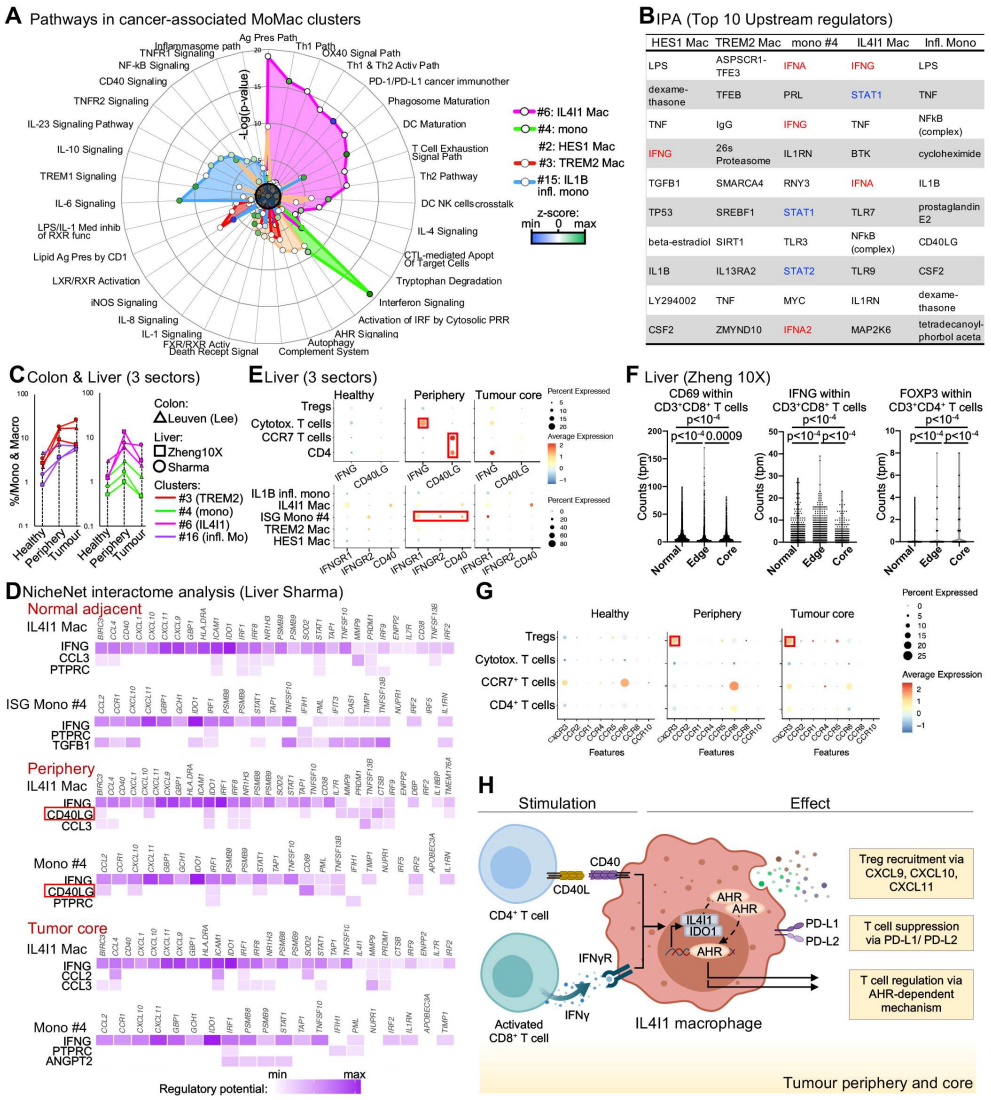

Figure 6. Potential mechanisms leading to pathogenic macrophage states in human tumours. *(**A**) Pathway analysis for individual tumour-associated macrophage clusters. (**B**) Top 10 upstream regulators for each cluster determined by ingenuity pathway analysis (IPA). (**C**) Repartition of cells from the indicated clusters in cancer sub-cellular localisations for one colon cancer and the two liver cancer studies included. (**D**) Visualisation of the regulatory potential of the top 3 predicted ligands associated with DEtG and DER expression in IL4I1_Mac (#6) and ISG_Mo (#4) across liver sections in the Sharma dataset as determined by NicheNet analysis. (**E**) Visualisation of the expression of IFNG and CD40LG by T cell subsets and of IFNGR1, IFNGR2*

*and CD40 by macrophage subsets in the different liver cancer sections. (**F**) Violin plots of CD69 and IFNG gene counts within CD3⁺CD8⁺ T cells and of FOXP3 within CD3⁺CD4⁺ T cells in real tpm of the indicated dataset. (**G**) Visualisation of the expression of transcripts coding for selected chemokine receptors by T cell subsets. (**H**) Potential mechanism leading to IL4I1 macrophage programming and function. P values were calculated with one-way ANOVA test in (**F**).*

Validation of the macrophage heterogeneity in human tissues

Following the establishment of the universal landscape of human macrophages, we applied multiparametric flow cytometry to validate our findings focusing on the IL4I1_Mac (#6). Our DEtG analysis (**Figure 2A**, **Figure S3A** and **Table S5**) indicated that *CD274* (PD-L1), *PDCD1LG2* (PD-L2), *CCR7*, isoforms of *HLA-DP/DQ, CD40*, *CD86* and *CD38* were highly expressed by IL4I1_Mac (#6) (**Figure 7A**). The MoMac-VERSE also included a scRNAseq/CITE-seq breast cancer dataset (Wu et al., 2021), which revealed that at the protein level, IL4I1_Mac (#6) significantly expressed more PD-L1, PD-L2, MHC-II, CD80 and CD86 proteins as compared to the other monocytes and macrophages analysed in this study, thus validating their unique genotype and associated phenotype (**Figure 7B**). We thus combined antibodies against the corresponding proteins encoded by these genes together with TREM2, FOLR2, CD206 (MRC1, which we recently described as a defining marker of HES1/FOLR2 macrophages in liver cancer (Sharma et al., 2020)) and monocyte/macrophage lineage markers and analysed first by flow cytometry healthy human lung, a tissue in which IL4I1_Mac (#6) could be detected even at steady state (**Figure S7A-B**, **Table S2**). Data were analysed within a first UMAP space (**Figure S7A-B**), from which MNP were extracted and re-analysed (**Figure 7C-D**). We detected three major clusters of HLA-DR⁺ MNP, a major population of alveolar macrophages, a population of CD16⁺ monocytes and a population of monocyte/macrophages. While we could not clearly identify TREM2_Mac (#3) using an anti-TREM2 antibody in this healthy human lung sample, within monocyte/macrophages we detected FOLR2⁺CD206⁺ cells

corresponding to the HES1_Mac (#2), FOLR2^{-}CD206^{+} macrophages corresponding to macrophages #16 and notably, a minor population of PD-L1^{hi}PL-L2^{hi}HLA-DP^{hi}HA-DQ^{hi}CD40^{hi}CD86^{hi} cells that corresponded to the IL4I1_Mac (#6) (**Figure 7C-D** and **Figure S7C**). We next established a classical manual gating strategy that allows to define these several macrophage populations in human lung (**Figure S7C-E**).

Flow cytometry analyses were subsequently performed on matched samples obtained from the normal adjacent and tumour cells of three lung adenocarcinoma (LUAD) patients (**Figure 7E-J** and **Figure S7F-I**). In these samples, CD9 was used as a TREM2 surrogate marker to identify TREM2_Mac (#3) since TREM2 could not be detected previously in healthy human lungs (**Figure 7C**). Data were analysed within a first UMAP space (**Figure 7E-F** and **Figure S7C**), from which non-alveolar macrophage MNP (Non-Alv. Mac MNP) were extracted and re-analysed (**Figure 7H-J** and **Figure S7G-I**). While IL4I1_Mac (#6) and TREM2_Mac (#3) increased in tumours for all three patients, HES1/FOLR2_Mac (#2) only increased in the tumours of two out of the three patients, although all three populations were found to be increased in the MoMac-VERSE (**Figure 7J**). Note also that IL4I1_Mac had the highest expression of CD38 and HLA-DP, confirming our findings from the MoMac-VERSE at the protein level (**Figure S7I**).

We also performed flow cytometry analysis on cells from the normal adjacent, the tumour periphery and the tumour core of the liver of a patient with Hepatocellular carcinoma (HCC, **Figure 7K-L** and **Figure S7J**). Similar to what was observed in the MoMac-VERSE (**Figure 6C**), IL4I1_Mac (#6) were mostly retrieved in the tumour periphery and were totally absent from normal adjacent liver (**Figure 7K-L**). We also confirmed our previous observation of progressive accumulation of HES1/FOLR2_Mac (#2) and TREM2_Mac (#3) from normal adjacent tissue towards the liver tumour core (**Figure 7K-L**) (Sharma et al., 2020).

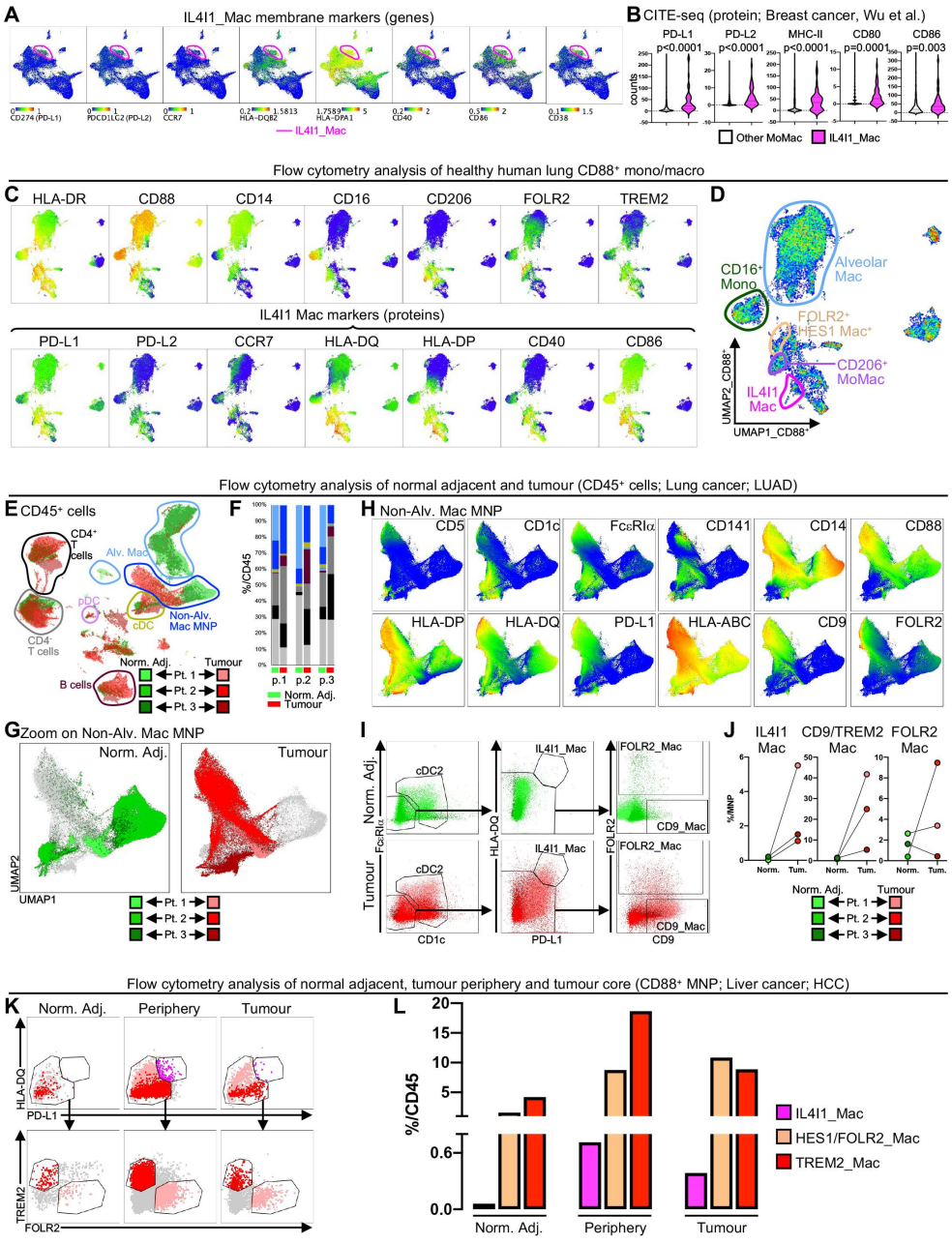

Figure 7. Flow cytometry validation of the MoMac-VERSE macrophage subsets (***A***) *Expression of IL4I1_Mac (#6) marker genes overlaid onto the MoMac-VERSE UMAP space.* (***B***) *Expression of IL4I1_Mac (#6) marker proteins revealed by CITE-seq data from the Wu et al. Breast cancer CITE-seq/10X scRNAseq data included in the MoMac-VERSE.* (***C***) *Flow cytometry analysis of healthy human lung using antibodies binding proteins of the IL4I1_Mac (#6) markers shown in*

*panel **(A)**. Relative expression of surface markers used to define the distinct populations as shown in (**D**)**. (**E-I**) Flow cytometry analysis of normal adjacent and tumour obtained from three lung cancer (LUAD) patients. (**E**) Mapping of Normal Adjacent (Norm. Adj.) and tumour CD45^{+} cells from the three included patients and (**F**) frequency among CD45^{+} cells of the populations defined in where histogram colours correspond to populations defined in (**E**). (**G-I**) For non-alveolar MNP (**G**) visualisation of detected in the Norm. Adj, and tumour tissues of the three patients and (**H**) relative expression of surface markers defining cDC2 (CD5, CD1c, FcεR1α), cDC1 (CD141) and macrophage subsets (other markers). (**I-J**) Within non-alveolar MNP, (**I**) gating strategy defining cDC2 and macrophage and (**J**) quantification of IL4I1, CD9/TREM2 and FOLR2 macrophages in healthy tissues and corresponding tumours in each patient. **(K)** Flow cytometry analysis of Norm. Adj, and Tumour Periphery and Tumour Core obtained from a liver cancer (HCC) patient. Cells falling within the MNP and defined as HLA-DR^{+}CD88^{+} macrophages are displayed (see **Figure S7J** for the upstream gating strategy). Within macrophages, PD-L1^{hi}HLA-DQ^{hi} IL4I1_Mac (#6) were gated. Next, among PD-L1$^{lo/-}$HLA-DQ$^{lo/-}$ cells, gating of TREM2^{+}FOLR2$^{lo/-}$ TREM2_Mac (#3) and of TREM2$^{lo/-}$FOLR2^{+} FOLR2_Mac. (**L**) Frequency among CD45^{+} mononuclear cells of macrophage subsets from the analysis of panel (**K**). P values were calculated using the non-parametric Mann-Whitney in **Figure 7B**.*

DISCUSSION

Here, we have compiled and meta-analysed a large number of available MNP single-cell transcriptomic datasets and built comprehensive integrated MNP- and MoMac- VERSEs. These exploratory tools allowed us to propose a unified annotation of human monocytes and macrophages. Furthermore, they enabled us to identify immunosuppressive macrophage populations present and potentially involved in the progression of tumours. To our knowledge, this study constitutes the largest meta-analysis of human monocytes and macrophages, and we believe that it will be helpful for the scientific community to better apprehend myeloid cell diversity in normal and diseased tissues. As well as elucidating key transcriptional programs at play in the different subpopulations of cells, we also validated the identities of many of the clusters by integrating large unanchored datasets with the more restricted, but index-sorted populations. Of note is that the data integration of these two distinct but complementary analyses yielded remarkably powerful and unified results from many laboratories. Moreover, this "probes and references" approach, which we used previously (Dutertre et al., 2019), increases the resolution of current analytic pipelines and generates comprehensive cell universes (Stuart et al., 2019). Importantly, this requires the generation of a transformed matrix comprising all those genes that are common to integrated studies. However, a limitation of this approach is that during the generation of the transf.matrix, each integrated dataset goes through the normalisation of counts, which can result in an apparent reduction of the expression of some highly expressed genes. On the other hand, this transformation limits the artefactual detection of non-relevant genes in isolated datasets and provides very accurate targets - in other words, conserved clusters are defined by fewer but far more relevant DEtGs. Another very recent study (currently at a preprint stage) used a similar strategy to resolve lung MNP populations (Peters et al., 2020); our findings here fully corroborate this approach while extending it across additional tissues and diseases. Furthermore, the possibility offered by workflows such as Azimuth, which allows the mapping of "query" datasets to our reference MoMac-VERSE, should facilitate the integration of upcoming studies by providing a unified framework (Hao et al., 2020). Indeed, by

projecting data from published COVID-19 datasets onto the MoMac-VERSE, we were able to recapitulate findings of previous works along with providing novel insight to the biology of macrophage and monocytes. The analysis of COVID-19 monocytes and macrophages highlighted an increased ISG signature in monocytes as observed by Silvin et al. (Silvin et al., 2020). Additionally, we observed an increased abundance of IL4I1_Mac expressing *CXCL9*, *CXCL10*, *CXCL11*, *IDO1*, and *IL4I1* as found by Zhang *et al.* in inflammatory diseases and severe COVID-19 (F. Zhang et al., 2020). Considering the relationship between interferon signalling and the presence of IL4I1 macrophages as shown by the MoMac-VERSE, the MoMac-VERSE can be used to unify the findings of these two publications to reveal a more robust analysis of the biology of monocytes and macrophages in severe COVID-19.

The integration here of data from healthy and diseased tissues revealed conserved pathologic programs, calling for re-visitation of the niche concept (Guilliams et al., 2020; Guilliams and Scott, 2017; Okabe and Medzhitov, 2014). Indeed, even in distinct tissues and so distinct niches, disease-associated programs become predominant and therefore strongly imprint myeloid cells (Sharma et al., 2020). In this context, the niche should not be conceptually restricted only to the tissue of residence, but should incorporate other important modifiers, including the sub-tissular niche and the inflammatory status of the tissue (Blériot et al., 2020). Previously, we identified two distinct subpopulations of interstitial macrophages present across tissues in both mice and humans (Chakarov et al., 2019). While confirming these findings, the current study improves their resolution considerably. It also raises the question of the ontogeny of human macrophages: in mice we now know that macrophages can either be derived from adult circulating monocytes or from embryonic precursors seeded in tissues during early development (Florent Ginhoux et al., 2010; Hashimoto et al., 2013; Mass et al., 2016; Perdiguero and Geissmann, 2016; Schulz et al., 2012; Yona et al., 2013). These seminal studies used powerful fate-mapping models but it has been challenging to understand their implications for human biology. While single-cell transcriptomics approaches go some way towards overcoming such challenges (Bian et al., 2020), our observation here that LYVE1^{+} macrophages harbour a signature overlapping with human fetal liver macrophages. Herein,

we focused our attention on the three main subsets of macrophages present across tissues, designed as TREM2, HES1 and IL4I1 macrophages. The integrated data (MoMac-VERSE) suggest that TREM2 and IL4I1 macs could be mostly monocyte-derived, whereas HES1 macs harbour an embryonic signature. To validate this hypothesis, we have used our mouse fate-mapping model to identify the equivalent murine populations and revealed their ontogeny. This further extends the aforementioned "probes and references" approach by extending it across species and renders possible the use of fate-mapping tools that have been developed along the years in animal models to reveal human cell population origins.

Another important point is that these three macrophage populations have been reported separately in many isolated studies, but our integrated approach reveals them as major conserved subsets. Many studies still use the M1/M2 classification initially developed for *in vitro* monocyte-derived macrophages and which indeed splits efficiently human primary macrophages. But as demonstrated previously, this dichotomy is limited to embrace macrophage diversity, especially in the cancer context in which TAM differentiation from circulating monocytes appear to be a distinct pathway from the assumed M2 anti-inflammatory (pro-tumoral) status (R A Franklin et al., 2014). For example, although IL4I1 have a strong M1 program, *in vitro* generated M1 monocyte-derived macrophages might not recapitulate the primary M1-like macrophages that contrary to *in vitro* M1 macrophages, do not produce *IL12B*, production which is restricted to primary tissue activated cDC1 and mregDC. Therefore, the versatility of resident macrophages and TAM needs to be taken into account to refine our understanding of healthy and diseased tissues. In addition to cancer, $CD38^{+}$ M1-like macrophages have recently been described in the context of ageing and ageing-related disease (Covarrubias et al., 2020), which may correspond to the IL4I1_Mac. Further validation is necessary to understand the role of IL4I1_Mac in this context.

Until recently TREM2 macrophages were mostly studied in the brain due to their role in the development of neurodegenerative disorders such as Alzheimer's disease (Krasemann et al., 2017; Parhizkar et al., 2019). However, a TREM2 macrophage population involved in metabolic disorders and obesity has now been detected in adipose

tissue (Jaitin et al., 2019); as well as in tumours, where they occupy a potentially immune-suppressive position (Katzenelenbogen et al., 2020; Molgora et al., 2020). In parallel, a subset of immunosuppressive IL4I1^{+} TAM was detected almost a decade ago (Zhao et al., 2012) and reconfirmed more recently (Sadik et al., 2020). Herein, the combination of data from multiple studies focusing on different cancers and the unbiased analytic approach has fully validated these discoveries, and accordingly we have detected these populations in all of the 6 cancers analysed. From a mechanistic point of view, even if it is clear that these TAM are involved in dampening anti-tumoral T cell responses, the precise pathways involved are still unclear and deserve further investigation to fully decipher the T cell (*IFNG*$^{+}$ CD8 T cells and `$^{+}$ CD4 T cells)/TAM relationship (Gordon et al., 2017). The third population of macrophages on which we focused our attention was the HES1 mac subset which corresponds to FOLR2^{+} mac that were notably detected recently in liver cancer (Sharma et al., 2020). Interestingly, these macrophages seem to undergo reprogramming towards a fetal macrophage identity during cancer development, which is mediated by the tumour vasculature. These macrophages could support tumour growth by being reprogrammed "as if" they were part of an embryo and should support its development. This raises the possibility that blocking this reprogramming and thereby promoting anti-tumoral responses of TAM could be a novel therapeutic strategy in the fight against cancer.

A major strength of the MoMac-VERSE that we propose is the inclusive focus on monocytes as well as macrophages. Within the literature, two major monocyte populations (CD16^{+} and CD16^{-}) have been recognised (Passlick et al., 1989; Ziegler-Heitbrock et al., 2010a) which we also saw within the MoMac-VERSE. In addition, however, we observed further heterogeneity, as in the case of ISG monocytes (#4) and their particular enrichment within the tumour periphery of liver and colon cancer patients. The resemblance of these cells to IL4I1_Mac (#6) further highlighted a potential precursor-product relationship that would have been missed in separate analyses.

Finally, we have validated hypotheses raised by the MoMac-VERSE by using multiparametric spectral flow cytometry, quantifying protein markers validated thanks to the RNA/protein expression connexion

brought by the integrated CITE-seq/scRNAseq breast cancer dataset (Wu et al., 2021). Indeed, even if we fully recognise the relevance of the *in silico* approach to integrate large and widespread datasets, ones could argue that such analyses require biological validation before to be used in clinical settings. Data obtained from tumour biopsies herein were in full accordance with the predictions from the MoMac-VERSE and so we believed that such results should accelerate translational research by providing markers and potential targets for new treatments.

In conclusion, we have revealed here the diverse but conserved array of human monocyte and macrophage populations in both health and disease. This study also provides an online tool to explore human MNP and we believe that this diversity should now be taken into account for further studies. The time when cancer-associated myeloid cell were called myeloid-suppressor derived cells based on the expression of few common but non-specific surface markers is now over: this paradigm shift, allowed by the new era of single-cell transcriptomics and their integration, will now lead us to go beyond the establishment of atlases, descriptive catalogues of cell subsets, and will pave the way to help the scientific community better design innovative and more specific macrophage-based immunotherapy strategies.

Limitations of the study:

The transformed matrix is made in such a way that only genes common to all included datasets are taken forward. Consequently, some genes are lost in this process but those included are conserved across studies and thus, have a greater chance to be also detected in any other study not included here. As a consequence, most genes included in our universal MNP subsets and individual monocyte and macrophage subset gene expression signatures should also be detected in any other study. Since we only included scRNAseq datasets that were available at the time when these VERSES were generated, the MNP- and MoMac- VERSES could continuously be improved by mapping more recent and upcoming datasets through reintegration or using Azimuth (Hao et al., 2021). We were also limited by the number of data sets that had separately sequenced normal adjacent tissue, periphery and tumour core. Consequently, our findings on the accumulation of IL4I1_Mac and their IFN-primed monocytes precurors (cluster #4) within the tumour periphery were limited to liver and colon. Therefore, further validation is required for other tumours. Nevertheless, the interactive MNP- and MoMac- VERSES can be used to explore and align new findings to the data published here.

ACKNOWLEDGMENTS

We thank L. Robinson of Insight Editing London for critical review and editing of the manuscript; F.G is an EMBO YIP awardee and is supported by Singapore Immunology Network (SIgN) core funding as well as a Singapore National Research Foundation Senior Investigatorship (NRFI) NRF2016NRF-NRFI001-02. The bioinformatics and immunogenomics platforms are part of the SIgN Immunomonitoring platform (supported by a BMRC IAF 311006 grant and BMRC transition funds #H16/99/b0/011).

AUTHOR CONTRIBUTIONS

Experiments, K.M., W.T.K, A.A.P., S.K., S.E.I. and C.A.D.; Data analysis, K.M. W.T.K, C.P., A.A.P., E.H., G.D., M.C., X.M.Z., R.M.M.W., R.P., A.I.S.K., A.S., C.B. and C.A.D.; providing human samples: J.K.C.T and provided the healthy lung sample, T.K.H.L., P.K.H.C. and A.B. and provided liver samples, A.D., L.D. and L.Z. provided the matched normal adjacent and lung tumour (LUAD) samples; G.A. and A.S. provided the breast cancer CITE-seq/scRNAseq data; Writing of the manuscript, C.B., C.A.D. and F.G.; Intellectual input, A.S., A.B.; Project supervision, C.A.D. and F.G.; Study conceptualization, C.A.D. and F.G.

DECLARATION OF INTERESTS

The authors declare no conflict of interest.

STAR METHODS

LEAD CONTACT

Further information and requests for resources and reagents should be directed to and will be fulfilled by the Lead Contact, Charles-Antoine Dutertre (charles-antoine.dutertre@inserm.fr) and Florent Ginhoux (Florent_Ginhoux@immunol.a-star.edu.sg).

DATA AND CODE AVAILABILITY

The MNP- and MoMac- VERSES can be explored and downloaded at https://gustaveroussy.github.io/FG-Lab/. Previously unpublished single-cell RNA-seq data have been deposited at GEO and are publicly available as of the date of publication. Accession numbers are listed in the key resources table.

EXPERIMENTAL MODELS AND SUBJECT DETAILS

Human samples

Human samples were obtained in accordance with a favourable ethical opinion from Singapore SingHealth and National Health Care Group Research Ethics Committees. Liver tissues were obtained from living donor transplantations (Asian American Liver Centre, Gleneagles Hospital, Singapore). Healthy liver perfusates were obtained from the liver grafts of donors by flushing intrahepatic veins with cold saline prior to transplantation. Explanted liver tissues from patients with advanced cirrhosis and/or HCC were obtained and perfused in a similar manner *in vitro* (using syringe and needle) and leukocytes isolated as previously described (Tan-Garcia et al., 2017). Spleen tissue was obtained from patients with tumours in the pancreas who underwent distal pancreatomy (Singapore General Hospital, Singapore). Tonsil tissue was obtained from patients with adeno-tonsillar obstruction and who underwent adeno-tonsillectomy (KK Hospital, Singapore). Lung

tissue was obtained from pancreatic cancer patients from the Department of Surgery, Yong Loo Lin School of Medicine, National University of Singapore. Tumour and healthy adjacent tissue from lung were obtained from lung adenocarcinoma patients following written informed consent (Marie Lannelongue Hospital, Paris) and ethical approval (N°ID-RCB: 2016-A00732-49). Spleen, lung, liver and tonsil tissues were processed as previously described (Dutertre et al., 2019) for SMARTseq2. Liver samples for flow cytometry validation were processed as previously described (Sharma et al., 2020). All subjects provided IRB-approved consent.

METHOD DETAILS

Flow cytometry and cell sorting

Cells were thawed from liquid nitrogen and transferred into RPMI (ThermoFischer) with 20% decomplemented FCS (ThermoFischer). Samples were treated with 1mg/ml DNase I (Sigma-Aldrich) at 37℃. Cells were incubated with Live/Dead blue dye (Invitrogen) or with Zombie NIR (Invitrogen) for 30 min at 4℃ in phosphate buffered saline (PBS) and then incubated in 5% heat-inactivated fetal calf serum (FCS) for 15 min at 4℃ (Sigma Aldrich). Cells were stained with appropriate antibodies (listed in the STAR METHODS key resources table) in PBS with 2% FCS and 2mM EDTA (Sigma Aldrich) and Brilliant Stain buffer (BD) and incubated for 30 min at 4℃, and then washed. For indexed-sorting, cells were sorted using a an ARIAIII (70µm nozzle; BD Biosciences) and for macrophage phenotyping, cells were analysed using a Cytek Aurora 4-laser or 5-laser spectral analyser. Fcs files were exported and analysed using FlowJo v10.5.3.

Algorithms for dimensionality reduction

For flow cytometry data, marker expression values were transformed using the auto-logicle transformation function from the flowCore R package. Uniform Manifold Approximation and Projection (UMAP) were carried out using all markers (flow cytometry) or significant PCs (based on Seurat analysis for scRNAseq data). UMAP was run using 15 nearest neighbours (*nn*), a *min_dist* of 0.001 to 0.2 and Euclidean distance (Becht et al., 2018; McInnes et al., 2018). Phenograph clustering (Levine et al., 2015) was performed using all markers or significant PCs (based on Seurat analysis) before dimension reduction, and with the number of nearest neighbours equal to 150 and 100, for MoMac-VERSE and MNP-VERSE, respectively, 30 for flow cytometry and equal to 15 for scRNAseq analysis.

MNP extraction and Seurat V3 integration

The 41 datasets used (Table S1) were either at the raw count matrix or already pre-processed and at the filtered stage. We first integrated all the datasets in an organ-specific manner. Before running the datasets through the integration, we applied universal quality control to keep everything in a unified matter. Cells that expressed fewer than 500 genes and had more than 20% mitochondrial reads were filtered out. All datasets where then unified in the same expression matrix format. Integration was initiated using the Seurat V3 anchoring method (Stuart et al., 2019) and log normalized. The matrix was scaled and a Principal Component Analysis (PCA) was performed (Becht et al., 2018) from which the first 50 Principal Components (PCs) were selected for UMAP analysis. Following the identification of mononuclear phagocytes (MNPs) using canonical markers, a global integration (using 100 PCs for dimensional reduction) of monocytes and macrophages from all tissues was carried out as above.

Generation of indexed-sorting and SMARTseq2 single-cell transcriptome data

Cells isolated from organs were indexed-sorted using the Indexed-sorting panel (Table S2) on a BD FACS ARIAIII (BD Biosciences) into 96 well plates containing 3 µL Lysis buffer (see below) using a 70 µm nozzle. Single-cell cDNA libraries were prepared using the SMARTSeq v2 protocol (Picelli et al., 2014) with the following modifications: (i) 1 mg/ml BSA Lysis buffer (Ambion Thermo Fisher Scientific, Waltham, MA, USA); and (ii) 200 pg cDNA with 1/5 reaction of Illumina Nextera XT kit (Illumina, San Diego, CA, USA). The length distribution of the cDNA libraries was monitored using a DNA High Sensitivity Reagent Kit on the Perkin Elmer Labchip (Perkin Elmer, Waltham, MA, USA). All samples were subjected to an indexed paired-end sequencing run of 2x151 cycles on an Illumina HiSeq 4000 system (Illumina, San Diego, CA, USA), with 300 samples/lane. Data are available through GEO (GEO: GSExxx).

Pre-processing, quality assessment and control and analysis of SMARTseq2 single-cell transcriptome data

Paired-end raw reads were aligned to the human reference genome (GRCh38 version 25 release; Gencode) using RSEM version 1.3.0. Transcript Per Million read (TPM) values were calculated using RSEM and used for downstream analysis. Quality control, selection of highly variable genes, PCA, and differential gene expression analysis was performed using the Seurat R package. All scRNAseq dot plots and meaning plots displaying the gene expression levels or mean signature genes were generated using SeqGeq v1.6 (Flow Jo LLC).

Generation of transformed matrix

To allow for universal analyses across all datasets, a transformed matrix was generated using datasets that contain more than 10,000 common genes inclusive of FOLR2. Datasets of (Cheng et al., 2018; James et al., 2020; MacParland et al., 2018; Stewart et al., 2019; Vieira Braga et al., 2019; Xue et al., 2019; Zheng et al., 2017) were excluded as they did

not meet the above criteria (Fig S1). The pipeline for the generation was adapted from Seurat V3. When loading in the selected datasets, we increased the amount of anchoring points (*anchor features)* and also the number of gene features *(nfeatures)*. Both values were set to the highest number of genes (56,000) in all the datasets. The normalized matrix was extracted from the Seurat object.

QUANTIFICATION AND STATISTICAL ANALYSIS

Differentially expressed genes (DEGs) and "transformed" genes (DEtGs) analysis

DEG and DEtG analyses were performed using the Seurat v3 package (Stuart et al., 2019). All DEtGs obtained from the transformed matrix were calculated on non-normalised values with a logFC threshold of 0.25 (unless specified otherwise) and DEGs obtained from real tpm/count matrixes were calculated on normalised values with a logFC threshold of 0.25. In both cases, the likelihood-ratio test for single-cell gene expression (bimodal test) was used and correction for multiple testing was carried out using the Bonferroni method. DEtGs between healthy and cancer tissues (**Figure 2E and F**), healthy and inflammation (**Figure 2H and I**) were calculated with a logFC threshold of 0.025. The heatmap was generated using the top 50 significant DEtGs from each cluster. All DEtGs calculated from the transformed matrix are depicted in a red/white/blue colour scheme, whilst DEGs calculated from original TPM are shown in a yellow/black/purple colour scheme.

Metadata analysis

Metadata analysis was performed for selected studies with paired conditions (healthy versus cancer or inflammation). The proportion of phenograph clusters were plotted for each condition as charts and density plots for the selected studies. Further analysis was performed

to deconvolute at the patient level in datasets where this information was provided. We only analysed datasets where more than 35 cells were present. Charts and density plots were made in GraphPad Prism v6 and SeqGeq v1.6, respectively. Statistical tests were performed using GraphPad Prism v6 and are specified within the figure legends.

M1 and M2 signature

M1 and M2 signatures were derived from Table 1 published by Martinez *et al.* (Martinez et al., 2006). Those in common with DEtGs obtained across phenograph clusters were used to define M1- and M2-like signatures. The mean gene expression of M1- and M2-like gene signatures were analysed in SeqGeq v1.6 (**Figure 2C and Figure S3F**). We also graphed the number of common genes between the DEtGs from each cluster (**Figure 2D)**.

Generation of the major MNP subset DEGs

Six datasets (Azizi et al., 2018; Cillo et al., 2020; Kim et al., 2020; Smillie et al., 2019; Zhang et al., 2019; Zilionis et al., 2019) that cover the UMAP space of the MNP-VERSE were selected for calculating DEGs across major MNP subsets using the original TPMs. Unique DEG to each of these subsets that were common across the six datasets were identified as the universal gene signatures. Expression of these universal gene signatures on the transformed matrix (DEtGs) was plotted as a heatmap (**Figure 1G**). The mean expression of the universal gene signatures for each MNP subset was visualised using SeqGeq v1.6 (**Figure 1H**).

Scenic gene regulatory network analyses

To infer gene regulatory networks (GRNs) from TPM-normalized expression matrices of colon (L. Zhang et al., 2020), liver (Sharma et al., 2020), and lung (Kim et al., 2020), a pySCENIC (single-cell regulatory network inference and clustering) v0.10.3 analysis was performed (Van de Sande et al., 2020). The analysis consisted of three main steps (GitHub/pySCENIC): generation of co-expression modules with GRNBoost2, refinement of these modules with RcisTarget and evaluation of the regulon activity with AUCell (Van de Sande et al., 2020). Differentially expressed regulons (DER) were calculated using the Seurat pipeline with the same parameters as described above for DEG/DEtG analysis (adjusted p-value lower or equal to 0.05 and Log2FC cut-off of 0.25). Phenograph cluster-specific DER, as well as DER that had similar expression patterns across closely-related phenograph clusters were identified and subsequently used to generate a heatmap (**Figure 2B**).

Pathway analysis

Subset-specific and/or condition specific DEtGs, together with the respective fold-change and p-values, were uploaded to the Ingenuity Pathway Analysis (IPA) software (QIAGEN). IPA analysis reported the p-value of canonical pathways and upstream regulators. Predicted upregulated or downregulated pathways were represented by a positive or negative Z-score, respectively. Canonical pathways determined by IPA's default threshold [–log. (p-value)>1.3] were then shortlisted and radar plots were used to visualize the p-values and Z-scores as previously described in (Dutertre et al., 2019). Full lists of pathways can be found in Tables S9 and S10.

NicheNet analysis

NicheNet is a computational method that uses scRNAseq data to predict interactions between cell populations (Browaeys et al., 2019). To identify potential interactions between T cells and subsets of macrophages in cancer, we used the HCC dataset from Sharma et al. (Sharma et al., 2020), that includes transcriptomic data for MNPs, lymphocytes and non-immune cells. The phenograph clusters that were enriched in cancer (clusters #2, #3, #4, #6 and # 15) were set as "receiver" populations, while the subsets of T cells were set as "sender" populations. Ligand-receptor pairs were included in the analysis when a minimum of 15% of the cells in the respective population expressed the protein (pct=15 in the *get_expressed_genes* function). The genes identified by DEtGs and DER in the MoMac-VERSE were used to predict the T cell ligands activities for each phenograph cluster ("geneset" input in the *predict_ligand_activities* function). The putative T cells ligands (the output of the *predict_ligand_activities* function) were ranked according to their ability to predict the gene signatures using Pearson correlation coefficients and can be found for each MNP phenograph cluster in Table S11. The top 3 ligands and their regulatory potential were represented in a heatmap following the NicheNet pipeline, using the function *get_weighted_ligand_target_links* on the top 20 predicted ligands with n=200 (top target genes), and a cutoff of 0.33 in the function *prepare_ligand_target_visualization*.

KEY RESOURCES TABLE

REAGENT or RESOURCE	SOURCE	IDENTIFIER
Antibodies		
Anti-goat (Polyclonal) AF488	Jackson Immuno-Research Laboratory	Cat# 705-545-147, RRID:AB_2336933
BTLA (Clone743986) BV605	BD Biosciences	Cat# 743986, RRID:AB_2741906
CCR2 (Clone LS132.1D9) BUV563	BD Biosciences	Cat# 749076, RRID:AB_2873470
CCR7 (Clone G043H7) Biotin	BD Biosciences	Cat# 552174, RRID:AB_394352
CD11b (Clone M1/70) Biotin	BD Biosciences	Cat# 553309, RRID:AB_394773
CD11b (Clone M1/70) BV570	Biolegend	Cat# 101233, RRID:AB_10896949
CD123 (Clone 6H6) PE/Daz594	Biolegend	Cat# 306034, RRID:AB_2566450
CD123 (Clone 7G3) BUV395	BD Biosciences	Cat# 564195, RRID:AB_2714171
CD14 (Clone 63D3) SparkB550	Biolegend	Cat# 367148, RRID:AB_2832724
CD14 (Clone M5E2) BV650	BD Biosciences	Cat# 563419, RRID:AB_2744286
CD141 (Clone AD5-14H12) APC	Miltenyi	Cat# 130-113-314, RRID:AB_2733313
CD141 (Clone M81) BV421	Biolegend	Cat# 344114, RRID:AB_2562956
CD16 (Clone 3G8) APC/Cy7	Biolegend	Cat# 302017, RRID:AB_314217
CD16 (Clone 3G8) APC/Cy7	Biolegend	Cat# 302018, RRID: AB_314218
CD16 (Clone 3G8) BV650	Biolegend	Cat# 302042, RRID:AB_2563801
CD163 (Clone GHI/61) BV605	Biolegend	Cat# 333615, RRID:AB_2562712
CD163 (Clone GHI/61) BV605	Biolegend	Cat# 333616, RRID: AB_2616879
CD169 (Clone 7-239) BUV661	BD Biosciences	Cat# 750363, RRID:AB_2874538
CD169 (Clone 7-239) PE	BD Biosciences	Cat# 565248, RRID:AB_2732051
CD19 (Clone HIB19) BV650	Biolegend	Cat# 302238, RRID:AB_2562097
CD19 (Clone SJ25C1) BV650	BD Biosciences	Cat# 563226, RRID: AB_2744313

CD1a (Clone HI149) AF700	Biolegend	Cat# 300120, RRID:AB_528764
CD1c (Clone L161) BV421	Biolegend	Cat# 331525, RRID:AB_10933249
CD1c (Clone L161) BV421	Biolegend	Cat# 331526, RRID: AB_10962909
CD1c (Clone L161) SB436	Invitrogen	Cat# 62-0015-42, RRID:AB_2762426
CD20 (Clone 2H7) BV650	Biolegend	Cat# 302336, RRID:AB_2563806
CD20 (Clone 2H7) BV650	BD Biosciences	Cat# 563780, RRID: AB_2744327
CD206 (Clone 15-2) PP/Cy5.5	Biolegend	Cat# 321122, RRID:AB_10899411
CD206 (Clone 19.2) PE/CF594	BD Biosciences	Cat# 564063, RRID:AB_2732052
CD209 (Clone 9E9A8) PE/Cy7	Biolegend	Cat# 330114, RRID:AB_10719953
CD209 (eB-h209) PercP/Cy5.5	ThermoFisher Scientific	Cat# 45-2099-73, RRID:AB_1106983
CD3 (Clone SP34-2) BV650	BD Biosciences	Cat# 563916, RRID:AB_2738486
CD3 (Clone UCHT1) BUV805	BD Biosciences	Cat# 612895, RRID:AB_2870183
CD301 (Clone H037G3) PE	Biolegend	Cat# 354704, RRID:AB_11219002
CD38 (Clone HIT2) BB515	BD Biosciences	Cat# 564498, RRID:AB_2744374
CD4 (Clone SK3) Cfl.YG584	Cytek Biosciences	Cat# R7-20041, RRID:AB_2885083
CD40 (Clone 5C3) BV750	BD Biosciences	Cat# 746948, RRID:AB_2871735
CD45 (Clone 30-F11) PercP	Biolegend	Cat# 103130, RRID:AB_893339
CD45 (Clone HI30) BV510	BD Biosciences	Cat# 563204, RRID:AB_2738067
CD45 (Clone HI30) V500	BD Biosciences	Cat# 560777, RRID:AB_1937324
CD45RA (Clone 5H9) FITC	BD Biosciences	Cat# 556626, RRID:AB_396498
CD5 (Clone UCHT2) APC/R700	BD Biosciences	Cat# 565121, RRID:AB_2744433
CD5 (Clone UCHT2) BV711	BD Biosciences	Cat# 563170, RRID:AB_2738044
CD86 (Clone 2331) BV786	BD Biosciences	Cat# 740990, RRID:AB_2870657

CD86 (Clone IT2.2) BV605	Biolegend	Cat# 305429, RRID:AB_11203889
CD88 (Clone S5/1) APC/Fire750	Biolegend	Cat# 344316, RRID:AB_2750445
CD88 (Clone S5/1) PE/Cy7	Biolegend	Cat# 344307, RRID:AB_11125761
CD88 (Clone S5/1) PE/Cy7	Biolegend	Cat# 344308, RRID: AB_11126750
CD89 (Clone A59) BUV496	BD Biosciences	Cat# 750617, RRID:AB_2874749
CD9 (Clone M-L13) BV480	BD Biosciences	Cat# 746356, RRID:AB_2743675
CTLA4 (Clone 14D3) PP/eF710	Invitrogen	Cat# 46-1529-42, RRID:AB_2573718
FcεRIα (Clone AER-37 (CRA-1)) BV711	Biolegend	Cat# 334638, RRID:AB_2687186
FcεRIα (Clone AER-37 (CRA-1)) PerCP	Biolegend	Cat# 334616, RRID:AB_2168079
FOLR2 (Clone 94b/FOLR2) PE	Biolegend	Cat# 391704, RRID:AB_2721336
FOLR2 (Clone 94b/FOLR2) APC	Biolegend	Cat# 391706, RRID:AB_2721303
HLA-ABC (Clone W6/32) Pacific Blue	Biolegend	Cat# 311417, RRID:AB_493668
HLA-ABC (Clone W6/32) Spark	Biolegend	Cat# 311453, RRID:AB_2876612
HLA-DP (Clone B7/21) BUV395	BD Biosciences	Cat# 750866, RRID:AB_2874962
HLA-DP (Clone B7/21) eFluor506	BD Biosciences	Cat# 334609, RRID:AB_1227656
HLA-DQ (Clone Tu169) AF647	BD Biosciences	Cat# 564806, RRID:AB_2738963
HLA-DQ (Clone Tu169) BV510	BD Biosciences	Cat# 742609, RRID:AB_2740907
HLA-DR (Clone L243) BV785	Biolegend	Cat# 307641, RRID:AB_2561360
HLA-DR (Clone L243) BV785	Biolegend	Cat# 307642, RRID: AB_2563461
HLADR (Clone L243) APC/Fire810	Biolegend	Cat# 307673, RRID:AB_2876603
NOTCH2 (Clone MHN2-25) BUV615	BD Biosciences	Cat# 752315, RRID:AB_2875832
PD-L1 (Clone MIH1) R700	BD Biosciences	Cat# 565188, RRID:AB_2739101
PD-L1 (Clone MIH1) PE/Cy5	Invitrogen	Cat# 15-5983-42, RRID:AB_2802211
PD-L2 (Clone 24F.10Ca12) APC	Biolegend	Cat# 329608, RRID:AB_1089013

PD-L2 (Clone MIH18) BUV737	BD Biosciences	Cat# 748698, RRID:AB_2873102
PD-1 (Clone EH12.1) BV750	BD Biosciences	Cat# 747446, RRID:AB_2872125
PD-1 (Clone PD1.3) PE/Cy5.5	Beckman Coulter	Cat# B36123
SLAN (Clone DD-1) VioBlue	Miltenyi Biotec	Cat# 130-119-868, RRID:AB_2733608
Streptavidin (Polyclonal) BV570	Biolegend	Cat# 405227
TREM2 (Polyclonal) pure	R&D Systems	Cat# AF1828, RRID:AB_2208689
TREM2 (Clone #237920) AF647	R&D Systems	Cat# FAB17291P, RRID:AB_884528
XCR1 (Clone S15046E) FITC	Biolegend	Cat# 372612, RRID:AB_2715831
Zombie NIR™ Fixable Viability Kit	Biolegend	Cat# 423106
LIVE/DEAD™ Fixable Blue Dead Cell	Invitrogen	Cat# L23105
Chemicals, Peptides, and Recombinant Proteins		
DNAse I	Sigma Aldrich	Cat# 48024000
PBS	ThermoFisher	Cat# 20012-027
Collagenase IV	Sigma Aldrich	Cat# C5138-500MG
RPMI	ThermoFisher	Cat# 31870-025
Brilliant Stain Buffer	BD Biosciences	Cat# 563794
FCS	ThermoFisher	Cat# 26140079
Deposited Data		
SMARTseq2 single cell transcriptome data of human blood and tissue MNP	This paper	GSE178209

Biological samples		
Healthy Lung sample	National University Hospital (NUH), Singapore	Healthy Lung sample

Matched LUAD lung sample	Marie Lannelongue Hospital, Paris	Matched LUAD lung sample
Matched HCC liver sample	Singapore General Hospital (SGH) and National University (NUH)	Matched HCC liver sample
Software and Algorithms		
Anaconda 2018.12	Anaconda	https://www.anaconda.com
DIVA	BD Biosciences	https://www.bdbiosciences.com/en-us
FlowJo v10.5.3	Tree Star	https://www.flowjo.com
GraphPad Prism 6	GraphPad	https://www.graphpad.com/scientificsoftware/prism/
Ingenuity Pathway Analysis v01-16	QIAGEN	https://www.qiagenbioinformatics.com/products/ingenuity-pathway-analysis/
NicheNet	Browaeys *et al.*, 2019	https://github.com/saeyslab/nichenetr
Phenograph	Levine *et al.*, 2015	https://github.com/JinmiaoChenLab/Rphenograph
Python v3.7.1	Python Software Foundation	https://www.python.org
R v4.4	The R Foundation	https://www.r-project.org
SCENIC	Van de Sande *et al.*, 2020	https://github.com/aertslab/pySCENIC
SeqGeq v1.6	FlowJo	https://www.flowjo.com/solutions/seqgeq
Seurat v3	Stuart *et al.*, 2019	https://satijalab.org/seurat/
Seurat v4	Hao *et al.*, 2020	https://satijalab.org/seurat/
UMAP	McInnes *et al.*, 2018	https://github.com/lmcinnes/umap

SUPPLEMENTAL FIGURES

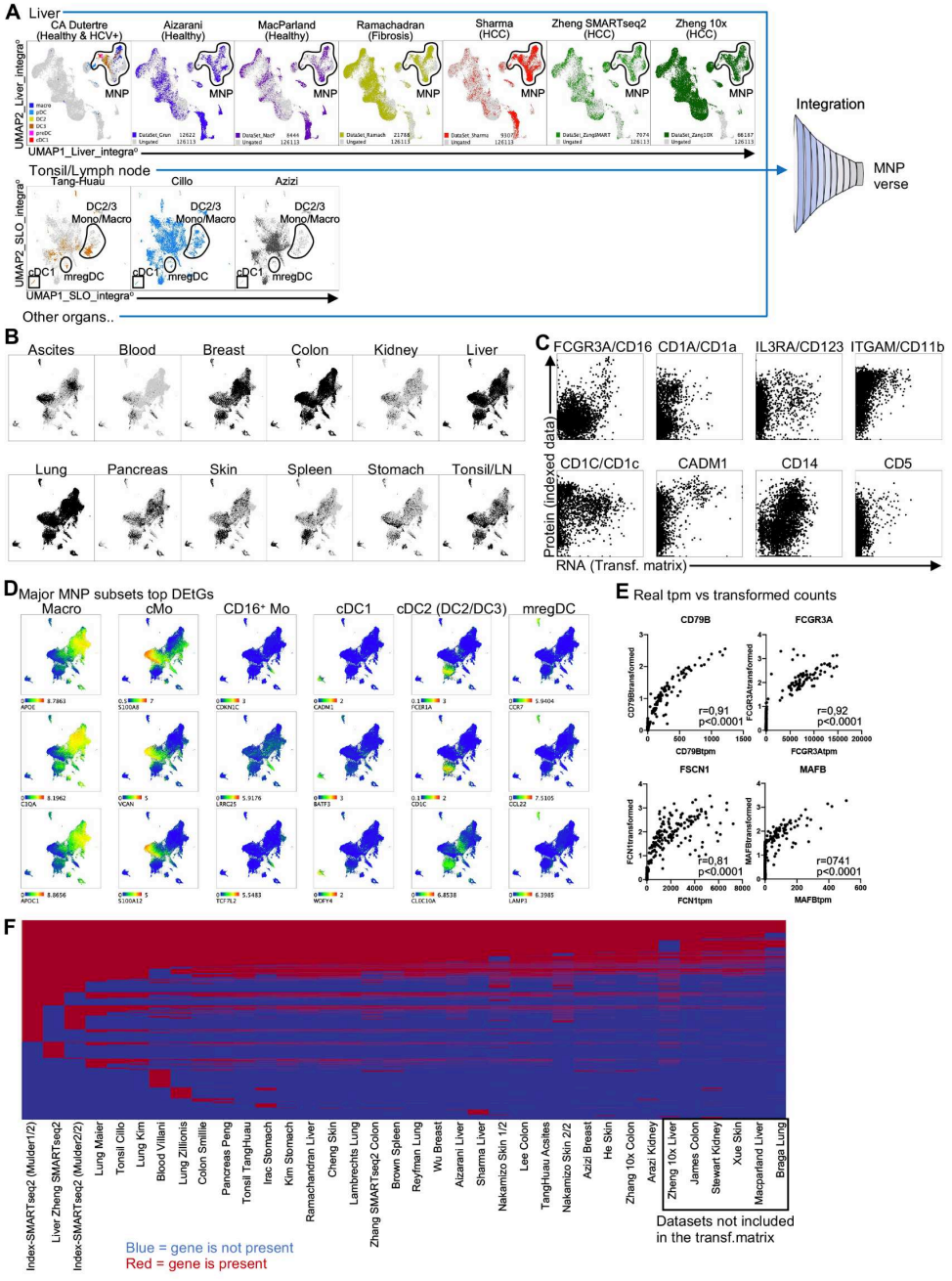

Figure S1 related to Figure 1: The MNP-VERSE reveals universal signatures of major MNP subsets across human tissues. *(**A**) Integration Strategy at the organ level (up: Liver – down: Tonsil/Lymph node). Cells form a common organ but coming from different studies*

*were integrated in a common 2D UMAP space and index sort data was used when available to annotate MNPs. (**B**) Overlay of cells from each organ on the MNP-VERSE. (**C**) Dot plots of RNA (X-axis) versus protein (Y-axis) expressions for the indicated markers. (**D**) Overlay of the expression of selected Universal signature genes (defined in **Figure 1G**) of the major MNP subsets. (**E**) Dot plots of real (X-axis) versus transformed matrix (Y-axis) counts for the indicated genes. The Pearson correlation co-efficient (r) was calculated alongside the p-value. (**F**) Heatmap showing the presence or absence of any given gene from human translatome in all the integrated datasets.*

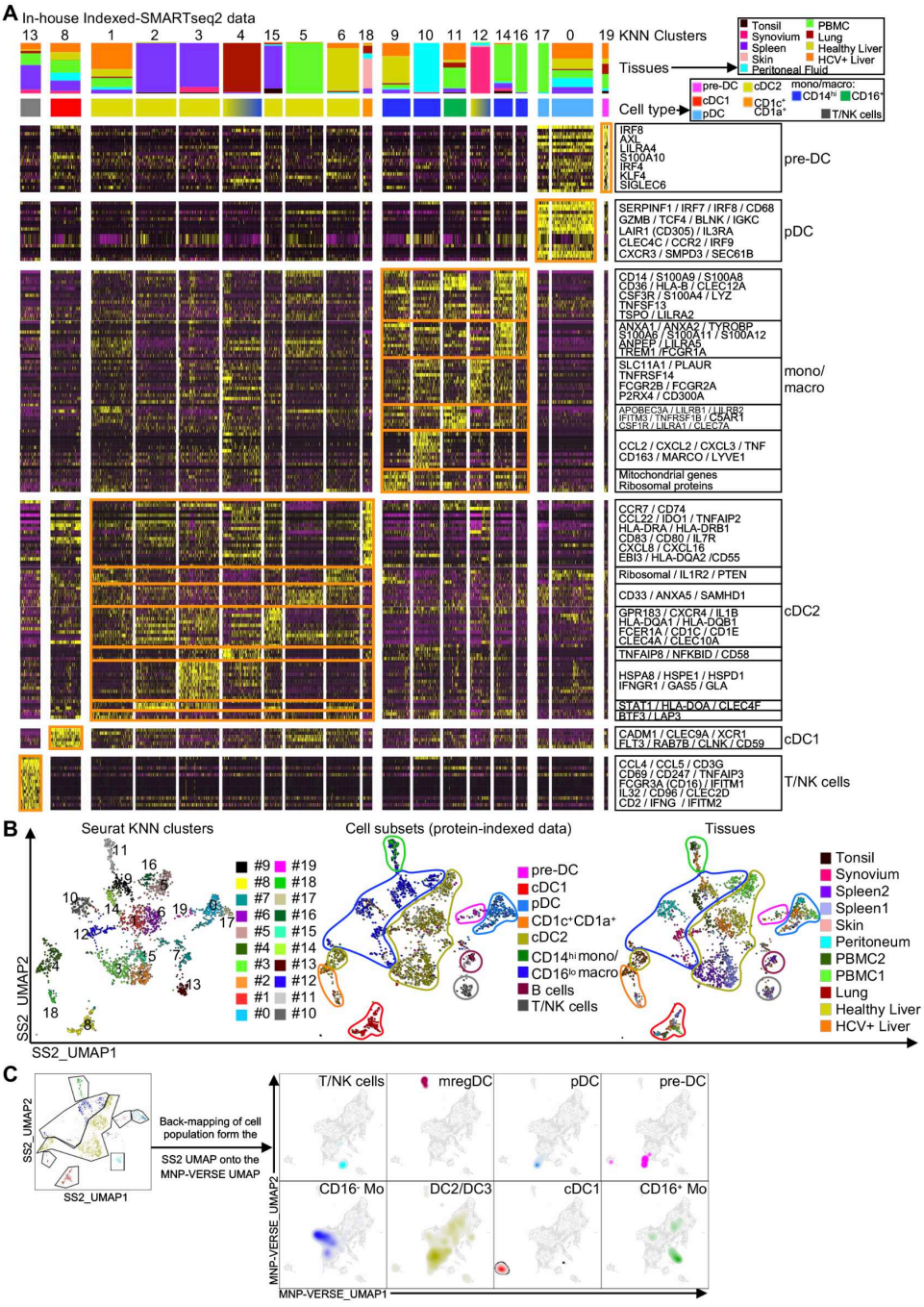

Figure S2 related to Figure 1: Analysis of indexed-SMARTseq2 scRNAseq data and back-mapping onto the MNP-VERSE. *(**A**) DEG heatmap obtained from SNN clusters of our in-house indexed-SMARTseq2 (SS2) scRNAseq data. The heat map is annotated to display relative frequency in each cluster of tissues and cell type annotation*

*(obtained from DEGs and from indexed-data protein expression analysis, not shown). (**B**) Overlay of KNN clusters (upper panel), cell subsets identification based on indexed-data protein expression analysis (middle panel) and of tissue of origin (lower panel) onto the UMAP space. (**C**) Back-mapping of cell subsets defined in the SS2 UMAP space onto the MNP-VERSE UMAP space.*

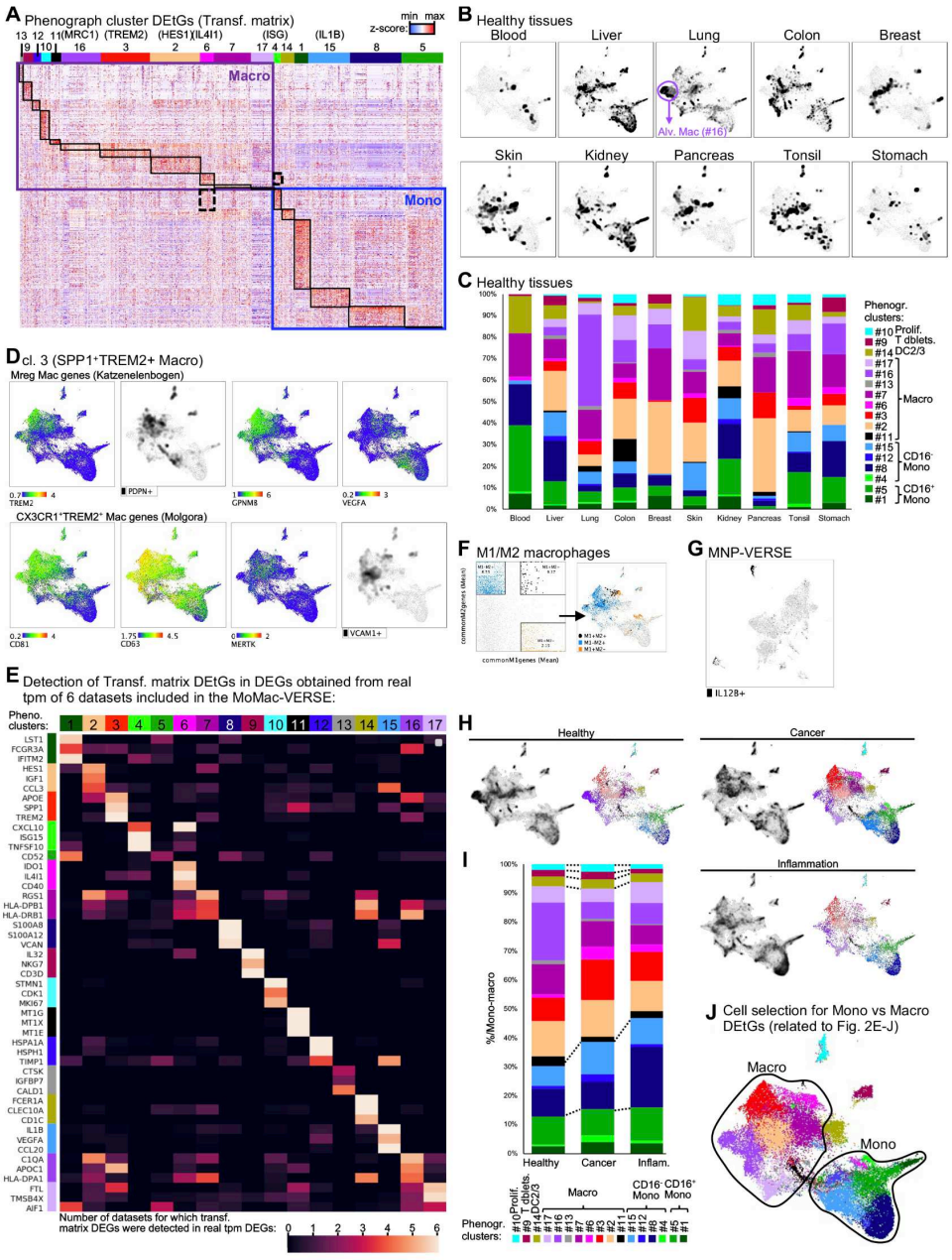

Figure S3 related to Figure 2: The MoMac-VERSE identifies conserved monocyte and macrophage states and global imprinting across human tissues *(**A**) Heatmap of the MoMac Phenograph cluster DEtGs. (**B**) Overlay of cells from healthy tissues on the MoMac-VERSE. (**C**) Quantification of the different Phenograph clusters in each healthy tissue. (**D**) Visualisation of the mean expression of cells positive for indicated genes used as biomarkers in the mentioned studies and overlaid on the MoMac-VERSE. (**E**) Gene expression in the*

*transformed matrix of the MoMac-VERSE. Heatmap showing the number of Phenograph clusters' DEGs defined on real counts from 6 datasets that are also defined as DEtGs when using the transf.matrix. (**F**) Visualisation of $M1^{+}M2^{+}$, $M1^{-}M2^{+}$, $M1^{+}M2^{-}$ macrophage polarisation states defined by mean signatures obtained from Martinez et al (Martinez et al., 2006) onto the MoMac-VERSE. (**G**) Profile of IL12B RNA expression in the MNP-VERSE. (H) Density plots and clustering information of the healthy, cancer or inflammatory diseased MoMac-VERSE. (**I**) Quantification of the different clusters in the indicated conditions. (**J**) Definition of monocytes and macrophages in the MoMac-VERSE used to analyse these cell subsets in **Figure 2E-J**.*

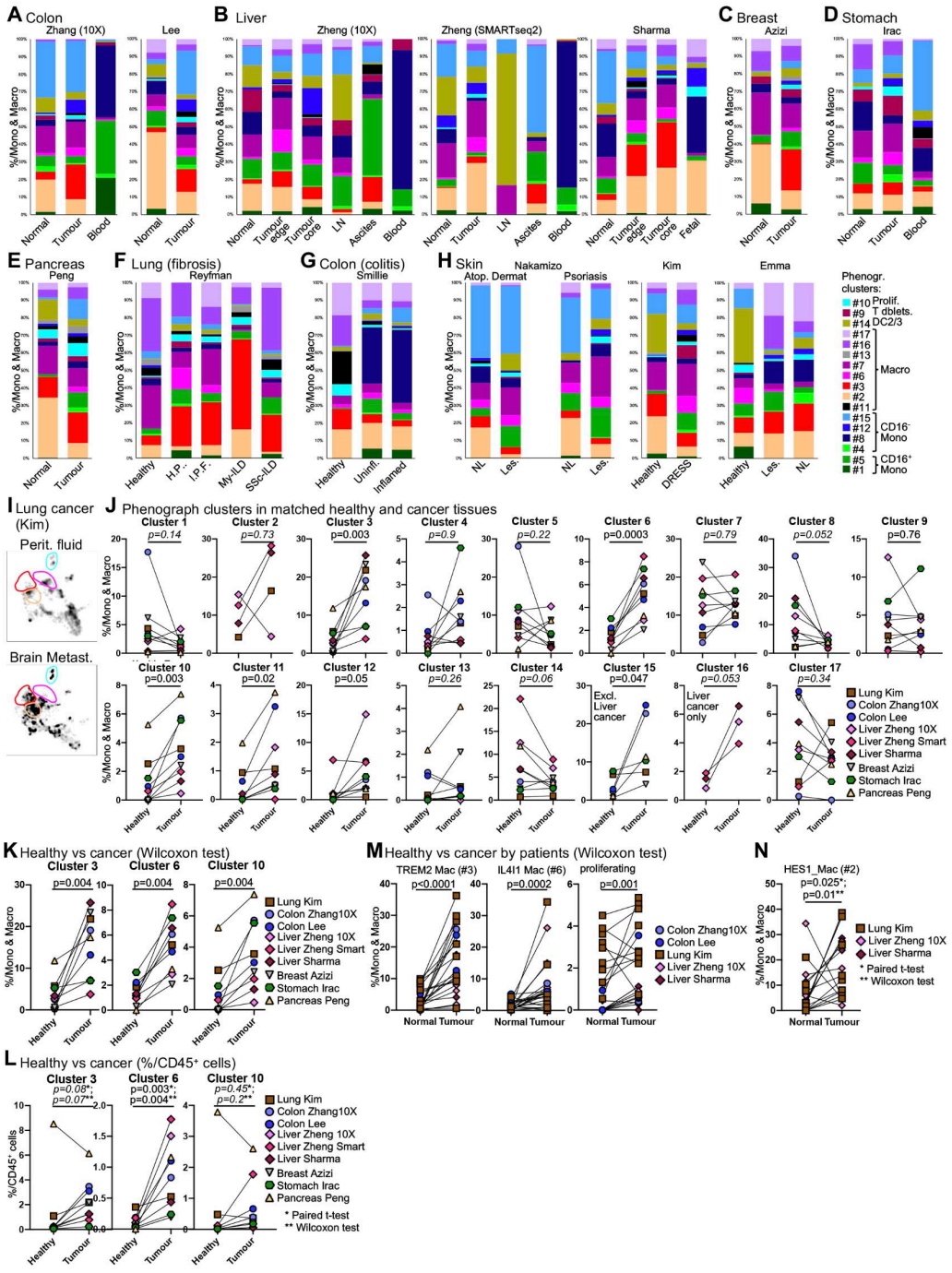

Figure S4 related to Figure 4: Definition of monocyte and macrophage states triggered in inflamed and cancerous tissue. *(**A-H**) Percentage of the different clusters in the indicated studies and in the corresponding organs: colon – cancer (**A**), liver (**B**), breast (**C**), stomach (**D**), pancreas (**E**), lung (**F**), colon - colitis (**G**) and skin (**H**). (**I**) Overlay of*

*metastatic cells of lung cancer data from the indicated dataset on the MoMac-VERSE. (**J**) Quantification of the different phenograph clusters in healthy tissues and corresponding tumours. P values were using a paired t-test (**K,M,N**) Graphical representation of the relative proportion of clusters increased using Wilcoxon test (related to **Figure 4O-P**). (**L**) Graphical representation of the relative proportion among CD45^{+} cells of clusters increased in all cancer studies. P values were using a paired t-test (*) and a Wilcoxon test (**).*

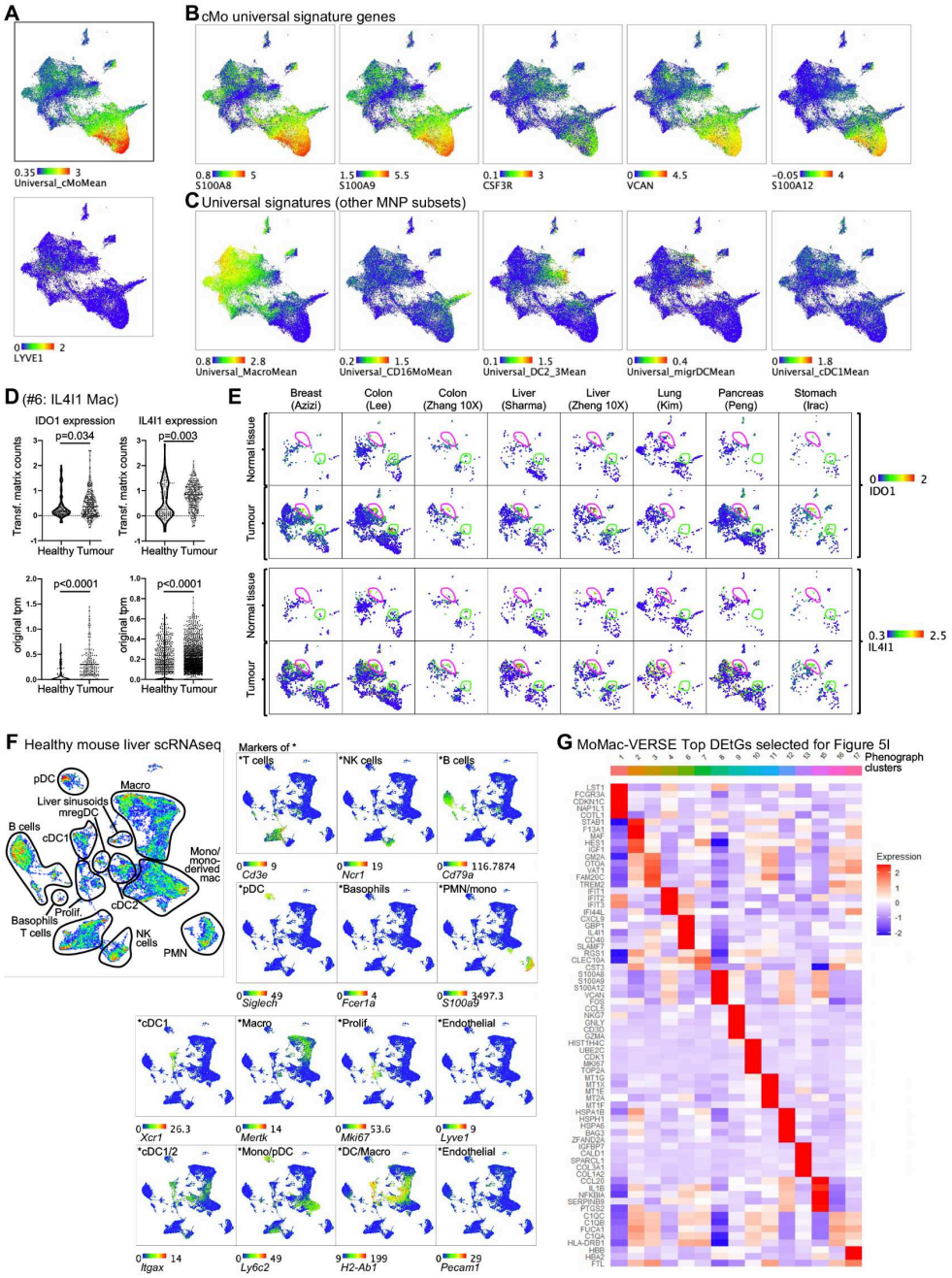

Figure S5 related to Figure 5: Characterisation of human embryonic-like resident and of monocyte-derived macrophages. *(**A**) Overlay of the expression of the mean universal monocyte signature and of LYVE1 on the MoMac-VERSE. (**B-C**) Overlay of the expression of indicated (**B**) monocyte markers, and other (**C**) mean Universal signatures. (**D**) Violin plots of IDO1 and IL4I1 transf.matrix counts (upper panels) or of real TPM (lower panels) in healthy or tumour tissues. (**E**)*

*Overlay of the expression of IDO1 and IL4I1 genes across tissues. (**F**) Annotation of the mouse liver integration data. P values were calculated with two-tailed unpaired t-test for (**D**). (**G**) Heat map showing the mean expression of DEtGs of the MoMac-VERSE selected for Figure 5I within each of the displayed Phenograph clusters.*

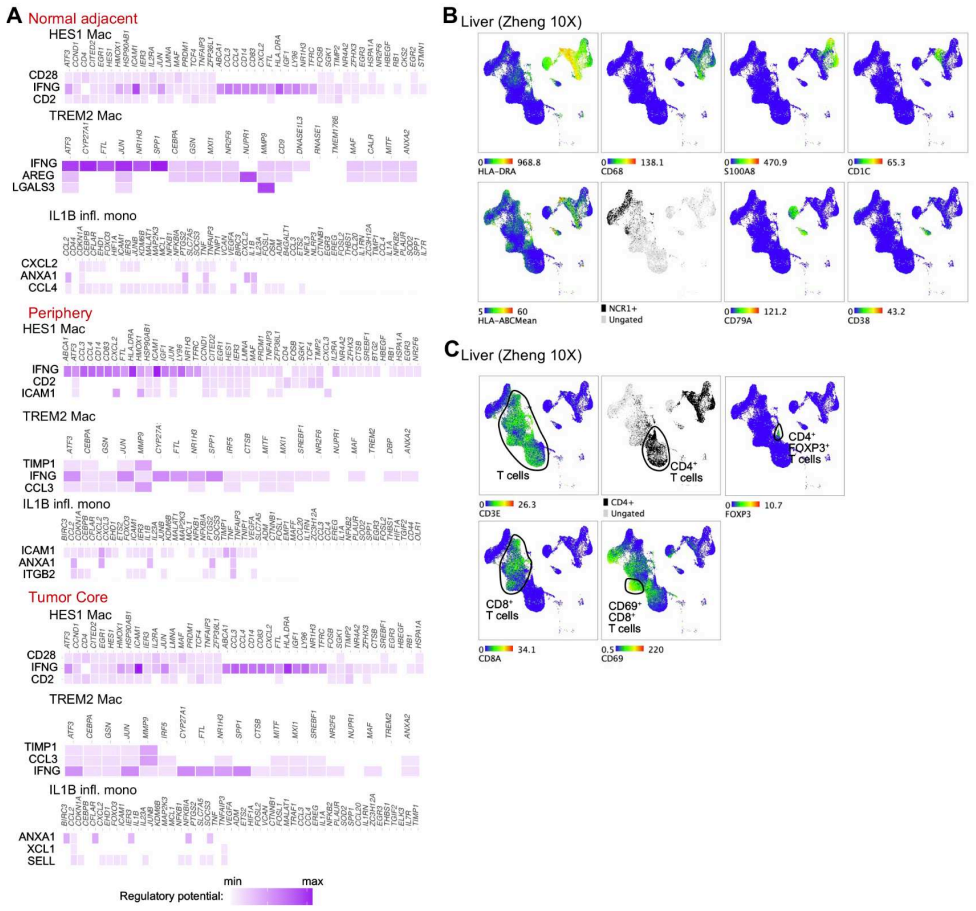

Figure S6 related to Figure 6: Potential mechanisms leading to pathogenic macrophage states in human tumours. *(**A**) Visualisation of the regulatory potential of the top 3 predicted ligands associated with DEtG and DER expression in the indicated myeloid cell populations across liver sections in the Sharma dataset as determined by NicheNet analysis. (**B-C**) Identification of (**B**) major cell subsets and of (**C**) the different T cell populations in the indicated liver dataset.*

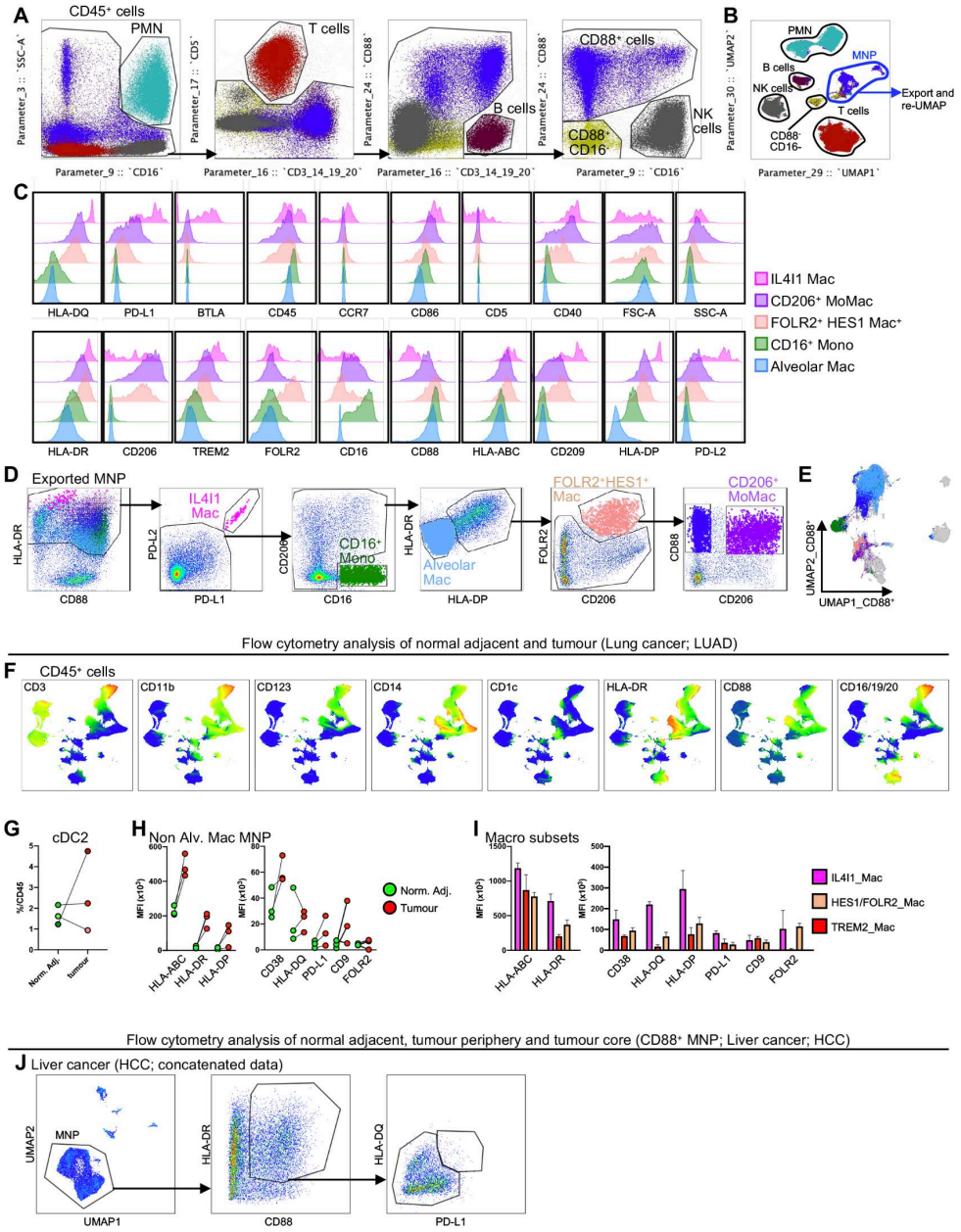

Figure S7 related to Figure 7. Validation of the MoMac-VERSE macrophage subsets in healthy human lung and in human lung (LUAD) and liver (HCC) cancers. *(**A**) Overlay of defined cell populations in the manual gating strategy on the (**B**) UMAP analysis used to resolve human CD45⁺ immune cell populations in healthy lungs. (**C**) Relative expression of surface markers by the defined cell populations. (**D**) Cell populations within the MNP gate from **Figure S5B** are further defined in the manual gating strategy and overlaid on the*

*(**E**) UMAP analysis of exported MNP in healthy lungs. (**F**) Meaning plots of surface markers used to define the distinct populations as shown in **Figure 5D**. (**G**) Quantification of cDC2 in healthy tissues and corresponding tumours in each patient. (**H-I**) Comparison of protein expression represented as mean fluorescence intensity (MFI) on (**H**) normal adjacent and tumour MNP, and on (**I**) IL4I1_Mac (#6) , HES1/FOLR2_Mac and TREM2_Mac. (**J**) Flow cytometry analysis of normal adjacent, tumour periphery and tumour core obtained a liver cancer (HCC) patient. With the UMAP of flow cytometry data, MNP were gated and macrophages were subsequently gated ad HLA-DR^{+}CD88^{+}.*

2.2 UNRAVELLING DC SUBSETS AND STATES ACROSS HUMAN NORMAL ADJACENT AND MALIGNANT TISSUES

Kevin Mulder,[1,2,3]* Wan Ting Kong,[1,2,*] Margaux Gardet,[1,2,*] Amit Ashok Patel,[1,2,*] Anne Calvez,[4] Grégoire Gessain,[1,2] Cécile Piot,[5] Quentin Blampey,[1,3,6] Thomas Jaffrezic,[1,2] Elisa Poupaud,[1,2] Emma Loubersac,[1,2] Louis Romette,[1,2] Ahmed-Amine Anzali,[1,2] Garett Dunsmore,[1,2] Antoine Bougouin,[4] Guilhem Pupier,[4] Lizhe He,[7] Timothy Wiggins,[7] Jiang He,[7] George Emanuel,[7] Anne-Gaëlle Goubet,[1,2] Ghamdan Al-Eryani,[8,9] Alexander Swarbrick,[8,9] Regine J. Dress,[10] Marc Deloger,[1,11] Antonio Bertoletti,[12] Vincent Thomas de Montpreville,[13] Catherine Sautès-Fridman,[4] Wolf H. Fridman,[4] Laurence Zitvogel,[1,2,3,14] Florent Ginhoux,[1,2,15,16,17]**,*** and Charles-Antoine Dutertre[1,2,**,***]

[1]Gustave Roussy Cancer Campus, Villejuif, France
[2]Institut National de la Santé Et de la Recherche Médicale (INSERM) U1015, Equipe Labellisée—Ligue Nationale contre le Cancer, Villejuif, France
[3]Université Paris-Saclay, Ile-de-France, France
[4]Centre de Recherche des Cordeliers, INSERM, Sorbonne Université, USPC Université Paris Cité, Equipe Labellisée Ligue Nationale Contre le Cancer, Paris, France
[5]Immunobiology Laboratory, The Francis Crick Institute, 1 Midland Road, London NW1 1AT, UK
[6]Paris-Saclay University, Gustave Roussy, INSERM U981, PRISM Center, Villejuif, France
[7]Vizgen, 61 Moulton St, Cambridge, MA, USA
[8]Garvan Institute of Medical Research, Darlinghurst, NSW 2010, Australia
[9]St Vincent's Clinical School, Faculty of Medicine, UNSW Sydney, NSW 2052, Australia
[10]Institute of Systems Immunology, Hamburg Center for Translational Immunology (HCTI), University Medical Center Hamburg-Eppendorf, Hamburg, Germany
[11]Plateforme de bioinformatique, Université Paris-Saclay, INSERM US23, CNRS UMS 3655, F-94805, VILLEJUIF France
[12]Program in Emerging Infectious Disease, Duke-NUS Medical School, 8 College Road, Singapore 169857, Singapore
[13]Pathology Department, Marie Lannelongue Center, Le Plessis Robinson, France
[14]Center of Clinical Investigations in Biotherapies of Cancer (BIOTHERIS) 1428, Villejuif, France.
[15]Singapore Immunology Network (SIgN), A*STAR, 8A Biomedical Grove, Immunos Building, Singapore 138648, Singapore [16]Shanghai Institute of Immunology, Shanghai Jiao Tong University School of Medicine, Shanghai 200025, China
[17]Lead Contact

* Equal contribution
** Equal contribution
*** Correspondence: charles-antoine.dutertre@inserm.fr, Florent_Ginhoux@immunol.a-star.edu.sg

SUMMARY

Dendritic cells (DCs) are professional antigen presenting cells (APCs). While plasmacytoid DCs (pDCs) are poor APCs at a steady state, myeloid progenitor-derived DCs (mDCs) comprise DC1s, DC2s and DC3s specialised in T-cell priming. To have unbiased DC atlases, we integrated DCs from 13 tissues across 40 datasets to generate a pDC+mDC-VERSE (DC-VERSE) and an mDC-VERSE scRNAseq compendiums. We characterised DC subsets and "states" across tissues. We found that most studied tumours contained $CD207^+$ DCs whose expansion inversely correlated with tumour $CD8^+$ resident memory T-cells (T_{RMs}), T-cell clonality and survival of patients that received immune checkpoint blockade treatment. Similarly to *CCR7*-expressing mDCs (a common "state" of DC1s, DC2s and DC3s), $CD207^+$ mDCs were a common state of DC2+DC3s. Spatially-resolved single-cell transcriptomic and immunohisto-fluorescence of human carcinomas demonstrated that lymphocytes and most DCs were enriched within tumour stroma, while $CD207^+$ DC2+DC3s were mostly embedded within tumour nests.

Keywords: Dendritic cells, DC1, DC2, DC3, Heterogeneity, Cancer, cell state, DC-VERSE, mDC-VERSE, CD207, T_{RM}, T_{EMRA}, T-cell clonality, Immune checkpoint blockade, ICB, scRNAseq, Single-cell spatial transcriptomics.

Link to the online website for DC-VERSE and mDC-VERSE exploration:

https://macroverse.gustaveroussy.fr/2021_DC-VERSE/

https://github.com/gustaveroussy/FG-Lab

INTRODUCTION

The mononuclear phagocyte system (MPS) was initially comprised of monocytes and macrophages, which later included conventional dendritic cells (cDCs) discovered by Ralph Steinman and colleagues (Steinman and Cohn, 1973). These cells were shown to be the unique potent activators of naïve T-cells and were viewed as 'accessory' cells bridging the innate and adaptive immune response (Nussenzweig et al., 1980; Steinman et al., 1983; Steinman and Witmer, 1978). Over time, the identification of common DC progenitors (CDPs) has aided in defining the cDC lineage and understanding the origin of various DC subsets (Lee et al., 2015; Liu et al., 2009; Naik et al., 2007; Onai et al., 2007), including cDC1s (referred to here as DC1s), $CD1c^+$ DCs (initially termed cDC2s), and plasmacytoid DCs (pDCs), found across tissues and species (Guilliams et al., 2016). However, the advent of high-dimensional single-cell technologies has unveiled additional subsets and states, particularly within human $CD1c^+$ DCs (referred to here as DC2s and DC3s, collectively termed DC2+DC3 throughout this study) and pDC compartments(Bourdely et al., 2020; Cytlak et al., 2019; Dutertre et al., 2019; See et al., 2017; Villani et al., 2017). Notably, $CD123^+$ DCs were revealed to harbour both *bona fide* pDCs and DC precursors (pre-DCs) (See et al., 2017; Villani et al., 2017). Within $CD1c^+$ DCs, $CD5^+$ DC2s and CD5-$CD14^{+/-}$ DC3s were identified, with the latter expanding during inflammation (Bourdely et al., 2020; Dutertre et al., 2019). The classification of DC3s within the cDC lineage has remained a significant question, with recent studies suggesting that DC3s might originate directly from a GMP/MDP progenitor, independent of CDPs/pre-DCs (Bourdely et al., 2020; Cytlak et al., 2019). The DC nomenclature is intricately linked by their ontogeny, and it was established that the term "conventional" DC (cDC) would qualify CDP/pre-DC-derived DCs (Guilliams et al., 2014). Consequently, the common myeloid progenitor origin of pre-DC-derived DC1 and DC2, as well as GMP/MDP-derived DC3, allows us to classify these three cell subsets as myeloid DCs (mDCs).

While cell lineages/subsets are determined by their ontogeny, cell states are molecular programs that could be acquired in a cell's lifespan in response to specific tissue or inflammatory cues (Ginhoux

et al., 2022). One example is the CCR7-expressing mDCs (*CCR7* mDCs, also called mature DCs enriched in immunoregulatory molecules, mregDCs), which represent terminally differentiated and matured states of DC1s, DC2s, and potentially DC3s, playing essential roles in tumour immunity (Di Pilato et al., 2021; Maier et al., 2020; Zheng et al., 2017).

The increased accessibility and feasibility of single-cell RNA sequencing (scRNAseq) is a double-edged sword. Whilst the public database continues to expand, we are left overwhelmed with numerous publications with different annotations and names of DC clusters, resulting in confusing misalignment of the nomenclature of cell populations (Ginhoux et al., 2022). For example, 'DC3' was initially coined to describe a subset of inflammatory $CD5^{-}CD14^{+/-}$ "$CD1c^{+}$ mDCs" (Bourdely et al., 2020; Cytlak et al., 2019; Dutertre et al., 2019), whereas others have used this term to describe cells (Di Pilato et al., 2021; Gerhard et al., 2020; Zilionis et al., 2019) that have an apparent transcriptomic alignment to *CCR7* mDCs (called mregDCs by the authors of this study) (Maier et al., 2020). Furthermore, a $CD207^{+}$ (Langerin) population has been described in various contexts (Bell et al., 1999; Leader et al., 2021; Y. Zhang et al., 2021). Evidently, there is little consensus on how these subsets are characterised, creating confusion among experts and newcomers in the field (Ginhoux et al., 2022).

In a recent study, we integrated monocytes and macrophages from 41 scRNAseq datasets across various human tissues in health and disease to unify the identities of these cells (Mulder et al., 2021). Building upon this approach, we present the pDC+mDC-VERSE (DC-VERSE) and, specifically, the mDC-VERSE to unravel the mDC heterogeneity to realign the mDC nomenclature comprehensively. The mDC-VERSE allowed us to provide an in-depth analysis of DC2 and DC3 heterogeneity, shedding light on their potential significance in various cancers. Notably, a common state of DC2+DC3s that co-expressed CD207 and CD1a receptors ($CD207^{+}$ DC2+DC3s) was observed to: (1) accumulate inside the tumour of most cancer studied; (2) inversely correlate with T-cell clonal expansion, and the frequency of $CD8^{+}$ resident memory T-cells (T_{RMs}, classically defined as co-expressing CD69 and CD103); (3) predominantly embedded within tumour nests

while all the other DCs, T and B-cells were mainly detected within the tumour stroma of breast and lung adenocarcinomas. Altogether, this work provides a comprehensive resource to explore DC heterogeneity, including subsets and states across various tissues and will provide the foundation for an open discussion on a unified DC nomenclature.

RESULTS

DC-VERSE

We recently performed a meta-analysis of human macrophages and monocytes sequenced from 41 published datasets across 13 tissues, including healthy, normal adjacent (to tumours) and tumour tissues (Mulder et al., 2021) (**Table S1**). We adopted a similar approach for dendritic cells (DCs), where datasets were first integrated tissue by tissue, from which mDC and pDC were extracted and re-integrated to generate the DC-VERSE (**Figure 1A and Table S1**). To validate our integrated DC-VERSE, we employed established gene markers, confirming the presence of pDCs (*LILRA4/CLEC4C* transcripts), pre-DCs (*CD5/AXL* transcripts), DC2+DC3s (*CD1C/FCER1A* transcripts), DC1s (*CLEC9A/CADM1* transcripts), CCR7 mDCs (*CCR7/LAMP3* transcripts), and proliferating DCs (*MKI67/CDK1* transcripts) (**Figure 1B**). We used Phenograph (Levine et al., 2015) to define clusters and calculated the differentially expressed genes (DEGs) for all Phenograph clusters (cl. #) using the RNA matrix (**Figure 1C, Table S2**).

We next implemented dendrogram clustering to understand the relationship of Phenograph clusters (cl. #) to one another. We identified ten DC mega-clusters, which included known subsets and novel ones such as heat shock protein-expressing DCs (cl. #16), low nFeature cells (Low nFeat., cl. #3), T-cell-containing doublets (cl. #1), and Langerhans cell-like DCs (LC-like DC, cl. #5, #17). (**Figure 1D,E**).

DEG analysis of the DC-VERSE mega-clusters showed distinct signature genes associated with each mega-clusters (**Figure 1F, Table S2**). Such "universal" signatures can be used to identify all these DC populations in scRNAseq data obtained from most human tissues.

We next evaluated the relative frequency of DC populations across normal adjacent (Norm. adj.) "healthy" tissues included in this study (**Figure 1G)**. We first focused on pDCs and observed that pDCs were detected at the highest frequency in blood compared to other tissues. Examination of transcription factors IRF4 and IRF8 showed variations in their expression levels among pDC subsets, indicating differences in

maturation states (**Figure 1H,I,J**). However, our meta-analysis comparing matched normal adjacent tissues and tumours did not reveal significant differences in the frequency of pDC subsets (**Figure 1K**).

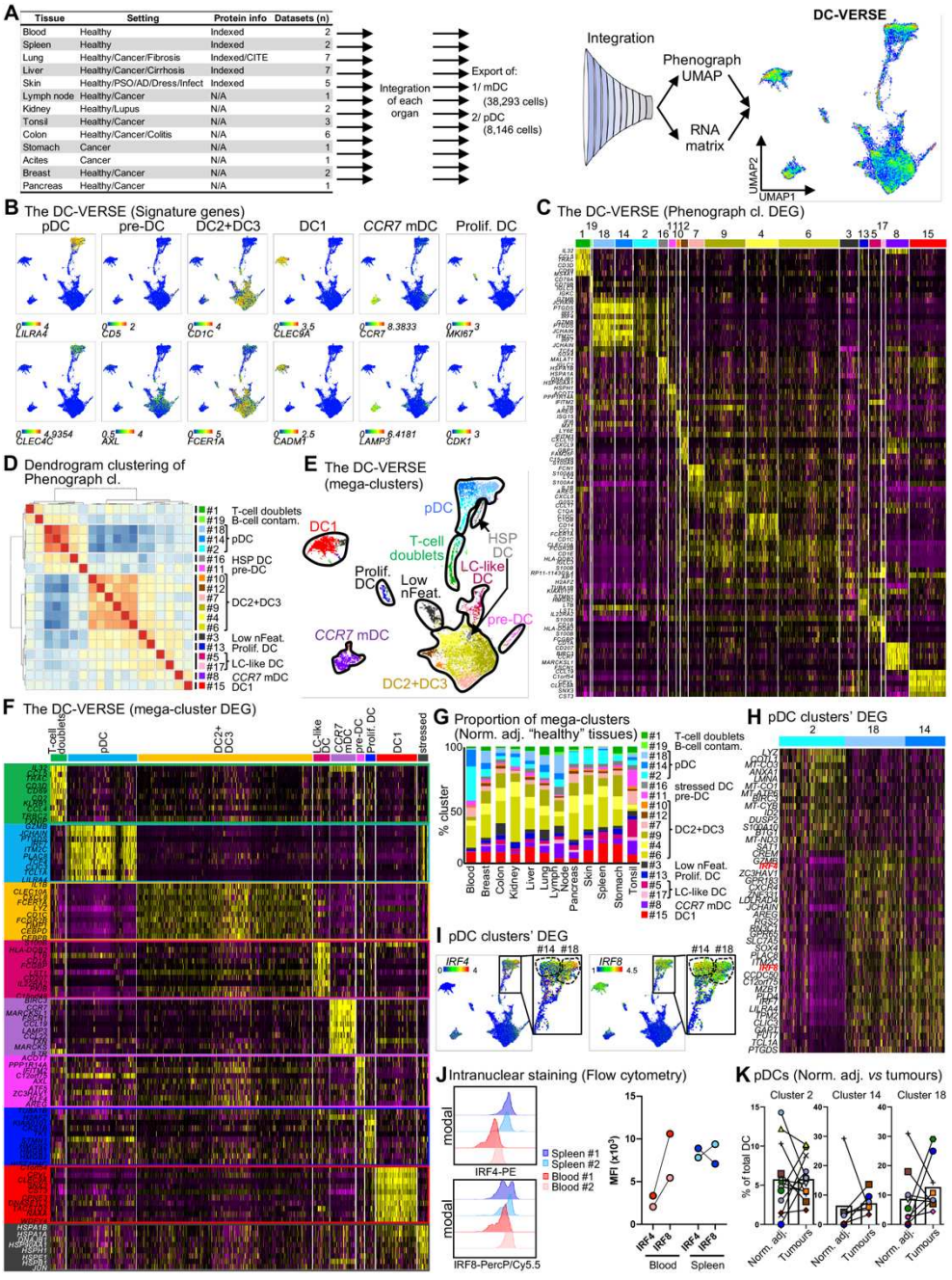

Figure 1. The DC-VERSE reveals signatures of major DC populations across human tissues *(**A**) Summary of the integrated*

*datasets and schematic overview of the meta-analysis. Integration was first performed at the organ level, and pDCs and mDCs were extracted. Extracted cells were then combined and integrated to generate the DC-VERSE. (**B**) Signature genes of major populations (pre-DC, pDC, DC1, DC2+DC3 subpopulations, CCR7 mDCs and Prolif. DCs) are shown on the DC-VERSE UMAP space. (**C**) Heatmap showing the expression of the top 5 DEGs per phenograph clusters. (**D**) Dendrogram clustering of Phenograph clusters. (**E**) UMAP where the Phenograph clusters and corresponding mega-clusters are overlaid. (**F**) Heatmap showing the expression of the top 15 DEGs per mega-clusters. (**G**) Composition of pDC and mDC clusters across normal adjacent "healthy" tissues. (**H**) Heatmap showing DEGs when comparing only pDC clusters. (**I**) Flow cytometry intranuclear staining of IRF4 and IRF8 in the blood and the spleen from different donors. The MFIs are shown in the right panel graphic. (**K**) Percentage of pDC clusters in all integrated datasets between matched normal adjacent and tumours.*

mDC-VERSE

In this study, an effort was made to enhance the resolution of myeloid DCs (mDCs), specifically focusing on DC2- and DC3-related cell subsets and states. The mDCs were extracted from integrated datasets (tissue by tissue) to generate the mDC-VERSE (**Figure 2 and Table S1**). Clusters were defined using Phenograph (Levine et al., 2015), and differentially expressed genes (DEGs) and differentially expressed regulons (DERs) were calculated for all Phenograph clusters (cl. #) (**Figure S1A,B, Table S2 and Table S3**). Cl. #20 consisted of cells with a relatively low nFeature_RNA (Low nFeat., **Figure S1C**), and cl. #15 was a minor population of 118 cells (Minor) that were consequently not examined further (**Figure S1D**).

We examined the expression of well-established signature genes and proteins (using CITE-seq data provided by Maier *et al.*) to identify major DC subsets broadly (**Figure 2A**). Specifically, *TCF4/AXL* transcripts and CD45RA/CD123 protein expression characterized pre-DCs, while *CADM1/CLEC9A* transcripts and CD141/CD26 proteins identified DC1s. *FCER1A/CD1C* transcripts and CD33/CD1c proteins

marked DC2+DC3s, and *CCR7/BIRC3* transcripts along with PD-L1/PD-L2 proteins denoted CCR7-expressing mDCs. Furthermore, *PCNA/MKI67* transcripts identified proliferating mDCs (Prolif. mDC). Notably, cl. #11 cells expressed T-cell specific membrane proteins, which likely represent T/DC cell doublets (Doublets) (**Figure S1E**). Dendrogram clustering was employed to comprehend the relationships among Phenograph clusters, leading to the recognition of twelve mDC mega-clusters (**Figure 2B, Table S2**). We identified regions encompassing previously defined subsets including pre-DCs (cl. #19), DC1s (cl. #8 and #10), DC2s (cl. #12, #13 and #17), DC3s (cl. #1, #4 and #9), *CCR7* mDCs (cl. #14 & #16), proliferating mDCs (Prolif. mDC, cl. #2 and #6) and T/DC doublets (Doublets, cl. #11). The CITE-seq data from Maier *et al.*, allowed us to quantify the expression of CD5 and CD14 proteins and, thus, identify $CD5^+$ DC2s and $CD14^+$ DC3s (Maier et al., 2020). Furthermore, DC2 and DC3 gene signatures from Dutertre *et al.* (Dutertre et al., 2019) confirmed the proper identification of DC2 and DC3 mega-clusters (**Figure 2C** and **Figure S1F-H**). The mDC-VERSE also revealed mDC populations that could not be clearly associated with the major mDC subsets described above, namely *CD207* DCs (cl. #7), *LTB* DCs (cl. #3 and #5) and *IL1B* DCs (cl. #18) (**Figure 2B**). Lastly, although cl. #17 was clustered with DC2s, and its unique gene expression pattern related to IFN-related genes led to its classification as an independent mega-cluster termed IFN-primed DCs (**Figure 2B, Figure S1A**).

The mDC-VERSE establishes conserved DC subsets and states across human tissues

In the exploration of human dendritic cell (DC) subsets and states, the mDC-VERSE framework provided a meticulous analysis, offering insights into their nuanced heterogeneity. Employing sophisticated computational techniques, including Label Transfer (SeuratV4) and cMAP analysis (Lamb et al., 2006), the study meticulously investigated puzzling mDC populations (*CD207*, *IL1B*, *LTB*, and *IFN* DCs), deciphering their categorisation as either distinct cell subsets or states (**Figure 2D,E and Figure S2I**). Both the Label Transfer and cMAP showed that while *CCR7* mDCs appeared as a common maturation

state shared by DC1s, DC2s and DC3s, the *CD207*, *LTB*, *IFN,* and *IL1B* mDC mega-clusters could be a transcriptomic state shared by DC2s and DC3s and will then be referred to DC2+DC3 states from now on.

In addition to finding signature genes for widely recognised mDC subsets (pre-DCs, DC2s, DC3s and DC1s) and state (*CCR7* mDCs), DEGs of mega-clusters also identified genes for the less characterised/well-known DC2+DC3 states such as *LTB* and *LST1* for *LTB* DC2+DC3s; *CD1A*, *CD207* and *HLA-DQB2* for *CD207* DC2+DC3s; *ISG15*, *IFI6*, *IFI44L* and *IFIT3* for *IFN*-primed DC2+DC3s and *AREG*, *IL1B*, *CCL17* and *NFKB1* for *IL1B* DC2+DC3s (**Figure 2F** and **Figure S1J**).

Since DC3s share transcriptomic and phenotypic similarities with monocytes(Dutertre et al., 2019), we aimed to address the potential contamination of monocyte-derived cells. We observed that the monocyte-derived DCs (moDCs) signature was obtained from Gao *et al*. (Gao et al., 2021) mapped mostly within macrophages when overlapped onto the MNP-VERSE (**Figure S1K**) (Mulder et al., 2021). This signature could only be detected within the DC-VERSE with a lower mean expression within the DC3 cluster cl. #1 (**Figure S1K,L**). Moreover, several genes related to monocytes (*C1QA, B, C* or *CD14*) are also identified in the DEGs of DC3s (**Figure S1A**).

When exploring only healthy tissues (mostly normal adjacent to tumours), DC populations were detected in varying frequencies, with some clusters such as *CCR7* mDCs, *LTB* and *CD207* DC2+DC3s detected in tissues but at a low frequency in the blood (**Figure S1M,N**). Note that in the skin datasets, few Langerhans cells were detected and regrouped within the CD207 DC2+DC3 cluster.

DC2+DC3 heterogeneity in humans has also been recognised by Brown *et al*. that described two subsets of $CD1c^+$ DCs in the spleen, namely $CLEC4A^+$ cDC2As (cDC2A_Brown) and cDC2Bs (cDC2B_Brown), these latter being defined as expressing higher levels of *CLEC10A* (CD301) and *CLEC12A* (CD371) transcripts (Brown et al., 2019). To define cDC2A, Brown *et al*. regrouped clusters (cl.), cl.3 and cl.4 that they described in their analysis. Back-mapping Brown *et al*.'s. cl.3 and cl.4 (cDC2A_Brown) on the mDC-VERSE revealed that cl.3 corresponded to *LTB* DC2+DC3s while cells from cl.4 were detected

within $CD5^+$ DC2s (**Figure S1O**). The study of Cheng *et al.* also evaluated the heterogeneity of human DC2+DC3s in various human tumours, describing six DC2+DC3 subsets (Cheng et al., 2021). As these data were not integrated with the initial 40 datasets, we used multimodal reference mapping to project Cheng *et al.*'s DC populations onto the mDC-VERSE as a reference map (Hao et al., 2021). We could observe which mega-cluster these cells were assigned to (**Figure S2A,B**). This method also showed that the mDC-VERSE could filter out cells with a low nFeature_RNA as they mapped to the mDC-VERSE cl. #20 (**Figure S2C**), allowing us to perform a second round of quality control to further identify and exclude low-quality cells for downstream analyses. When examining the mean expression of the top 50 DEGs of all DC2+DC3 mDC-VERSE mega-clusters on the UMAP from Cheng *et al.,* we observed how the populations identified by these authors corresponded to the mDC-VERSE mega-clusters (**Figure S2D,E**) and vice versa (**Figure S2F**). The cDC2_*ISG15* cluster, defined by Cheng *et al.*, corresponded to the *IFN*-primed DC2+DC3s and the cDC2_*FCN1* cluster, defined by Cheng *et al.*, corresponded to DC3s. In turn, cells with the signature of *LTB* DC2+DC3s and of *CD207* DC2+DC3s (both defined within the mDC-VERSE) corresponded to unique subsets of Cheng *et al.*'s cDC2_*CD1A* (**Figure S2E**), highlighting the strength of the mDC-VERSE to identify small discrete populations which might otherwise be missed.

After performing DEG analysis of the mDC-VERSE mega-clusters, we performed a gene regulatory network analysis (SCENIC) to identify mega-cluster-specific regulons common for two datasets [Lung (Maier) and Head & Neck (Cillo)] (Cillo et al., 2020; Maier et al., 2020), which adequately represented the UMAP space (**Figure 2G** and **Table S3**). Regulons included *SOX4* and *KLF3* for pre-DCs, *IRF8*, *KLF8*, *FOXB1*, *HOXA7* for DC1s, *MEF2C* for DC2s, *MAFB*, *CEBPA*, *STAT2* for DC3s, *RXRA* and *RUNX3* for *CD207* DC2+DC3s, *RFX2* for *LTB* DC2+DC3s and *ZEB1*, *IRF4*, *RELB* for *CCR7* mDCs.

To gain insights into these cells' biological processes and functional relevance, we performed pathway analysis for major DC mega-clusters (**Figure 2H** and **Table S4**). We identified pathways including "Integrin signalling" and "mTOR signalling" for *LTB* DC2+DC3s; "IL-10 signalling" and "IL-6 signalling" for *IL1B* DC2+DC3s, "Aryl Hydrocarbon Receptor

(AHR) signalling" and "Dendritic Cell Maturation" for *CCR7* mDCs, "Phagosome formation" and "complement system" for DC3s, and "ERK/MAPK signalling" and "HIF1α signalling" for *CD207* DC2+DC3s.

Given the vast number of recent publications examining DC subsets, various names have been assigned to DC subsets due to a lack of unity between publications, creating confusion within the field (Ginhoux et al., 2022). For example, the denomination 'DC3' was initially used to describe a subset of $CD14^+$ inflammatory DCs (Dutertre et al., 2019), whilst others have used 'DC3' to describe DC that have an apparent transcriptomic alignment to *CCR7* mDCs (Maier et al., 2020), because of the shared expression of transcripts such as *CCR7*, *BIRC3*, *FSCN1* and *LAMP3* among others. Addressing the prevailing challenge of inconsistent nomenclature in the field of dendritic cell research, we sought to align the subsets identified in the mDC-VERSE with the published DEG signatures (**Figure 2I**). This heatmap proposes a nomenclature unification to mDCs, which have been given multiple identities. It also demonstrates that mature 'DC3s' defined by Gerhard *et al.*, and Zilionis *et al.* (Gerhard et al., 2020; Zilionis et al., 2019), mregDCs defined by Maier *et al.*(Maier et al., 2020)*, LAMP3* DCs or *CCR7* DCs identified by Zhang *et al.* and Qian *et al.*, respectively (Qian et al., 2020; Zhang et al., 2019) all shared the gene expression signature of *CCR7* mDCs defined here. Whilst the DC3 signatures [DC3s as defined by Dutertre *et al.* (Dutertre et al., 2019)] could be appreciated, some published signatures are only weakly associated with DC2s or DC3s.

Altogether, the integrative approach used to generate the mDC-VERSE allowed us to appreciate the heterogeneity of mDCs and define universal signatures of their subsets/states, thus offering the possibility to reconcile the different studies that focused on the single-cell transcriptomic analysis of these cells. Next, we set out to unravel the heterogeneity of mDCs further and study their potential association with pathology.

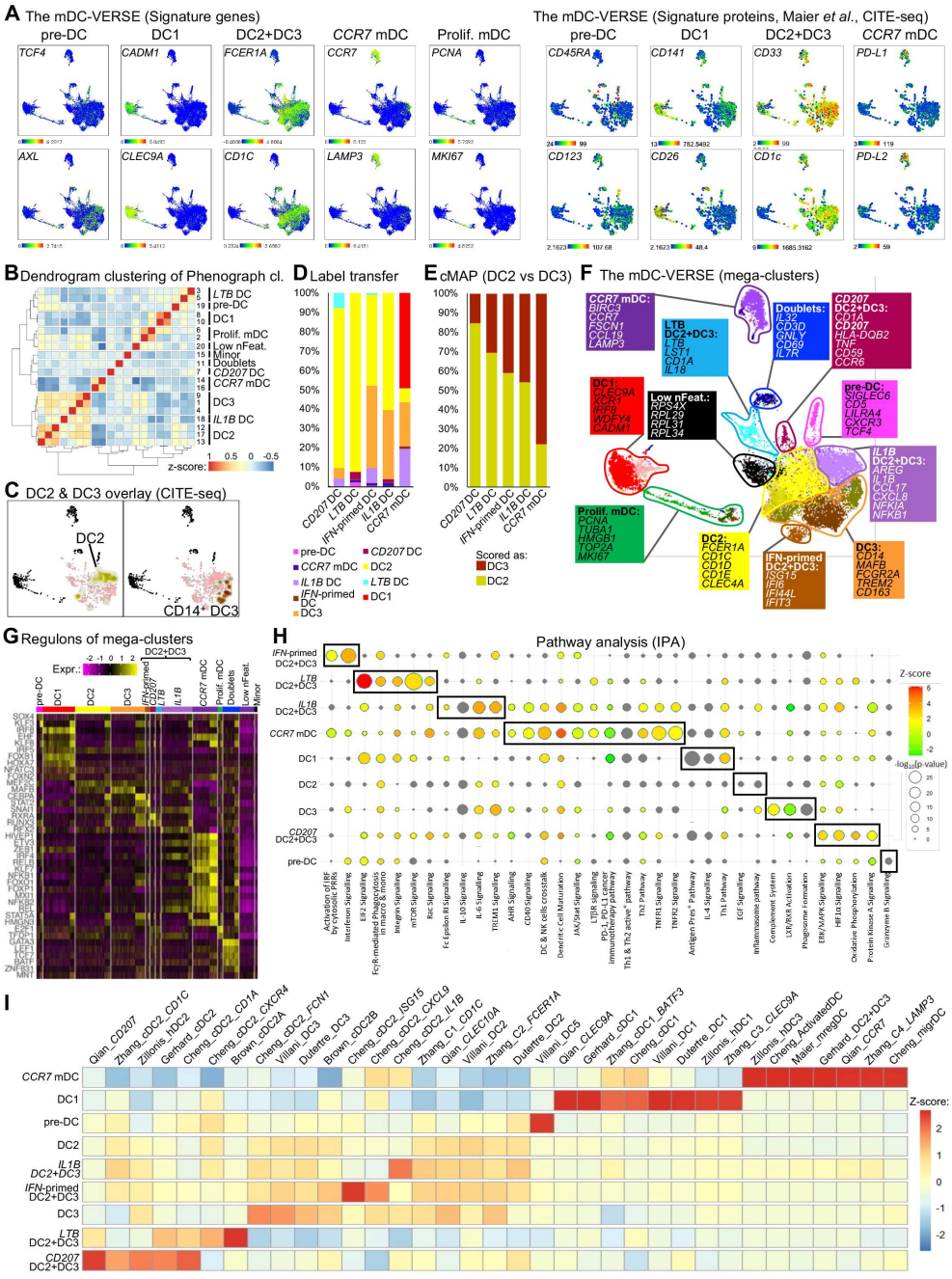

Figure 2. The mDC-VERSE identifies mDC subsets and states across human tissues. *(**A**) Signature genes (from mDC-VERSE) and protein markers (from Maier CITE-seq data) of major DC subsets (pre-DCs, DC1s, DC2+DC3 subpopulations, CCR7 mDCs and Prolif. mDCs) are shown on the mDC-VERSE. (**B**) Dendrogram clustering of Phenograph clusters to define mega-clusters. (**C**) Overlay on the mDC-VERSE of DC2*

*and DC3 cells defined based on CITE-seq CD5 and CD14 protein expression. (**D**) Label Transfer of identified cell states onto the mDC-VERSE. (**E**) cMAP analysis of identified cell states showing their enrichment for DC2 or DC3 gene sets. cMAP permutation p-value < 0.05. (**F**) Annotation of mega-clusters within the UMAP space of the mDC-VERSE. (**G**) Heatmap showing the relative expression levels of differentially expressed regulons (DERs) between mega-clusters common to Lung (Maier) and Head & Neck (Cillo) (Cillo et al., 2020; Maier et al., 2020) cancer datasets. (**H**) Ingenuity Pathway Analysis of mDC mega-clusters. (**I**) Heatmap showing the score of published DC signatures and nomenclature against DC mega-clusters.*

The mDC-VERSE reveals changes in DC distribution across matched normal adjacent tissues and tumours

To assess the significance of the identified dendritic cell (DC) subsets, a comprehensive metadata analysis was conducted, comparing matched normal adjacent tissues with tumours. Initially, DEG analysis were performed between matched normal adjacent tissue and tumour across all mDCs (**Figure 3A,B** and **Table S1**). Notable differentially expressed genes (DEGs), including *SPP1*, *CD14*, *LTB*, *CD1A*, *BIRC3* and *CD207*, were found to be upregulated in tumours, whereas *CLEC9A* (a DC1-specific gene) and *CPVL* were found to be enriched in the normal adjacent tissues. Several of the DEGs corresponded to the mDC-VERSE mega-cluster DEGs, prompting an exploration of their relative proportions across matched normal adjacent tissues and tumours. A global comparison of mega-cluster proportions indicated a potential increase in *CCR7* mDCs, *IFN*-primed DCs, *CD207* and *LTB* DC2+DC3s in tumours (**Figure 3C** and **Figure S3A**). For datasets where tumour localisation was available, normal adjacent tissue, tumour periphery and tumour core had been analysed separately. We observed that *CCR7* mDCs trended to accumulate in the tumour periphery while proliferating mDCs trended to accumulate in the tumour core (**Figure S3B**). Additionally, the ratio of DC3s to DC2s (DC3/DC2 ratio), representing functionally similar but pro-inflammatory counterparts, showed an increasing trend in the tumour core (**Figure S3A,B**). A meta-analysis was then conducted on studies with matched normal

adjacent and tumour across the identified mDC-VERSE mega-clusters, incorporating the predicted clusters from Cheng *et al*., (Cheng et al., 2021) (**Figure 3D** and **Figure S3C,D**). Only studies with at least 8 cells detected were plotted for each cell population. Thus, for datasets with enough cells, this meta-analysis revealed a significant increase of *CD207* DC2+DC3s in tumours where we could identify CD207 DC2+DC3s, while *IFN*-primed DCs, *CCR7* mDCs, the DC3/DC2 ratio and Prolif. mDCs significantly accumulated in most, but not all, tumours (**Figure 3D,E**). Conversely, a significant decrease in DC1s was also observed. Interestingly, when examining the constitution of Prolif. mDCs using Label Transfer (Seurat V4), the frequency of *CD207* DC2+DC3s among Prolif. mDCs exhibited a 10.75-fold increase in the tumour relative to normal adjacent tissue (**Figure 3F**). Moreover, compared to other mega-clusters, *CD207* DC2+DC3s and DC1s comprised a greater percentage of proliferation in the tumour than in their normal adjacent tissue counterpart (**Figure 3G**).

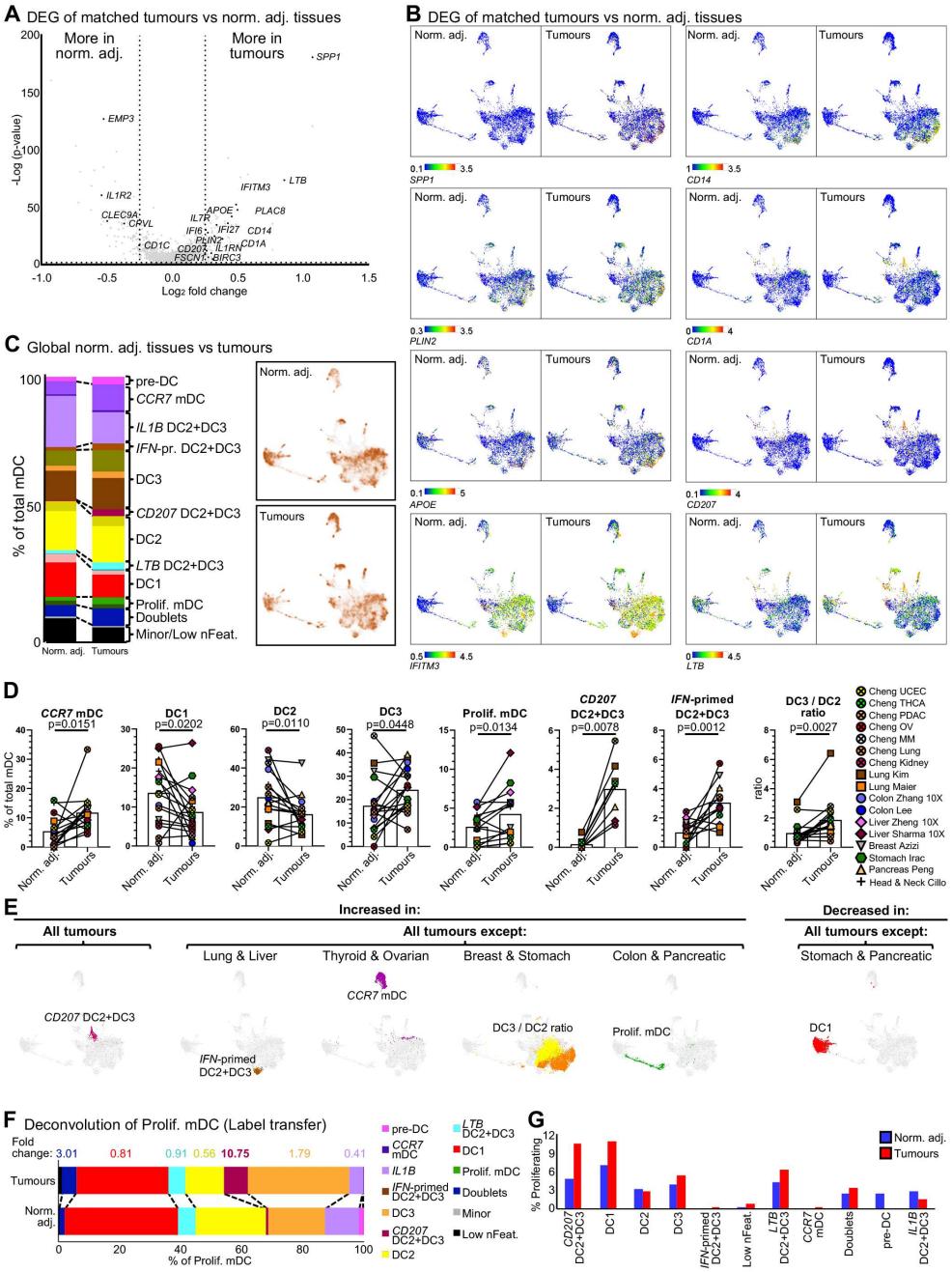

Figure 3. Metadata analysis of mDC populations in cancer. *(**A**) Volcano plot and (**B**) meaningplots of DEGs between globally matched normal adjacent and tumour for all cells included in the mDC-VERSE. (**C**) Bar plot of the percentage of mega-clusters and density plot of global matched normal adjacent and tumour. (**D**) Percentage of each mDC mega-cluster of the mDC-VERSE in all integrated datasets and query datasets (mapped through multimodal reference mapping and*

*annotated with cross symbols) between matched normal adjacent and tumour. (**E**) Overview of all included cancer datasets depicting a change in the distribution of DC populations between normal adjacent and tumour. (**F**) Percentage of DC mega-clusters predicted through Label Transfer (Seurat V4) within the Prolif. mDC mega-cluster with corresponding fold change (Tumour vs normal adjacent tissue). (**G**) Percentage of proliferating cells within each DC mega-cluster in normal adjacent and tumour tissues. P-values were calculated using a Wilcoxon test.*

Flow cytometric evaluation of DC subsets and states in normal adjacent and tumour tissues from non-small-cell lung carcinoma patients

Following the identification of markers unravelling antigen presenting DCs' heterogeneity and the characterisation of their putative relative changes in tumours, a validation study was conducted using multiparametric flow cytometry in normal adjacent tissues and tumours from eight non-small-cell lung carcinoma patients (NSCLC, **Figure 4** and **Table S5**). Among $CD45^+$ leukocytes, mononuclear phagocytes (MNPs) were initially identified, from which we identified $CD123^+$ pre-DC+pDCs, DC1s, DC2+DC3s, and monocyte/macrophages (MoMac) (**Figure 4A** and **Figure S4A**). MNPs were exported and reanalysed, revealing all major MNP subsets (**Figure 4B** and **Figure S4B,C**). The frequencies of pDCs (data not shown), DC1s and total DC2+DC3s were comparable between normal adjacent and tumour tissues (**Figure 4C**). We next focused on specific DC populations, including DC2s and DC3s, where an increase in the percentage of $CD14^+$ DC3s was observed in the tumours of 6 of the 8 patients (**Figure 4D,E**). When looking at total DC3 (including $CD14^-$ DC3s), the DC3 to DC2 ratio was increased in the tumour of 7 of the 8 patients, as previously shown (**Figure 4F**). The mDC-VERSE revealed that *CD207* and *CD1A* were uniquely expressed genes by *CD207* DC2+DC3s. CITE-seq data also indicated that the CD103 protein was expressed on the membrane of all *LTB* DC2+DC3s and some *CD207* DC2+DC3s (**Figure 4G**).

Subsequently, we analysed CD1a, CD207 and CD103 at the protein level to define if cells expressing these membrane proteins correspond to unique subsets of $CD1c^+$ DC2+DC3s or if they correspond to cell "states" that could be acquired by DC2s and/or DC3s (**Figure 4H** and **Figure S4D**). This analysis showed that the *CCR7* mDC state is a shared maturation state of DC1s (*CCR7* DC1s), DC2s (*CCR7* DC2s) and DC3s (*CCR7* DC3s). Similarly, $CD103^+$ *LTB* DCs and $CD207^+$ DCs corresponded to shared phenotypic states of $CD5^+$ DC2s and $CD5^-$ $CD14^{+/-}$ DC3s ($CD103^+$ or $CD207^+$ DC2s or DC3s, respectively) since they did not constitute a specific subset of either DC2s or DC3s. Note that among mDCs, a minor fraction of DC1s was detected within $CD103^+$ cells (**Figure S4E**). Beyond CD5 and CD14, these $CD103^+$ and $CD207^+$ cell states also showed variable expression of other makers commonly expressed by DC3s, such as CD38 and CD11b (**Figure S4F,G**).

Upon comparing normal adjacent and tumour tissues, a significantly increased frequency of *CCR7* DC1 was observed in tumours, whereas the frequencies of *CCR7* DC2+DC3s (and of *CCR7* DC2s or *CCR7* DC3s) were not significantly different (**Figure 4I,J** and **Figure S4H**).

While $CD103^+$ *LTB* DC2+DC3s were not expanded in tumours (**Figure 4K,L** and **Figure S4H**), we confirmed that the frequency of $CD1a^+CD207^+$ DC2+DC3s was increased in the tumour tissue of all lung cancer patients with a fold increase ranging from 1.48 to 209.11 (**Figure 4M,N** and **Figure S4H,I**). Notably, $CD1a^+CD207^+CD5^-$ DC3s showed a more significant increase as compared to $CD1a^+CD207^+CD5^+$ DC2s in the tumour tissues (**Figure S4H**), mirroring the trend to an increased proportion of total DC3s (**Figure 4D,E**).

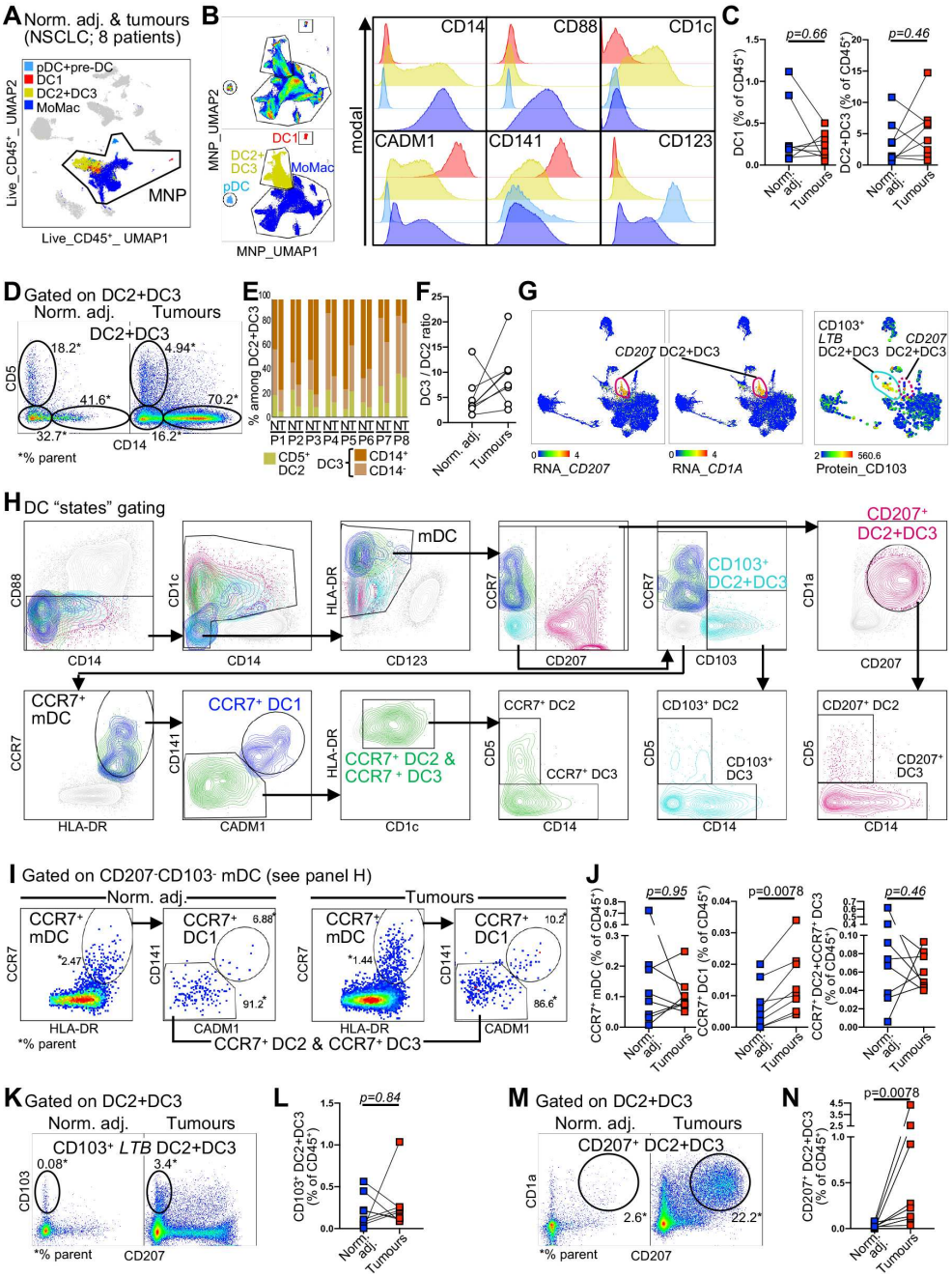

Figure 4. Spectral flow cytometric analysis of DC subsets and states in 8 NSCLC patients. *(**A**) UMAP of singlet, live, CD45⁺ cells from normal adjacent and tumour samples obtained from 8 NSCLC patients. (**B**) UMAP of extracted MNPs showing delineation of DC1s, DC2+DC3s, CD123⁺ DCs (pDCs and pre-DCs, see **Figure S6C**) and monocytes/macrophages (MoMac). (**C**) Percentage of DC1s and DC2+DC3s among total CD45⁺ cells. (**D,E**) Identification and*

*quantification of DC2s and DC3s and (**F**) DC3s/DC2s ratio in normal adjacent and tumour samples. (**G**) RNA expression of CD207 and CD1A and protein expression of CD103 overlayed on the mDC-VERSE. (**H**) Gating strategy starting from MNPs extracted in panel (**B**) to define the various states of mDCs. (**I-J**) Identification and percentage of total CCR7$^+$ mDCs, CCR7$^+$ DC1s and CCR7$^+$ DC2+DC3s among total CD45$^+$ cells. (**K-L**) Identification and percentage of CD103$^+$ LTB DC2+DC3s among total CD45$^+$ cells. (**M-N**) Identification and percentage of CD207$^+$ DC2+DC3s among total CD45$^+$ cells. P-values were calculated using a Wilcoxon test.*

Spatial mapping of DC subsets and states in breast and lung tumours

Following our transcriptomic and phenotypic analyses, the spatial distribution of dendritic cell (DC) subsets defined in the mDC-VERSE was explored within tumour lesions from patients with three triple-negative breast cancer (TNBC) and two estrogen receptor-positive (ER) (**Figure 5A,B** and **Figure S5A,B**). To this end, we reanalysed Visium spatial data of breast cancer tumours (Wu et al., 2021), where we performed z-scoring of mDC transcriptomic signatures identified in the mDC-VERSE. Most DC subsets and states were found in immune-enriched/tertiary lymphoid structure (TLS) niches, including CD207 DC2+DC3s. CD207 DC2+DC3s, and to a lesser extent, IL1B DC2+DC3s, were also detected in the "invasive cancer+stroma" niche.

To have a more refined understanding of the *in situ* localisation of the various subsets and states of DCs at the single-cell resolution and to define their localisation in regard to the other immune subsets, breast and lung tumours were analysed using Merscope data (Vizgen) (Chen et al., 2015). Following the delineation of cells within tissue cross-sections (segmentation) and the quantification of their transcripts, we carried out a principal component analysis (PCA) followed by UMAP projection using principal components (PCs) selected for their high loading with immune-related genes (**Figure S5C)**. This identified major cell populations, including *EPCAM*-expressing tumour cells, fibroblasts, endothelial cells and *PTPRC* (CD45)-expressing immune cells. Immune

cells were next extracted and analysed again as described above, revealing some B-cells, subsets of T-cells (*CD4* T-cells, *CD4* &*FOXP*3 -expressing regulatory T-cells (Tregs) and *CD8* T-cells), monocytes, macrophages and DC populations, including *CLEC4C*(CD303) *& IL3RA*(CD123) -expressing pDCs (**Figure S5D)**. Notably, *CD207* DC2+DC3s expressed the highest quantity of *TNF* transcripts among all immune cells (**Figure S5D**), consistent with our observation from the mDC-VERSE where *TNF* was one of the top DEGs of *CD207* DC2+DC3s (**Figure 2F**). To improve the resolution of mDCs, we extracted mDCs for reanalysis, allowing us to identify *CCR7* mDCs, DC1s, *CD207*$^{-}$ and *CD207*$^{+}$ DC2+DC3s (**Figure S5C-E)**.

The above-mentioned cell populations were then mapped onto the lung and breast tumour cross-sections (**Figure S5F**), in which insets were defined to visualise better the localisation of each immune cell population (**Figure 5C,D**). While pDCs, *CCR7* mDCs and DC1s were detected within the tumour stroma in close contact with B-cells and T-cells, *CD207* DC2+DC3s were located within tumour nests (surrounded by tumour cells) in both cancers. Besides the *CD207* DC2+DC3s, a few Tregs and CD8^{+} T-cells were observed within tumours nest in both cancers.

To validate the observation of CD207^{+} DC2+DC3s' localisation within the tumour nests in a greater number of patients, immunohisto-fluorescence (IHF) analyses were conducted on formalin-fixed paraffin-embedded (FFPE) non-small-cell lung carcinoma (NSCLC) tumours obtained from 16 patients where CD207, CD3, CD8 and CD20 proteins were stained simultaneously (**Figure 5E-J** and **Figure S5G**). By re-analysing our spectral flow cytometry data from **Figure 4**, we confirmed that among live cells of the NSCLC tumour, CD207 expression was only observed within CD45^{+} cells and that it was solely expressed by CD1a^{+}CD1c^{+}HLA-DR^{+}HLA-DP^{+} cells (all markers of CD207^{+}CD1a^{+} DC2+DC3s) and that it was not expressed by CD88^{+} cells (monocyte/macrophages), CD3^{+} cells (T-cells), CD16^{+} cells (NK cells, monocyte/macrophages) nor by CD19^{+}CD20^{+} cells (B-cells) (**Figure S4J**). Thus, the CD207 membrane protein staining is sufficient to identify CD207^{+} DC2+DC3s specifically. Normal adjacent and tumour regions were defined by a pathologist (G.G.) and are delineated in green and brown, respectively (**Figure 5E,F**).

Quantification of $CD207^+$ cells ($CD207^+$ DC2+DC3s) confirmed the significantly higher density of $CD207^+$ DC2+DC3s in the tumour compared to the normal adjacent lung (**Figure 5F,G**). TLSs were detected (inset #2), and $CD207^+$ DC2+DC3s appeared to be excluded from these structures (**Figure 5H** and **Figure S5G**). Within the tumour, $CD3^+$ T-cells (including $CD3^+CD8^+$ T-cells) and $CD20^+$ B-cells predominantly accumulated in the tumour stroma, while $CD207^+$ DC2+DC3s were primarily detected in tumour nests, particularly in glandular structures (**Figure 5H,I** and **Figure S5G**). The Halo10 software allowed us to perform an unsupervised delineation of the stroma and tumour area only in 13 of the 16 stained cross-sections. Quantitative analyses confirmed the significantly higher density of $CD207^+$ DC2+DC3s in the tumour nests compared to the tumour stroma, while $CD3^+CD8^+$ T-cells were accumulating more in the tumour stroma than in the tumour nests (**Figure 5I,J**).

Thus, these data not only confirmed the intratumoral accumulation of $CD207^+$ DC2+DC3s but also allowed us to observe that these cells were embedded in between tumour cells, while the other DC populations, as well as T and B-cells, were mostly detected within the stroma.

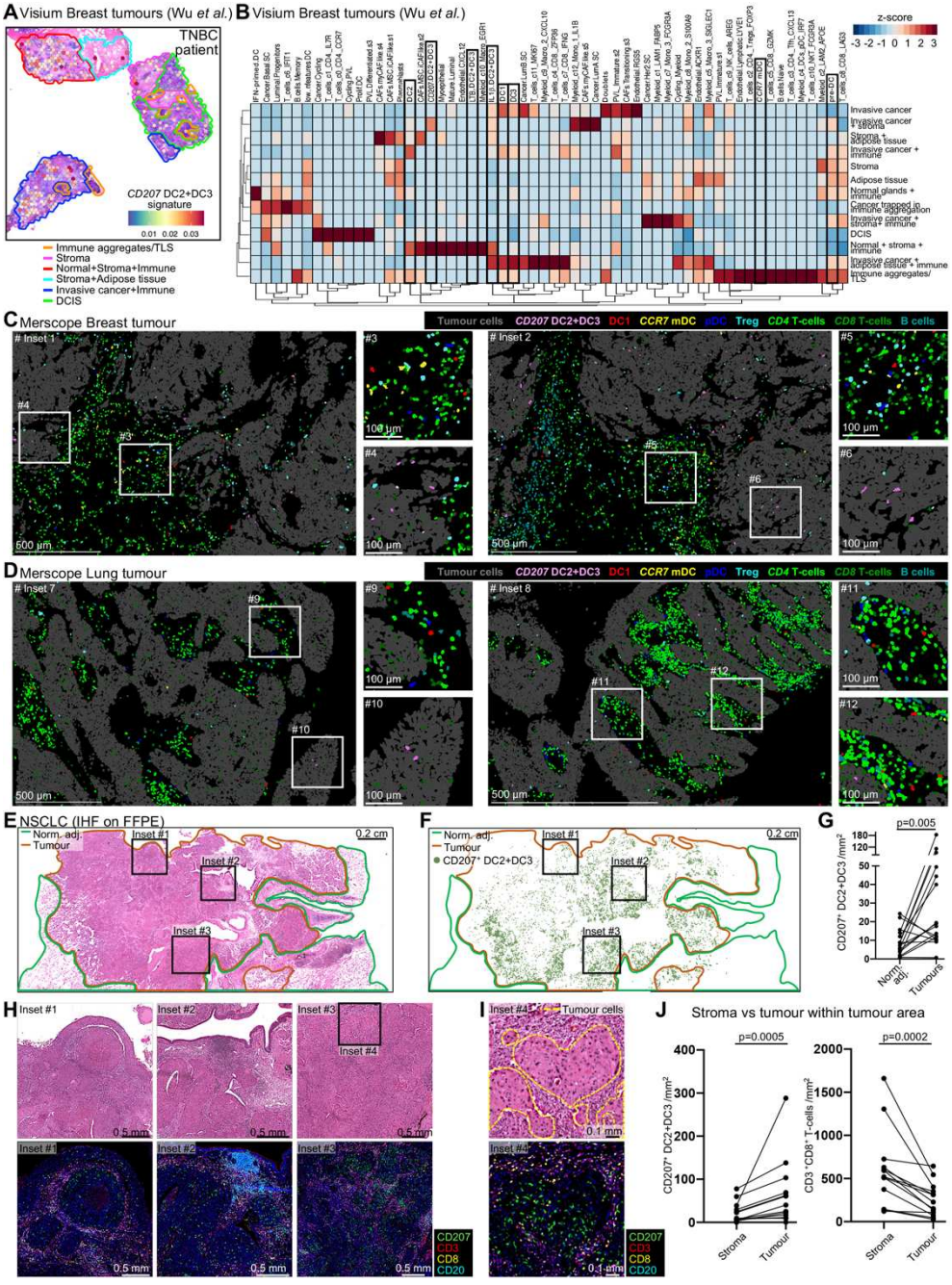

Figure 5. Spatial analysis of DC subsets and states in lung and breast tumours. *(**A**) Visium spatial transcriptomic profiling of TNBC breast tumours was initially published by Wu et al. (Wu et al., 2021) outlining various tissue compartments in addition to spots showing the scaled median enrichment of CD207 DC2+DC3's signature, overlayed on the Hematoxylin and Eosin (H&E) stainings. DCIS = Ductal*

*Carcinoma in situ. (**B**) Heatmap depicting the correlation of both immune and non-immune cell types within tissue niches. Certain non-immune populations were mapped using the nomenclature and signatures from the study of Wu et al. (**C-D**) Visualisation of insets defined in **Figure S5F** of tumour cells and immune cells in (**C**) breast and (**D**) lung tumour cross-sections using the Merscope visualiser (Vizgen). (**E-F**) Visualisation of a full NSCLC FFPE cross-section where normal adjacent tissues and tumour regions are delineated by a green and brown line, respectively, and where insets #1 to #3 magnified in (**H**) are depicted. (**E**,**F**) Visualisation of (**E**) H&E stainings or of (**F**) the spatial mapping of CD207$^+$ cells (CD207$^+$ DC2+DC3s) of the same tumour cross-section is shown. (**G**) Density of CD207$^+$ DC2+DC3s in normal adjacent lungs and the tumour regions from the 16 NSCLC tumours analysed. (**H**) Magnified insets defined in (**E-F**) are shown. (**I**) H&E stainings (upper panels) and the multiplexed fluorescent image (middle panel) from inset #4 [defined in (**H**)] are shown. The yellow dotted line delineates the tumour glandular areas from the tumour stroma. (**J**) Density of CD207$^+$ DC2+DC3s and of CD3$^+$CD8$^+$ T-cells from 13 of the 16 NSCLC tumours that could be analysed for tumour vs stroma regions. P-values were calculated using the Wilcoxon paired non-parametric test in (**G**) and (**J**).*

CD207 DC2+DC3s are associated with an unfavourable outcome in cancer

Since mDCs are professional antigen-presenting cells that can prime naïve T-cells or reactivate memory T-cells, we explored the potential relationship of mDCs with T-cells. To address this, we mapped the breast cancer dataset from Bassez *et al*. (Bassez et al., 2021), where T-cell clonality was evaluated before and after anti-PD-1 therapy onto the mDC-VERSE (using multimodal reference mapping (Hao et al., 2021), **Figure 6A-C** and **Figure S6A**). Contrary to *CCR7* mDCs, *IFN*-primed DC2+DC3s and DC1s, the percentage of *CD207* DC2+DC3s among total DCs increased only in tumours of patients without a clonal T-cell expansion (**Figure 6A** and **Figure S6B**). Interestingly, T-cell clonal expansion was only observed in patients with a DC1 to *CD207* DC2+DC3 ratio >1 (both pre-and post-treatment) (**Figure 6B**).

However, T-cell clonality quantification requires single-cell TcR-sequencing, which is not used routinely due to technical limitations. If validated in other cohorts, the DC1s to CD207 DC2+DC3s ratio could become a means to predict T-cell clonality within tumours. Further analysis correlated mDC-VERSE populations against T_{EMRAs}, T_{RMs} and total $CD8^+$ T-cells. This revealed that CD207 DC2+DC3s exhibited a negative correlation with *CD8* T-cells' frequency and showed a significant inverse correlation with resident memory *CD8* T-cells (T_{RMs}) **(Figure 6C)**, specifically in patients without T-cell clonal expansion. This trend was extended to lung tumours scRNAseq data from Leader *et al.* (Leader et al., 2021), where the percentage of *CD207* DC2+DC3s but not that of the other DC populations, trended to be higher in patients with a low frequency of *CD8* T_{RMs} (**Figure 6D** and **Figure S6C**). We also observed a significant positive correlation between the frequencies of DC1 and *CD8* T_{RMs} (**Figure S6C**). Additionally, within the Bassez *et al.* breast cancer data, *CD207* DC2+DC3s strongly correlated with effector memory T-cells that re-express CD45RA (T_{EMRAs}), which are terminally differentiated senescent and hypofunctional cells (Reading et al., 2018) (**Figure 6C**). Reanalysing our flow cytometry data from **Figure 4**, we also observed that the frequencies of $CD207^+$ DC2+DC3s significantly negatively correlated with those of $CD8^+$ T-cells but not with that of $CD4^+$ T-cells, while no correlation was observed between the other DC populations and T-cell subsets (**Figure 6E** and **Figure S6D**).

To confirm these observations in other datasets, bulk RNA-seq data from breast (BRCA) and lung (LUAD) adenocarcinoma patients obtained from The Cancer Genome Atlas Program (TCGA) were analysed (TCGA; **Figure 6F** and **Table S6**). DC population signatures were obtained from the mDC-VERSE, and other signatures were from the study of Nalio Ramos *et al.* (Nalio Ramos et al., 2022). In both the BRCA and LUAD cohorts, among all mDC signatures, the *CD207* DC2+DC3 signature showed the most negative correlation with T-cell subset signatures (*CD8* T-cells, *CD8* T_{RMs}, exhausted T-cells and only for LUAD, Tregs) and with the DC1 signature. Furthermore, among the different T-cell subsets, the *CD8* T_{RM} signature showed the most negative correlation with the *CD207* DC2+DC3s.

Finally, we further explored cohorts of patients whose tumours were sampled and analysed by bulk RNAseq before receiving an immune checkpoint blockade treatment (Lánczky and Győrffy, 2021) to evaluate the prognostic value when using the gene signatures of major DC populations (**Figure 6G** and **Figure S6E**). While the mean expression of DC1s (*XCR1*, *CLEC9A*) and *CCR7* mDCs (*LAMP3*, *BIRC3*) gene signatures correlated with a statistically significant increase in overall survival (OS), the mean expression of *CD207* DC2+DC3s (*CD207*, *CD1A*) gene signature was associated to a statistically significant decrease in OS. There was also a statistically significant increase in OS when looking at individual defining genes for each DC population (*XCR1/CADM1/CLEC9A* for DC1, *LAMP3/BIRC3/MARCKS* for *CCR7* mDCs, and *CD1C*, a pan DC2+DC3 gene). Since the *CD1C* pan DC2+DC3 gene was significantly associated with an increased OS, this analysis points out that the "*CD207*" state of DC2+DC3s was specifically of poor prognosis (**Figure S6E**). Notably, the ratio of DC1 to CD207 DC2+DC3 transcripts (*XCR1/ CD207*) was predictive of patient survival (**Figure 6G**), consistent with the observations made regarding the expansion of T-cell clonality (**Figure 6B**). Altogether, this analysis suggests that patients with low *CD207* DC2+DC3 and high DC1 and *CCR7* mDC tumour infiltrates respond better to ICB treatment and vice versa.

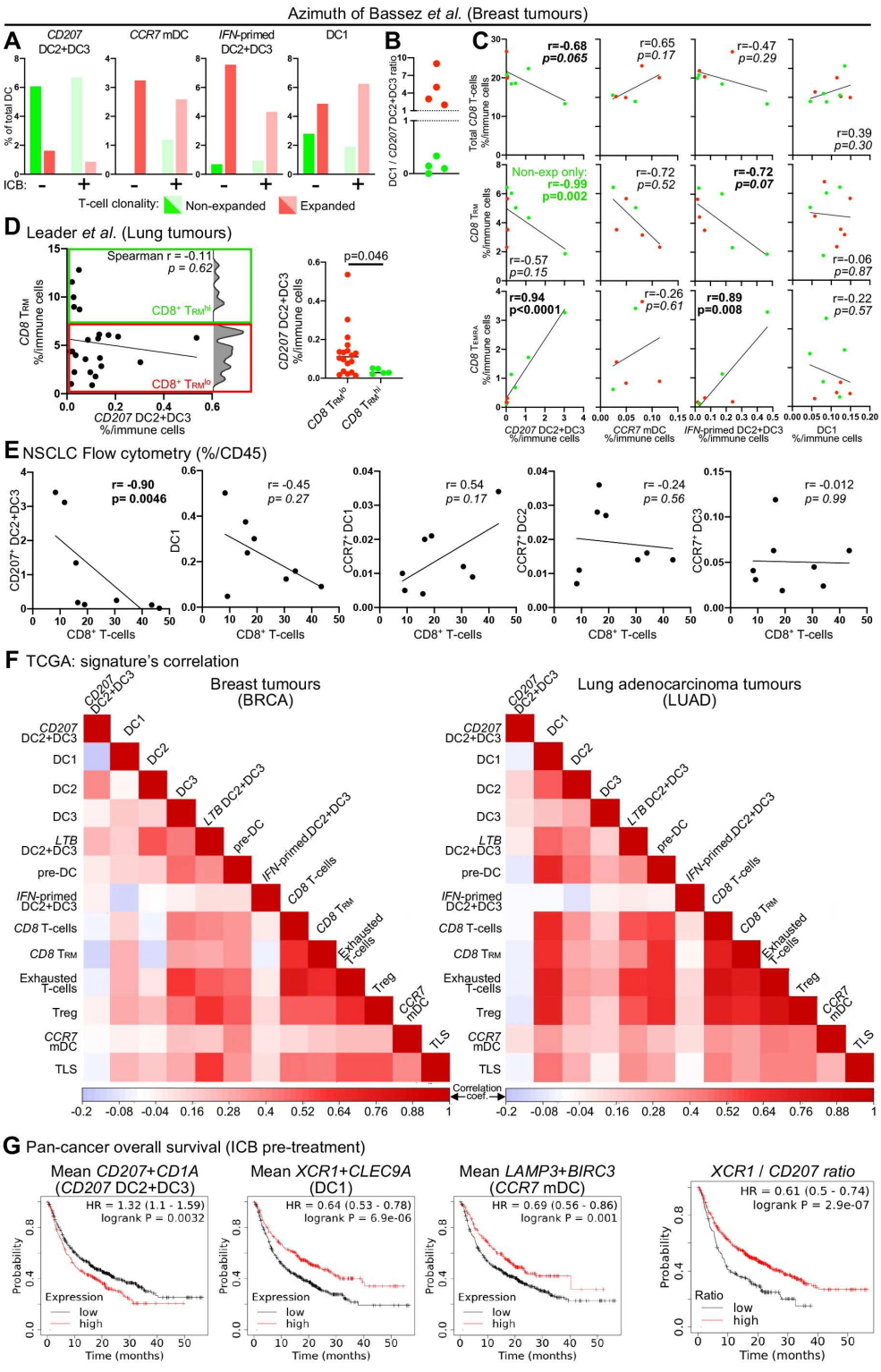

Figure 6. Characterisation of the pathophysiological involvement of mDC populations in human cancer patients. *(**A**) Percentage of*

*predicted mega-clusters by multimodal reference mapping of query data from breast cancer patients (Bassez et al., 2021) categorised by T-cell clonality and treatment status (anti-PD-1 therapeutic monoclonal antibody = Immune Checkpoint Blockade = ICB). (**B**) DC1 to CD207 DC2+DC3 ratio for patients from Bassez et al. (Bassez et al., 2021), with at least one CD207 DC2+DC3. (**C**) Pearson correlations between the percentage among PTPRC(CD45)-expressing immune cells of CD207 DC2+DC3s, CCR7 mDCs, IFN DC2+DC3s, or DC1s against total CD8 T-cells (top), CD8 T_{RMs} (middle) or CD8 T_{EMRAs} (bottom). (**D**) Correlation between the frequencies of CD207 DC2+DC3s and CD8 T_{RMs} among immune cells in lung tumours within the Leader et al. scRNAseq data (Leader et al., 2021). (**E**) Pearson correlation between the frequencies among $CD45^+$ cells of CD207 DC2+DC3s, DC1s, $CCR7^+$ DC1s, $CCR7^+$ DC2s and $CCR7^+$ DC3s against $CD8^+$ T-cells from flow cytometry analysis of tumours cells obtained from 8 NSCLC patients. (**F**) Correlation map of DC population signatures (defined in the mDC-VERSE) and of other signatures obtained from Ramos et al. (Nalio Ramos et al., 2022) in the BRCA (Breast) and the LUAD (Lung) adenocarcinoma TCGA datasets. (**G**) Kaplan-Meier plot of the overall survival (OS) of patients with different cancers whose tumours were sampled and analysed by bulk RNAseq before ICB treatment. Patients were separated based on the high or low expression of mDC populations' mean gene signatures (left and middle panels) or the ratio of XCR1 to CD207 transcripts (right panel). P-values were calculated using a Wilcoxon non-parametric paired test. Correlations were evaluated using the Pearson correlation (r) with two-tailed test.*

DISCUSSION

Similar to our previous study investigating monocyte and macrophage heterogeneity (Mulder et al., 2021), we provide an integrated analysis across multiple tissues in various pathologies to build an in-depth overview of human DC heterogeneity. This analysis took advantage of 40 scRNAseq datasets, along with flow cytometry validation, CITE-seq protein expression data, spatial genomics and immunohisto-fluorescence, and various analytical pipelines to help define a robust characterisation of human DCs.

The DC-VERSE can be useful for the scientific community to map all DCs from any scRNAseq dataset using multimodal reference mapping, but a more refined mapping of mDCs will be obtained using the mDC-VERSE. Such an approach allows the mapping of different cells, including HSP-expressing DCs that could correspond to stressed cells, cells with low viability, B-cell contaminants, and T-cell doublets. Importantly, the DC-VERSE has provided "universal" DC population signatures applicable to defining these cells within any scRNAseq dataset. The DC-VERSE also revealed differences between blood and tissue pDCs, the latter presenting a higher IRF4 transcript. Such differences, together with the other DEGs, could also help identify blood-derived pDCs within tissue scRNAseq datasets.

By integrating a vast number of cells based on their transcriptome and incorporating protein expression data (CITE-seq and indexed-FACS data), the mDC-VERSE revealed an unprecedented level of resolution of discrete cell subsets/lineages as well as transcriptomic/phenotypic states that the different subsets/lineages of DC2s and DC3s can share. For example, the CITE-seq data of Maier *et al.* allowed us to confirm the identification of DC2s and DC3s by overlaying the expression of CD5 and CD14 proteins. This CITE-seq data also helped us to define that *LTB* DC2+DC3s, and to a lesser extent, CD207 DC2+DC3s, expressed CD103 protein at their membrane, information that was used to detect and quantify $CD103^+$ *LTB* DC2+DC3s by flow cytometry.

Our integrative approach also allowed us to better appreciate the heterogeneity of the cDC2A_Brown defined in the study of Brown *et al.* (Brown et al., 2019). Indeed, when mapping cDC2A_Brown in the

mDC-VERSE, we observed that these cells were composed of *LTB* DC2+DC3s and $CD5^+$ DC2s, while cDC2B_Brown overlapped with DC3s. Furthermore, cDC2A_Brown was described by Brown *et al.,* to comprise two clusters (Brown clusters 3 and 4). When back mapping Brown clusters 3 and 4 onto the mDC-VERSE, we observed that Brown cluster 3 overlapped with *LTB* DC2+DC3s while Brown cluster 4 overlapped with DC2s, highlighting that our approach allowed us to delineate DC subsets with a higher resolution. Cheng *et al.*, also examined DC2 and DC3 heterogeneity by scRNAseq (Cheng et al., 2021). The "*CD1A* DC2*s*" cluster from Cheng *et al*., was in fact, composed of the *LTB* and *CD207* DC2+DC3 populations, which had not been appreciated in their study, most probably due to the low abundance of these cells. Within the DC-VERSE, LC-like DCs also comprised *CD207* DC2+DC3s that accumulated in tumours and *LTB* DC2+DC3s that did not. These two cell states could only be defined when we analysed only mDCs (mDC-VERSE), pointing out that reducing the global variance of the dataset by analysing less heterogeneous cells makes it possible to define discrete cell subsets and states.

The increasing number of scRNAseq studies has resulted in various names assigned to DC populations that share strong similarities, which calls for a nomenclature unification. DC3s were initially proposed as a subset of $CD1c^+$ DCs harbouring pro-inflammatory $CD14^+$ cells (Bourdely et al., 2020; Dutertre et al., 2019). Despite these observations, the term "DC3" has also been used to describe cells (Di Pilato et al., 2021; Gerhard et al., 2020; Zilionis et al., 2019), that have an obvious transcriptomic alignment to *CCR7* mDCs (Di Pilato et al., 2021; Maier et al., 2020; Zheng et al., 2017). Consequently, using the term "DC3" to describe these two fundamentally different populations can be confusing for researchers, especially since $CD5^-CD14^{+/-}$ DC3s correspond to a cell subset while *CCR7* mDCs correspond to a state shared by DC1, DC2s and DC3s (Ginhoux et al., 2022). To resolve this, we showed how published signatures aligned with the DC populations identified in the mDC-VERSE. For example, the various published nomenclature assigned to *CCR7* mDCs included mregDC/migratory/activated/*LAMP3*/*CCR7*/"DC3". Since the mDC-VERSE considers several datasets across various diseases and tissues, our analysis allows for a comprehensive analysis of mDC

heterogeneity.

In our meta-analysis, we particularly focused on the changes of mDC heterogeneity between normal adjacent and tumour tissues and observed genes such as *SPP1*, which was highly expressed in tumour tissues, mirroring findings also observed in monocytes and macrophages (Mulder et al., 2021). We also revealed a downregulation of genes, such as the DC1-specific *CLEC9A* gene, that suggests a reduction of DC1s' density within human tumours (Kvedaraite and Ginhoux, 2022). This was in contrast to $CCR7^+$ DC1s (but not of $CCR7^+$ DC2s nor $CCR7^+$ DC3s), whose frequency, evaluated by flow cytometry, was increased in the tumour of all the lung cancer patients assessed as compared to their matched normal adjacent lung tissue. Recently, an enrichment of "ISG^+ DC2s" was observed in the tumours of mice, which efficiently activate $CD8^+$ T-cells, thus promoting anti-tumour immunity (Duong et al., 2021). We also identified *IFN*-primed DC2+DC3s in human tumours, which were increased in most cancers studied when comparing tumours to normal adjacent tissues. Additionally, the expansion of *CCR7* mDCs and DC3s has been reported in lung cancer patients (Leader et al., 2021; Maier et al., 2020), which we extended to several other cancers.

While Leader *et al*. observed an expression of *CD1A* and *CD207* transcripts by total tumour DC2+DC3s, we could delineate $CD207^+CD1A^+$ DC2+DC3s (*CD207* DC2+DC3s), which correspond to a tumour-associated state common to DC2s and DC3s. This population was of significant interest as its intratumoral expansion was observed in the mDC-VERSE with further validation by spectral flow cytometry and IHF in NSCLC patients. Our spectral flow cytometry analysis also confirmed that the $CD103^+$ *LTB* and $CD207^+CD1a^+$ DC2+DC3 populations could correspond to cellular states rather than ontogenically distinct cell subsets (or lineage) since they both exhibited DC2 ($CD5^+$) and DC3 ($CD5^-CD14^{+/-}$) phenotypes. This is similar to *CCR7* mDCs, which we also described by flow cytometry as a mature (potentially migratory) state shared by DC1s, DC2s and DC3s.

Our investigation into the spatial distribution of DC subsets within

tumour tissues has yielded crucial insights into the role of *CD207* DC2+DC3s. Visium spatial transcriptomic analysis of human breast tumours suggested that *CD207* DC2+DC3s were detected within the tumour region, contrary to most other immune cells, including the other DC subsets and states detected within normal tissue or immune-rich niches. To corroborate these observations at the single-cell resolution, we analysed one lung and one breast cancer patient using the Merfish technology (Merscope, Vizgen). As mentioned above, cell segmentation followed by a sequential dimensionality reduction approach allowed us to define tumour and stroma niches within the two tumours analysed, as well as major immune cell populations (B-cells, major T-cell subsets) and most DC subsets and states that we had defined in the DC- and mDC- VERSEs. This revealed the spatial localisation of all these cells, including discrete DC populations, whose identification usually requires multiple markers. In the two tumour cross-sections, like most lymphocytes, all DC subsets and states, except for the *CD207* DC2+DC3s, were detected in greater abundance within the tumour stroma. *CD207* DC2+DC3s were the only DCs detected in greater abundance within the tumour nests (surrounded by tumour cells). To validate this observation, we carried out 4-colour IHF stainings of 16 lung adenocarcinoma patients, focusing on $CD207^+$ DC2+DC3s. Our IHF data also confirmed a significant intratumoral accumulation of $CD207^+$ DC2+DC3s, specifically within the tumour glandular areas of patients' tumours (tumour nests), while B and T lymphocytes, including $CD8^+$ T-cells, were significantly accumulating in the tumour stroma.

Furthermore, our study has delved into the potential implications of *CD207* DC2+DC3s in the context of immunotherapy. By analysing data from immune checkpoint blockade-treated breast cancer patients, we observed that *CD207* DC2+DC3s, contrary to *CCR7* mDCs and DC1s, were predominantly enriched in patients without T-cell clonal expansion. Together with the finding that *CD207* DC2+DC3s have a negative correlation with CD8 T-cells in ICB scRNAseq, our flow cytometry data and TCGA analysis suggest a role in limiting T-cell clonality. However, it cannot be ruled out that these are independent events requiring further investigation. Furthermore, *CD207* DC2+DC3s inversely correlate with $CD8^+$ T_{RM} cells, which accumulate in various

tumours and are associated with improved disease outcomes and survival (Park et al., 2019). Conversely, these DCs strongly positively correlated with $CD8^+$ T_{EMRA} cells, which are senescent/hypofunctional cells (Reading et al., 2018). Two hypotheses could explain why *CD207* DC2+DC3s, but not any other DC subset or state, inversely correlated with $CD8^+$ T_{RMs}: (1) Many studies have demonstrated that TGF-β can induce a $CD1a^+CD207^+$ Langerhans cell-like phenotype from blood $CD1c^+$ DCs and a $CD103^+$ T_{RM}-like phenotype from $CD103^-$ T-cells. These two cell types could compete for TGF-β, a phenomenon which could explain their inverse correlation; (2) The combined negative and positive correlations with T_{RMs} and T_{EMRAs}, respectively, make it possible to hypothesise that *CD207* DC2+DC3s could favour the progression of $CD8^+$ T-cells towards the T_{EMRA} state to the detriment of T_{RMs} through a mechanism that we haven't identified in our study. These data provide potential therapeutic targets in favour of reducing the abundance of *CD207* DC2+DC3s. Furthermore, *CD207* DC2+DC3s could also serve as a prognostic factor alongside DC1s as the ratio of these cells predicted whether patients would develop a T-cell clonal expansion, but this will require further investigation in larger prospective cancer patient cohorts.

In summary, our study offers a comprehensive analysis of human DC heterogeneity, integrating diverse datasets and techniques to elucidate their roles in health and disease. The DC-VERSE and mDC-VERSE platforms provide valuable resources for researchers, enabling a deeper understanding of DCs and their implications for immunotherapy strategies. By providing an online tool for exploration, unifying nomenclature and shedding light on the spatial distribution and potential prognostic significance of specific DC subsets, our study paves the way for further research and targeted therapeutic interventions in the realm of dendritic cell biology.

Limitations of the study:

The DC-VERSE and mDC-VERSE are generated based on integrating various datasets, which comes naturally with the limitation of single-cell analyses. Since the study was performed using a limited number of datasets based on availability at the point of analysis, these VERSEs could be improved by including newer datasets that have new cancer types and other disease datasets. The multimodal reference mapping algorithm makes it possible to overcome this feature by using these VERSEs as reference maps to query the new, non-integrated datasets. Additionally, the inverse correlation of *CD207* DC2+DC3s and T-cell clonality observed in the study was restricted to one dataset, requiring further exploration and validation.

ACKNOWLEDGMENTS

We thank L. Robinson of Insight Editing London for critical review and editing of the manuscript; We thank Yoan Velut for providing the immunohisto-fluorescence and the cell imaging and flow cytometry platform (CHIC) from Centre de Recherche des Cordeliers for their help on this study; This work was supported by INSERM, Sorbonne Université, Université de Paris, Ligue Contre le Cancer (Equipe labellisée), CARPEM (Cancer Research for Personalized Medicine) programme of the Sites Integrés de Recherche sur le Cancer (SIRIC), LabeX Immunooncology; F.G. is an EMBO YIP awardee and is supported by Singapore Immunology Network (SIgN) core funding as well as a Singapore National Research Foundation Senior Investigatorship (NRFI) NRF2016NRF-NRFI001-02 and the Foundation Gustave Roussy. C.A.D. is an INSERM researcher supported by INSERM.

AUTHOR CONTRIBUTIONS

Experiments, K.M., W.T.K., M.G, A.A.P., A.C., T.J., E.P., L.R., A.B., S.K. and A.G.G.; Data analysis, K.M. W.T.K., M.G, A.A.P., A.C., G.G., C.P., Q.B., E.L., A.A.A., G.D., G.P., G.A., R.D. and C.A.D.; Providing human NSCLC samples: A.G.G. and L.Z.; Providing human NSCLC FFPE blocks: V.T.D.M.; Providing Breast cancer Visium spatial transcriptomic data, A.S.; Generating, providing and segmentation of Merfish data: L.H., T.W., J.H. and G.E.; Establishment of the publicly available online DC-

VERSE and mDC-VERSE, M.D.; Writing of the manuscript, K.M., W.T.K., A.A.P., F.G. and C.A.D.; Online cellXgene VERSEs: M.D.; Intellectual input, C.S.F, W.H.F., A.B.; Project supervision, F.G. and C.A.D.; Study conceptualisation, F.G. and C.A.D.

DECLARATION OF INTERESTS

Florent Ginhoux and Charles-Antoine Dutertre are co-inventors of a patent related to the findings described in this manuscript.

STAR METHODS

LEAD CONTACT

Further information and requests for resources and reagents should be directed to and will be fulfilled by the Lead Contacts, Charles-Antoine Dutertre (charles-antoine.dutertre@inserm.fr) and Florent Ginhoux (Florent_Ginhoux@immunol.a-star.edu.sg).

DATA AND CODE AVAILABILITY

The DC-VERSE and the mDC-VERSE can be explored and downloaded at https://gustaveroussy.github.io/FG-Lab/.

EXPERIMENTAL MODELS AND SUBJECT DETAILS

Human tissue and blood samples

Spleen tissue used for flow cytometry was obtained in accordance with a favourable ethical opinion from Singapore SingHealth and National Health Care Group Research Ethics Committees. Spleen tissue was obtained from patients with tumours in the pancreas who underwent distal pancreatectomy (Singapore General Hospital, Singapore).

Tumour and normal adjacent tissue from the lung, as well as FFPE blocks, were obtained from Non-Small Cell Lung Cancer patients

following written informed consent (Marie Lannelongue Hospital, Paris) and ethical approval (N°ID-RCB: 2016-A00732-49). All subjects provided IRB-approved consent. Human tissues were cut into 0.5 cm squares and incubated with 0.8 mg/mL collagenase (Type IV, Worthington-Biochemical) in RPMI (PAA) with 10% FCS (AutogenBioclear) for 2 and 8 h, respectively, or when stated mechanically dispersed.

METHOD DETAILS

Flow cytometry

For the NSCLC normal adjacent and tumour samples, cells were thawed and transferred into RPMI (Thermo Fischer) with 20% decomplemented FCS (Thermo Fischer). Samples were treated with 1mg/ml DNase I (Sigma-Aldrich) at 37℃. Cells were incubated with Live/Dead blue dye (Invitrogen) for 30 min at 4℃ in phosphate buffered saline (PBS) and then incubated in 5% heat-inactivated fetal calf serum (FCS, Sigma Aldrich) for 15 min at 4℃. Cells were stained with appropriate antibodies (listed in the STAR METHODS key resources table and **Table S5** in PBS with 2% FCS, 2mM EDTA (Sigma Aldrich) and Brilliant Stain buffer (BD), incubated for 30 min at 4℃, and then washed. Cells were analysed using a Cytek Aurora 5-laser spectral analyser. FCS files were exported and analysed using FlowJo v10.8.1.

Immunohisto-fluorescence labelling assays

All immunostainings were performed on 4 µm thick whole sections prepared from FFPE blocks of human NSCLC (Marie Lannelongue Hospital, Paris). Antigen retrieval was carried out on a PT-link (Dako) using the EnVision FLEX Target Retrieval Solutions at High pH (Dako, K8004) or Low pH (Dako, K8005). Endogenous peroxidase activity and non-specific Fc receptor binding were blocked with 3% H_2O_2 (Gilbert, 3518646067907) and Protein Block (Dako, X0909), respectively. Necrotic, serous, folded and blurred areas were excluded from image analyses. The CD20/CD3/CD207**/**CD8 4-plex staining was performed

manually using the OPAL tyramide system amplification (TSA, Akoya Biosciences). Nuclei were stained with DAPI Solution (Thermofisher, 62248) at 2µg/ml for 5 minutes. After mounting with ProLong™ Glass Antifade Mountant (Thermofisher, P36980), the slides were scanned at 20X magnification using a Zeiss Axio scan Z1 device. The primary, secondary antibodies and TSA used are listed in the key resources table.

Algorithms for dimensionality reduction

For flow cytometry data, marker expression values were transformed using the auto-logicle transformation function from the flowCore R package. Uniform Manifold Approximation and Projection (UMAP) were carried out using all markers (flow cytometry) or significant PCs (based on Seurat analysis for scRNAseq data). UMAP was run using 15 nearest neighbours (*nn*), a *min_dist* of 0.01 to 0.2 and Euclidean distance (Becht et al., 2018; McInnes et al., 2018). Phenograph clustering (Levine et al., 2015) was performed using all markers or significant PCs (based on Seurat analysis) before dimension reduction. The number of PCs selected was equal to 50 for the mDC-VERSE, 30 for flow cytometry and equal to 15 for scRNAseq analysis.

MNP extraction and Seurat V3 integration

We previously integrated 41 datasets examining monocyte and macrophage heterogeneity (Mulder et al., 2021). Similarly, for DCs, we integrated 40 of the 41 datasets (1 of the 41 datasets did not meet the cell number criteria for integration). The 40 datasets used (**Table S2**) were either at the raw count matrix or already pre-processed and filtered. As previously described (Mulder *et al.),* we first integrated all the datasets in an organ-specific manner. Before integrating the datasets, we applied universal quality control to keep everything unified. Cells with fewer than 500 genes or more than 20% mitochondrial reads were filtered out. All datasets were then unified in the same expression matrix format. Integration was initiated using the Seurat V3 anchoring method (Stuart et al., 2019) and log-normalised. The matrix was scaled, and a Principal Component Analysis (PCA) was

performed (Becht et al., 2018), from which the first 50 significant Principal Components (PCs) were selected for UMAP analysis. Following the identification of MNPs using canonical markers, a global integration (using 50 PCs for dimensional reduction) of dendritic cells from all tissues was carried out as above.

Label Transfer/ Multimodal reference mapping

For cell metadata transfer and multimodal reference mapping, we used the Label Transfer and the multimodal reference mapping pipeline from Seurat (Hao et al., 2021; Stuart et al., 2019). The algorithm returns a prediction score for each class for every cell in the query dataset, and a cutoff score was set at 0.3.

QUANTIFICATION AND STATISTICAL ANALYSIS

Differentially expressed genes (DEGs)

DEG analyses were performed using the Seurat v3 package (Stuart et al., 2019). DEGs obtained from the "RNA" matrix of the Seurat object were calculated on normalised values with a logFC threshold of 0.25, and the threshold for false discovery is 0.05. The likelihood-ratio test for single-cell gene expression (bimodal test) was used, and correction for multiple testing was carried out using the Bonferroni method.

Dendrogram Heatmap to define mDC-VERSE mega-clusters

The average expression of each gene obtained from the DEG analysis for each Phenograph cluster was first obtained, and a Spearman correlation was calculated. A Dendrogram heatmap was then generated using pHeatmap using Ward's method for hierarchical cluster analysis.

Published DC Signature score Heatmap

For the generation of the signature score heatmap, the package pHeatmap was used as described above. The signatures were obtained from various public datasets. The mDC-VERSE was split into the defined mega-clusters in which we obtained the average gene expression of every mega-cluster for all the genes present. Following this, the mean expression of the signature is calculated and plotted by the mega-clusters in the heatmap.

Metadata analysis

Metadata analysis was performed for selected studies with paired conditions (normal adjacent tissues versus tumours). The proportion of mega-clusters was plotted for each state as charts and density plots for the selected studies. Further analysis was performed to deconvolute at the patient level in datasets where this information was provided. We only analysed datasets where more than 7 cells were present. Charts and density plots were made in GraphPad Prism v6 and SeqGeq v1.6, respectively. Statistical tests were performed using GraphPad Prism v6 and are specified within the figure legends.

Scenic gene regulatory network analyses

To infer gene regulatory networks (GRNs) from tpm-normalized expression matrices of Lung (Maier et al., 2020) and Head/Neck (Cillo et al., 2020), a pySCENIC (single-cell regulatory network inference and clustering) v0.10.3 analysis was performed (Van de Sande et al., 2020). The analysis consisted of three main steps (GitHub/pySCENIC): generation of co-expression modules with GRNBoost2, refinement of these modules with RcisTarget and evaluation of the regulon activity with AUCell (Van de Sande et al., 2020). Differentially expressed regulons (DERs) were calculated using the Seurat pipeline with the same parameters described above for DEGs analysis (adjusted p-value lower or equal to 0.05 and Log2FC cut-off of 0.25). Phenograph cluster-specific DERs and DERs with similar expression patterns across closely

related Phenograph clusters were identified and subsequently used to generate a heatmap.

Spatial transcriptomic analysis (Visium 10X Genomics)

The analysis is performed as previously described in the paper of Wu *et al.* (Wu et al., 2021). Spatial transcriptomic data for Visium samples were deconvoluted using Stereoscope 0.3.1 using Wu *et al.* Breast cancer scRNAseq reference (Wu et al., 2021). Cells in the scRNAseq reference were filtered with the --sc_upper_bound option so that no more than 1000 (randomly selected) cells of any given cell type were used to fit the model. Similarly, genes were filtered by a list of 3695 highly variable genes, as identified using the sc.pp.highly_variable_genes() function from Scanpy with default parameters and the --filter-genes option was also enabled. Both model fitting and model application was run for 75000 epochs each, with a batch size of 100. Wu *et al.* pathology annotations were used to calculate the enrichment of spatially deconvoluted cell subsets, and deconvoluted proportion results were mapped onto H&E images using Seurat v4.

MERFISH analysis

Samples from patients with breast and lung cancer were preserved in FFPE. Slices from each block were prepared following Vizgen's FFPE protocol using Vizgen's Cell Boundary Kit (10400009) and imaged on the MERSCOPE system (Vizgen 10000001) using a panel of 500 genes (**Table S7**). Cell boundaries were determined using Cellpose (Stringer et al., 2021) using boundaries identified from the CLAHE filtered DAPI and cell boundary 3 images merged with boundaries identified from only CLAHE filtered DAPI images. Segmentation was performed on the center z plane imaged on the MERSCOPE system and extrapolated across all 7 z planes. Transcripts within each cell boundary were tabulated to construct a cell by gene matrix used for cell clustering analysis. All MERSCOPE output data is available as part of Vizgen's data release program (https://info.vizgen.com/merscope-ffpe-solution).

Following segmentation, a single-cell analysis was performed using the Scanpy library. MERFISH single-cell gene expression data were first filtered to remove cells with low count or a low number of unique genes expressed (25 genes and 10 counts, respectively). Cells were then normalised to have equal counts (set to a default median of total counts), and gene expression counts were log-transformed and scaled to unit variance. PCA, UMAP embedding (10 neighbours, 0.1 min distance, and spread 3.0), and Leiden clustering (resolution of 1.5) were performed. Leiden clusters were manually labelled for global annotation. A PCA was performed for the immune compartment and consecutively on the myeloid department, in which the PCs with strong loading on immune-associated genes were selected for running UMAP embedding (15 neighbours, 0.01 min distance, and spread 3.0) and Phenograph clustering (K50).

Pathway analysis

DEGs of DC populations, together with the respective fold-change and p-values, were uploaded to the Ingenuity Pathway Analysis (IPA) software (QIAGEN). IPA analysis reported the p-value of canonical pathways. Predicted upregulated or downregulated pathways were represented by a positive or negative Z-score, respectively. Canonical pathways are determined by IPA's default threshold [–log. (p-value)>1.3] were then shortlisted, and bubble plots were used to visualise the p-values and Z-scores. Complete lists of pathways can be found in **Table S4**.

TCGA analysis

For the generation of the correlation matrix, signatures were used from Mulder *et al.*, Nalio Ramos *et al.* and Mackay *et al*. (Mackay et al., 2016; Mulder et al., 2021; Nalio Ramos et al., 2022). The TCGA datasets were scaled by Z-score per patient, of which the average of every signature was calculated. A Pearson correlation (r) with two-tailed test was used to obtain the correlation matrix and plotted using the corrplot R package (0.84).

Quantification and statistical analysis of the immunohisto-fluorescence labelling

Tumour and normal adjacent tissue areas were defined by a pathologist (G.G.). Tumours, tumour nests and stromal regions were identified using the Halo10 software (Indica Labs) with a classifier based on examples of the two areas. The density of positive cells/mm^2: CD3$^+$, CD8$^+$, CD20$^+$, and CD207$^+$ cells were quantified in the different zones with Halo10 software (Indica Labs) using the fitting counting algorithms.

KEY RESOURCES TABLE

REAGENT or RESOURCE	SOURCE	IDENTIFIER
Antibodies for spectral flow cytometry		
Anti-goat (Polyclonal) AF488	Jackson Immuno-Research Laboratory	Cat# 705-545-147, RRID:AB_2336933
CCR2 (Clone LS132.1D9) BUV563	BD Biosciences	Cat# 749076, RRID:AB_2873470
CD11b (Clone M1/70) BV570	Biolegend	Cat# 101233, RRID:AB_10896949
CD117 (Clone 104D2) APC	Biolegend	Cat# 313206, RRID:AB_314985
CD123 (Clone 6H6) PE/Daz594	Biolegend	Cat# 306034, RRID:AB_2566450
CD103 (Clone Ber-ACT8) BV605	Biolegend	Cat# 350217, RRID:AB_2564282
CD14 (Clone 63D3) SparkB550	Biolegend	Cat# 367148, RRID:AB_2832724
CD141 (Clone M81) BV421	Biolegend	Cat# 344114, RRID:AB_2562956
CD169 (Clone 7-239) BUV661	BD Biosciences	Cat# 750363, RRID:AB_2874538

CD19 (Clone HIB19) BV650	Biolegend	Cat# 302238, RRID:AB_2562097
CD1a (Clone SK9) BB660	BD Biosciences	Custom
CD1c (Clone L161) SB436	Invitrogen	Cat# 62-0015-42, RRID:AB_2762426
CD20 (Clone 2H7) BV650	Biolegend	Cat# 302336, RRID:AB_2563806
CD25 (Clone CD25-3G10) PE/AF700	Thermo Fisher Scientific	Cat# MHCD2524, RRID:AB_2539740
CD206 (Clone 19.2) PercP/eFluor 710	Thermo Fisher Scientific	Cat# 46-2069-42, RRID:AB_10853034
CD207 (Clone 2G3) BB755	BD Biosciences	Custom
CD209 (Clone 9E9A8) PE/Cy7	Biolegend	Cat# 330114, RRID:AB_10719953
CD3 (Clone SP34-2) BV650	BD Biosciences	Cat# 563916, RRID:AB_2738486
CD301 (Clone H037G3) PE	Biolegend	Cat# 354704, RRID:AB_11219002
CD38 (Clone HB7) BUV805	BD Biosciences	Cat# 742074, RRID:AB_2871359
CD4 (Clone SK3) Cfl.YG584	Cytek Biosciences	Cat# R7-20041, RRID:AB_2885083
CD45 (Clone 30-F11) PercP	Biolegend	Cat# 103130, RRID:AB_893339
CD5 (Clone UCHT2) APC/R700	BD Biosciences	Cat# 565121, RRID:AB_2744433
CD8 (Clone SK1) APC/Fire 810	Biolegend	Cat# 344764, RRID:AB_2860890
CD127 (Clone HIL-7R-M21) BB510	BD Biosciences	Custom
CD86 (Clone 2331) BV786	BD Biosciences	Cat# 740990, RRID:AB_2870657
CD88 (Clone S5/1) APC/Fire750	Biolegend	Cat# 344316, RRID:AB_2750445
CD89 (Clone A59) BUV496	BD Biosciences	Cat# 750617, RRID:AB_2874749

CD9 (Clone M-L13) BV480	BD Biosciences	Cat# 746356, RRID:AB_2743675
FcεRIα (Clone AER-37 (CRA-1)) BV711	Biolegend	Cat# 334638, RRID:AB_2687186
HLA-ABC (Clone W6/32) Sp. NIR 685	Biolegend	Cat# 311453, RRID:AB_2876612
HLA-DP (Clone B7/21) BUV395	BD Biosciences	Cat# 750866, RRID:AB_2874962
HLA-DQ (Clone Tu169) BV510	BD Biosciences	Cat# 742609, RRID:AB_2740907
HLA-DR (Clone L243) PE/Fire 810	Biolegend	Custom
PD-L1 (Clone MIH1) PE/Cy5	Invitrogen	Cat# 15-5983-42, RRID:AB_2802211
PD-1 (Clone EH12.1) BV750	BD Biosciences	Cat# 747446, RRID:AB_2872125
SLAN (Clone DD-1) VioBlue	Miltenyi Biotec	Cat# 130-119-868, RRID:AB_2733608
CADM1 (Clone 3E1)	MBL International	Cat# CM004-3, RRID:AB_592783
IRF4 (Clone 3E4) PE	Thermo Fisher Scientific	Cat# 12-9858-82, RRID:AB_10852721
IRF8 (Clone V3GYWCH) PercP/eFluor 710	Thermo Fisher Scientific	Cat# 46-9852-82, RRID:AB_2573904
CD11c (Clone 3.9) BV605	BioLegend	Cat# 301636, RRID:AB_2563796
CD16 (Clone 3G8) APC/Cy7	BioLegend	Cat# 302017, RRID:AB_314217
HLA-DR (Clone L243) BV785	BioLegend	Cat# 307641, RRID:AB_2561360
CD14 (Clone RMO52) ECD	Beckamn Coulter	Cat# B92391
CD123 (Clone 7G3) BUV395	BD Biosciences	Cat# 564195, RRID:AB_2714171
CD45 (Clone HI30) V500	BD Biosciences	Cat# 560777, RRID:AB_1937324
ViaDye™ Red Fixable Viability Dye Kit	Cytek Biosciences	Cat# SKU R7-60008

LIVE/DEAD™ Fixable Blue Dead Cell	Invitrogen	Cat# L23105
CCR7 (Clone 2-L1-A) BUV737	BD Biosciences	Cat# 749676, RRID:AB_2873937
Antibodies and reagents for immunohisto-fluorescence experiments		
Rabbit IgG polyclonal anti-CD3 (6 µg/mL)	Agilent	Cat# : A0452, RRID: AB_2335677
Mouse IgG1 mAb (C8/144B) anti-CD8 (1.6 µg/mL)	Agilent	Cat# : M7103, RRID: AB_2075537
Mouse IgG2a mAb (L26) anti-CD20 concentrated at 0.3 µg/mL	Agilent	Cat# : M0755, RRID: AB_2282030
Rat IgG2a mAb (929F3.01) anti-CD207/Langerin (2.5 µg/mL)	Eurobio Scientific	Cat# : DDX0362P-100, RRID : AB_2892751
Polymer anti-Mouse HRP	Agilent	Cat# : K4001, RRID: AB_2827819
Polyview® plus anti-Rabbit HRP	Enzo Life Sciences	Cat# : ENZ-ACC103-0150
Opal Polymer anti-Rabbit HRP	Akoya Biosciences	Cat# : ARR1001KT
Polymer IgG anti-rat HRP	Vector Laboratories	Cat# : MP-7404, RRID: AB_2336531
OPAL 520	Akoya Biosciences	Cat# : FP1487001KT
OPAL 570	Akoya Biosciences	Cat# : FP1488001KT
OPAL 690	Akoya Biosciences	Cat# : FP1497001KT
OPAL Polaris 780	Akoya Biosciences	Cat# : FP1501001KT
Chemicals, peptides, and recombinant proteins for immunohisto-fluorescence experiments		
EnVision FLEX Target Retrieval Solution, High pH	Agilent	Cat# : K8004
EnVision FLEX Target Retrieval Solution, Low pH	Agilent	Cat# : K8005
H2O2 3%	Gilbert	Cat# : 3518646067907
Protein Block	Agilent	Cat# : X0909
DAPI	Thermofisher	Cat# : 62248

ProLong™ Glass Antifade Mountant	Thermofisher	Cat# : P36980
Chemicals, Peptides, and Recombinant Proteins		
DNAse I	Sigma Aldrich	Cat# 48024000
PBS	ThermoFisher	Cat# 20012-027
Collagenase IV	Sigma Aldrich	Cat# C5138-500MG
RPMI	ThermoFisher	Cat# 31870-025
Brilliant Stain Buffer	BD Biosciences	Cat# 563794
FCS	ThermoFisher	Cat# 26140079
Biological samples		
Spleen sample	Singapore General Hospital (SGH)	
Matched LUAD lung sample	Marie Lannelongue Hospital, Paris	Matched LUAD lung sample
Software and Algorithms		
Anaconda 2018.12	Anaconda	https://www.anaconda.com
DIVA	BD Biosciences	https://www.bdbiosciences.com/en-us
FlowJo v10.5.3	Tree Star	https://www.flowjo.com
GraphPad Prism 6	GraphPad	https://www.graphpad.com/scientificsoftware/prism/
Ingenuity Pathway Analysis v01-16	QIAGEN	https://www.qiagenbioinformatics.com/products/ingenuity-pathway-analysis/
Phenograph	Levine *et al.*, 2015	https://github.com/JinmiaoChenLab/Rphenograph
Python v3.7.1	Python Software Foundation	https://www.python.org
R v4.4	The R Foundation	https://www.r-project.org

SCENIC	Van de Sande *et al*., 2020	https://github.com/aertslab/pySCENIC
SeqGeq v1.6	FlowJo	https://www.flowjo.com/solutions/seqgeq
Seurat v3	Stuart *et al*., 2019	https://satijalab.org/seurat/
Seurat v4	Hao *et al*., 2020	https://satijalab.org/seurat/
UMAP	McInnes *et al*., 2018	https://github.com/lmcinnes/umap
Halo version 3.4.2986.166	Indica Labs	RRID: SCR_018350 https://indicalab.com
MERSCOPE visualizer	Vizgen	https://vizgen.com/

SUPPLEMENTAL FIGURES

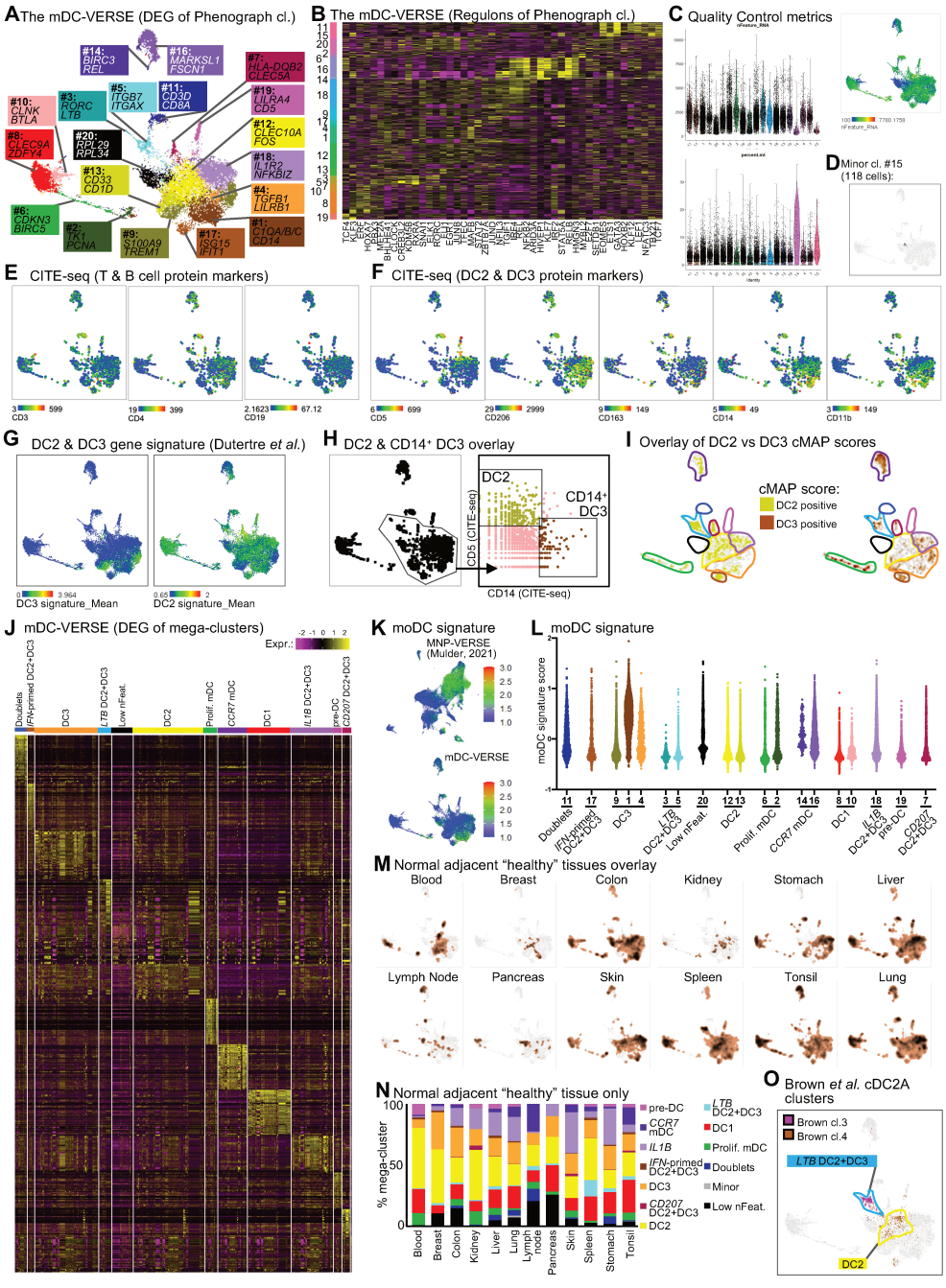

Figure S1 related to Figure 2: Identification of clusters within the mDC-VERSE and mDC mega clusters' distribution across normal adjacent "healthy" tissues. *(**A**) Phenograph clusters' annotation of the*

*mDC-VERSE. (**B**) Heatmap showing the relative expression levels of DERs between phenograph clusters common to Lung (Maier) and Tonsil (Cillo) cancer datasets. (**C**) Quality control metrics for each phenograph cluster and meaning plot of nFeature_RNA. (**D**) Annotation of cl. #15 on the mDC-VERSE. (**E-F**) CITE-seq data (from Maier et al.) showing expression of signature T & B cell protein markers and DC2 and DC3 protein markers (Maier et al., 2020). (**G**) Meaning plots of DC2 and DC3 gene signatures from Dutertre et al. on the DC-VERSE (Dutertre et al., 2019). (**H**) Identification of DC2s and DC3s using CD5 and CD14 protein expression from CITE-seq data within the DC2+DC3 region of the mDC-VERSE (Maier et al., 2020). (**I**) Overlay of cMAP scores onto the mDC-VERSE UMAP space. (**J**) DEG heatmap between mega clusters of the mDC-VERSE. (**K**) Mean expression of the moDC signature from Gao et al. (Gao et al., 2021) overlayed onto the MNP-VERSE (from Mulder et al.) (Mulder et al., 2021) and onto the mDC-VERSE UMAP spaces. (**L**) moDC signature score for each cell of the different mDC-VERSE Phenograph clusters. (**M,N**) Composition of DC mega clusters across normal adjacent "healthy" tissues. (**O**) Annotation of cl.3 & cl.4 (corresponding to cDC2As_Brown) from Brown et al. on the mDC-VERSE (Brown et al., 2019).*

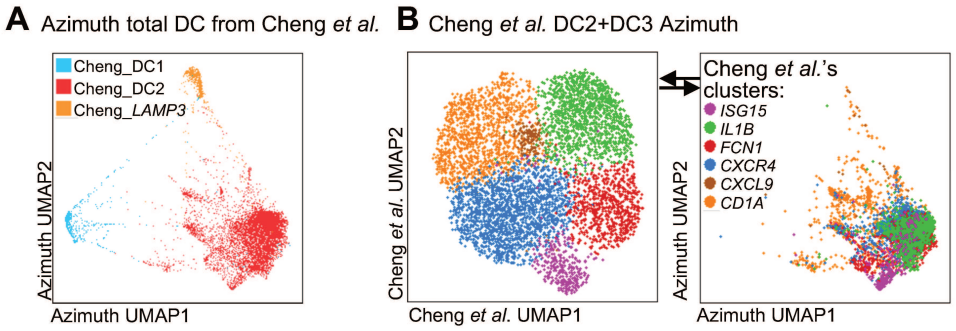
A Azimuth total DC from Cheng et al.
Cheng_DC1
Cheng_DC2
Cheng_LAMP3
Azimuth UMAP2
Azimuth UMAP1
B Cheng et al. DC2+DC3 Azimuth
Cheng et al. UMAP2
Cheng et al. UMAP1
Cheng et al.'s clusters:
ISG15
IL1B
FCN1
CXCR4
CXCL9
CD1A
Azimuth UMAP2
Azimuth UMAP1

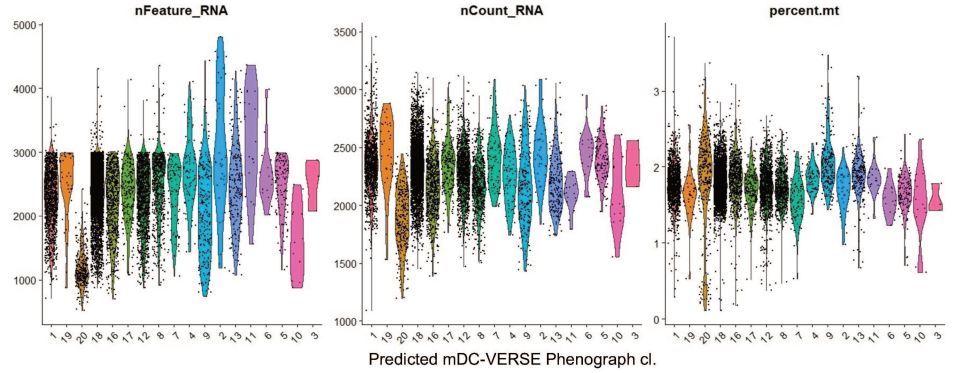
C Quality Control metrics (Azimuth of Cheng et al.)
nFeature_RNA
nCount_RNA
percent.mt
Predicted mDC-VERSE Phenograph cl.

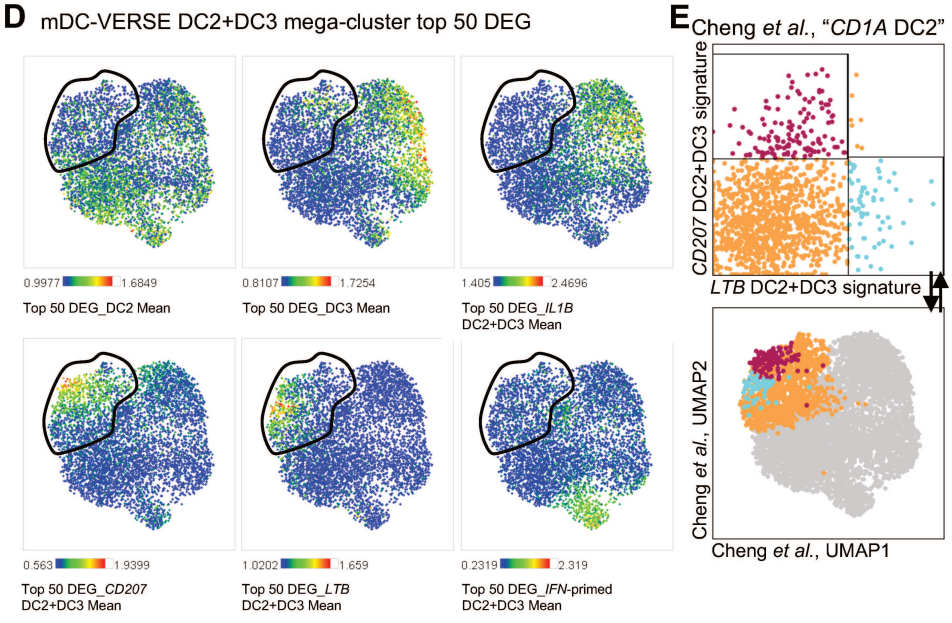
D mDC-VERSE DC2+DC3 mega-cluster top 50 DEG
Top 50 DEG_DC2 Mean
Top 50 DEG_DC3 Mean
Top 50 DEG_IL1B DC2+DC3 Mean
Top 50 DEG_CD207 DC2+DC3 Mean
Top 50 DEG_LTB DC2+DC3 Mean
Top 50 DEG_IFN-primed DC2+DC3 Mean
E Cheng et al., "CD1A DC2"
CD207 DC2+DC3 signature
LTB DC2+DC3 signature
Cheng et al., UMAP2
Cheng et al., UMAP1

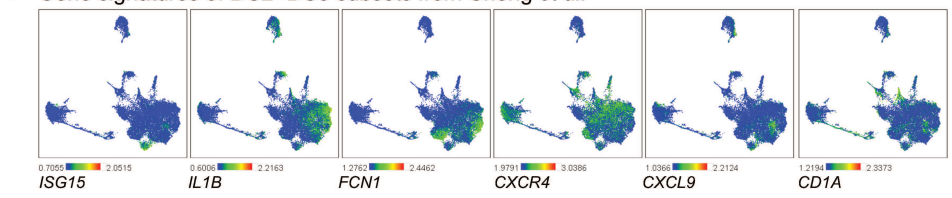
F Gene signatures of DC2+DC3 subsets from Cheng et al.
ISG15
IL1B
FCN1
CXCR4
CXCL9
CD1A

Figure S2 related to Figure 2: Comparison of mDC-VERSE DC2+DC3 populations to Cheng's cDC2 subsets. *(**A-B**) Projection of all mDC subsets and DC2+DC3 populations defined by Cheng et al.'s metadata (Cheng et al., 2021) on the mDC-VERSE using multimodal reference mapping (Azimuth). (**C**) Quality control metrics of predicted mDC-VERSE phenograph clusters from Cheng et al. data projected by multimodal reference mapping. (**D**) Mean expression of the top 50 genes of mega clusters from the mDC-VERSE mapped onto the UMAP from Cheng et al. (**E**) Mapping of cDC2_CD1A cells from Cheng et al., enriched in CD207 or LTB cDC2/DC3 signatures (from the mDC-VERSE) onto the UMAP from Cheng et al. (**F**) Meaning plots of the mean gene signatures of DC2+DC3 populations from Cheng et al. shown on the mDC-VERSE.*

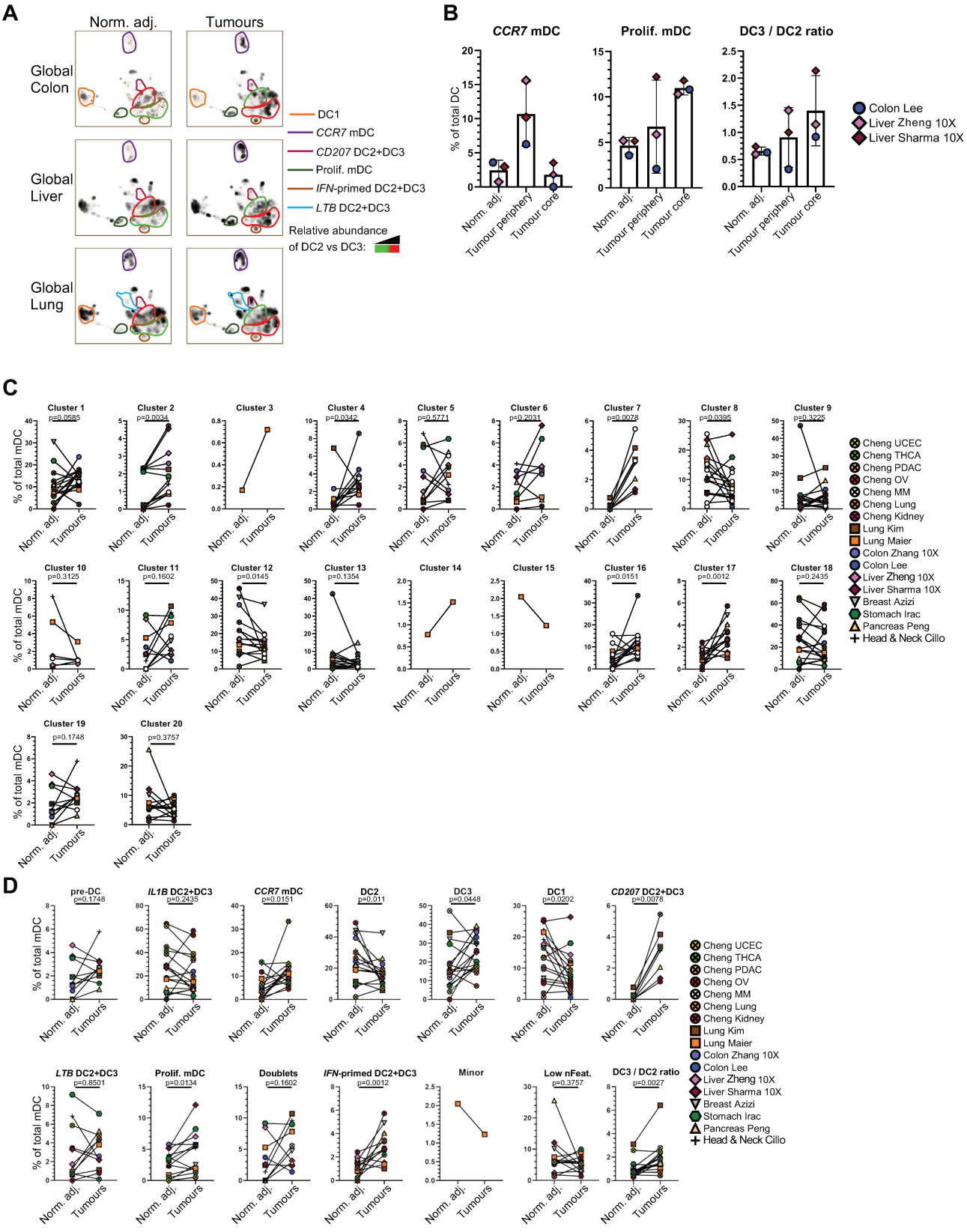
A
Norm. adj.
Tumours
Global Colon
Global Liver
Global Lung
DC1
CCR7 mDC
CD207 DC2+DC3
Prolif. mDC
IFN-primed DC2+DC3
LTB DC2+DC3
Relative abundance of DC2 vs DC3:
B
CCR7 mDC
Prolif. mDC
DC3 / DC2 ratio
% of total DC
Norm. adj.
Tumour periphery
Tumour core
Colon Lee
Liver Zheng 10X
Liver Sharma 10X
C
Cluster 1 p=0.0585
Cluster 2 p=0.0034
Cluster 3
Cluster 4 p=0.0342
Cluster 5 p=0.5771
Cluster 6 p=0.2031
Cluster 7 p=0.0078
Cluster 8 p=0.0395
Cluster 9 p=0.3225
Cluster 10 p=0.3125
Cluster 11 p=0.1602
Cluster 12 p=0.0145
Cluster 13 p=0.1354
Cluster 14
Cluster 15
Cluster 16 p=0.0151
Cluster 17 p=0.0012
Cluster 18 p=0.2435
Cluster 19 p=0.1748
Cluster 20 p=0.3757
% of total mDC
Norm. adj.
Tumours
Cheng UCEC
Cheng THCA
Cheng PDAC
Cheng OV
Cheng MM
Cheng Lung
Cheng Kidney
Lung Kim
Lung Maier
Colon Zhang 10X
Colon Lee
Liver Zheng 10X
Liver Sharma 10X
Breast Azizi
Stomach Irac
Pancreas Peng
Head & Neck Cillo
D
pre-DC p=0.1748
IL1B DC2+DC3 p=0.2435
CCR7 mDC p=0.0151
DC2 p=0.011
DC3 p=0.0448
DC1 p=0.0202
CD207 DC2+DC3 p=0.0078
LTB DC2+DC3 p=0.8501
Prolif. mDC p=0.0134
Doublets p=0.1602
IFN-primed DC2+DC3 p=0.0012
Minor
Low nFeat. p=0.3757
DC3 / DC2 ratio p=0.0027
% of total mDC
Norm. adj.
Tumours
Cheng UCEC
Cheng THCA
Cheng PDAC
Cheng OV
Cheng MM
Cheng Lung
Cheng Kidney
Lung Kim
Lung Maier
Colon Zhang 10X
Colon Lee
Liver Zheng 10X
Liver Sharma 10X
Breast Azizi
Stomach Irac
Pancreas Peng
Head & Neck Cillo

Figure S3 related to Figure 3: Metadata analysis of mDC populations in cancer. *(**A**) Density plots of global colon, liver and lung datasets highlighting changes in DC1s, CCR7 mDCs, CD207 DC2+DC3s, Prolif. mDCs, IFN-primed DC2+DC3s and LTB DC2+DC3s between normal adjacent and cancer tissues. (**B**) Percentage of CCR7 mDCs and Prolif. mDCs, and DC3/DC2 ratio in datasets which had analysed normal adjacent tissue, tumour periphery and tumour core. (**C**,**D**) Percentage of mDC-VERSE (**C**) phenograph clusters and (**D**) mega clusters in all integrated and query datasets (Obtained through multimodal reference mapping and annotated with cross symbol) between matched healthy and cancer tissues. P values were calculated using a Wilcoxon test.*

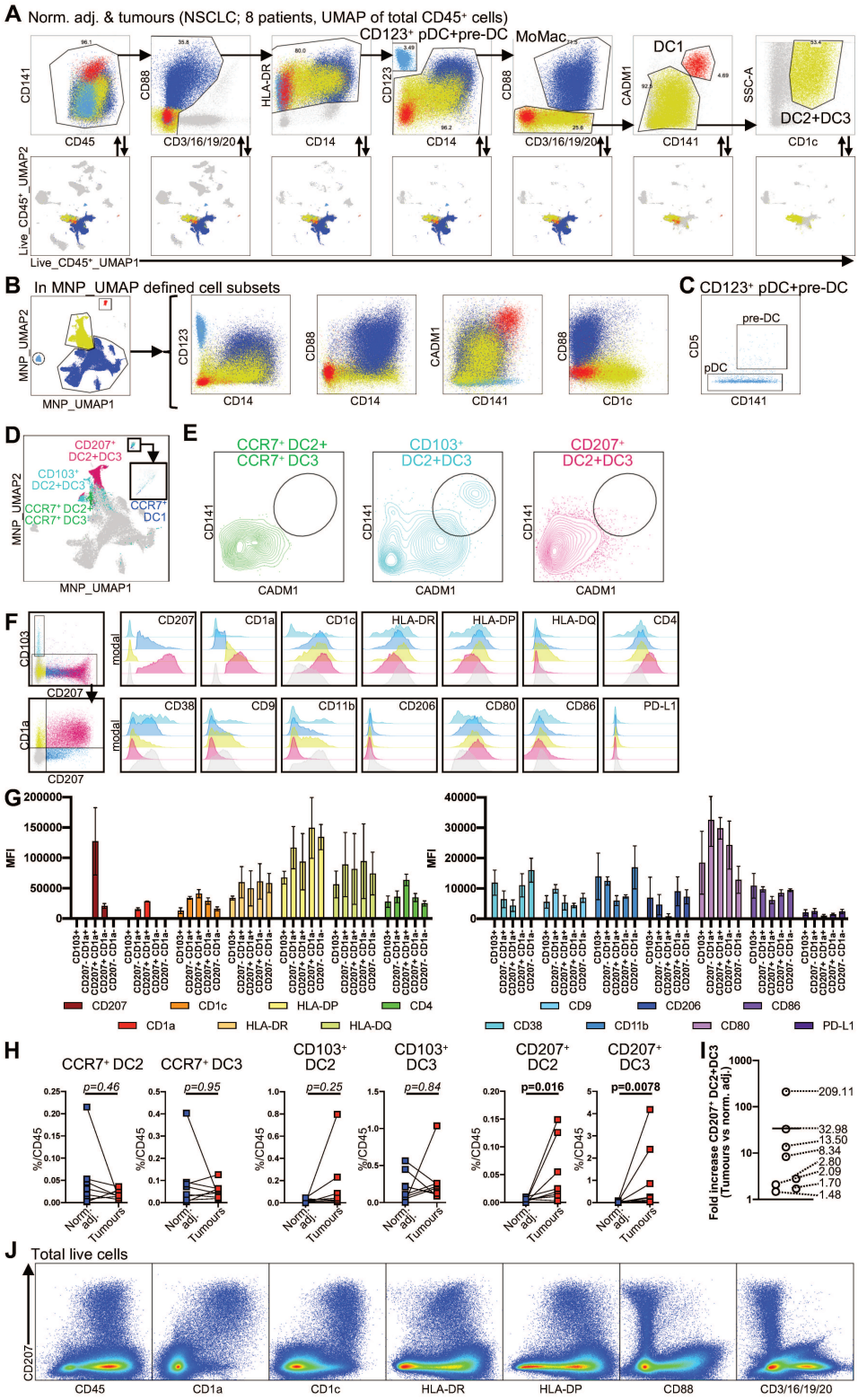
A
Norm. adj. & tumours (NSCLC; 8 patients, UMAP of total CD45⁺ cells)
CD123⁺ pDC+pre-DC
MoMac
DC1
DC2+DC3
CD141
CD45
CD88
CD3/16/19/20
HLA-DR
CD14
CD123
CADM1
SSC-A
CD1c
Live_CD45⁺_UMAP2
Live_CD45⁺_UMAP1
B
In MNP_UMAP defined cell subsets
MNP_UMAP2
MNP_UMAP1
C
CD123⁺ pDC+pre-DC
pre-DC
pDC
CD5
D
CD207⁺ DC2+DC3
CD103⁺ DC2+DC3
CCR7⁺ DC2+ CCR7⁺ DC3
CCR7⁺ DC1
E
CCR7⁺ DC2+ CCR7⁺ DC3
CD103⁺ DC2+DC3
CD207⁺ DC2+DC3
CADM1
F
modal
CD207
CD1a
CD1c
HLA-DR
HLA-DP
HLA-DQ
CD4
CD38
CD9
CD11b
CD206
CD80
CD86
PD-L1
G
MFI
H
CCR7⁺ DC2
CCR7⁺ DC3
CD103⁺ DC2
CD103⁺ DC3
CD207⁺ DC2
CD207⁺ DC3
p=0.46
p=0.95
p=0.25
p=0.84
p=0.016
p=0.0078
%/CD45
Norm. adj.
Tumours
I
Fold increase CD207⁺ DC2+DC3 (Tumours vs norm. adj.)
209.11
32.98
13.50
8.34
2.80
2.09
1.70
1.48
J
Total live cells
CD45
CD1a
CD1c
HLA-DR
HLA-DP
CD88
CD3/16/19/20

Figure S4 related to Figure 4 and Figure 5: Gating strategy to define DC populations and states and evaluation of their phenotype in NSCLC spectral flow cytometry data. *(**A**) Gating strategy from singlets, live, CD45$^+$ cells and projection of each gated population onto the MNP_UMAP space. (**B**) MNP_UMAP annotation confirmed by protein expression. (**C**) Gating of pDCs and pre-DCs within CD123$^+$ DCs defined in **Figure 4A-B**. (**D**) Overlay of DC "states" identified in **Figure 4H** onto the MNP_UMAP space. (**E**) Expression of CADM1 and CD141 by CCR7$^+$ DC2+CCR7$^+$ DC3, by CD103$^+$ DC2+DC3s and by CD207$^+$ DC2+DC3s. (**F**) Gating and phenotype of CD103$^+$ "LTB" and CD1a$^+$CD207$^+$ DC2+DC3s. (**G**) Mean fluorescence intensity (MFI) of markers expressed by populations of DC2+DC3s defined in panel (**F**). (**H**) Percentage of DC "states" identified in (**Figure 4H,I**, **Figure 4K** and **Figure 4M**) among total CD45$^+$ cells in normal adjacent tissue versus tumour. (**I**) Fold increase of CD207$^+$ DC2+DC3s in tumour versus normal adjacent tissue. (**J**) Expression of CD45, CD1a, CD1c, HLA-DR, HLA-DP, CD88 and CD3/CD16/CD19/CD20 versus CD207 by total live cells (including CD45$^-$ non-immune cells) from a NSCLC tumour.*

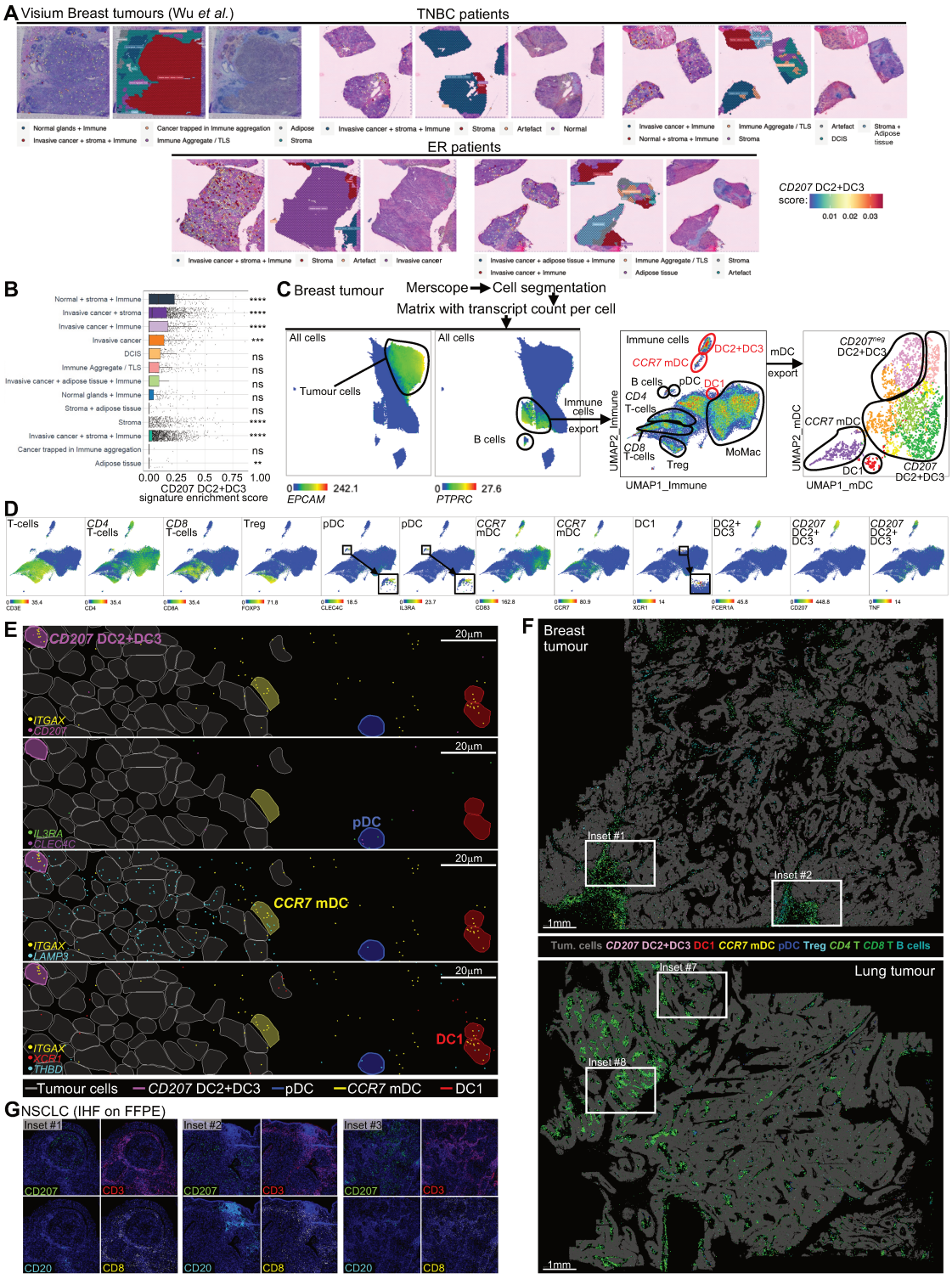

Figure S5 related to Figure 5: Spatial mapping and characterisation of the pathophysiological involvement of DC

populations in human breast and lung cancer patients. *(**A**) Visium spatial transcriptomic profiling of 3 TNBC and 2 ER breast cancer patients from Wu et al. (Wu et al., 2021). For each patient, the left panel shows the CD207 DC2+DC3 signature score, middle panel shows tissue niches and the right panel shows haematoxylin and eosin (H&E) staining. (**B**) Enrichment score of CD207 DC2+DC3 signature across different tissue niches identified in (**A**). (**C**) Meaning plots of EPCAM and PTPRC expression visualised on the UMAP generated with all cells from the Merscope data of the breast cancer patient. Immune cells were extracted, and different cell populations were annotated based on a curated list of genes. mDCs were then extracted to generate a mDC UMAP identifying mDC populations. (**D**) Meaning plots of representative genes used to define the immune populations identified in the Immune cells' UMAP from panel (**C**). (**E,F**) Merfish analysis of breast cancer and lung cancer cross-sections. (**E**) Visualisation of the expression of DC population-defining transcripts in the segmented Merfish spatial data. (**F**) Spatial distribution of tumour cells (grey) and immune populations within the breast and lung tumour cross-sections analysed by Merfish. (**G**) Single fluorescent images for CD207 (green), CD3 (red), CD8 (yellow) and CD20 (cyan) of the IHF data shown in **Figure 5H**.*

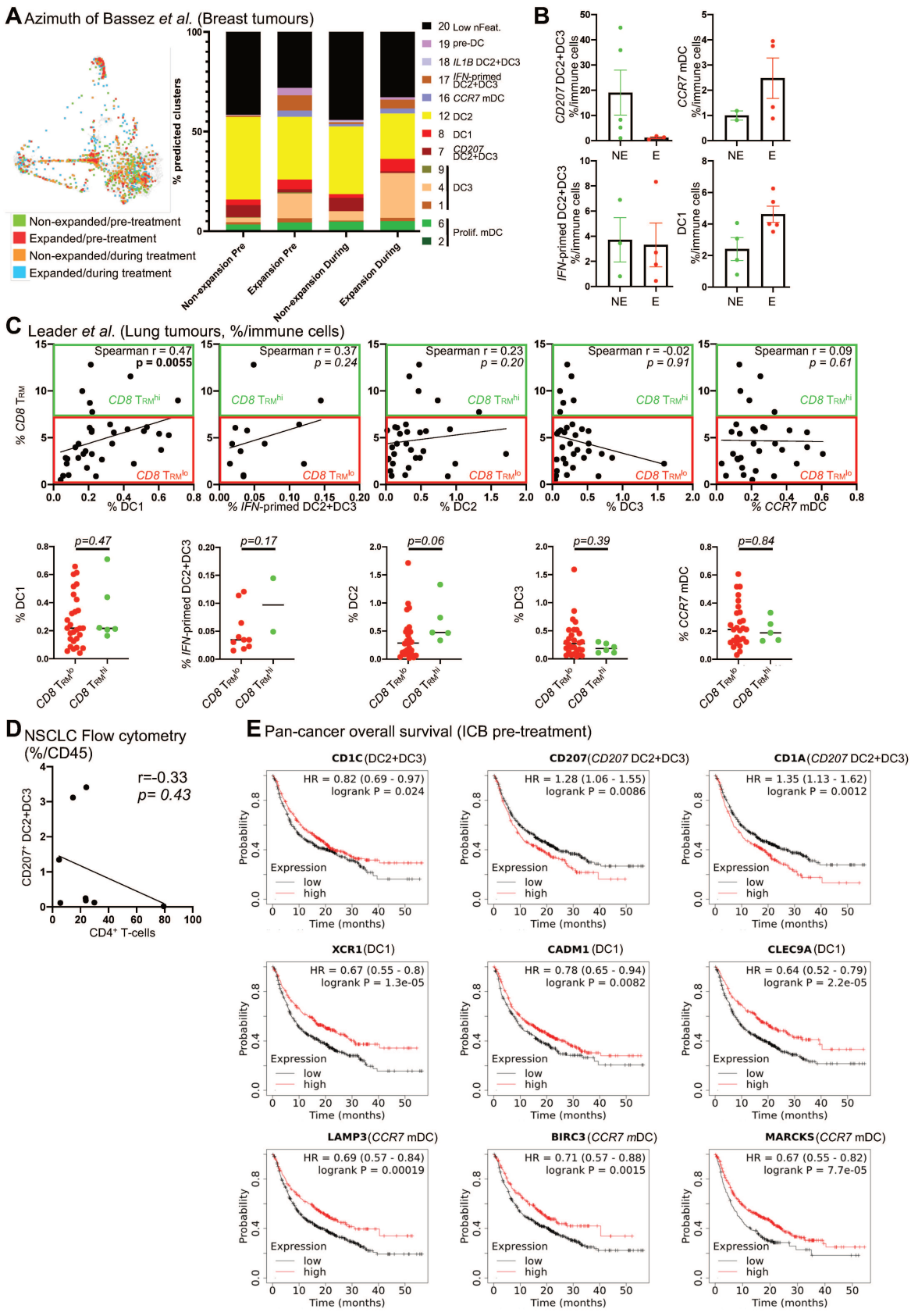
A Azimuth of Bassez et al. (Breast tumours)
Non-expanded/pre-treatment
Expanded/pre-treatment
Non-expanded/during treatment
Expanded/during treatment
% predicted clusters
20 Low nFeat.
19 pre-DC
18 IL1B DC2+DC3
17 IFN-primed DC2+DC3
16 CCR7 mDC
12 DC2
8 DC1
7 CD207 DC2+DC3
9
4
1
DC3
6
2
Prolif. mDC
Non-expansion Pre
Expansion Pre
Non-expansion During
Expansion During
B
CD207 DC2+DC3 %/immune cells
CCR7 mDC %/immune cells
IFN-primed DC2+DC3 %/immune cells
DC1 %/immune cells
NE
E
C Leader et al. (Lung tumours, %/immune cells)
Spearman r = 0.47
p = 0.0055
Spearman r = 0.37
p = 0.24
Spearman r = 0.23
p = 0.20
Spearman r = -0.02
p = 0.91
Spearman r = 0.09
p = 0.61
% CD8 TRM
CD8 TRMhi
CD8 TRMlo
% DC1
% IFN-primed DC2+DC3
% DC2
% DC3
% CCR7 mDC
p=0.47
p=0.17
p=0.06
p=0.39
p=0.84
D NSCLC Flow cytometry (%/CD45)
r=-0.33
p= 0.43
CD207+ DC2+DC3
CD4+ T-cells
E Pan-cancer overall survival (ICB pre-treatment)
CD1C (DC2+DC3)
HR = 0.82 (0.69 - 0.97)
logrank P = 0.024
CD207 (CD207 DC2+DC3)
HR = 1.28 (1.06 - 1.55)
logrank P = 0.0086
CD1A (CD207 DC2+DC3)
HR = 1.35 (1.13 - 1.62)
logrank P = 0.0012
XCR1 (DC1)
HR = 0.67 (0.55 - 0.8)
logrank P = 1.3e-05
CADM1 (DC1)
HR = 0.78 (0.65 - 0.94)
logrank P = 0.0082
CLEC9A (DC1)
HR = 0.64 (0.52 - 0.79)
logrank P = 2.2e-05
LAMP3 (CCR7 mDC)
HR = 0.69 (0.57 - 0.84)
logrank P = 0.00019
BIRC3 (CCR7 mDC)
HR = 0.71 (0.57 - 0.88)
logrank P = 0.0015
MARCKS (CCR7 mDC)
HR = 0.67 (0.55 - 0.82)
logrank P = 7.7e-05
Probability
Expression
low
high
Time (months)

Figure S6 related to Figure 6: Characterisation of the pathophysiological involvement of mDC populations in human cancer patients. *(**A**) Percentage of predicted phenograph clusters from query dataset (Bassez et al.) projected using multimodal reference mapping (Azimuth) (Bassez et al., 2021). (**B**) Percentage of CD207 DC2+DC3s between patients with non-expanded and expanded T-cell clonality in the Bassez et al. data. (**C**) Upper panel shows the correlation between the frequencies among CD45^{+} cells of DC populations (DC1s, IFN DC2+DC3s, DC2s, DC3s and CCR7 mDCs) and CD8 T_{RMs} in lung tumours within the Leader et al. scRNAseq data (Leader et al., 2021). Lower panel shows the frequencies among PTPRC(CD45)-expressing immune cells of the same DC populations split by CD8 T_{RMs}^{hi} and CD8 T_{RMs}^{lo}. (**D**) Correlation between the frequencies of CD207^{+} DC2+DC3s and CD4^{+} T-cells from flow cytometry analysis of 8 NSCLC patients. (**E**) Kaplan-Meier plots of the overall survival (OS) of patients with different cancers whose tumour was sampled and analysed by bulk RNAseq prior to immune checkpoint blockade (ICB) treatment. Patients were separated based on high or low expression of genes specifically expressed by total DC2+DC3s (CD1C), by CD207 DC2+DC3s, by DC1s or by CCR7 mDCs. Correlations were evaluated using the Pearson correlation (r) with two-tailed p values. P values were calculated using a t-test.*

2.3 SOPA: A TECHNOLOGY-INVARIANT PIPELINE FOR ANALYSES OF IMAGE-BASED SPATIAL OMICS

Quentin Blampey[1,2*#], Kevin Mulder[3#], Margaux Gardet[3], Stergios Christodoulidis[1], Charles- Antoine Dutertre[3], Fabrice André[2,4], Florent Ginhoux[3] & Paul-Henry Cournède[1*]

[1]Paris-Saclay University, CentraleSupélec, Laboratory of Mathematics and Computer Science (MICS), Gif-sur-Yvette, France

[2]Paris-Saclay University, Gustave Roussy, INSERM U981, Villejuif, France

[3]Paris-Saclay University, Gustave Roussy, INSERM U1015, Villejuif, France

[4]Gustave Roussy, Department of Medical Oncology, Villejuif, France

# These authors contributed equally

*Correspondence to: quentin.blampey@gmail.com (Quentin Blampey)

*Correspondence to: paul-henry.cournede@centralesupelec.fr (Paul-Henry Cournède)

Abstract

Spatial omics data allow in-depth analysis of tissue architectures, opening new opportunities for biological discovery. In particular, imaging techniques offer single-cell resolutions, providing essential insights into cellular organizations and dynamics. Yet, the complexity of such data presents analytical challenges and demands substantial computing resources. Moreover, the proliferation of diverse spatial omics technologies, such as Xenium, MERSCOPE, CosMX in spatial-transcriptomics, and MACSima and PhenoCycler in multiplex imaging, hinders the generality of existing tools. We introduce Sopa (https://github.com/gustaveroussy/sopa), a technology-invariant, memory-efficient pipeline with a unified visualizer for all image-based spatial omics. Built upon the universal SpatialData framework, Sopa optimizes tasks like segmentation, transcript/channel aggregation, annotation, and geometric/spatial analysis. Its output includes user-friendly web reports and visualizer files, as well as comprehensive data files for in-depth analysis. Overall, Sopa represents a significant step toward unifying spatial data analysis, enabling a more comprehensive understanding of cellular interactions and tissue organization in biological systems.

Introduction

Spatial omics data offer opportunities to improve our understanding of cellular interactions within their micro-environment and the intricacies of tissue organization (Bressan et al., 2023; Rao et al., 2021). Recent advancements in imaging technologies have expanded these capabilities, enabling the measurement of 1000+ genes through Spatial Transcriptomics (Moses and Pachter, 2022) and/or the analysis of 50+ proteins via Multiplex Imaging (Lewis et al., 2021). These include Merfish (Chen et al., 2015), ISH (Jin and Lloyd, 1997), ISS (He et al., 2022), MICS (Kinkhabwala et al., 2022), PhenoCycler (Jhaveri et al., 2023) and IMC (Chang et al., 2017), all of which provide single-cell resolution that could not be achieved by previous spot-based techniques like 10X Visium or Nanostring GeoMX (Merritt et al., 2020). Therefore, image-based technologies provide a higher resolution — up to the subcellular level — which is needed for a detailed exploration of individual cells and their gene expression profiles within their spatial context. This level of precision has been essential for unravelling tissue architecture and understanding cellular interactions; it marks the beginning of a significant leap forward in our comprehension of biological systems (Chu et al., 2023; Jhaveri et al., 2023; Kumar et al., 2023).

In parallel with these technological advancements, the analysis of image-based spatial omics has encountered significant computational challenges and limitations (Atta and Fan, 2021; Dries et al., 2021; Moses and Pachter, 2022; Vandereyken et al., 2023; Zeng et al., 2022). Most existing methods (Biancalani et al., 2021; Petukhov et al., 2021; Stringer et al., 2021) are not designed to handle large images with millions of cells. Their usage typically demands high- performance computational clusters with substantial memory resources, which limits accessibility

to spatial omics due to cost and hardware constraints. As a result, most companies have developed proprietary tools for their own data types, primarily focusing only on segmentation and visualiza- tion. Yet, these proprietary tools have certain constraints, such as (i) a limit on specific function- alities, (ii) no incorporation of the latest state-of-the-art methods, and (iii) a lack of versatility, as they cannot be applied to other technologies. This tool diversity has other limitations in that each

suite has a learning and adaptation process and that the tools' specificities lead to variations in the analysis of comparable data types. Similarly, current open-source analysis libraries often rely on (i) already-segmented data (Hao et al., 2024; Palla et al., 2022), (ii) specific data types (Axelrod et al., 2021; Cisar et al., 2023)23,24, or (iii) a subset of analysis tasks (Axelrod et al., 2021; Cisar et al., 2023), resulting in fragmented approaches and difficulty in adapting one approach to a different type of technology. The absence of a unified data representation and modular programming interface further complicates the integration of various analysis steps.

To address these gaps, our work introduces Spatial Omics Pipeline and Analysis, or Sopa, a computational framework that enhances the accessibility, efficiency, and interpretability of image- based spatial omics data. Sopa is a memory-efficient pipeline that works across all image-based spatial omics technologies and that can display results in a common visualizer. This includes the most recent Spatial Transcriptomics technologies (Xenium, MERSCOPE, CosMX) and also the multiplex imaging techniques (e.g., MACSima, PhenoCycler, Hyperion). Sopa's capabilities in- clude segmentation and multilevel annotation, both based on transcripts and/or stainings, as well as spatial statistics and niche geometry analysis. We demonstrate Sopa's performance on four public datasets: two spatial-transcriptomics (MERSCOPE, Xenium) and two multiplex imaging technolo- gies (PhenoCycler, MACSima), and provide a memory and time benchmark over multiple dataset sizes. Additionally, we demonstrate Sopa's capabilities for geometric and spatial analysis on the MERSCOPE dataset by analyzing cell colocalization with regard to cell types and niches, show- ing promise for biological discoveries. All these functionalities are accessible via our open-source code, which includes a Command Line Interface (CLI), an Application Programming Interface (API), and a flexible Snakemake workflow (Köster and Rahmann, 2012), enabling users with various levels of expertise to pro- cess spatial omics data seamlessly, from no-code simplicity to full flexibility. The pipeline's generic nature ensures effortless transitions to other types of spatial omics data, making it a versatile and powerful tool for the scientific community.

Results

Technology-invariant pipeline for spatial omics

To establish versatile tools, a common strategy involves adopting a shared data structure that seamlessly integrates across diverse technologies. SpatialData serves as one such comprehensive framework, including readers tailored for the most widely used spatial omics technologies (Marconato et al., 2024). Building upon this, Sopa converts any data into a SpatialData object, on which all of the six following tasks are performed. First, if needed, users can interactively select a region of interest, facilitating the exclusion of less relevant or lower-quality areas. Next, we generate overlapping patches of images and/or transcripts. Segmentation can then be performed for each individual patch, and we currently support Cellpose (Stringer et al., 2021) (image-based segmentation) and Baysor (Petukhov et al., 2021) (transcripts-based segmentation). Afterwards, the cell segmentation masks are converted into polygons and merged over all patches to remove potential artefacts. Following these first four steps, we average the staining intensities and count the transcripts inside each cell, allowing further tasks such as annotation. For example, Sopa currently supports Tangram (Biancalani et al., 2021) for transcript-based annotation, and a simple Z-score method for staining-based annotation. Finally, we implemented spatial and geometric analysis tools to fully exploit the spatial nature of the data. For convenience, all image-based technologies can be visualized in a shared explorer, and an HTML report is provided for pipeline quality checks. The full process described above is summarised in **Figure 1**.

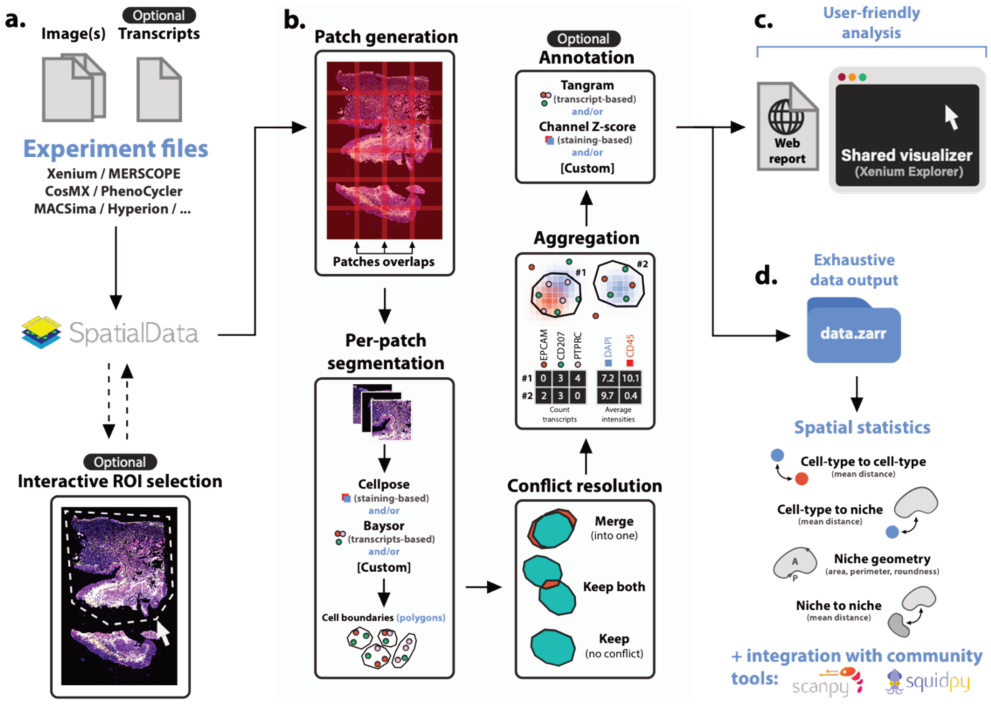

Figure 1: Overview of Sopa. ***a.*** *The pipeline input consists of experimental files of any image-based spatial omics. It is transformed into a SpatialData object, on which we can optionally select a region of interest (ROI) interactively.* ***b.*** *Afterwards, the data is split into overlapping patches, and segmentation is run on each patch (for instance, Cellpose, Baysor, or a custom segmentation tool). Since patches are overlapping, some cells can be segmented multiple times on different patches. Therefore, these conflicts have to be resolved: two boundaries with a significant overlap are merged into one cell, while two cells barely touching are kept separate. The next step is aggregation, i.e., counting transcripts and averaging each channel intensity inside each cell. This allows annotation, either based on transcripts (using Tangram) or on channel intensities.* ***c.*** *Afterwards, Sopa outputs a user-friendly report and files to be opened in the Xenium Explorer (whatever the input technology).* ***d.*** *All data files are kept for further analysis in Sopa, such as spatial statistics, or integration with community tools.*

Visualisation of spatial omics in a cross-technology interactive visualizer

In spatial omics analysis, effective visualization is crucial but has presented challenges due to the size of the datasets. While open-source initiatives like Napari are emerging, they currently face limitations in handling large amounts of transcripts. Also, most companies provide technology-specific visualizers, offering limited user possibilities (see Supplementary Notes). Yet, 10X Genomics has introduced the Xenium Explorer, an optimized visualizer whose file format is open, i.e., formats that can be generated for various SpatialData types. In Sopa, we have incorporated a converter that transforms the pipeline output into the input files compatible with the Xenium Explorer (**see Figure 1c**). This integration ensures access to an efficient and robust visualizer, extending its functionalities to any technology whose data is readable by Sopa. Importantly, this adaptation applies to both spatial transcriptomics and multiplex imaging data, with the "Transcripts" panel selectively available for transcriptomics data. **Figure 3b/e** shows views using this Explorer, while Supplementary **Fig. 2, 3** provide full-window examples. In addition to visualisation, the Xenium Explorer contains an interactive tool to align images from which we can export a transformation matrix and use it to align images on the SpatialData object to benefit from all the functionalities in Sopa.

Memory and time efficient analysis of spatial omics

Managing large datasets is a critical challenge in spatial omics, particularly when dealing with im- ages that can reach hundreds of gigabytes and contain hundreds of millions of transcripts in spatial transcriptomics data. This necessitates implementing memory optimization techniques to ensure the scalability of the analysis. Notably, segmentation algorithms like Cellpose (Stringer et al., 2021) and Baysor (Petukhov et al., 2021) encounter scalability issues with large images, as illustrated in **Figure 2a/b**. To tackle this, these segmentation models are applied to smaller regions called patches, drastically decreasing random- access-memory (RAM) usage and time. While this patching process generates possible segmentation conflicts, we show in **Figure 2d/e** and in Supplementary **Fig. 1** that this does not impact segmentation quality, since most conflicting cell boundaries have an intersection-over-min-area (IOMA) lower than 0.07 or higher than 0.8 Indeed, for cells on overlapping regions, most of the boundary conflicts correspond to either (i) the same cell segmented twice on the two patches (at least one cell is complete, as shown in **Figure 2c**, with one boundary being included in the other), or (ii) different cells slightly overlapping (as shown in the right of **Figure 2c**). Additionally, the conventional storage of cell boundaries as raster masks demands significant memory for storage and processing (see **Figure 2f).** To address this, we adopt a more efficient approach by storing cell boundaries as polygons using Shapely28, which proves highly effective for both on-disk and in-memory storage. This also facilitates geometry-related operations, such as cell expansion, area/perimeter computations, and cell-cell intersections. Combined with the image lazy loading feature from SpatialData (Marconato et al., 2024) and Xarray (Hoyer and Hamman, 2017), we implement a fast channel averaging on cell boundaries by combining geometry operations and image chunk lazy loading (see **Figure 2f**), i.e., deferring memory loading until needed for processing. Additionally, using memory-efficient tools like Dask ("Dask | Scale the Python tools you love," n.d.), we extend geometric operations of GeoPandas31 on chunks of transcripts, ensuring parallel processing of as many chunks as possible without exceeding memory limits (see **Figure 2g**). For image conversion to a pyramidal '.tif', we significantly

lower the memory usage compared to what is recommended by 10X Genomics by writing tiles in a lazy manner, which avoids loading the full image in memory (see **Figure 2h**). To highlight Sopa's memory efficiency, we compared its RAM usage against standard methods for all tasks mentioned above across various dataset sizes, summarized in **Figure 2**. Overall, the latter figure shows significant improvements in terms of RAM and time: depending on the tasks, Sopa can require between 10 and 100 times less memory than normal techniques and can be up to 100 times faster. Even on the largest image, Sopa can be run with a simple laptop with 16GB of RAM.

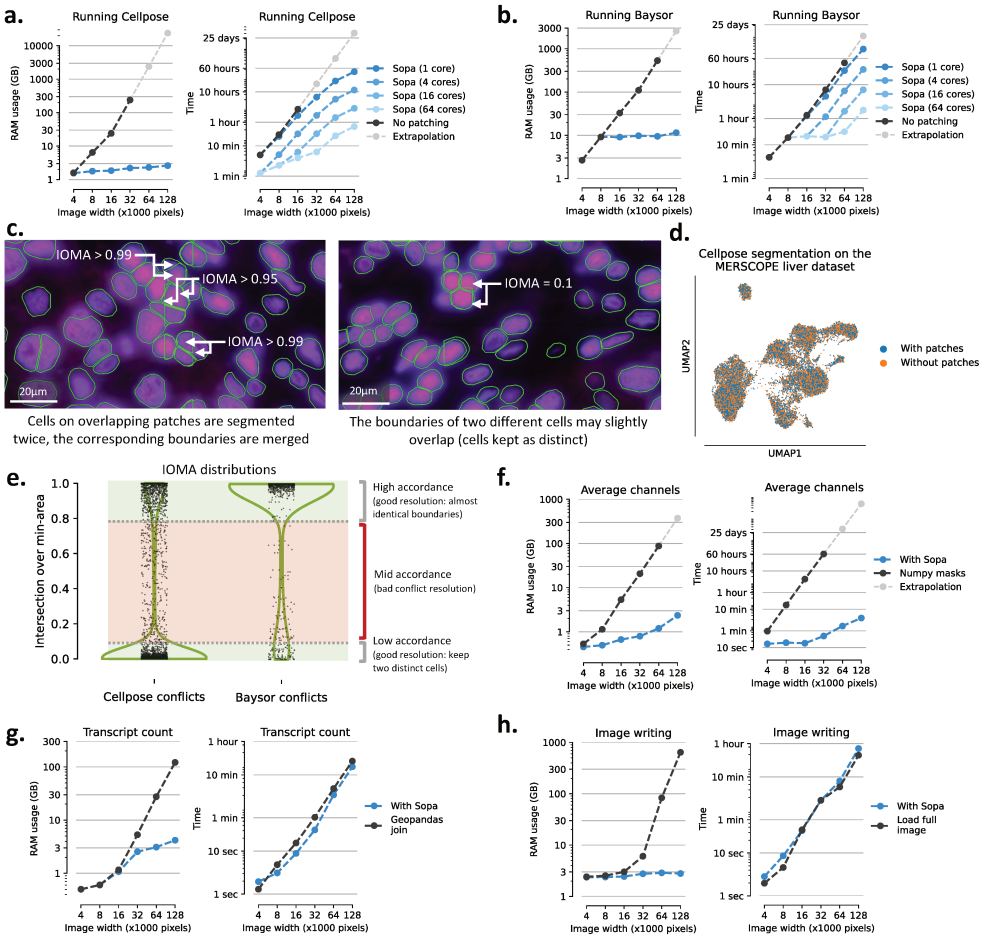

Figure 2: Computational efficiency of Sopa in terms of RAM and time on different dataset sizes. a. *Cellpose segmentation comparison: with and without patching. The RAM usage is given per core.* ***b.*** *Baysor segmentation comparison: with and without patching. The RAM usage is given per core.* ***c.*** *Examples of cell boundaries before resolving the conflicts over overlapping patches when running Cellpose segmentation on DAPI staining (MERSCOPE human liver hepatocellular carcinoma dataset). On overlapping regions, cells are segmented twice (middle and right). For each conflict, their IOMA determines whether or not to merge the two cell boundaries.* ***d.*** *UMAP showing the difference between the resolution with and without the patching process.* ***e.*** *Violin plots showing the intersection-over-min-area density of segmentation conflicts when using patches (for both Cellpose and Baysor). When resolving a conflict, the two good cases are either (i) a high concordance between the two cells (which will be merged), or (ii) a low concordance between them (the two cells are kept). IOMA below 0.07 or above 0.8 correspond to good conflict resolution cases.* ***f.*** *Channels averaging for each cell: Sopa and standard average inside numpy masks.* ***g.*** *Counting each gene inside each cell: with Sopa compared to GeoPandas join operation on the whole DataFrame.* ***h.*** *Writing image as a tiff file for the Xenium Explorer: with Sopa compared to what is recommended by 10X Genomics, i.e. loading the whole image in memory. Source data are provided as a Source Data file.*

A wide range of use cases for different levels of expertise

Sopa offers three distinct options, each tailored to different use cases: (i) a Snakemake (Köster and Rahmann, 2012) pipeline that enables a quick start within minutes, (ii) a CLI that facilitates rapid prototyping of a personized pipeline, and (iii) an API that allows direct usage of Sopa as a Python package (https://github.com/gustaveroussy/sopa), providing full flexibility and customization. The Snakemake pipeline remains consistent across various technologies, with only its configuration dif- fering. Users can leverage existing configuration files, selecting one that aligns with their technology, which then enables them to execute the pipeline without any code updates. Another advantage of Sopa's generality and scalability is that more

advanced users seeking customisable pipelines can use the CLI. Notably, Sopa's general design allows for an easy integration of any state-of- the-art or custom segmentation methods such as BIDCell (Fu et al., 2024), rendering them memory-efficient and accessible for all image-based spatial omics applications. Additionally, the Python API is avail- able for users interested in incorporating specific parts of Sopa into their personal libraries. This API also facilitates integration with other tools of the scverse (Virshup et al., 2023) ecosystem, such as Scanpy or Squidpy (Palla et al., 2022). In particular, the integration with Squidpy enables the use of post-processing tools for cell-cell interaction and spatially variable gene analysis.

High resolution of the tumour microenvironment

Segmentation plays a crucial role in image-based spatial omics analysis. Sopa focuses significantly on improving this step by enabling the usage of state-of-the-art segmentation models like Baysor19 on large datasets. Indeed, as shown on **Figure 2a/b**, these high-quality segmentation tools use a lot of memory, which hinders their usage on large spatial datasets. To evaluate the reso- lution provided by Sopa after segmentation, we annotated major cell types and conducted tests on four datasets: two spatial-transcriptomics datasets (MERSCOPE and Xenium) and two multiplex-imaging datasets (PhenoCycler and MACSima), see section and Supplementary Notes for more details. For the MERSCOPE and Xenium datasets, proprietary segmentations were provided by Vizgen and 10X Genomics, respectively. In comparison to these segmentations, Sopa shows an improved cell-type distinction on UMAP (McInnes et al., 2018) plots (see **Figure 3a/d**) by leveraging Baysor. To support these visual observations, we used multiple metrics , indicating that Sopa can generate more significant population-specific genes, greater intra-cluster distance, and improved cluster separation (see **Figure 3c/f**). The increased resolution in spatial omics data allows for a more in-depth exploration compared to previous segmentations (see Supplementary **Fig. 4** for more details).

Sopa also facilitates the concurrent analysis of both RNA and proteins. To demonstrate this, we used the Xenium dataset, which includes transcriptomic expression and protein stainings (CD20, PPY and TROP2). CD20 is a common marker for B cells, PPY is expressed by endocrine cells, and TROP2 is overexpressed in tumour cells. 10X Genomics currently does not produce files with protein expression per cell, while Sopa does support the analysis of proteins. To demonstrate this feature, we aligned the Xenium staining image to the original coordinate system, and Sopa computed the CD20/PPY/TROP2 intensity within all cell boundaries. Combined with transcriptomic expression, CD20 staining greatly facilitates the annotation of B cells, as shown by their clear delimitation on **Figure 3d** and Supplementary **Fig. 4c**. In the future, we expect technologies to be able to run more

protein stainings in parallel with transcriptomics data, making this kind of analysis even more valuable.

Regarding multiplex imaging, Sopa shows efficiency in (i) managing large protein staining panels and (ii) segmenting millions of cells (using Cellpose). The former is exemplified by the MACSima dataset with 61 stained proteins. Again, we computed staining intensity per cell, and **Figure 3g** demonstrates Sopa's capacity to annotate high-resolution cell types. Secondly, the PhenoCycler dataset underscores Sopa's ability to handle datasets of substantial size, with an area of $3cm^2$, containing approximately 2,500,000 cells. The corresponding cell resolution is shown in **Figure 3h/i**. In summary, these studies demonstrate that Sopa can (i) be applied across diverse technologies, (ii) efficiently handle millions of cells, and (iii) seamlessly operate on both transcriptomics and protein stainings.

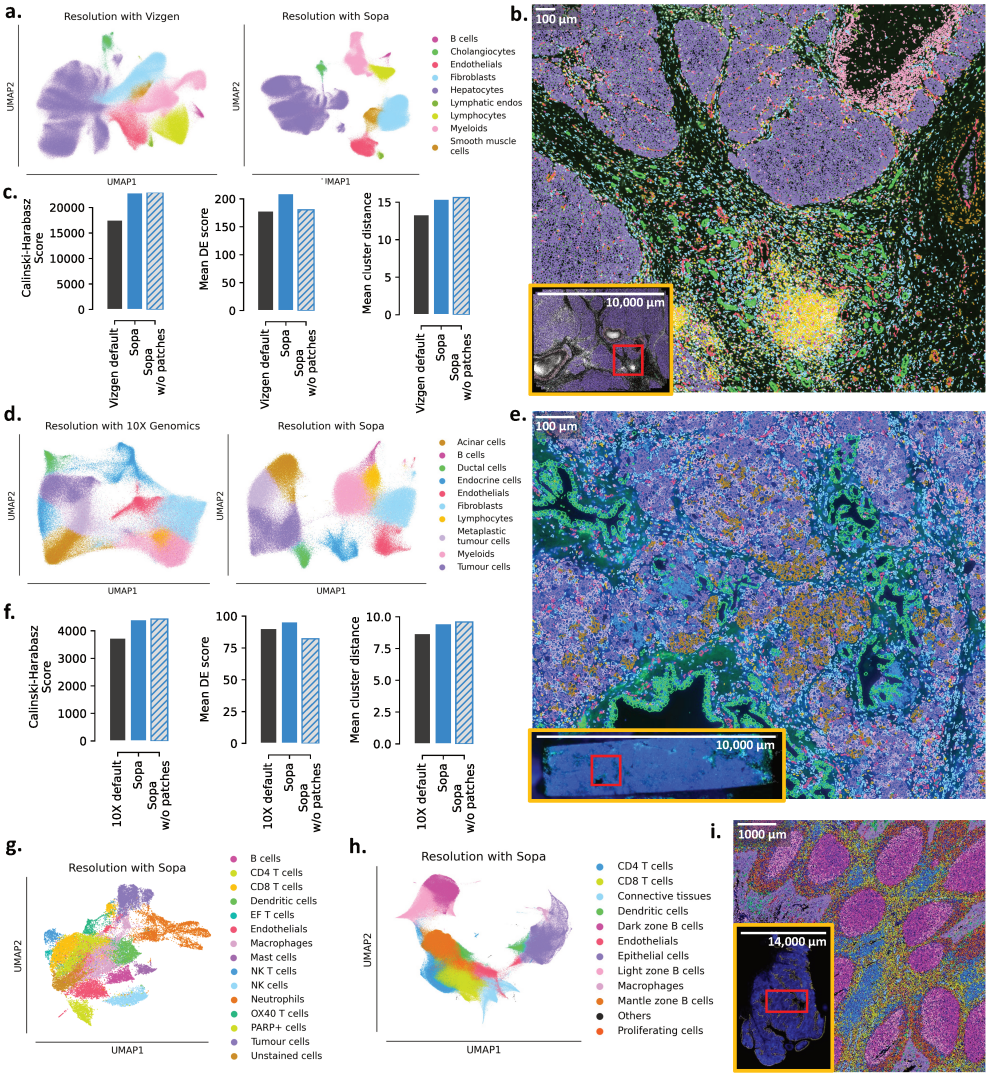

Figure 3: Data resolution after Sopa segmentation over two spatial-transcriptomics technologies (MERSCOPE (a-c) and Xenium (d-f)) and over two multiplex-imaging technologies (g-i). a. *UMAPs after Vizgen proprietary segmentation on the MERSCOPE human liver hepatocellular carcinoma dataset (left) and after Sopa segmentation on the same dataset (right).* ***b.*** *Visualization of cell types on the MERSCOPE dataset after annotation with Sopa. Colours correspond to the legend of (a).* ***c.*** *Three cluster separation metrics compare the quality of these two segmentations on the MERSCOPE dataset. The grey hatched boxes extrapolate the score Sopa would have without running on patches.* ***d.*** *UMAPs of cells after 10X Genomics proprietary segmentation on the Xenium human pancreatic cancer*

dataset (left) and after Sopa segmentation on the same dataset (right). ***e.*** *Visualization of cell types on the Xenium dataset after annotation with Sopa. Colours correspond to the legend of (d).* ***f.*** *Three cluster separation metrics compare the quality of these two segmentations on the Xenium dataset. The grey hatched boxes extrapolate the score Sopa would have without running on patches.* ***g.*** *UMAP of cell types on the MACSima dataset (head and neck squamous cell carcinoma), based on 61 protein stainings.* ***h.*** *UMAP of cell types on the PhenoCycler dataset (human tonsil), based on 31 protein stainings.* ***i.*** *Cells of the PhenoCycler dataset visualized. The colours correspond to the legend of (h). Source data for (c, f) are provided as a Source Data file.*

Demonstration of geometric and spatial analyses capabilities

Spatial omics naturally unlocks multiple biological questions related to spatial organization. While some are addressed in libraries such as Squidpy (Palla et al., 2022), metrics related to the distance between cell- types/niches and the geometric characteristics of those niches are not provided. These metrics could help in the understanding of the morphology of the tumour micro-environment and its location with regard to different cell types. Such statistics have been shown to be relevant for predicting disease progression or response to treatment (Jass, 2007; Sharma et al., 2005). For instance, it is known that tertiary lymphoid structures (TLS) have a good prognosis (Sautès-Fridman et al., 2019), but their geometry has not been studied. TLS may come in different sizes, shapes, occurrences, or locations with regard to other niches. Such statistics are generalized in section for all cell categories (usually, cell types or niches). Leveraging this spatial analysis, we demonstrate a better understanding of the dynamics among different cell types and their relation to different spatial niches on the MERSCOPE liver dataset (**Figure 4**). To use Sopa geometric analysis, we run STAGATE (Dong and Zhang, 2022) to identify eight distinct niches (or "spatial domains") across various tumour regions (**Figure 4a**). First, we show in **Figure 4b** four geometric properties related to these niches: for each niche compartment, we counted their occurrence on the same slide, as well as their mean area, perimeter, and roundness. For instance, our geometric analysis shows a high

occurrence of vascular niches, that are small in area and perimeter, but have a high roundness. Conversely, the stroma has only one occurrence and is highly "unround", and **Figure 4c** shows that this shape enables a "proximity" to every other niche. **Figure 4c** also highlights how far the vascular niche is from the necrosis. While such observations are not novel, our geometric computation allows for statistical comparisons over multiple patients, which could lead to the discovery of significant geometric biomarkers in large-scale studies. Finally, Squidpy (Palla et al., 2022) already incorporates functionalities on neighbourhood enrichments, which is a local metric and, therefore, not suited to capture niche-level information. In comparison, the distance metric used in Sopa can capture asymmetrical observations and global organizations (see Supplementary **Fig. 6** for more details).

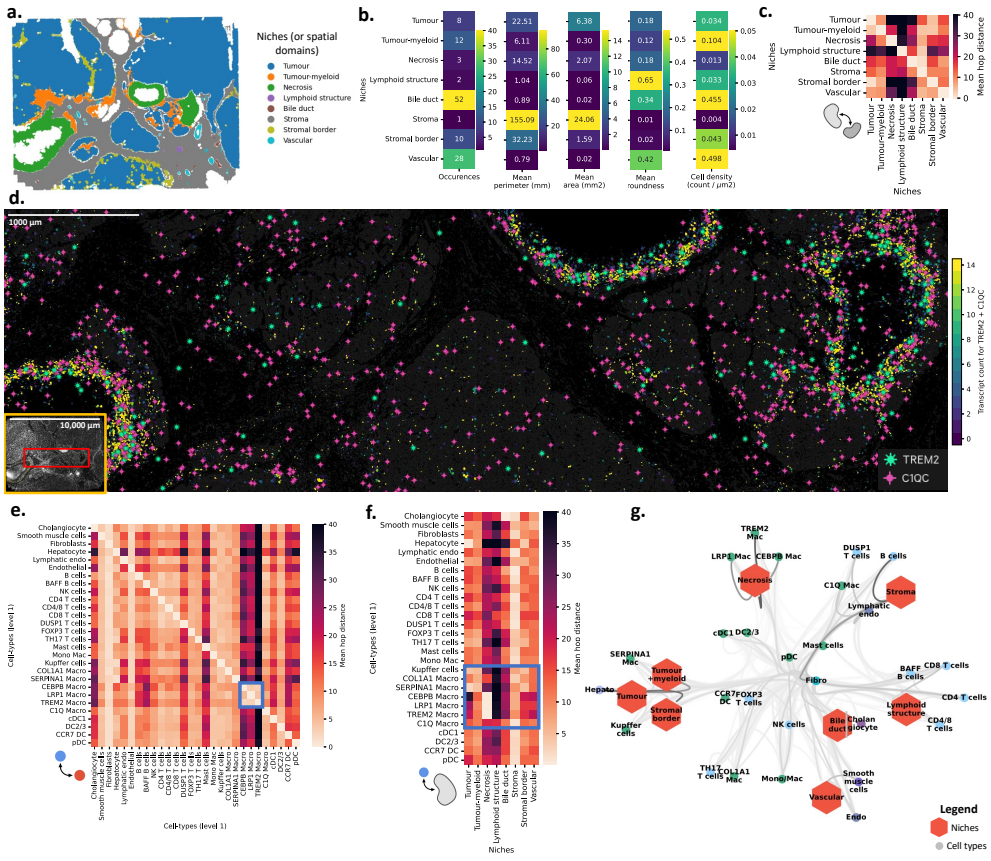

Figure 4: **Geometric analyses and spatial statistics on the MERSCOPE human liver hepatocellular carcinoma dataset. a.** Niches (or spatial domains) after geometric conversion to shapely

polygons. **b.** Geometric statistics of the niches: their occurrence, perimeter, area, roundness, and inner cell density. **c.** Heatmap of average hop distance between niches and niches. **d.** Localisation of *TREM2* macrophages shown in the visualizer. The *TREM2* and *C1QC* genes are shown, and cells are coloured by their gene counts for the two selected genes. **e.** Heatmap of average hop distance between cell types and all other cell types. *LRP1*, *CEBP*, and *TREM2* macrophages show a high proximity. **f.** Heatmap of average hop distance between cell types and niches. The macrophage subpopulations show heterogeneous localisation with respect to the niches. *LRP1*, *CEBP*, and *TREM2* macrophages are enriched in the necrosis niche. **g.** Network plot summarising the distance metrics of (c)/(e)/(f). Each node of the network corresponds either to a niche (hexagon) or a cell type (circle). The lower the mean distance between the two nodes, the higher the weight of the edge between these two nodes. A high node-node proximity is shown by a dark edge. Overall, it provides an overview of the colocalisation of cell types and niches in the tumour environment.

We also utilised Sopa to assess the intricacies of the tumour complexity. We annotated the immune populations of the MERSCOPE dataset in higher definition (see Supplementary **Fig. 5a/b**) and, in parallel, performed a differential analysis on each niche to better understand niche complexity. This revealed a distinct necrotic niche correlated with *TREM2* macrophages (expressing *TREM2, C1QC and CSF1R)*, a population of macrophages reported across cancer types and of- ten associated with bad prognosis (Binnewies et al., 2021; Molgora et al., 2020) (see **Figure 4d** and Supplementary **Fig. 5c**). To deepen this understanding of tissue intricacies, we investigated whether these *TREM2* macrophages were in close distance with any other cell type (see **Figure 4e**). Strikingly, this figure highlighted that three macrophage populations (*LRP1, CEBP*, and *TREM2*-macrophages) exclusively interacted with themselves. Correlating their location with the niche revealed that their co-occurrence is specific to the necrotic niche (see **Figure 4f**). When combining all (cell-cell/cell-niche/niche-niche) interactions, this affirms again the association of *LRP1/CEBP/TREM2*-macrophages in the necrotic niche, yet it also highlights the heterogeneity of all macrophage populations and their

relation to the niche in the whole tissue environment (see **Figure 4g**). These combined interactions also showed

that, inversely, the conventional dendritic cells (DCs) are not associated with any niche environment, accentuating how some populations can also be niche-independent. This observed spatial location underscores a potential reprogramming feature of macrophages based on their specific niche. While it is known that the accumulation of TREM2 macrophages has been associated with enrichment in the tumour regions (Mulder et al., 2021; Sharma et al., 2020; Zhou et al., 2022), Sopa can provide insights for a refined understanding of a macrophage-specific tumour-associated phenotype. These examples illustrate that this geometric and spatial analysis — computed with Sopa — helps better understand the tumour's architecture and its relationship with cell type phenotypes.

Incorporation of H&E into the multi-omics spatial analysis

Some technologies, such as the Xenium, have been developed to get Hematoxylin and Eosin (H&E) staining and protein staining on the same slide used for Spatial Transcriptomics. By aligning the modalities (with the Xenium Explorer, as detailed in the Supplementary Notes), Sopa enables analyses that can interplay with all three modalities. Especially, the H&E modality, via the colour and texture, captures extra information that the two other modalities do not contain. For instance, H&E may be stronger in regions with low RNA information, such as high collagen regions (see Supplementary **Fig. 7**). In **Figure 5**, we perform analyses that couple the three layers to provide interpretability to the H&E niches (see section for more details on the niches computation). **Figure 5c** shows that H&E-based niches are highly heterogeneous in terms of cell types, with some niches being highly enriched in some particular populations. Notably, niche 3 is highly specific to Acinar cells, niche 5 is specific to Ductal cells, while niche 4 is enriched in B cells and Myeloid cells. Also, **Figure 5d** shows differentially expressed genes inside each niche, providing

complementary insights to **Figure 5c**, such as *TM4SF4* and *APCDD1* being highly specific to niche 5. Finally, **Figure 5e** exemplifies the analysis of the distribution of protein stainings inside these H&E niches, with TROP2 being more expressed in niche 0 and 3, which correspond to the tumour-specific niches identified in **Figure 5c**. Overall, these examples show the capability of Sopa to use one spatial modality to bring insights into another spatial modality.

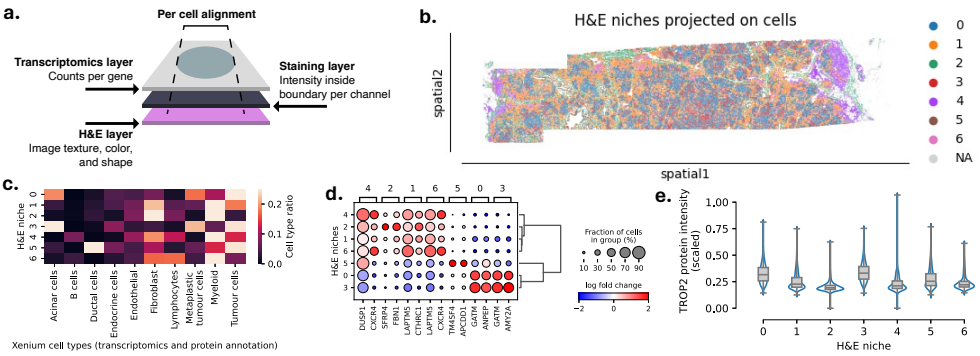

Figure 5: Spatial multi-omics analyses on the Xenium pancreatic cancer dataset. a. *Overview of spatial multi-omics alignment. For each single cell, the information of (i) transcriptomics, (ii) stainings, and (iii) H&E is combined after the alignment of all the different layers.* ***b.*** *H&E clusters of patch-level embeddings based on a pre-trained computer vision model (denoted as H&E niches). The figure shows the cells obtained from spatial transcriptomics data and coloured by the H&E patch cluster inside which they are included.* ***c.*** *Proportion of cell types inside each H&E niche. The cell types are the cell types annotated using both spatial transcriptomics and protein information as in Figure 3.* ***d.*** *Differential gene expression performed on the H&E niches using single-cell resolution.* ***e.*** *Distribution of TROP2 intensities per cell (N=175,022) inside each H&E niche, showcasing the usage of the staining layer coupled with the H&E information. Source data for (e) are provided as a Source Data file.*

Discussion

Advances in technology development for spatial omics hold great promise for biological discoveries. Yet, to build strong and unified foundations for spatial omics data analysis, more tools are required. With this purpose in mind, we designed and built Sopa to address several crucial aspects of spatial omics analysis: versatility, reproducibility, and scalability. It offers a suite of tools — or building blocks — designed for spatial omics, which are assembled to build a pipeline for any image-based spatial omics technology. At the end of the pipeline, it produces standardized outputs, which ease exploration and visualization. While each company's technology comes with its own suite of tools — which differ in terms of capabilities and functionalities — Sopa does not require learning from multiple data types and software. In addition, Sopa is scalable from simple laptops to high-performance clusters, offering further versatility for users.

Moreover, Sopa can easily integrate recent methods and tools: as future segmentation or annotation methods are developed, they can be added to Sopa once published and validated. This incorporation into Sopa enables scalability and availability to any future technology with only minor configuration changes. As datasets become increasingly bigger, Sopa's scalability is crucial. For instance, Sopa enabled the possibility of running Baysor on data produced by the MERSCOPE, which was previously impossible due to RAM usage and time. Assessing the effect of patch-based segmentation showed no significant difference in segmentation quality. We also demonstrated that Baysor significantly increases data quality compared to the default Vizgen and 10X Genomics segmentation tools, which aligns with Hartman et al. (Hartman and Satija, 2024).

As shown on the MERSCOPE liver dataset, we were able to annotate spatial-specific macrophages, particularly *TREM2* macrophages, in the necrotic niche. Additionally, *TREM2* has been shown to increase with HCC, suggesting a potential immunosuppressive role of *TREM2* (Molgora et al., 2020), while necrosis has been associated with worse prognosis (Bijelic and Rubio, 2021; Wei et al., 2021). With the help of

Sopa, the exploration of this relationship between tissue architecture and cell phenotypes can advance biological knowledge.

Besides higher data resolution, Sopa can also incorporate protein and H&E information into spatial analysis. Without this protein layer, extracting the B cell population in the Xenium data would not have been possible. Concerning the H&E layer, we can benefit from the transcriptomics layer to bring interpretability to the H&E tissue characterization or also build upon Sopa to develop tools that predict refined spatial-transcriptomics cell types based on H&E images. While current spatial technologies involve either a high number of proteins or transcripts, future developments could add extra layers of information, contributing to a better understanding of biological systems. This paper has demonstrated through various techniques that Sopa is ready to handle large multi-modal spatial technologies.

Acknowledgement

This work is supported by Prism – National Precision Medicine Center in Oncology funded by the France 2030 programme, the French National Research Agency (ANR) under grant number ANR-18-IBHU-0002, ARC Foundation and Fondation Gustave Roussy.

Author Contributions

Q.B. implemented the Sopa library, performed the computational benchmark, and wrote the manuscript. K.M. defined the biological aims of the project, performed the biological analysis, and wrote the manuscript. M.G. performed experiments as part of a clinical study involving private data. S.C. implemented capabilities for handling H&E data to the Sopa package. C.A.D. detailed the need for a new method to standardize the analysis of spatial omics data. F.G. supervised K.M. with a particular focus on the biological aspect of the project. P.H.C supervised Q.B., concentrating on the methodological aspects of the work and manuscript development. Finally, F.A. and P.H.C. acquired the grant to fund the project.

Methods

Datasets used

Four public datasets were used to demonstrate Sopa's abilities. First, we used a MERSCOPE dataset (from Vizgen) of the human liver hepatocellular carcinoma (HCC), called FFPE Human Immuno-oncology Data Set May 2022. It is composed of a 500-gene panel, and has DAPI staining and PolyT staining. It contains about 500,000 cells, depending on the segmentation. Secondly, we used a Xenium dataset (from 10X Genomics) of pancreatic cancer (adenocarcinoma, Grade I-II) with the Xenium Human Multi-Tissue and Cancer Panel, in parallel with corresponding H&E image, and a protein-staining image with DAPI/CD20/PPY/TROP2. Note that the two latter images has to be aligned on the default main DAPI image. It contains about 180,000 cells, depending on the segmentation. Thirdly, we used a PhenoCycler dataset (from Akoya Biosciences) of the human tonsil (FFPE) with 31 protein stainings. It contains about 2,500,000 cells, depending on the segmentation. Finally, we used a MACSima dataset (from Miltenyi) of head and neck squamous cell carcinoma (HNSCC) with 61 protein stainings. It contains about 40,000 cells, depending on the segmentation. For more details about the accessibility of these datasets, see section .

Metrics used and computational details

The Calinski-Harabasz-Score is defined as the ratio of the sum of between-cluster dispersion and of within-cluster dispersion. To compute this score, we used the implementation in scikit-learn. The mean cluster distance is the average distance between all pairwise combinations of cells between two different clusters; thus, a higher distance indicates a better cluster separation. For the differential expression analysis, we ran the scanpy *rank genes groups* function, and we averaged the score of the 20 most significant genes for each cell type. Since we could not run Baysor on the full datasets in Figure 2, we run it on 16,000-pixels-wide crops of the MERSCOPE and Xenium datasets, and we computed the ratios between the run with the

patches and without patches. We then averaged these ratios across these two datasets, with two runs on each dataset, for each of theabove metrics and used the resulting ratios to extrapolate the Baysor score on the full datasets. Thetime and memory benchmarks were performed on a Slurm cluster on the same CPU nodes. The benchmark related to Cellpose was performed on crops of the MERSCOPE dataset, while the othertime and memory benchmarks were performed on a synthetic dataset.

Figure 2e was generated based on the corresponding 16,000-pixels-wide datasets; this involves 25 Cellpose patches and 4 Baysor patches. The percentage of conflicts for Cellpose (compared to allpairs of cells) was 0.007%, while this percentage was 0.001% for Baysor. The UMAPs of Fig- ure 3 were generated with scanpy, using the default parameters. The MERSCOPE and Xenium datasets have been segmented with Baysor, while the PhenoCycler and MACSima datasets have been segmented with Cellpose. Both the MERSCOPE and Xenium datasets have been annotated using Tangram (see Supplementary Notes for more details). Concerning the H&E niches, they were obtained by running a ResNet model pre-trained on ImageNet and applied on patches of size 250x250 pixels.

Segmentation on patches

For computational efficiency, segmentation is performed on patches, i.e., small image regions. These patches have a certain overlap, which is typically chosen to be at least twice as big asthe average diameter of cells (e.g., 20 microns). This way, each cell should be complete in at least one patch, which avoids artefacts due to cutting cells at the border of the patches. Subsequently, any segmentation algorithm compatible with images and/or transcripts can be applied. While Cellpose and/or Baysor are commonly used, Sopa does allow the integration of other segmentation algorithms. Following segmentation on individual tiles, the cell boundaries are transformed into polygons using Shapely. Since patches overlap, some cells may be segmented

across different patches, leading to segmentation conflicts where multiple polygons correspond to a single cell. To resolve this, we adopt a method similar to the one used in Vizgen's preprocessing tool (VPT). Specifically, we merge pairs of cells when the intersection area exceeds half the area of the smaller cell, ensuring a substantial overlap. If the intersection area is too small, indicating distinct cells, both polygons are retained. When the overlap area divided by the smallest cell area is close to 1, this corresponds to two almost identical cells, while a score close to 0 corresponds to two cells barely touching. On **Figure 2e**, we studied the distribution of this score, showing that most of the conflicts are associated with a score that is either very close to 0 or very close to 1, indicating a good conflict resolution. Indeed, statistical considerations indicate that scores above 0.8 or below 0.07 are good resolutions. Additionally, note that, before segmentation, the user can decide to select a region of interest: this can be done interactively with matplotlib on a low-resolution image.

When dealing with image-based technologies, a crucial step involves averaging the intensity of each channel within each cell. While this task can be achieved using cell masks, it proves highly inefficient in terms of both time and memory consumption. To address this challenge, we adopt a chunk-level approach: (i) For each chunk, we identify cell boundaries (i.e., polygons) that intersect with the chunk coordinates, then (ii) we determine the bounding box for each of these cells, then (iii) we extract the image values for each of these bounding boxes, and finally (iv) we rasterize the cell polygons to average the staining intensity over the local bounding box. In this way, we only load small arrays corresponding to each cell, instead of loading large cell masks. This process is repeated over all chunks, and we make sure that the channel intensity for cells located on multiple chunks is computed correctly.

Counting transcripts

GeoPandas is a Python library that enhances Pandas Dataframes by incorporating support for Shapely geometries. It facilitates scaling operations on geometries, making it particularly suit- able for transcript counting, where transcripts can be represented as Shapely points and cells as Shapely polygons. However, without Sopa, the memory requirements for such operations can be substantial, especially for spatial transcriptomics datasets that may contain up to one billion tran-scripts. To optimize this process, we leverage Dask and execute the GeoPandas "join" operationat the partition level to assign each point (i.e., a transcript) to a polygon (i.e., a cell). Thus, each op-eration is carried out on smaller data frames, each less than 100MB in size. Dask efficiently assigns each partition to different workers in parallel, mitigating memory concerns. This approach proveshighly effective on both laptops and high-performance clusters, as Dask is designed to seamlessly scale these processes without necessitating any code modifications.

Con-verting a spatial omics object into the Xenium Explorer requires the creation of six files: (i) theimage, (ii) a JSON metadata file, (iii) the cell boundaries, (iv) the cell categories (e.g., cell type orclustering), (v) the gene counts table, and (vi) the transcripts (if they exist). The conversion is doneautomatically by Sopa, but it can also be done manually via our CLI: `sopa explorer write <sdata path> <output path>`.

For image creation, a Python function is recommended in the Xenium Explorer documentation (`https://www.10xgenomics.com/support/software/xenium-explorer/tutorials/ xe-image-file-conversion`) but is not optimized for large images. We updated it to support Dask arrays, i.e. (the image type used by Sopa). Pyramids of resolutions are generated via the SpatialData library. To decrease memory usage, each

(1024x1024) image tile is generated using an iterator that only computes the minimally required data from the Dask array at each tile generation. For higher pyramidal levels, where the image size decreases, we allow loading an image into memory if it fits, accelerating conversion.

As transcripts typically cannot be loaded entirely into memory, the Xenium Explorer avoidsloading all transcripts. On low-resolution levels, only a subset of transcripts is displayed (sub- sampled), while zooming in reveals all transcripts from the current field of view. This pyramidal transcript view ensures low memory usage during visualization. The highest-resolution tiles are 250-micron-wide squares. For each pyramid level, the tile width doubles, and only one-fourth of the transcripts from the previous level are retained. The process stops when there is only one remaining tile that is larger than the original slide. Transcript coordinates are stored as separate chunks for each tile and resolution, saved as a Zarr file. This allows loading only the transcripts corresponding to the displayed tiles when zooming in.

Cell boundaries are padded to have the same number of vertices (13). Polygon simplification is applied to polygons with more than 13 vertices using the Shapely library, reducing the number of vertices while preserving shape geometry. A fixed number of vertices enables lighter cell-boundary storage and faster visualization.

Transcript counts (cell-by-gene table) use sparse array storage. One 1D array stores all non-zero transcript counts, another array stores the cell index for each count, and a third array is a pointer indicating the gene index for these counts. Cell categories are similarly saved using indices and corresponding pointers. Once again, the file format employed is a Zarr file.

Cell-type annotation

Transcript-based annotation. Tangram is used for cell-type annotation based on an anno-tated scRNAseq reference. To make Tangram scalable for large datasets, we adopt a strategy of splitting the data into "bags of cells", with the size determined by the user. This approach ensures that each Tangram iteration operates within manageable memory limits, and we subsequently merge the results to obtain the annotation for the entire dataset. Following this, Leiden[53] clustering can be applied to refine the annotation, associating each Leiden cluster with its most prevalent Tangram cell type. Additionally, we have implemented a multi-level annotation feature based on Tangram to enhance the annotation of minor cell types if needed. The process involves initially annotating global cell populations, followed by running Tangram on specific cell groups (e.g., Myeloid cells) for a more detailed annotation (e.g., pDCs, *TREM2* macrophages, etc.). All that is required is to provide multiple cell-type annotation columns in the reference scRNAseq data, and Sopa will seamlessly execute the multi-level annotation.

Staining-based annotation. For non-transcriptomics data, we also provide a fluorescence- based annotation. As each channel intensity is averaged inside each cell, we obtain a matrix $\mathbf{X}$ of shape (N, P), where N is the number of cells, and P the number of stainings/channels. Then, these intensities are preprocessed as in a recent article[52]:

$$\mathbf{X}' = (\mathbf{X'}_j)_{1 \leq j \leq P}, \text{ with } \mathbf{X'_j} = \operatorname{arcsinh}\left(\frac{\mathbf{X_j}}{5Q(0.2, \mathbf{X_j})}\right),$$

where $\mathbf{X}'$ is the preprocessed matrix, arcsinh is the inverse hyperbolic sinus function, and $Q(0.2, \mathbf{X_j})$is the 20th percentile of $\mathbf{X_j}$. Afterwards, we use a list of stainings corresponding to a population, and each cell is annotated according to the channel whose preprocessed intensity is the highest. If desired, Leiden clustering can be run to have a deeper annotation. Each cluster can be annotated via differential analysis or by showing a heatmap of staining expression per cluster.

Spatial statistics

All spatial statistics are performed after computing a Delaunay graph based on the spatial locationof cells. This is done with Squidpy, which is itself based on Scipy. We also prune long edges that cannot correspond to a physical cell-cell interaction (typically, edges longer than 40 microns). In the paragraphs below, N denotes the number of cells.

***** Cell category to cell-category statistics. One relevant spatial statistic is the computation of the mean or minimum distance between two cell categories. This includes the pairwise distance be- tween cell types (e.g., the mean distance between CD8 T cells and tumour cells), as well as the distance between cell types and niches (e.g., the distance between tumour cells and tertiary lym- phoid structures). Let ($C_1, \ldots, C_N$) represent categories assigned to the N cells (e.g., cell types), and ($C'_1, \ldots, C'_N$) represent other categories (such as the niche to which the cell belongs). For instance, if cell "i" is a T cell inside the stroma,

then C_i = "T cell" and C_i' = "stroma". The sets ofunique categories are denoted G and G', respectively; for instance, G can be the set of unique cell types, and G' can be the set of unique niches. Then, $\forall g \in G$ and $\forall g' \in G'$, we define the mean distance between the category g and g' as follow:

$$D(g, g') = \frac{1}{\mathrm{Card}(\{i \mid C_i = g\})} \sum_{i \mid C_i = g} \min_{j \mid C'_j = g'} d_{ij},$$

where Card represents the cardinal, and d_{ij} is the hop-distance between cell i and cell j. Note

that $\min_{j \mid C_j' = g'} d_{ij}$ is the distance between cell i and the closest cell of category g', that is how many hops are needed for cell i to "find" the category of interest. In practice, we compute $D(g, g')$ by multi-node graph traversal, starting from all nodes whose category is g'. In this way, for each $g' \in G'$, we compute $(\min_{j \mid C_j' = g'} d_{ij})_{1 \le i \le N}$ in a single graph traversal. All the resulting distances can be stored in a matrix $((D(g, g')))_{g \in G, g' \in G'}$ and shown as a heatmap. Note that this

heatmap is asymmetric because of the "minimum" usage in the above distance definition. To prevent confusion while reading the asymmetrical heatmaps, we precise that one row corresponds tothe distances from the cell type of the row index to all other cell types. Additionally, we combinethe four matrices of distances (cell-type to cell-type, cell-type to niches, niches to cell type, and niches to niches) into an adjacency matrix whose weights are the inverse of the distance. Then, thecorresponding network can be plotted using the netgraph library, as in **Figure 4g**, providing an interpretable visualization of the tumour microenvironment's structure.

***** Niche geometry statistics. When niches (or spatial domains) are performed with an algorithm such as STAGATE[39], users can decide to extract these niches as geometries to compute some relevant statistics, such as their area, perimeter, or roundness. From now on, for each cell i, $1 \leq i \leq N$, C_i denotes the niche to which the cell belongs, and G is the corresponding set of unique niches (i.e., for all cell i, $C_i \in G$). First, we prune all the edges (i, j) that are in between niches from the Delaunay graph, i.e., if $C_i \neq C_j$. Then, we extract the connected components of the graph. Because of the way we pruned the edges, each component corresponds to one niche, but one niche can be composed of multiple components (or occurrences). For each component, we search simplices (i.e., triangles from the Delaunay graph) at the component's border, that is, the simplices that have one or two simplex neighbours. From all the border simplices, we extract the corresponding border edges; these edges are then linked to make one or multiple rings (i.e. cyclic lines). If we have only one ring, it is transformed into a polygon, which corresponds to a "full" component. If there are multiple rings, the largest ring is the outer polygon, and the others correspond to "holes" inside the main polygon: this can happen when some components are completely surrounded by another niche. Repeating this process for all components allows the transformation of each niche $g \in G$ into multiple polygons. We can then count how many occurrences (or polygons) each niche is made of, and we can also compute the mean area A_g, perimeter L_g, and roundness R_g of each niche using Shapely[28]. Note that $R_g = \frac{4\pi A_g}{L_g^2} \in [0, 1]$, where higher values correspond to a "circle-like" shape. The density of cells inside a niche is computed as the total number of cells in this niche divided by the total area of the niche. Also, for each niche, we filter out components whose areas are less than 5% of the area of the same niche's largest component, as they usually correspond to low-quality artefacts from the clustering of niches.

Data availabilty

The MERSCOPE dataset is available online at https://info.vizgen.com/merscope- ffpe-solution. The Xenium dataset is available at https://www.10xgenomics.com/resources/datasets/pancreatic-cancer-with-xenium-human-multi-tissue- and-cancer-panel-1-standard. The PhenoCycler dataset is available upon request to Akoya Biosciences, see https://www.akoyabio.com/fusion/data-gallery/. The MACSima dataset is available upon request to Miltenyi Biotec. Source data are provided with this paper.

Code availability

The code developed in this article is available as an open-source Python package, accessible on Github at https://github.com/gustaveroussy/sopa, or with the Zenodo DOI 11084433[56]. The code used to run the benchmark is available at https://github.com/quentinblampey/ sopa_benchmark.

Supplementary Figures

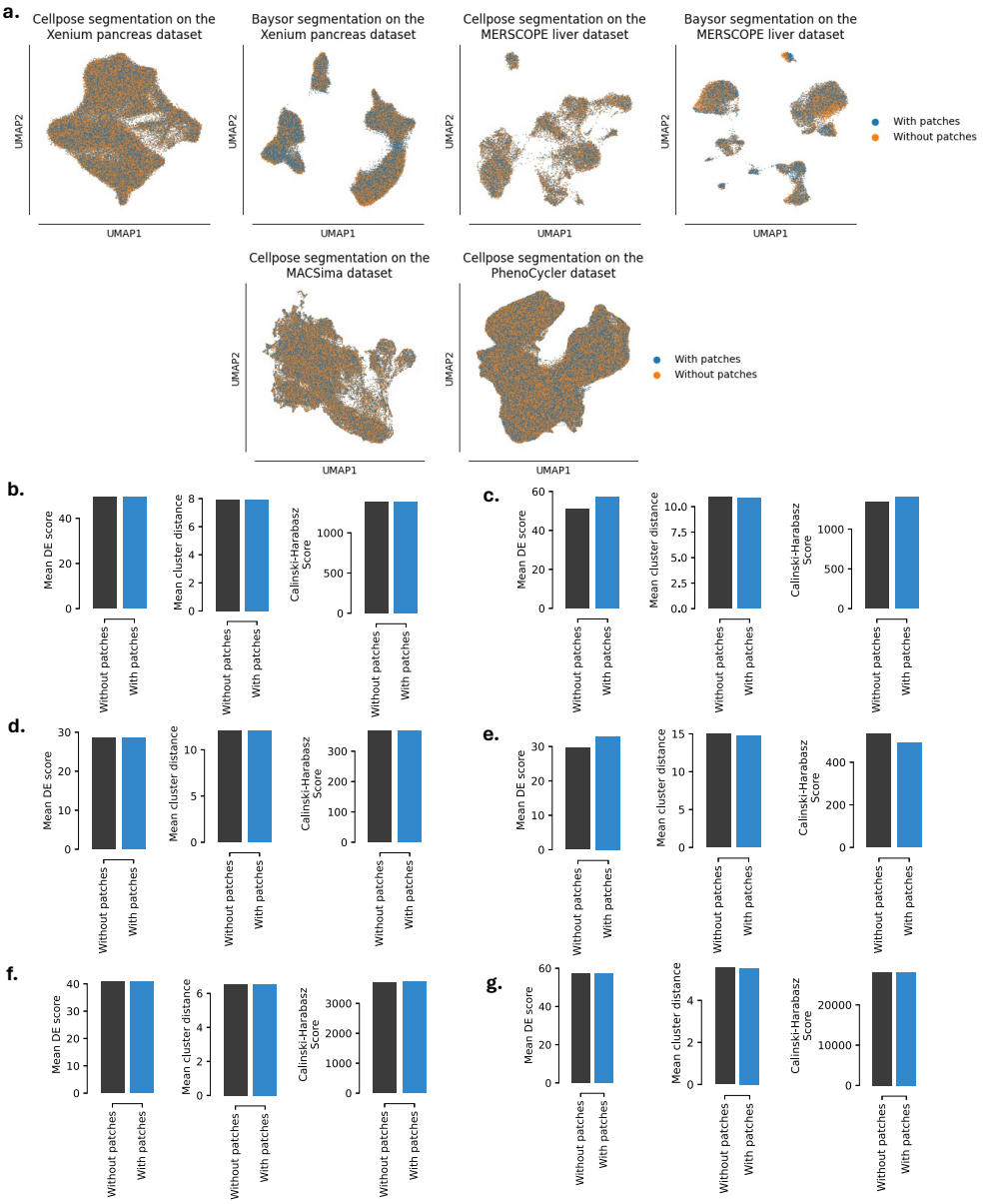

Supplementary Figure 1: *Impact of patched-based segmentation over the data quality, based on crops of size (16000x16000) of the original image. a. UMAPs comparing the representation of the cells obtained while running segmentation over the whole image and using patches (as in Sopa). This was tested over multiple datasets, for Cellpose (for all datasets) and Baysor (for spatial transcriptomics datasets). b.*

Comparison of segmentation quality metrics for Cellpose run on the Xenium dataset. c. Comparison of segmentation quality metrics for Baysor run on the Xenium dataset. d. Comparison of segmentation quality metrics for Cellpose run on the MERSCOPE dataset. e. Comparison of segmentation quality metrics for Baysor run on the MERSCOPE dataset. f. Comparison of segmentation quality metrics for Cellpose run on the MACSima dataset. g. Comparison of segmentation quality metrics for Cellpose run on the PhenoCycler dataset.

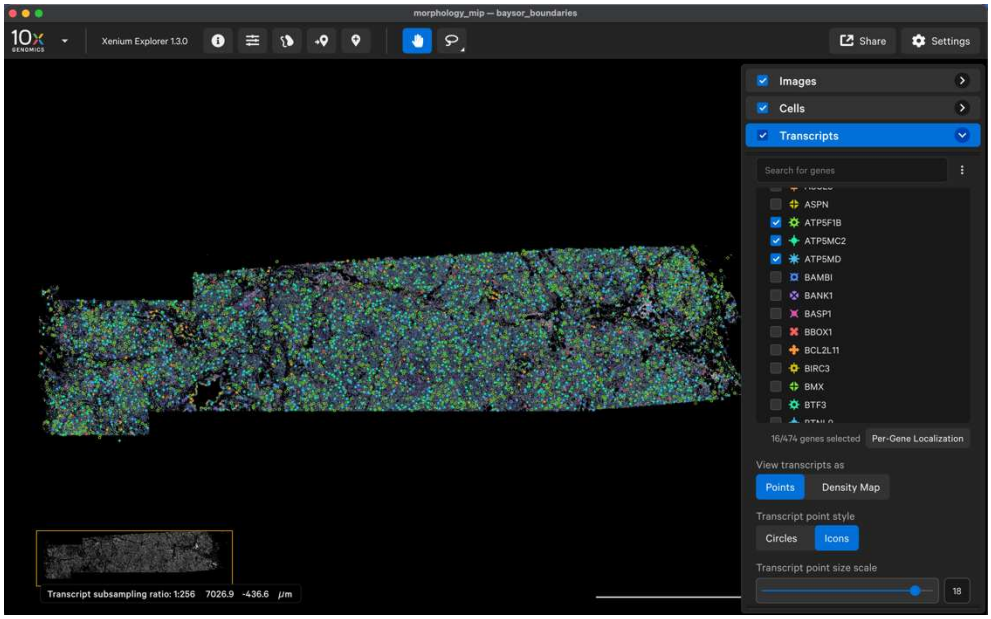

***Supplementary Figure 2**: Xenium human pancreatic cancer dataset (10X Genomics) open in the Xenium Explorer. The transcript panel is shown, with a few genes selected. Cells are coloured by a colour gradient representing transcript count.*

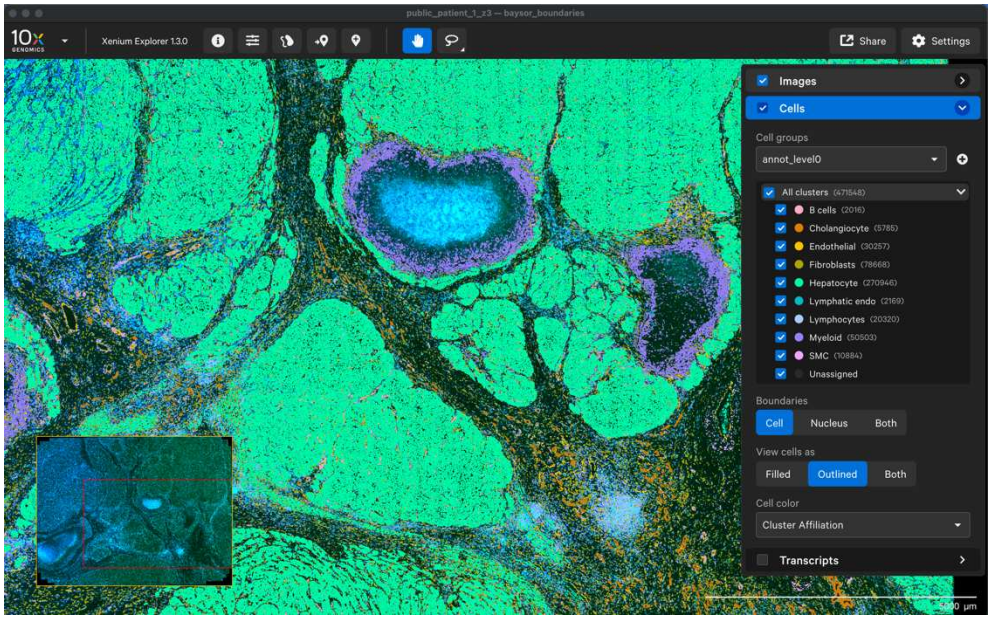

Supplementary Figure 3: *MERSCOPE human liver hepatocellular carcinoma dataset (Vizgen) open in the Xenium Explorer. The cell panel is shown, and the "annot level0" category is displayed. Colors correspond to a cell-type.*

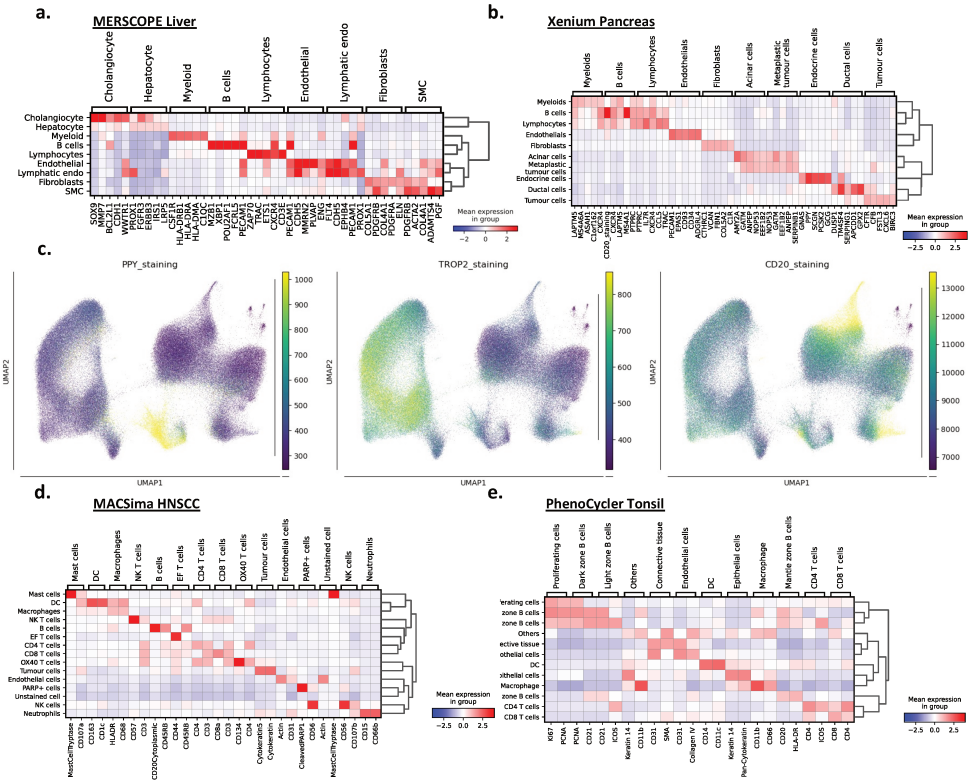

Supplementary Figure 4: *Visual validation of the annotations. a. Heatmap of genes expression per population on the MERSCOPE human liver hepatocellular carcinoma dataset. b. Heatmap of genes expression per population on the Xenium pancreas dataset. c. Protein staining per cell on the Xenium human pancreatic cancer dataset after aligning the staining image to the original Xenium image. d. Heatmap of protein expression per population on the MACSima HNSCC dataset. e. Heatmap of protein expression per population on the Phenocycler tonsil dataset.*

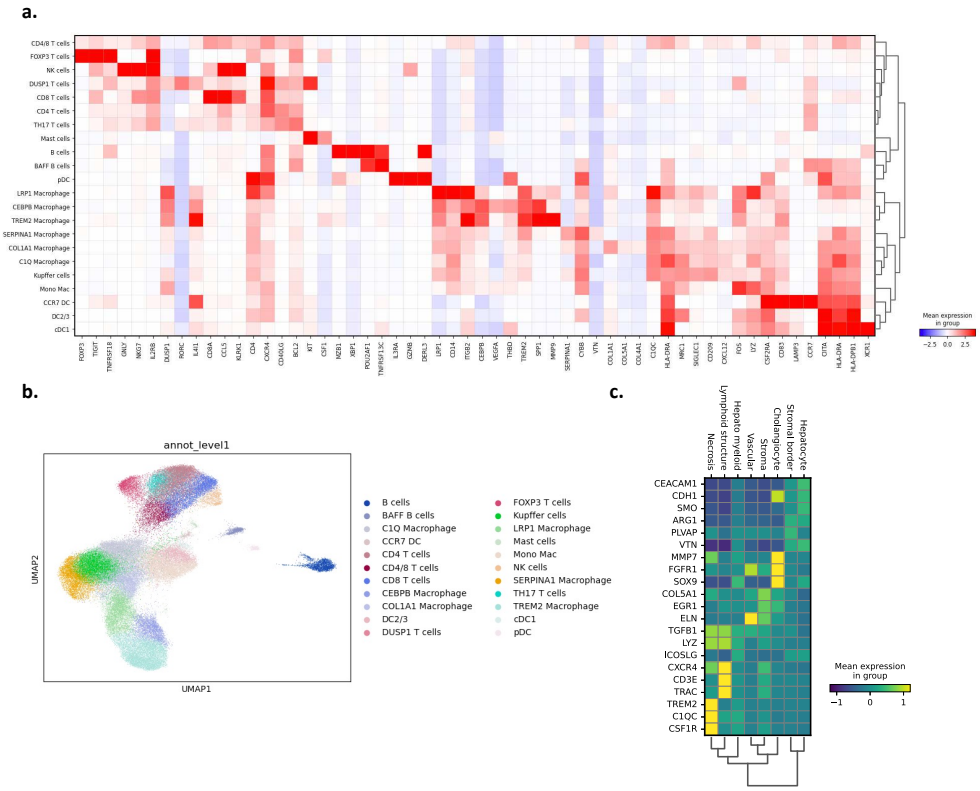

Supplementary Figure 5: *Annotation of the immune cells of the MERSCOPE human liver hepatocellular carcinoma dataset and niche differential gene expressions (DEGs). a. Heatmap of DEGs per immune population on the MERSCOPE liver dataset. b. UMAP of immune cells of the MERSCOPE liver dataset c. Heatmap of DEGs per niche of the MERSCOPE liver dataset.*

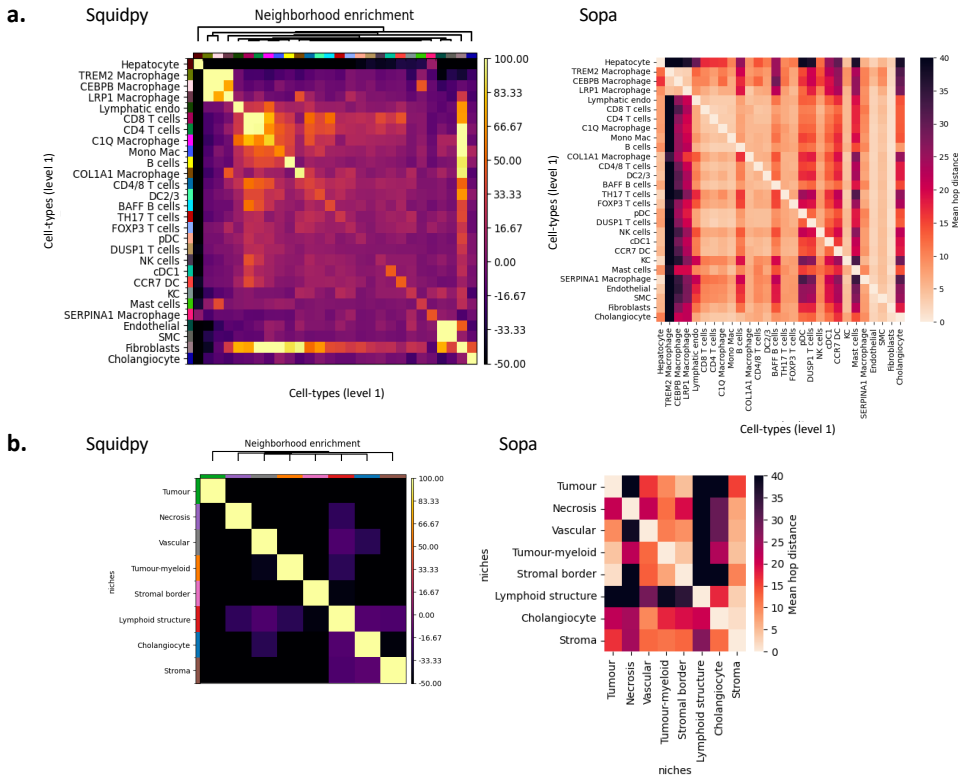

Supplementary Figure 6: *Comparison between Squidpy and Sopa post-processing analyses a. Comparison of Squidpy neighbourhood enrichment (cell to cell) and Sopa cell to cell average hop distance. While the neighbourhood enrichment is symmetric, the distances are not. In terms of insights, this asymmetry can, for instance, show that TREM2 macrophages are relatively close to the Hepatocytes, while the Hepatocytes are generally far from the TREM2 Macrophages. To prevent confusion while reading this heatmap, we precise that one row corresponds to the distances from the cell type of the row index to all other cell types. b. Comparison of Squidpy neighbourhood enrichment (niche to niche) and Sopa niche to niche average hop distance. Since niches are more global structures, their neighbourhood usually includes only the same niche (left), while the distances can capture more global organizations and information (right).*

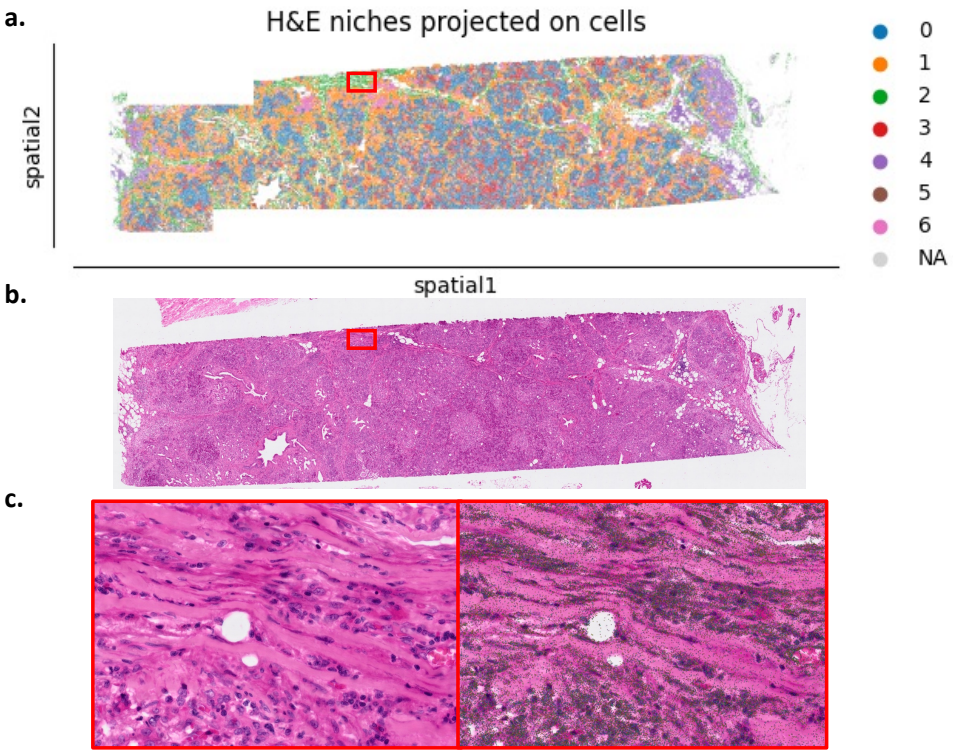

Supplementary Figure 7: *Zoom on Xenium human pancreatic cancer dataset a. H&E clusters of patch-level embeddings based on a pre-trained computer vision model (denoted as H&E niches), red box highlighting the image in c. b. H&E image of human pancreatic cancer dataset (10X Genomics dataset), red box highlighting the image in c. c. Left, zoom of H&E image of human pancreatic cancer dataset (10X Genomics dataset). Right, zoom of H&E image with all transcript overlay of human pancreatic cancer dataset (10X Genomics dataset).*

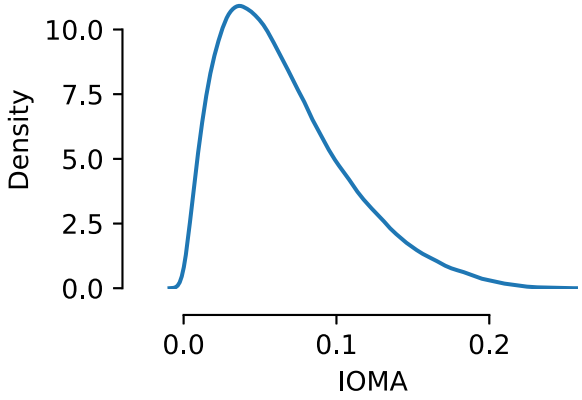

Supplementary Figure 8: *Distribution of IOMA when non-touching 3D cells are projected on a 2D plane. This computation has been performed by simulating random non-touching 3D cells.*

3 DISCUSSION

Mononuclear phagocytes (MNPs), a diverse group of immune cells that includes dendritic cells, monocytes, and macrophages, play critical roles in antimicrobial defence, homeostasis, and immunoregulation. However, the complexity and varied nomenclature used to describe MNPs across different tissues and diseases have presented challenges for the field. To address this, we integrated data from MNPs across a multitude of tissues and datasets, creating the MNP-VERSE, a comprehensive single-cell RNA sequencing (scRNAseq) compendium.

3.1 CONSOLIDATING THE HETEROGENEOUS MOMAC POPULATIONS

The generation of the MoMac-VERSE allowed us to propose a unified annotation of human monocytes and macrophages. By elucidating key transcriptional programs across different cell subpopulations, we validated the identities of numerous clusters by integrating large transcriptomics datasets with more restricted but index-sorted populations. This required generating a transformed matrix comprising all genes common to the integrated studies. As with continuous development, the limitation of this approach is that during the generation of the transformed matrix, it is not needed anymore, making the integration of datasets an even more powerful approach. Furthermore, the possibility offered by workflows such as reference mapping (Azimuth), which allows the mapping of "query" datasets to our reference MoMac-VERSE, has given the framework that has been a valuable tool to the community (Hao et al., 2020).

One of the key findings from our analysis was the increased abundance of IL4I1_Mac expressing *CXCL9*, *CXCL10*, *CXCL11*, *IDO1*, and *IL4I1* within tumours, with specific enrichment at the tumour periphery compared to normal adjacent tissue. A subset of immunosuppressive *IL4I1*+ tumour-associated macrophages (TAMs) was first detected over a decade ago (Zhao et al., 2012) and reconfirmed more recently (Sadik et al., 2020). Our integration of data from multiple cancer studies, coupled with an unbiased analytic approach, has validated these

findings, revealing the presence of these populations in all six cancers we analysed.

From a mechanistic standpoint, the exact pathways involved in the T cell (*IFNG*$^+$ CD8 T cells and *CD40L*$^+$ CD4 T cells)/TAM interaction remains unclear (Gordon et al., 2017). While these TAMs are here associated with dampening anti-tumoral T-cell responses, more recent studies suggest they may play a more favourable role (Bill et al., 2023; Chen et al., 2024). Although there is overlap in the programs observed, these findings highlight the need for more robust and detailed investigations to better understand the complexities of these TAMs in cancer.

TREM2 macrophages were mostly studied in the brain due to their role in the development of neurodegenerative disorders such as Alzheimer's disease (Krasemann et al., 2017; Parhizkar et al., 2019) . They are also involved in metabolic disorders, and obesity have now been detected in adipose tissue (Jaitin et al., 2019). However, there has recently been a surge in the association with the tumour microenvironment (Colonna, 2023). *TREM2* macrophage populations have increased in various tumours, occupying a potentially immune-suppressive position in the TME. With more recent studies, the location of *TREM2* mac has come more to light in cancer and seems to have a unique location based on the disease (Matusiak et al., 2024; Ramos et al., 2022).

The third population of macrophages we focused on were the HES1 macrophage subset, which corresponds to *FOLR2*$^+$ macrophages. These cells were identified in various cancer types like liver cancer (Li et al., 2024; Ramos et al., 2022; Sharma et al., 2020). These macrophages exhibit a signature similar to that of resident, fetal-derived macrophages in mice, aligning with the concept of oncofetal reprogramming (Sharma et al., 2022). This reprogramming could play a role in supporting tumour vasculature and growth, as these macrophages may be "tricked" into functioning as if they were part of an embryo, promoting development in a way that aids the tumour. This finding opens up the possibility that targeting this reprogramming process could be a novel therapeutic strategy to shift tumor-associated macrophages (TAMs) toward anti-tumor activity. However,

it's important to note that the role of these macrophages can vary depending on the tumour type and location. For instance, in breast cancer, these macrophages have been shown to enhance $CD8^+$ T cell infiltration, contributing to an anti-tumor response (Ramos et al., 2022).

A key insight from our research is that these three macrophage populations, often reported separately in various isolated studies, actually represent major conserved subsets when viewed through an integrated approach. Traditionally, macrophages have been classified using the M1/M2 framework, a system originally developed for in vitro monocyte-derived macrophages (Charles D. Mills et al., 2000; Stein et al., 1992). While this classification efficiently distinguishes between certain macrophage types, it falls short of capturing the full diversity of macrophages, particularly in the context of cancer. TAM differentiation from circulating monocytes follows a distinct pathway that does not align neatly with the M2 anti-inflammatory (pro-tumoral) classification (Ruth A. Franklin et al., 2014).

For example, although *IL4I1*$^+$ macrophages exhibit a strong M1 program, in vitro-generated M1 monocyte-derived macrophages might not fully represent the primary M1-like macrophages found in tissues. Unlike in vitro M1 macrophages, these primary macrophages do not produce IL12B, which is instead produced by tissue-activated cDC1 and *CCR7*$^+$ dendritic cells (Maier et al., 2020). This highlights the importance of avoiding oversimplified classifications, which can lead to a narrow and potentially misleading understanding of the tumour environment. Our findings emphasize the need for a more nuanced approach to characterizing macrophage diversity in cancer.

It is well established that macrophages display distinct tissue-specific characteristics, particularly under homeostatic conditions, and their origin often influences their function. However, an intriguing observation from the MoMac-VERSE dataset is the lower influence of tissue specificity. While this may reflect a limitation of the approach, it also highlights the presence of conserved programs that span across different diseases. For example, the *TREM2* macrophage program is prevalent not only in various cancers but also in other disease states, such as inflammatory conditions like atherosclerosis (Colonna, 2023;

Patterson et al., 2023).

In cancer, there are well-known hallmarks that remain consistent across different tissue types, and similarly, certain macrophage populations exhibit similar patterns across cancers (Haigis et al., 2019). Although the significance of tissue specificity is increasingly recognised in understanding cancer heterogeneity, these conserved programs can also be observed in the macrophage function regardless of the tissue type. While disease and tissue-specific targets have a high potential for efficiency and precision, these consistencies across tissue and disease types give an opportunity to find and improve treatments that could be used in a universal manner.

3.2 STANDARDISING THE HETEROGENEOUS STATES WITHIN DC SUBSETS

Similar to our previous study investigating monocyte and macrophage heterogeneity, we provide an integrated analysis across multiple tissues in various pathologies to build an in-depth overview of human DC heterogeneity. This analysis took advantage of 40 scRNAseq datasets, along with flow cytometry validation, CITE-seq protein expression data, spatial genomics and immunohisto-fluorescence, and various analytical pipelines to help define a robust characterisation of human DCs.

By continuing an integration of dendritic cells based on their transcriptome and incorporating protein expression data (through CITE-seq and indexed-FACS), the mDC-VERSE has provided an unprecedented level of detail in identifying discrete cell subsets and lineages. For instance, we confirmed the identification of DC2s and DC3s by examining the expression of CD5 and CD14 proteins. This data also revealed that LTB DC2+DC3s, and to a lesser extent, CD207 DC2+DC3s, express the CD103 protein on their membranes, which was used to detect and quantify $CD103^{+}$ LTB DC2+DC3s through flow cytometry. This integrative approach allowed us to compare multiple studies, clarify the annotation in a unifying way, and increase the resolution of their defined populations (Brown et al., 2019; Cheng et al., 2021).

The increasing number of scRNAseq studies has led to various names being assigned to DC populations with strong similarities, which calls for a unified nomenclature. For example, DC3s were initially described as a subset of $CD1c^+$ DCs containing pro-inflammatory $CD14^+$ cells (Bourdely et al., 2020; Dutertre et al., 2019). However, the term "DC3" has also been used to describe cells that align transcriptomically with *CCR7* mDCs (Di Pilato et al., 2021; Gerhard et al., 2020; Zilionis et al., 2019). This dual usage of the term "DC3" can create confusion, as $CD5^-CD14^{+/-}$ DC3s represent a cell subset, whereas *CCR7* mDCs represent a state shared by DC1, DC2s, and DC3s (Ginhoux et al., 2022). To clarify this, we aligned published signatures with the DC populations identified in the mDC-VERSE, providing a more consistent framework for understanding DC heterogeneity.

Another key aspect of our study was distinguishing between cell subsets and cell states. For example, we showed that the *CD207* program is a shared program, similar to the $CCR7^+$ migration program, which can be acquired by cell subsets/types of different lineages. In contrast, a subset is defined as a population that does not revert to its original state, such as DC1 not becoming DC2. This distinction is crucial for extending and clarifying current literature and understanding the complexity of the tumour microenvironment.

The term "lineage" is often used to describe a population of cells that lack specific combinations of surface markers associated with other lineages (Merad et al., 2013). However, when we think of a "state," we refer to a condition or way of being at a particular moment in time. Applying this concept to populations identified in datasets is crucial, especially considering that the environment highly influences states without being predetermined.

In the context of macrophages, there is a general agreement that these cells exhibit significant plasticity, adapting to their surroundings. The identification of various macrophage populations underscores the presence of numerous states, which are sometimes labelled as subsets. It's more accurate to consider these as states, as this approach better reflects the dynamic nature of macrophages. Whether macrophages have the inherent ability to switch states or are locked into a particular state still requires further investigation (Dunsmore et al., 2024;

Guilliams and Svedberg, 2021).

For DCs, the situation is more complex, particularly with recent insights into the DC3 population (Bourdely et al., 2020; Liu et al., 2023; Rodrigues et al., 2024). This new understanding suggests that DC3s have an independent determination, distinct from other DC subsets. If this distinction is not maintained, the ontological significance could be lost in the issues of nomenclature.

Understanding the difference between a subset and a state is crucial, especially when translating these findings into therapeutic strategies. The distinction can have a significant impact on the timing and location of targeted interventions, influencing the effectiveness of modulating immune responses.

Our meta-analysis focused on the differences in mDC heterogeneity between normal adjacent and tumour tissues. We found that genes like *SPP1* were highly expressed in tumours, consistent with findings in monocytes and macrophages. Additionally, the cDC1-specific gene *CLEC9A* was downregulated in tumours, indicating a reduced presence of cDC1s (Kvedaraite and Ginhoux, 2022). Notably, $CCR7^+$ cDC1s, unlike $CCR7^+$ DC2s or DC3s, were more frequent in tumours than adjacent normal lung tissue. We also identified an increase in IFN-primed DC2+DC3s in various cancers, a trend previously observed in lung cancer and now extended to other types (Leader, 2021; Maier et al., 2020).

Further analysis revealed that while *CD1A* and *CD207* transcripts were broadly expressed by tumour-associated DC2+DC3s, we specifically identified $CD207^+CD1A^+$ DC2+DC3s as a distinct tumour-associated state. This population's expansion was validated in NSCLC patients using spectral flow cytometry and immunohistochemistry.

We also examined the role of *CD207* DC2+DC3s in immunotherapy. In breast cancer patients treated with immune checkpoint blockade, *CD207* DC2+DC3s were more prevalent in those without T-cell clonal expansion. This, along with a negative correlation with CD8 T-cells in scRNAseq data, suggests these cells may limit T-cell clonality. Additionally, *CD207* DC2+DC3s inversely correlated with $CD8^+$ TRM

cells, which are linked to better outcomes, while positively correlating with senescent/hypofunctional $CD8^+$ TEMRA cells (Park et al., 2019; Reading et al., 2018).

There are two potential explanations for why *CD207* DC2+DC3s, unlike other DC subsets or states, show an inverse correlation with *CD8*$^+$ TRMs. The first possibility is that TGF-β, a cytokine known to induce a *CD1a*$^+$*CD207*$^+$ Langerhans cell-like phenotype from blood *CD1c*$^+$ DCs and a *CD103*$^+$ TRM-like phenotype from *CD103*- T-cells, could be a factor. These two cell types might compete for TGF-β, which could account for their inverse relationship (Bigley et al., 2015; Yu et al., 2013). The second hypothesis is that *CD207* DC2+DC3s might promote the differentiation of *CD8*$^+$ T-cells into TEMRA cells rather than TRMs through a mechanism not yet identified in our study. This could explain the observed negative correlation with TRMs and positive correlation with TEMRAs.

These data provide potential therapeutic targets in favour of reducing the abundance of *CD207* DC2+DC3s. Furthermore, *CD207* DC2+DC3s could also serve as a prognostic factor alongside cDC1s as the ratio of these cells predicted whether patients would develop a T-cell clonal expansion, but this will require further investigation in larger prospective cancer patient cohorts.

Our investigation into the spatial distribution of dendritic cell (DC) subsets within tumour tissues has provided valuable insights, particularly concerning *CD207* DC2+DC3s. Visium spatial transcriptomics of human breast tumours indicated that *CD207* DC2+DC3s were located within the tumour region itself, unlike most other immune cells, including other DC subsets, which were primarily found in normal tissue or immune-rich niches. To further validate these findings at single-cell resolution, we used Merfish technology (Merscope, Vizgen) to analyse one lung and one breast cancer patient.

This analysis involved cell segmentation followed by dimensionality reduction, allowing us to identify tumour and stroma niches as well as major immune cell populations, including B-cells, T-cell subsets, and most DC subsets. In both tumour cross-sections, all DC subsets and states, except for *CD207* DC2+DC3s, were more abundant in the tumour stroma. *CD207* DC2+DC3s were uniquely concentrated within the tumour nests, surrounded by tumour cells. To confirm this observation, we performed 4-colour immunohistofluorescence (IHF) staining on 16 lung adenocarcinoma patients, which corroborated the significant intratumoral presence of *CD207*$^+$ DC2$^+$DC3s specifically within the tumour glandular areas, while B and T lymphocytes, including CD8$^+$ T-cells, were more prevalent in the tumour stroma.

Our findings, coupled with advancements in spatial omics technologies, highlighted the need for robust, unified tools for data analysis. To address this, we developed Sopa, a versatile, reproducible, and scalable platform designed for spatial omics analysis. Sopa offers a suite of tools that can be assembled to create pipelines tailored to any image-based spatial omics technology, producing standardized outputs that facilitate exploration and visualization. Unlike other tools tied to specific technologies, Sopa does not require learning multiple data types and software, and it is scalable from laptops to high-performance clusters.

While the DC-VERSE has expanded our knowledge of dendritic cells, including those involved in the CD207 program, achieving a comprehensive functional understanding of these cells remains a considerable challenge. Single-cell analysis offers valuable insights and suggests potential regulatory mechanisms, such as TGF-β. However, the interaction between dendritic cells and their surrounding environment needs further exploration, particularly from a biological perspective. For example, *CD207* DC2+DC3 cells exhibit lower expression of *CXCR4*, a marker known to be essential for cell migration, which may influence their behaviour within tissue (Liu et al., 2021).

Although research into the spatial context of macrophages and dendritic cells is progressing, it still falls short of the depth achieved through single-cell analysis. A key area for future exploration is whether the conserved programs observed in macrophages during

disease states are also reflected in their spatial distribution within tissues. Understanding this could provide new perspectives on how these cells interact with their environment and may inform the development of new therapeutic strategies. Moreover, beyond the *CD207* DC2+DC3s, it will also be of interest to explore the relationship of the other DC populations within their environment.

3.3 STREAMLINING MULTI-LEVEL SPATIAL OMICS

Sopa is also adaptable, integrating new methods and tools as they are developed. For instance, as future segmentation or annotation methods are validated, they can be incorporated into Sopa with minor configuration changes, ensuring that Sopa remains relevant with the advancement of new technologies.

As datasets continue to grow in size, Sopa's scalability becomes increasingly crucial. It enabled us to run high-demand algorithms that were previously challenging due to RAM limitations and processing time. Our assessments showed no significant differences in segmentation quality, and Baysor notably enhanced the data quality compared to default segmentation tools from Vizgen and 10X Genomics.

Beyond high-resolution data, Sopa also integrates protein and H&E information into spatial analysis. This capability allowed us to extract B cell populations in Xenium data and enhance the interpretability of H&E tissue characterisation using transcriptomics. While current spatial technologies primarily focus on either a high number of proteins or transcripts, future developments could add additional layers of information, further enhancing our understanding of biological systems. This study demonstrates that Sopa is equipped to handle the demands of large, multi-modal spatial technologies.

Using the MERSCOPE liver dataset, we could annotate spatial-specific macrophages, particularly macrophages within the necrotic niche. The presence of macrophages, which are known to increase hepatocellular carcinoma (HCC) (Molgora et al., 2020; Sharma et al., 2020), suggests

a potential immunosuppressive role, especially since necrosis is associated with a poorer prognosis (Wei et al., 2021). With Sopa, the relationship between tissue architecture and cell phenotypes can be explored more effectively, advancing our understanding of these interactions.

The concept of a subtissular or niche environment has gained significant importance, especially with recent technological advancements. Various populations within the mononuclear phagocyte system occupy unique locations and perform specific functions in both health and disease. While our understanding of their relationship with the environment has traditionally been viewed in a somewhat linear manner, the full complexity of this ecosystem remains largely unexplored. As combinatory treatments become more prevalent, there is a growing emphasis on targeting the entire ecosystem rather than isolated components. Through our research and the development of advanced tools, we aim to deepen the understanding of mononuclear phagocytes in the tumour microenvironment, ultimately contributing to the development of more effective and targeted therapies.

4 CONCLUSION

In conclusion, our research has unveiled the diverse yet conserved array of human monocyte and macrophage populations in both health and disease. By offering a comprehensive analysis and an online tool for exploring human mononuclear phagocytes (MNPs), we hope to influence future studies to consider this diversity more fully. The era of broadly categorizing cancer-associated myeloid cells based on a few common but nonspecific surface markers is ending. The advent of single-cell transcriptomics and their integration marks a paradigm shift, moving beyond mere atlases and descriptive catalogues of cell subsets. This new approach will enable the scientific community to design more innovative and specific macrophage-based immunotherapy strategies.

Furthermore, our study provides an extensive examination of human dendritic cell (DC) heterogeneity, integrating various datasets and methodologies to clarify their roles in health and disease. The DC-VERSE and mDC-VERSE platforms serve as valuable resources, enhancing the understanding of DCs and their implications for immunotherapy. By unifying nomenclature and highlighting the spatial distribution and potential prognostic significance of specific DC subsets, our work lays the groundwork for further research and targeted therapeutic interventions in dendritic cell biology.

The integration of spatial omics data offers profound insights into tissue architectures, creating new opportunities for biological discovery. Imaging techniques now provide single-cell resolutions, revealing the intricacies of cellular organisation and dynamics. However, the complexity of such data requires advanced analytical tools and significant computing power. The diversity of spatial omics technologies further complicates the generalisation of existing tools, necessitating the development of versatile, scalable platforms.

As we continue to explore the subtissular or niche environments, the significance of these ecosystems becomes increasingly clear. The various populations within the mononuclear phagocyte system, each with unique locations and functions, play critical roles in both health and disease. While our understanding of these relationships has often been linear, the true complexity of the ecosystem is still unfolding. With combinatory treatments becoming more common, there is a growing focus on targeting the entire ecosystem rather than isolated components. Our research and the development of advanced tools aim to deepen the understanding of mononuclear phagocytes in the tumour microenvironment, ultimately contributing to creating more effective and targeted therapies.

5 REFERENCES

Aegerter, H., Lambrecht, B.N., Jakubzick, C.V., 2022. Biology of lung macrophages in health and disease. Immunity 55, 1564–1580. https://doi.org/10.1016/j.immuni.2022.08.010

Aibar, S., González-Blas, C.B., Moerman, T., Huynh-Thu, V.A., Imrichova, H., Hulselmans, G., Rambow, F., Marine, J.-C., Geurts, P., Aerts, J., van den Oord, J., Atak, Z.K., Wouters, J., Aerts, S., 2017. SCENIC: single-cell regulatory network inference and clustering. Nat. Methods 14, 1083–1086. https://doi.org/10.1038/nmeth.4463

Ajami, B., Bennett, J.L., Krieger, C., Tetzlaff, W., Rossi, F.M.V., 2007. Local self-renewal can sustain CNS microglia maintenance and function throughout adult life. Nat. Neurosci. 10, 1538–1543. https://doi.org/10.1038/nn2014

Akashi, K., Traver, D., Miyamoto, T., Weissman, I.L., 2000. A clonogenic common myeloid progenitor that gives rise to all myeloid lineages. Nature 404, 193–197. https://doi.org/10.1038/35004599

Al, B., Suen, T.K., Placek, K., Netea, M.G., 2023. Innate (learned) memory. J. Allergy Clin. Immunol. 152, 551–566. https://doi.org/10.1016/j.jaci.2023.06.014

Alcántara-Hernández, M., Leylek, R., Wagar, L.E., Engleman, E.G., Keler, T., Marinkovich, M.P., Davis, M.M., Nolan, G.P., Idoyaga, J., 2017. High-Dimensional Phenotypic Mapping of Human Dendritic Cells Reveals Interindividual Variation and Tissue Specialization. Immunity 47, 1037-1050.e6. https://doi.org/10.1016/j.immuni.2017.11.001

Allan, L.L., Stax, A.M., Zheng, D.-J., Chung, B.K., Kozak, F.K., Tan, R., van den Elzen, P., 2011. CD1d and CD1c expression in human B cells is regulated by activation and retinoic acid receptor signaling. J. Immunol. Baltim. Md 1950 186, 5261–5272. https://doi.org/10.4049/jimmunol.1003615

Ardouin, L., Luche, H., Chelbi, R., Carpentier, S., Shawket, A., Sanchis, F.M., Maria, C.S., Grenot, P., Alexandre, Y., Grégoire, C., Fries, A., Manh, T.-P.V., Tamoutounour, S., Crozat, K., Tomasello, E., Jorquera, A., Fossum, E., Bogen, B., Azukizawa, H., Bajenoff, M., Henri, S., Dalod, M., Malissen, B., 2016. Broad and Largely Concordant Molecular Changes Characterize Tolerogenic and Immunogenic Dendritic Cell Maturation in Thymus and Periphery. Immunity 45, 305–318. https://doi.org/10.1016/j.immuni.2016.07.019

Atta, L., Fan, J., 2021. Computational challenges and opportunities in spatially resolved transcriptomic data analysis. Nat. Commun. 12, 5283. https://doi.org/10.1038/s41467-021-25557-9

Auffray, C., Fogg, D., Garfa, M., Elain, G., Join-Lambert, O., Kayal, S., Sarnacki, S., Cumano, A., Lauvau, G., Geissmann, F., 2007. Monitoring of blood vessels and tissues by a population of monocytes with patrolling behavior. Science 317, 666–70. https://doi.org/10.1126/science.1142883

Axelrod, S., Cai, M., Carr, A.J., Freeman, J., Ganguli, D., Kiggins, J.T., Long, B., Tung, T., Yamauchi, K.A., 2021. starfish: scalable pipelines for image-based transcriptomics. J. Open Source Softw. 6, 2440. https://doi.org/10.21105/joss.02440

Azizi, E., Carr, A.J., Plitas, G., Cornish, A.E., Konopacki, C., Prabhakaran, S., Nainys, J., Wu, K., Kiseliovas, V., Setty, M., Choi, K., Fromme, R.M., Dao, P., McKenney, P.T., Wasti, R.C., Kadaveru, K., Mazutis, L., Rudensky, A.Y., Pe'er, D., 2018. Single-Cell Map of Diverse Immune Phenotypes in the Breast Tumor Microenvironment. Cell 174, 1293-1308.e36. https://doi.org/10.1016/j.cell.2018.05.060

Baer, J.M., Zuo, C., Kang, L.-I., de la Lastra, A.A., Borcherding, N.C., Knolhoff, B.L., Bogner, S.J., Zhu, Y., Yang, L., Laurent, J., Lewis, M.A., Zhang, N., Kim, K.-W., Fields, R.C., Yokoyama, W.M., Mills, J.C., Ding, L., Randolph, G.J., DeNardo, D.G., 2023. Fibrosis induced by resident macrophages has divergent roles in pancreas inflammatory injury and PDAC. Nat. Immunol. 24, 1443–1457. https://doi.org/10.1038/s41590-023-01579-x

Bain, C.C., Bravo-Blas, A., Scott, C.L., Gomez Perdiguero, E., Geissmann, F., Henri, S., Malissen, B., Osborne, L.C., Artis, D., Mowat, A.M., 2014. Constant replenishment from circulating monocytes maintains the macrophage pool in the intestine of adult mice. Nat. Immunol. 15, 929–937. https://doi.org/10.1038/ni.2967

Balan, S., Dalod, M., 2016. In Vitro Generation of Human XCR1+ Dendritic Cells from CD34+ Hematopoietic Progenitors, in: Segura, E., Onai, N. (Eds.), Dendritic Cell Protocols. Springer, New York, NY, pp. 19–37. https://doi.org/10.1007/978-1-4939-3606-9_2

Balan, S., Saxena, M., Bhardwaj, N., 2019. Dendritic cell subsets and locations. Int. Rev. Cell Mol. Biol. 348, 1–68. https://doi.org/10.1016/bs.ircmb.2019.07.004

Barry, K.C., Hsu, J., Broz, M.L., Cueto, F.J., Binnewies, M., Combes, A.J., Nelson, A.E., Loo, K., Kumar, R., Rosenblum, M.D., Alvarado, M.D., Wolf, D.M., Bogunovic, D., Bhardwaj, N., Daud, A.I., Ha, P.K., Ryan, W.R., Pollack, J.L., Samad, B., Asthana, S., Chan, V., Krummel, M.F., 2018. A natural killer–dendritic cell axis defines checkpoint therapy–responsive tumor microenvironments. Nat. Med. 24, 1178–1191. https://doi.org/10.1038/s41591-018-0085-8

Bassez, A., Vos, H., Van Dyck, L., Floris, G., Arijs, I., Desmedt, C., Boeckx, B., Vanden Bempt, M., Nevelsteen, I., Lambein, K., Punie, K., Neven, P., Garg, A.D., Wildiers, H., Qian, J., Smeets, A.,

Lambrechts, D., 2021. A single-cell map of intratumoral changes during anti-PD1 treatment of patients with breast cancer. Nat. Med. 27, 820–832. https://doi.org/10.1038/s41591-021-01323-8

Becht, E., McInnes, L., Healy, J., Dutertre, C.-A., Kwok, I.W.H., Ng, L.G., Ginhoux, F., Newell, E.W., 2019. Dimensionality reduction for visualizing single-cell data using UMAP. Nat. Biotechnol. 37, 38–44. https://doi.org/10.1038/nbt.4314

Becht, E., McInnes, L., Healy, J., Dutertre, C.-A., Kwok, I.W.H., Ng, L.G., Ginhoux, F., Newell, E.W., 2018. Dimensionality reduction for visualizing single-cell data using UMAP. Nat. Biotechnol. https://doi.org/10.1038/nbt.4314

Becht, E., Tolstrup, D., Dutertre, C.A., Morawski, P.A., Campbell, D.J., Ginhoux, F., Newell, E.W., Gottardo, R., Headley, M.B., 2021. High-throughput single-cell quantification of hundreds of proteins using conventional flow cytometry and machine learning. Sci. Adv. 7, 505–527. https://doi.org/10.1126/SCIADV.ABG0505/SUPPL_FILE/SCIADV.ABG0505_MOVIE_S1.ZIP

Becker, A.M.D., Decker, A.H., Flórez-Grau, G., Bakdash, G., Röring, R.J., Stelloo, S., Vermeulen, M., Piet, B., Aarntzen, E.H.J.G., Verdoes, M., de Vries, I.J.M., 2024. Inhibition of CSF-1R and IL-6R prevents conversion of cDC2s into immune incompetent tumor-induced DC3s boosting DC-driven therapy potential. Cell Rep. Med. 5, 101386. https://doi.org/10.1016/j.xcrm.2023.101386

Bell, D., Chomarat, P., Broyles, D., Netto, G., Harb, G.M., Lebecque, S., Valladeau, J., Davoust, J., Palucka, K.A., Banchereau, J., 1999. In Breast Carcinoma Tissue, Immature Dendritic Cells Reside within the Tumor, Whereas Mature Dendritic Cells Are Located in Peritumoral Areas. J. Exp. Med. 190, 1417–1426. https://doi.org/10.1084/jem.190.10.1417

Bian, Z., Gong, Y., Huang, T., Lee, C.Z.W., Bian, L., Bai, Z., Shi, H., Zeng, Y., Liu, C., He, J., Zhou, J., Li, X., Li, Z., Ni, Y., Ma, C., Cui, L., Zhang, R., Chan, J.K.Y., Ng, L.G., Lan, Y., Ginhoux, F., Liu, B., 2020. Deciphering human macrophage development at single-cell resolution. Nature 582, 571–576. https://doi.org/10.1038/s41586-020-2316-7

Biancalani, T., Scalia, G., Buffoni, L., Avasthi, R., Lu, Z., Sanger, A., Tokcan, N., Vanderburg, C.R., Segerstolpe, Å., Zhang, M., Avraham-Davidi, I., Vickovic, S., Nitzan, M., Ma, S., Subramanian, A., Lipinski, M., Buenrostro, J., Brown, N.B., Fanelli, D., Zhuang, X., Macosko, E.Z., Regev, A., 2021. Deep learning and alignment of spatially resolved single-cell transcriptomes with Tangram. Nat. Methods 2021 1–11. https://doi.org/10.1038/s41592-021-01264-7

Bigley, V., Cytlak, U., Collin, M., 2019. Human dendritic cell immunodeficiencies. Semin. Cell Dev. Biol., SI: Human dendritic cells 86, 50–61. https://doi.org/10.1016/j.semcdb.2018.02.020

Bigley, V., McGovern, N., Milne, P., Dickinson, R., Pagan, S., Cookson, S., Haniffa, M., Collin, M., 2015. Langerin-expressing dendritic cells in human tissues are related to CD1c+ dendritic cells and distinct from Langerhans cells and CD141high XCR1+ dendritic cells*. J. Leukoc. Biol. 97, 627–634. https://doi.org/10.1189/jlb.1HI0714-351R

Bijelic, L., Rubio, E.R., 2021. Tumor Necrosis in Hepatocellular Carcinoma—Unfairly Overlooked? Ann. Surg. Oncol. 28, 600–601. https://doi.org/10.1245/s10434-020-09402-9

Bill, R., Wirapati, P., Messemaker, M., Roh, W., Zitti, B., Duval, F., Kiss, M., Park, J.C., Saal, T.M., Hoelzl, J., Tarussio, D., Benedetti, F., Tissot, S., Kandalaft, L., Varrone, M., Ciriello, G., McKee, T.A., Monnier, Y., Mermod, M., Blaum, E.M., Gushterova, I., Gonye, A.L.K., Hacohen, N., Getz, G., Mempel, T.R., Klein, A.M., Weissleder, R., Faquin, W.C., Sadow, P.M., Lin, D., Pai, S.I., Sade-Feldman, M., Pittet, M.J., 2023. CXCL9:SPP1 macrophage polarity identifies a network of cellular programs that control human cancers. Science 381, 515–524. https://doi.org/10.1126/science.ade2292

Binnewies, M., Mujal, A.M., Pollack, J.L., Combes, A.J., Hardison, E.A., Barry, K.C., Tsui, J., Ruhland, M.K., Kersten, K., Abushawish, M.A., Spasic, M., Giurintano, J.P., Chan, V., Daud, A.I., Ha, P., Ye, C.J., Roberts, E.W., Krummel, M.F., 2019. Unleashing Type-2 Dendritic Cells to Drive Protective Antitumor CD4+ T Cell Immunity. Cell 177, 556-571.e16. https://doi.org/10.1016/j.cell.2019.02.005

Binnewies, M., Pollack, J.L., Rudolph, J., Dash, S., Abushawish, M., Lee, T., Jahchan, N.S., Canaday, P., Lu, E., Norng, M., Mankikar, S., Liu, V.M., Du, X., Chen, A., Mehta, R., Palmer, R., Juric, V., Liang, L., Baker, K.P., Reyno, L., Krummel, M.F., Streuli, M., Sriram, V., 2021. Targeting TREM2 on tumor-associated macrophages enhances immunotherapy. Cell Rep. 37, 109844. https://doi.org/10.1016/j.celrep.2021.109844

Bissinger, S., Hage, C., Wagner, V., Maser, I.-P., Brand, V., Schmittnaegel, M., Jegg, A.-M., Cannarile, M., Watson, C., Klaman, I., Rieder, N., González Loyola, A., Petrova, T.V., Cassier, P.A., Gomez-Roca, C., Sibaud, V., De Palma, M., Hoves, S., Ries, C.H., 2021. Macrophage depletion induces edema through release of matrix-degrading proteases and proteoglycan deposition. Sci. Transl. Med. 13, eabd4550. https://doi.org/10.1126/scitranslmed.abd4550

Blampey, Q., Bercovici, N., Dutertre, C.-A., Pic, I., Ribeiro, J.M., André, F., Cournède, P.-H., 2023. A biology-driven deep generative model for

cell-type annotation in cytometry. Brief. Bioinform. 24, bbad260. https://doi.org/10.1093/bib/bbad260
Blériot, C., Chakarov, S., Ginhoux, F., 2020. Determinants of Resident Tissue Macrophage Identity and Function. Immunity 52, 957–970. https://doi.org/10.1016/j.immuni.2020.05.014
Blériot, C., Dunsmore, G., Alonso-Curbelo, D., Ginhoux, F., 2024. A temporal perspective for tumor-associated macrophage identities and functions. Cancer Cell 42, 747–758. https://doi.org/10.1016/j.ccell.2024.04.002
Bonnardel, J., T'Jonck, W., Gaublomme, D., Browaeys, R., Scott, C.L., Martens, L., Vanneste, B., Prijck, S.D., Nedospasov, S.A., Kremer, A., Hamme, E.V., Borghgraef, P., Toussaint, W., Bleser, P.D., Mannaerts, I., Beschin, A., Grunsven, L.A. van, Lambrecht, B.N., Taghon, T., Lippens, S., Elewaut, D., Saeys, Y., Guilliams, M., 2019. Stellate Cells, Hepatocytes, and Endothelial Cells Imprint the Kupffer Cell Identity on Monocytes Colonizing the Liver Macrophage Niche. Immunity 51, 638-654.e9. https://doi.org/10.1016/j.immuni.2019.08.017
Böttcher, J., Bonavita, E., Chakravarty, P., Cell, H.B.-, 2018, undefined, 2018. NK cells stimulate recruitment of cDC1 into the tumor microenvironment promoting cancer immune control. Cell 172.
Böttcher, J.P., Reis e Sousa, C., 2018. The Role of Type 1 Conventional Dendritic Cells in Cancer Immunity. Trends Cancer 4, 784–792. https://doi.org/10.1016/j.trecan.2018.09.001
Bourdely, P., Anselmi, G., Vaivode, K., Ramos, R.N., Missolo-Koussou, Y., Hidalgo, S., Tosselo, J., Nuñez, N., Richer, W., Vincent-Salomon, A., Saxena, A., Wood, K., Lladser, A., Piaggio, E., Helft, J., Guermonprez, P., 2020. Transcriptional and Functional Analysis of CD1c+ Human Dendritic Cells Identifies a CD163+ Subset Priming CD8+CD103+ T Cells. Immunity 53, 335-352.e8. https://doi.org/10.1016/j.immuni.2020.06.002
Bressan, D., Battistoni, G., Hannon, G.J., 2023. The dawn of spatial omics. Science 381, eabq4964. https://doi.org/10.1126/science.abq4964
Brestoff, J.R., Wilen, C.B., Moley, J.R., Li, Y., Zou, W., Malvin, N.P., Rowen, M.N., Saunders, B.T., Ma, H., Mack, M.R., Hykes, B.L., Balce, D.R., Orvedahl, A., Williams, J.W., Rohatgi, N., Wang, X., McAllaster, M.R., Handley, S.A., Kim, B.S., Doench, J.G., Zinselmeyer, B.H., Diamond, M.S., Virgin, H.W., Gelman, A.E., Teitelbaum, S.L., 2021. Intercellular Mitochondria Transfer to Macrophages Regulates White Adipose Tissue Homeostasis and Is Impaired in Obesity. Cell Metab. 33, 270-282.e8. https://doi.org/10.1016/j.cmet.2020.11.008
Breton, G., Lee, J., Zhou, Y.J., Schreiber, J.J., Keler, T., Puhr, S., Anandasabapathy, N., Schlesinger, S., Caskey, M., Liu, K.,

Nussenzweig, M.C., 2015. Circulating precursors of human CD1c+ and CD141+ dendritic cells. J. Exp. Med. 212, 401–13. https://doi.org/10.1084/jem.20141441
Breton, G., Zheng, S., Valieris, R., Tojal da Silva, I., Satija, R., Nussenzweig, M.C., 2016. Human dendritic cells (DCs) are derived from distinct circulating precursors that are precommitted to become CD1c+ or CD141+ DCs. J. Exp. Med. 213, 2861–2870. https://doi.org/10.1084/jem.20161135
Browaeys, R., Saelens, W., Saeys, Y., 2019. NicheNet: modeling intercellular communication by linking ligands to target genes. Nat. Methods. https://doi.org/10.1038/s41592-019-0667-5
Brown, C.C., Gudjonson, H., Pritykin, Y., Deep, D., Lavallée, V.-P., Mendoza, A., Fromme, R., Mazutis, L., Ariyan, C., Leslie, C., Pe'er, D., Rudensky, A.Y., 2019. Transcriptional Basis of Mouse and Human Dendritic Cell Heterogeneity. Cell 179, 846-863.e24. https://doi.org/10.1016/j.cell.2019.09.035
Broz, M.L., Binnewies, M., Boldajipour, B., Nelson, A.E., Pollack, J.L., Erle, D.J., Barczak, A., Rosenblum, M.D., Daud, A., Barber, D.L., Amigorena, S., van'tVeer, L.J., Sperling, A.I., Wolf, D.M., Krummel, M.F., 2014. Dissecting the Tumor Myeloid Compartment Reveals Rare Activating Antigen-Presenting Cells Critical for T Cell Immunity. Cancer Cell 26, 638–652. https://doi.org/10.1016/j.ccell.2014.09.007
Busch, K., Klapproth, K., Barile, M., Flossdorf, M., Holland-Letz, T., Schlenner, S.M., Reth, M., Höfer, T., Rodewald, H.-R., 2015. Fundamental properties of unperturbed haematopoiesis from stem cells in vivo. Nature 518, 542–546. https://doi.org/10.1038/nature14242
Buus, T.B., Herrera, A., Ivanova, E., Mimitou, E., Cheng, A., Herati, R.S., Papagiannakopoulos, T., Smibert, P., Odum, N., Koralov, S.B., 2021. Improving oligo-conjugated antibody signal in multimodal single-cell analysis. eLife 10, e61973. https://doi.org/10.7554/eLife.61973
Cabeza-Cabrerizo, M., Cardoso, A., Minutti, C.M., Costa, M.P. da, Sousa, C.R. e, 2021. Dendritic Cells Revisited. Annu. Rev. Immunol. 39, 131–166. https://doi.org/10.1146/annurev-immunol-061020-053707
Caronni, N., La Terza, F., Vittoria, F.M., Barbiera, G., Mezzanzanica, L., Cuzzola, V., Barresi, S., Pellegatta, M., Canevazzi, P., Dunsmore, G., Leonardi, C., Montaldo, E., Lusito, E., Dugnani, E., Citro, A., Ng, M.S.F., Schiavo Lena, M., Drago, D., Andolfo, A., Brugiapaglia, S., Scagliotti, A., Mortellaro, A., Corbo, V., Liu, Z., Mondino, A., Dellabona, P., Piemonti, L., Taveggia, C., Doglioni, C., Cappello, P., Novelli, F., Iannacone, M., Ng, L.G., Ginhoux, F., Crippa, S., Falconi, M., Bonini, C., Naldini, L., Genua, M., Ostuni,

R., 2023. IL-1β+ macrophages fuel pathogenic inflammation in pancreatic cancer. Nature 623, 415–422. https://doi.org/10.1038/s41586-023-06685-2

Caronni, N., Piperno, G.M., Simoncello, F., Romano, O., Vodret, S., Yanagihashi, Y., Dress, R., Dutertre, C.-A., Bugatti, M., Bourdeley, P., Del Prete, A., Schioppa, T., Mazza, E.M.C., Collavin, L., Zacchigna, S., Ostuni, R., Guermonprez, P., Vermi, W., Ginhoux, F., Bicciato, S., Nagata, S., Benvenuti, F., 2021. TIM4 expression by dendritic cells mediates uptake of tumor-associated antigens and anti-tumor responses. Nat. Commun. 12, 2237. https://doi.org/10.1038/s41467-021-22535-z

Casanova-Acebes, M., Dalla, E., Leader, A.M., LeBerichel, J., Nikolic, J., Morales, B.M., Brown, M., Chang, C., Troncoso, L., Chen, S.T., Sastre-Perona, A., Park, M.D., Tabachnikova, A., Dhainaut, M., Hamon, P., Maier, B., Sawai, C.M., Agulló-Pascual, E., Schober, M., Brown, B.D., Reizis, B., Marron, T., Kenigsberg, E., Moussion, C., Benaroch, P., Aguirre-Ghiso, J.A., Merad, M., 2021. Tissue-resident macrophages provide a pro-tumorigenic niche to early NSCLC cells. Nature 595, 578–584. https://doi.org/10.1038/s41586-021-03651-8

Cassetta, L., Fragkogianni, S., Sims, A.H., Swierczak, A., Forrester, L.M., Zhang, H., Soong, D.Y.H., Cotechini, T., Anur, P., Lin, E.Y., Fidanza, A., Lopez-Yrigoyen, M., Millar, M.R., Urman, A., Ai, Z., Spellman, P.T., Hwang, E.S., Dixon, J.M., Wiechmann, L., Coussens, L.M., Smith, H.O., Pollard, J.W., 2019. Human Tumor-Associated Macrophage and Monocyte Transcriptional Landscapes Reveal Cancer-Specific Reprogramming, Biomarkers, and Therapeutic Targets. Cancer Cell 35, 588-602.e10. https://doi.org/10.1016/j.ccell.2019.02.009

Cassetta, L., Pollard, J.W., 2018. Targeting macrophages: therapeutic approaches in cancer. Nat. Rev. Drug Discov. 17, 887–904. https://doi.org/10.1038/nrd.2018.169

Chakarov, S., Lim, H.Y., Tan, L., Lim, S.Y., See, P., Lum, J., Zhang, X.-M., Foo, S., Nakamizo, S., Duan, K., Kong, W.T., Gentek, R., Balachander, A., Carbajo, D., Bleriot, C., Malleret, B., Tam, J.K.C., Baig, S., Shabeer, M., Toh, S.-A.E.S., Schlitzer, A., Larbi, A., Marichal, T., Malissen, B., Chen, J., Poidinger, M., Kabashima, K., Bajenoff, M., Ng, L.G., Angeli, V., Ginhoux, F., 2019. Two distinct interstitial macrophage populations coexist across tissues in specific subtissular niches. Science 363, eaau0964. https://doi.org/10.1126/science.aau0964

Chang, Q., Ornatsky, O.I., Siddiqui, I., Loboda, A., Baranov, V.I., Hedley, D.W., 2017. Imaging Mass Cytometry. Cytometry A 91, 160–169. https://doi.org/10.1002/cyto.a.23053

Chaplin, D.D., 2010. Overview of the Immune Response. J. Allergy Clin. Immunol. 125, S3-23. https://doi.org/10.1016/j.jaci.2009.12.980

Chaussabel, D., Quinn, C., Shen, J., Patel, P., Glaser, C., Baldwin, N., Stichweh, D., Blankenship, D., Li, L., Munagala, I., Bennett, L., Allantaz, F., Mejias, A., Ardura, M., Kaizer, E., Monnet, L., Allman, W., Randall, H., Johnson, D., Lanier, A., Punaro, M., Wittkowski, K.M., White, P., Fay, J., Klintmalm, G., Ramilo, O., Palucka, A.K., Banchereau, J., Pascual, V., 2008. A modular analysis framework for blood genomics studies: application to systemic lupus erythematosus. Immunity 29, 150–164. https://doi.org/10.1016/j.immuni.2008.05.012

Che, L.-H., Liu, J.-W., Huo, J.-P., Luo, R., Xu, R.-M., He, C., Li, Y.-Q., Zhou, A.-J., Huang, P., Chen, Y.-Y., Ni, W., Zhou, Y.-X., Liu, Y.-Y., Li, H.-Y., Zhou, R., Mo, H., Li, J.-M., 2021. A single-cell atlas of liver metastases of colorectal cancer reveals reprogramming of the tumor microenvironment in response to preoperative chemotherapy. Cell Discov. 7, 1–21. https://doi.org/10.1038/s41421-021-00312-y

Chen, J.H., Nieman, L.T., Spurrell, M., Jorgji, V., Elmelech, L., Richieri, P., Xu, K.H., Madhu, R., Parikh, M., Zamora, I., Mehta, A., Nabel, C.S., Freeman, S.S., Pirl, J.D., Lu, C., Meador, C.B., Barth, J.L., Sakhi, M., Tang, A.L., Sarkizova, S., Price, C., Fernandez, N.F., Emanuel, G., He, J., Van Raay, K., Reeves, J.W., Yizhak, K., Hofree, M., Shih, A., Sade-Feldman, M., Boland, G.M., Pelka, K., Aryee, M.J., Mino-Kenudson, M., Gainor, J.F., Korsunsky, I., Hacohen, N., 2024. Human lung cancer harbors spatially organized stem-immunity hubs associated with response to immunotherapy. Nat. Immunol. 25, 644–658. https://doi.org/10.1038/s41590-024-01792-2

Chen, K.H., Boettiger, A.N., Moffitt, J.R., Wang, S., Zhuang, X., 2015. Spatially resolved, highly multiplexed RNA profiling in single cells. Science 348, aaa6090. https://doi.org/10.1126/science.aaa6090

Cheng, J.B., Sedgewick, A.J., Finnegan, A.I., Harirchian, P., Lee, J., Kwon, S., Fassett, M.S., Golovato, J., Gray, M., Ghadially, R., Liao, W., Perez White, B.E., Mauro, T.M., Mully, T., Kim, E.A., Sbitany, H., Neuhaus, I.M., Grekin, R.C., Yu, S.S., Gray, J.W., Purdom, E., Paus, R., Vaske, C.J., Benz, S.C., Song, J.S., Cho, R.J., 2018. Transcriptional Programming of Normal and Inflamed Human Epidermis at Single-Cell Resolution. Cell Rep. 25, 871–883. https://doi.org/10.1016/j.celrep.2018.09.006

Cheng, S., Li, Z., Gao, R., Xing, B., Gao, Y., Yang, Yu, Qin, S., Zhang, L., Ouyang, H., Du, P., Jiang, L., Zhang, B., Yang, Yue, Wang, X., Ren, X., Bei, J.X., Hu, X., Bu, Z., Ji, J., Zhang, Z., 2021. A pan-cancer single-cell transcriptional atlas of tumor infiltrating myeloid cells. Cell 184, 792-809.e23. https://doi.org/10.1016/j.cell.2021.01.010

Chu, Y., Dai, E., Li, Y., Han, G., Pei, G., Ingram, D.R., Thakkar, K., Qin, J.-J., Dang, M., Le, X., Hu, C., Deng, Q., Sinjab, A., Gupta, P., Wang, R., Hao, D., Peng, F., Yan, X., Liu, Y., Song, S., Zhang, S., Heymach, J.V., Reuben, A., Elamin, Y.Y., Pizzi, M.P., Lu, Y., Lazcano, R., Hu, J., Li, M., Curran, M., Futreal, A., Maitra, A., Jazaeri, A.A., Ajani, J.A., Swanton, C., Cheng, X.-D., Abbas, H.A., Gillison, M., Bhat, K., Lazar, A.J., Green, M., Litchfield, K., Kadara, H., Yee, C., Wang, L., 2023. Pan-cancer T cell atlas links a cellular stress response state to immunotherapy resistance. Nat. Med. 29, 1550–1562. https://doi.org/10.1038/s41591-023-02371-y

Cillo, A.R., Kürten, C.H.L., Tabib, T., Qi, Z., Onkar, S., Wang, T., Liu, A., Duvvuri, U., Kim, S., Soose, R.J., Oesterreich, S., Chen, W., Lafyatis, R., Bruno, T.C., Ferris, R.L., Vignali, D.A.A., 2020. Immune Landscape of Viral- and Carcinogen-Driven Head and Neck Cancer. Immunity 52, 183-199.e9. https://doi.org/10.1016/j.immuni.2019.11.014

Cisar, C., Keener, N., Ruffalo, M., Paten, B., 2023. A unified pipeline for FISH spatial transcriptomics. Cell Genomics 3. https://doi.org/10.1016/j.xgen.2023.100384

Cohen, Y.C., Zada, M., Wang, S.-Y., Bornstein, C., David, E., Moshe, A., Li, B., Shlomi-Loubaton, S., Gatt, M.E., Gur, C., Lavi, N., Ganzel, C., Luttwak, E., Chubar, E., Rouvio, O., Vaxman, I., Pasvolsky, O., Ballan, M., Tadmor, T., Nemets, A., Jarchowcky-Dolberg, O., Shvetz, O., Laiba, M., Shpilberg, O., Dally, N., Avivi, I., Weiner, A., Amit, I., 2021. Identification of resistance pathways and therapeutic targets in relapsed multiple myeloma patients through single-cell sequencing. Nat. Med. 27, 491–503. https://doi.org/10.1038/s41591-021-01232-w

Coillard, A., Segura, E., 2019. In vivo Differentiation of Human Monocytes. Front. Immunol. 10. https://doi.org/10.3389/fimmu.2019.01907

Collin, M., Bigley, V., 2018. Human dendritic cell subsets: an update. Immunology 154, 3–20. https://doi.org/10.1111/imm.12888

Collin, M., Mcgovern, N., Haniffa, M., 2013. Human dendritic cell subsets. Immunology 140, 22–30. https://doi.org/10.1111/imm.12117

Collins, F.S., Morgan, M., Patrinos, A., 2003. The Human Genome Project: Lessons from Large-Scale Biology. Science 300, 286–290. https://doi.org/10.1126/science.1084564

Colonna, M., 2023. The biology of TREM receptors. Nat. Rev. Immunol. 23, 580–594. https://doi.org/10.1038/s41577-023-00837-1

Colonna, M., Trinchieri, G., Liu, Y.-J., 2004. Plasmacytoid dendritic cells in immunity. Nat. Immunol. 5, 1219–1226. https://doi.org/10.1038/ni1141

Cortez-Retamozo, V., Etzrodt, M., Newton, A., Rauch, P.J., Chudnovskiy, A., Berger, C., Ryan, R.J.H., Iwamoto, Y., Marinelli, B., Gorbatov,

R., Forghani, R., Novobrantseva, T.I., Koteliansky, V., Figueiredo, J.-L., Chen, J.W., Anderson, D.G., Nahrendorf, M., Swirski, F.K., Weissleder, R., Pittet, M.J., 2012. Origins of tumor-associated macrophages and neutrophils. Proc. Natl. Acad. Sci. 109, 2491–2496. https://doi.org/10.1073/pnas.1113744109

Covarrubias, A.J., Kale, A., Perrone, R., Lopez-Dominguez, J.A., Pisco, A.O., Kasler, H.G., Schmidt, M.S., Heckenbach, I., Kwok, R., Wiley, C.D., Wong, H.-S., Gibbs, E., Iyer, S.S., Basisty, N., Wu, Q., Kim, I.-J., Silva, E., Vitangcol, K., Shin, K.-O., Lee, Y.-M., Riley, R., Ben-Sahra, I., Ott, M., Schilling, B., Scheibye-Knudsen, M., Ishihara, K., Quake, S.R., Newman, J., Brenner, C., Campisi, J., Verdin, E., 2020. Senescent cells promote tissue NAD + decline during ageing via the activation of CD38 + macrophages. Nat. Metab. 2, 1265–1283. https://doi.org/10.1038/s42255-020-00305-3

Crozat, K., Guiton, R., Contreras, V., Feuillet, V., Dutertre, C.-A., Ventre, E., Vu Manh, T.-P., Baranek, T., Storset, A.K., Marvel, J., Boudinot, P., Hosmalin, A., Schwartz-Cornil, I., Dalod, M., 2010. The XC chemokine receptor 1 is a conserved selective marker of mammalian cells homologous to mouse CD8α+ dendritic cells. J. Exp. Med. 207, 1283–1292. https://doi.org/10.1084/jem.20100223

Cueto, F.J., Fresno, C. del, Brandi, P., Combes, A.J., Hernández-García, E., Sánchez-Paulete, A.R., Enamorado, M., Bromley, C.P., Gomez, M.J., Conde-Garrosa, R., Mañes, S., Zelenay, S., Melero, I., Iborra, S., Krummel, M.F., Sancho, D., 2021. DNGR-1 limits Flt3L-mediated antitumor immunity by restraining tumor-infiltrating type I conventional dendritic cells. J. Immunother. Cancer 9, e002054. https://doi.org/10.1136/jitc-2020-002054

Cytlak, U., Resteu, A., Pagan, S., Green, K., Milne, P., Maisuria, S., McDonald, D., Hulme, G., Filby, A., Carpenter, B., Queen, R., Hambleton, S., Hague, R., Allen, H.L., Thaventhiran, J., Doody, G., Collin, M., Bigley, V., 2019. Differential IRF8 Requirement Defines Two Pathways of Dendritic Cell Development in Humans (SSRN Scholarly Paper No. ID 3365028). Social Science Research Network, Rochester, NY.

Cytlak, U., Resteu, A., Pagan, S., Green, K., Milne, P., Maisuria, S., McDonald, D., Hulme, G., Filby, A., Carpenter, B., Queen, R., Hambleton, S., Hague, R., Lango Allen, H., Thaventhiran, J.E.D., Doody, G., Collin, M., Bigley, V., 2020. Differential IRF8 Transcription Factor Requirement Defines Two Pathways of Dendritic Cell Development in Humans. Immunity 53, 353-370.e8. https://doi.org/10.1016/j.immuni.2020.07.003

Dask | Scale the Python tools you love [WWW Document], n.d. URL https://www.dask.org/ (accessed 8.29.24).

de Mingo Pulido, Á., Hänggi, K., Celias, D.P., Gardner, A., Li, J., Batista-Bittencourt, B., Mohamed, E., Trillo-Tinoco, J., Osunmakinde, O., Peña, R., Onimus, A., Kaisho, T., Kaufmann, J., McEachern, K., Soliman, H., Luca, V.C., Rodriguez, P.C., Yu, X., Ruffell, B., 2021. The inhibitory receptor TIM-3 limits activation of the cGAS-STING pathway in intra-tumoral dendritic cells by suppressing extracellular DNA uptake. Immunity 54, 1154-1167.e7. https://doi.org/10.1016/J.IMMUNI.2021.04.019

De Monte, A., Olivieri, C.-V., Vitale, S., Bailleux, S., Castillo, L., Giordanengo, V., Maryanski, J.L., Segura, E., Doglio, A., 2016. CD1c-Related DCs that Express CD207/Langerin, but Are Distinguishable from Langerhans Cells, Are Consistently Present in Human Tonsils. Front. Immunol. 7. https://doi.org/10.3389/fimmu.2016.00197

De Schepper, S., Verheijden, S., Aguilera-Lizarraga, J., Viola, M.F., Boesmans, W., Stakenborg, N., Voytyuk, I., Schmidt, I., Boeckx, B., Dierckx de Casterlé, I., Baekelandt, V., Gonzalez Dominguez, E., Mack, M., Depoortere, I., De Strooper, B., Sprangers, B., Himmelreich, U., Soenen, S., Guilliams, M., Vanden Berghe, P., Jones, E., Lambrechts, D., Boeckxstaens, G., 2018. Self-Maintaining Gut Macrophages Are Essential for Intestinal Homeostasis. Cell 175, 400-415.e13. https://doi.org/10.1016/j.cell.2018.07.048

Delfini, M., Stakenborg, N., Viola, M.F., Boeckxstaens, G., 2022. Macrophages in the gut: Masters in multitasking. Immunity 55, 1530–1548. https://doi.org/10.1016/j.immuni.2022.08.005

den Haan, J.M.M., Lehar, S.M., Bevan, M.J., 2000. Cd8+ but Not Cd8− Dendritic Cells Cross-Prime Cytotoxic T Cells in Vivo. J. Exp. Med. 192, 1685–1696. https://doi.org/10.1084/jem.192.12.1685

Desai, J.V., Kumar, D., Freiwald, T., Chauss, D., Johnson, M.D., Abers, M.S., Steinbrink, J.M., Perfect, J.R., Alexander, B., Matzaraki, V., Snarr, B.D., Zarakas, M.A., Oikonomou, V., Silva, L.M., Shivarathri, R., Beltran, E., Demontel, L.N., Wang, L., Lim, J.K., Launder, D., Conti, H.R., Swamydas, M., McClain, M.T., Moutsopoulos, N.M., Kazemian, M., Netea, M.G., Kumar, V., Köhl, J., Kemper, C., Afzali, B., Lionakis, M.S., 2023. C5a-licensed phagocytes drive sterilizing immunity during systemic fungal infection. Cell 186, 2802-2822.e22. https://doi.org/10.1016/j.cell.2023.04.031

Deyell, M., Garris, C.S., Laughney, A.M., 2021. Cancer metastasis as a non-healing wound. Br. J. Cancer 124, 1491–1502. https://doi.org/10.1038/s41416-021-01309-w

Di Pilato, M., Kfuri-Rubens, R., Pruessmann, J.N., Ozga, A.J., Messemaker, M., Cadilha, B.L., Sivakumar, R., Cianciaruso, C., Warner, R.D., Marangoni, F., Carrizosa, E., Lesch, S., Billingsley, J., Perez-Ramos,

D., Zavala, F., Rheinbay, E., Luster, A.D., Gerner, M.Y., Kobold, S., Pittet, M.J., Mempel, T.R., 2021. CXCR6 positions cytotoxic T cells to receive critical survival signals in the tumor microenvironment. Cell 184, 4512-4530.e22. https://doi.org/10.1016/j.cell.2021.07.015

Diao, J., Winter, E., Cantin, C., Chen, W., Xu, L., Kelvin, D., Phillips, J., Cattral, M.S., 2006. In Situ Replication of Immediate Dendritic Cell (DC) Precursors Contributes to Conventional DC Homeostasis in Lymphoid Tissue1. J. Immunol. 176, 7196–7206. https://doi.org/10.4049/jimmunol.176.12.7196

Dieu-Nosjean, M.-C., Antoine, M., Danel, C., Heudes, D., Wislez, M., Poulot, V., Rabbe, N., Laurans, L., Tartour, E., de Chaisemartin, L., Lebecque, S., Fridman, W.-H., Cadranel, J., 2008. Long-Term Survival for Patients With Non–Small-Cell Lung Cancer With Intratumoral Lymphoid Structures. J. Clin. Oncol. 26, 4410–4417. https://doi.org/10.1200/JCO.2007.15.0284

Ding, Y., Chung, C.-S., Newton, S., Chen, Y., Carlton, S., Albina, J.E., Ayala, A., 2004. Polymicrobial sepsis induces divergent effects on splenic and peritoneal dendritic cell function in mice. Shock Augusta Ga 22, 137–44. https://doi.org/10.1097/01.shk.0000131194.80038.3f

Ding, Y., Wilkinson, A., Idris, A., Fancke, B., O'Keeffe, M., Khalil, D., Ju, X., Lahoud, M.H., Caminschi, I., Shortman, K., Rodwell, R., Vuckovic, S., Radford, K.J., 2014. FLT3-Ligand Treatment of Humanized Mice Results in the Generation of Large Numbers of CD141+ and CD1c+ Dendritic Cells In Vivo. J. Immunol. 192, 1982–1989. https://doi.org/10.4049/jimmunol.1302391

Dong, K., Zhang, S., 2022. Deciphering spatial domains from spatially resolved transcriptomics with an adaptive graph attention auto-encoder. Nat. Commun. 13, 1739. https://doi.org/10.1038/s41467-022-29439-6

Dress, R.J., Dutertre, C.A., Giladi, A., Schlitzer, A., Low, I., Shadan, N.B., Tay, A., Lum, J., Kairi, M.F.B.M., Hwang, Y.Y., Becht, E., Cheng, Y., Chevrier, M., Larbi, A., Newell, E.W., Amit, I., Chen, J., Ginhoux, F., 2019. Plasmacytoid dendritic cells develop from Ly6D+ lymphoid progenitors distinct from the myeloid lineage. Nat. Immunol. 20, 852–864. https://doi.org/10.1038/s41590-019-0420-3

Dries, R., Chen, J., del Rossi, N., Khan, M.M., Sistig, A., Yuan, G.-C., 2021. Advances in spatial transcriptomic data analysis. Genome Res. 31, 1706–1718. https://doi.org/10.1101/gr.275224.121

Dunn, G.P., Old, L.J., Schreiber, R.D., 2004. The three Es of cancer immunoediting. Annu. Rev. Immunol. 22, 329–360. https://doi.org/10.1146/annurev.immunol.22.012703.104803

Dunsmore, G., Guo, W., Li, Z., Bejarano, D.A., Pai, R., Yang, K., Kwok, I., Tan, L., Ng, M., De La Calle Fabregat, C., Yatim, A., Bougouin, A., Mulder, K., Thomas, J., Villar, J., Bied, M., Kloeckner, B., Dutertre,

C.-A., Gessain, G., Chakarov, S., Liu, Z., Scoazec, J.-Y., Lennon-Dumenil, A.-M., Marichal, T., Sautès-Fridman, C., Fridman, W.H., Sharma, A., Su, B., Schlitzer, A., Ng, L.G., Blériot, C., Ginhoux, F., 2024. Timing and location dictate monocyte fate and their transition to tumor-associated macrophages. Sci. Immunol. 9, eadk3981. https://doi.org/10.1126/sciimmunol.adk3981

Duong, E., Fessenden, T.B., Lutz, E., Dinter, T., Yim, L., Blatt, S., Bhutkar, A., Wittrup, K.D., Spranger, S., 2021. Type I interferon activates MHC class I-dressed CD11b+ conventional dendritic cells to promote protective anti-tumor CD8+ T cell immunity. Immunity. https://doi.org/10.1016/j.immuni.2021.10.020

Dutertre, C.-A., Becht, E., Irac, S.E., Khalilnezhad, A., Narang, V., Khalilnezhad, S., Ng, P.Y., van den Hoogen, L.L., Leong, J.Y., Lee, B., Chevrier, M., Zhang, X.M., Yong, P.J.A., Koh, G., Lum, J., Howland, S.W., Mok, E., Chen, J., Larbi, A., Tan, H.K.K., Lim, T.K.H., Karagianni, P., Tzioufas, A.G., Malleret, B., Brody, J., Albani, S., van Roon, J., Radstake, T., Newell, E.W., Ginhoux, F., 2019. Single-Cell Analysis of Human Mononuclear Phagocytes Reveals Subset-Defining Markers and Identifies Circulating Inflammatory Dendritic Cells. Immunity 51, 573-589.e8. https://doi.org/10.1016/j.immuni.2019.08.008

Dvorak, H.F., 1986. Tumors: Wounds That Do Not Heal. N. Engl. J. Med. 315, 1650–1659. https://doi.org/10.1056/NEJM198612253152606

Dzionek, A., Fuchs, A., Schmidt, P., Cremer, S., Zysk, M., Miltenyi, S., Buck, D.W., Schmitz, J., 2000. BDCA-2, BDCA-3, and BDCA-4: three markers for distinct subsets of dendritic cells in human peripheral blood. J. Immunol. Baltim. Md 1950 165, 6037–6046. https://doi.org/10.4049/jimmunol.165.11.6037

Engel, P., Boumsell, L., Balderas, R., Bensussan, A., Gattei, V., Horejsi, V., Jin, B.-Q., Malavasi, F., Mortari, F., Schwartz-Albiez, R., Stockinger, H., van Zelm, M.C., Zola, H., Clark, G., 2015. CD Nomenclature 2015: Human Leukocyte Differentiation Antigen Workshops as a Driving Force in Immunology. J. Immunol. 195, 4555–4563. https://doi.org/10.4049/jimmunol.1502033

Epelman, S., Lavine, K.J., Beaudin, A.E., Sojka, D.K., Carrero, J.A., Calderon, B., Brija, T., Gautier, E.L., Ivanov, S., Satpathy, A.T., Schilling, J.D., Schwendener, R., Sergin, I., Razani, B., Forsberg, E.C., Yokoyama, W.M., Unanue, E.R., Colonna, M., Randolph, G.J., Mann, D.L., 2014. Embryonic and adult-derived resident cardiac macrophages are maintained through distinct mechanisms at steady state and during inflammation. Immunity 40, 91–104. https://doi.org/10.1016/j.immuni.2013.11.019

Erblich, B., Zhu, L., Etgen, A.M., Dobrenis, K., Pollard, J.W., 2011. Absence of Colony Stimulation Factor-1 Receptor Results in Loss of

Microglia, Disrupted Brain Development and Olfactory Deficits. PLOS ONE 6, e26317. https://doi.org/10.1371/journal.pone.0026317
Esparza-Baquer, A., Labiano, I., Sharif, O., Agirre-Lizaso, A., Oakley, F., Rodrigues, P.M., Zhuravleva, E., O'Rourke, C.J., Hijona, E., Jimenez-Agüero, R., Riaño, I., Landa, A., Casta, A.L., Zaki, M.Y.W., Munoz-Garrido, P., Azkargorta, M., Elortza, F., Vogel, A., Schabbauer, G., Aspichueta, P., Andersen, J.B., Knapp, S., Mann, D.A., Bujanda, L., Banales, J.M., Perugorria, M.J., 2021. TREM-2 defends the liver against hepatocellular carcinoma through multifactorial protective mechanisms. Gut 70, 1345–1361. https://doi.org/10.1136/gutjnl-2019-319227
Fang, X., Zheng, Y., Duan, Y., Liu, Y., Zhong, W., 2019. Recent Advances in Design of Fluorescence-based Assays for High-throughput Screening. Anal. Chem. 91, 482–504. https://doi.org/10.1021/acs.analchem.8b05303
Ferchen, K., Salomonis, N., Grimes, H.L., 2023. pyInfinityFlow: optimized imputation and analysis of high-dimensional flow cytometry data for millions of cells. Bioinformatics 39, btad287. https://doi.org/10.1093/bioinformatics/btad287
Ferris, S.T., Durai, V., Wu, R., Theisen, D.J., Ward, J.P., Bern, M.D., Davidson, J.T., Bagadia, P., Liu, T., Briseño, C.G., Li, L., Gillanders, W.E., Wu, G.F., Yokoyama, W.M., Murphy, T.L., Schreiber, R.D., Murphy, K.M., 2020. cDC1 prime and are licensed by CD4+ T cells to induce anti-tumour immunity. Nature 584, 624–629. https://doi.org/10.1038/s41586-020-2611-3
Fogg, D.K., Sibon, C., Miled, C., Jung, S., Aucouturier, P., Littman, D.R., Cumano, A., Geissmann, F., 2006. A Clonogenic Bone Marrow Progenitor Specific for Macrophages and Dendritic Cells. Science 311, 83–87. https://doi.org/10.1126/science.1117729
Förster, R., Davalos-Misslitz, A.C., Rot, A., 2008. CCR7 and its ligands: balancing immunity and tolerance. Nat. Rev. Immunol. 8, 362–371. https://doi.org/10.1038/nri2297
Franklin, Ruth A., Liao, W., Sarkar, A., Kim, M.V., Bivona, M.R., Liu, K., Pamer, E.G., Li, M.O., 2014. The cellular and molecular origin of tumor-associated macrophages. Science 344, 921–925. https://doi.org/10.1126/science.1252510
Franklin, R A, Liao, W., Sarkar, A., Kim, M.V., Bivona, M.R., Liu, K., Pamer, E.G., Li, M.O., 2014. The cellular and molecular origin of tumor-associated macrophages. Science 344, 921–925. https://doi.org/10.1126/science.1252510
Fu, X., Lin, Y., Lin, D.M., Mechtersheimer, D., Wang, C., Ameen, F., Ghazanfar, S., Patrick, E., Kim, J., Yang, J.Y.H., 2024. BIDCell: Biologically-informed self-supervised learning for segmentation of

subcellular spatial transcriptomics data. Nat. Commun. 15, 509. https://doi.org/10.1038/s41467-023-44560-w
Fujimoto, Y., Tu, L., Miller, A.S., Bock, C., Fujimoto, M., Doyle, C., Steeber, D.A., Tedder, T.F., 2002. CD83 Expression Influences CD4+ T Cell Development in the Thymus. Cell 108, 755–767. https://doi.org/10.1016/S0092-8674(02)00673-6
Gabanyi, I., Muller, P.A., Feighery, L., Oliveira, T.Y., Costa-Pinto, F.A., Mucida, D., 2016. Neuro-immune Interactions Drive Tissue Programming in Intestinal Macrophages. Cell 164, 378–391. https://doi.org/10.1016/j.cell.2015.12.023
Gajewski, T.F., Schreiber, H., Fu, Y.-X., 2013. Innate and adaptive immune cells in the tumor microenvironment. Nat. Immunol. 14, 1014–1022. https://doi.org/10.1038/ni.2703
Gao, Y., Li, H., Li, Z., Xie, L., Liu, X., Huang, Z., Chen, B., Lin, X., Wang, X., Zheng, Y., Su, W., 2021. Single-Cell Analysis Reveals the Heterogeneity of Monocyte-Derived and Peripheral Type-2 Conventional Dendritic Cells. J. Immunol. Baltim. Md 1950 207, 837–848. https://doi.org/10.4049/jimmunol.2100094
Gautier, E.L., Shay, T., Miller, J., Greter, M., Jakubzick, C., Ivanov, S., Helft, J., Chow, A., Elpek, K.G., Gordonov, S., Mazloom, A.R., Ma'ayan, A., Chua, W.-J., Hansen, T.H., Turley, S.J., Merad, M., Randolph, G.J., 2012. Gene-expression profiles and transcriptional regulatory pathways that underlie the identity and diversity of mouse tissue macrophages. Nat. Immunol. 13, 1118–1128. https://doi.org/10.1038/ni.2419
Geissmann, F., Jung, S., Littman, D.R., 2003. Blood monocytes consist of two principal subsets with distinct migratory properties. Immunity 19, 71–82. https://doi.org/10.1016/S1074-7613(03)00174-2
Gerhard, G.M., Bill, R., Messemaker, M., Klein, A.M., Pittet, M.J., 2020. Tumor-infiltrating dendritic cell states are conserved across solid human cancers. J. Exp. Med. 218, e20200264. https://doi.org/10.1084/jem.20200264
Germain, C., Gnjatic, S., Tamzalit, F., Knockaert, S., Remark, R., Goc, J., Lepelley, A., Becht, E., Katsahian, S., Bizouard, G., Validire, P., Damotte, D., Alifano, M., Magdeleinat, P., Cremer, I., Teillaud, J.-L., Fridman, W.-H., Sautès-Fridman, C., Dieu-Nosjean, M.-C., 2014. Presence of B Cells in Tertiary Lymphoid Structures Is Associated with a Protective Immunity in Patients with Lung Cancer. Am. J. Respir. Crit. Care Med. 189, 832–844. https://doi.org/10.1164/rccm.201309-1611OC
Giampazolias, E., Schulz, O., Lim, K.H.J., Rogers, N.C., Chakravarty, P., Srinivasan, N., Gordon, O., Cardoso, A., Buck, M.D., Poirier, E.Z., Canton, J., Zelenay, S., Sammicheli, S., Moncaut, N., Varsani-Brown, S., Rosewell, I., Reis e Sousa, C., 2021. Secreted gelsolin

inhibits DNGR-1-dependent cross-presentation and cancer immunity. Cell 184, 4016-4031.e22. https://doi.org/10.1016/j.cell.2021.05.021
Giladi, A., Amit, I., 2018. Single-Cell Genomics: A Stepping Stone for Future Immunology Discoveries. Cell 172, 14–21. https://doi.org/10.1016/j.cell.2017.11.011
Ginhoux, F., Greter, M., Leboeuf, M., Nandi, S., See, P., Gokhan, S., Mehler, M.F., Conway, S.J., Ng, L.G., Stanley, E.R., Samokhvalov, I.M., Merad, M., 2010. Fate Mapping Analysis Reveals That Adult Microglia Derive from Primitive Macrophages. Science 330, 841–845. https://doi.org/10.1126/science.1194637
Ginhoux, Florent, Greter, M., Leboeuf, M., Nandi, S., See, P., Gokhan, S., Mehler, M.F., Conway, S.J., Ng, L.G., Stanley, E.R., Samokhvalov, I.M., Merad, M., 2010. Fate mapping analysis reveals that adult microglia derive from primitive macrophages. Science 330, 841–5. https://doi.org/10.1126/science.1194637
Ginhoux, F., Guilliams, M., Merad, M., 2022. Expanding dendritic cell nomenclature in the single-cell era. Nat. Rev. Immunol. 22, 67–68. https://doi.org/10.1038/s41577-022-00675-7
Ginhoux, F., Jung, S., 2014. Monocytes and macrophages: developmental pathways and tissue homeostasis. Nat. Rev. Immunol. 14, 392–404. https://doi.org/10.1038/nri3671
Ginhoux, F., Liu, K., Helft, J., Bogunovic, M., Greter, M., Hashimoto, D., Price, J., Yin, N., Bromberg, J., Lira, S.A., Stanley, E.R., Nussenzweig, M., Merad, M., 2009. The origin and development of nonlymphoid tissue CD103 + DCs. J. Exp. Med. 206, 3115–3130. https://doi.org/10.1084/jem.20091756
Goldmann, T., Wieghofer, P., Müller, P.F., Wolf, Y., Varol, D., Yona, S., Brendecke, S.M., Kierdorf, K., Staszewski, O., Datta, M., Luedde, T., Heikenwalder, M., Jung, S., Prinz, M., 2013. A new type of microglia gene targeting shows TAK1 to be pivotal in CNS autoimmune inflammation. Nat. Neurosci. 16, 1618–1626. https://doi.org/10.1038/nn.3531
Gonzalez, H., Mei, W., Robles, I., Hagerling, C., Allen, B.M., Hauge Okholm, T.L., Nanjaraj, A., Verbeek, T., Kalavacherla, S., van Gogh, M., Georgiou, S., Daras, M., Phillips, J.J., Spitzer, M.H., Roose, J.P., Werb, Z., 2022. Cellular architecture of human brain metastases. Cell 185, 729-745.e20. https://doi.org/10.1016/j.cell.2021.12.043
Gordon, S.R., Maute, R.L., Dulken, B.W., Hutter, G., George, B.M., McCracken, M.N., Gupta, R., Tsai, J.M., Sinha, R., Corey, D., Ring, A.M., Connolly, A.J., Weissman, I.L., 2017. PD-1 expression by tumour-associated macrophages inhibits phagocytosis and tumour

immunity. Nature 545, 495–499. https://doi.org/10.1038/nature22396
Gosselin, D., Link, V.M., Romanoski, C.E., Fonseca, G.J., Eichenfield, D.Z., Spann, N.J., Stender, J.D., Chun, H.B., Garner, H., Geissmann, F., Glass, C.K., 2014. Environment drives selection and function of enhancers controlling tissue-specific macrophage identities. Cell 159, 1327–1340. https://doi.org/10.1016/j.cell.2014.11.023
Greter, M., Lelios, I., Pelczar, P., Hoeffel, G., Price, J., Leboeuf, M., Kündig, T.M., Frei, K., Ginhoux, F., Merad, M., Becher, B., 2012. Stroma-Derived Interleukin-34 Controls the Development and Maintenance of Langerhans Cells and the Maintenance of Microglia. Immunity 37, 1050–1060. https://doi.org/10.1016/j.immuni.2012.11.001
Gschwend, J., Sherman, S.P.M., Ridder, F., Feng, X., Liang, H.-E., Locksley, R.M., Becher, B., Schneider, C., 2021. Alveolar macrophages rely on GM-CSF from alveolar epithelial type 2 cells before and after birth. J. Exp. Med. 218, e20210745. https://doi.org/10.1084/jem.20210745
Guilliams, M., De Kleer, I., Henri, S., Post, S., Vanhoutte, L., De Prijck, S., Deswarte, K., Malissen, B., Hammad, H., Lambrecht, B.N., 2013. Alveolar macrophages develop from fetal monocytes that differentiate into long-lived cells in the first week of life via GM-CSF. J. Exp. Med. 210, 1977–1992. https://doi.org/10.1084/jem.20131199
Guilliams, M., Dutertre, C.-A., Scott, C.L., McGovern, N., Sichien, D., Chakarov, S., Van Gassen, S., Chen, J., Poidinger, M., De Prijck, S., Tavernier, S.J., Low, I., Irac, S.E., Mattar, C.N., Sumatoh, H.R., Low, G.H.L., Chung, T.J.K., Chan, D.K.H., Tan, K.K., Hon, T.L.K., Fossum, E., Bogen, B., Choolani, M., Chan, J.K.Y., Larbi, A., Luche, H., Henri, S., Saeys, Y., Newell, E.W., Lambrecht, B.N., Malissen, B., Ginhoux, F., 2016a. Unsupervised High-Dimensional Analysis Aligns Dendritic Cells across Tissues and Species. Immunity 45, 669–684. https://doi.org/10.1016/j.immuni.2016.08.015
Guilliams, M., Dutertre, C.-A., Scott, C.L., McGovern, N., Sichien, D., Chakarov, S., Van Gassen, S., Chen, J., Poidinger, M., De Prijck, S., Tavernier, S.J., Low, I., Irac, S.E., Mattar, C.N., Sumatoh, H.R., Low, G.H.L., Chung, T.J.K., Chan, D.K.H., Tan, K.K., Hon, T.L.K., Fossum, E., Bogen, B., Choolani, M., Chan, J.K.Y., Larbi, A., Luche, H., Henri, S., Saeys, Y., Newell, E.W., Lambrecht, B.N., Malissen, B., Ginhoux, F., 2016b. Unsupervised High-Dimensional Analysis Aligns Dendritic Cells across Tissues and Species. Immunity 45, 669–684. https://doi.org/10.1016/j.immuni.2016.08.015

Guilliams, M., Ginhoux, F., Jakubzick, C., Naik, S.H., Onai, N., Schraml, B.U., Segura, E., Tussiwand, R., Yona, S., 2014. Dendritic cells, monocytes and macrophages: A unified nomenclature based on ontogeny. Nat. Rev. Immunol. 14, 571–578. https://doi.org/10.1038/nri3712

Guilliams, M., Mildner, A., Yona, S., 2018. Developmental and Functional Heterogeneity of Monocytes. Immunity 49, 595–613. https://doi.org/10.1016/j.immuni.2018.10.005

Guilliams, M., Scott, C.L., 2022. Liver macrophages in health and disease. Immunity 55, 1515–1529. https://doi.org/10.1016/j.immuni.2022.08.002

Guilliams, M., Scott, C.L., 2017. Does niche competition determine the origin of tissue-resident macrophages? Nat. Rev. Immunol. 17, 451–460. https://doi.org/10.1038/nri.2017.42

Guilliams, M., Svedberg, F.R., 2021. Does tissue imprinting restrict macrophage plasticity? Nat. Immunol. 22, 118–127. https://doi.org/10.1038/s41590-020-00849-2

Guilliams, M., Thierry, G.R., Bonnardel, J., Bajenoff, M., 2020. Establishment and Maintenance of the Macrophage Niche. Immunity 52, 434–451. https://doi.org/10.1016/j.immuni.2020.02.015

Hagemeyer, N., Kierdorf, K., Frenzel, K., Xue, J., Ringelhan, M., Abdullah, Z., Godin, I., Wieghofer, P., Costa Jordão, M.J., Ulas, T., Yorgancioglu, G., Rosenbauer, F., Knolle, P.A., Heikenwalder, M., Schultze, J.L., Prinz, M., 2016. Transcriptome-based profiling of yolk sac-derived macrophages reveals a role for Irf8 in macrophage maturation. EMBO J. 35, 1730–1744. https://doi.org/10.15252/embj.201693801

Haigis, K.M., Cichowski, K., Elledge, S.J., 2019. Tissue-specificity in cancer: The rule, not the exception. Science 363, 1150–1151. https://doi.org/10.1126/science.aaw3472

Hambleton, S., Salem, S., Bustamante, J., Bigley, V., Boisson-Dupuis, S., Azevedo, J., Fortin, A., Haniffa, M., Ceron-Gutierrez, L., Bacon, C.M., Menon, G., Trouillet, C., McDonald, D., Carey, P., Ginhoux, F., Alsina, L., Zumwalt, T.J., Kong, X.-F., Kumararatne, D., Butler, K., Hubeau, M., Feinberg, J., Al-Muhsen, S., Cant, A., Abel, L., Chaussabel, D., Doffinger, R., Talesnik, E., Grumach, A., Duarte, A., Abarca, K., Moraes-Vasconcelos, D., Burk, D., Berghuis, A., Geissmann, F., Collin, M., Casanova, J.-L., Gros, P., 2011. IRF8 Mutations and Human Dendritic-Cell Immunodeficiency. N. Engl. J. Med. 365, 127–138. https://doi.org/10.1056/NEJMoa1100066

Haniffa, M., Shin, A., Bigley, V., McGovern, N., Teo, P., See, P., Wasan, P.S., Wang, X.N., Malinarich, F., Malleret, B., Larbi, A., Tan, P., Zhao, H., Poidinger, M., Pagan, S., Cookson, S., Dickinson, R., Dimmick, I., Jarrett, R.F., Renia, L., Tam, J., Song, C., Connolly, J.,

Chan, J.K., Gehring, A., Bertoletti, A., Collin, M., Ginhoux, F., 2012. Human tissues contain CD141hi cross-presenting dendritic cells with functional homology to mouse CD103+ nonlymphoid dendritic cells. Immunity 37, 60–73. https://doi.org/10.1016/j.immuni.2012.04.012

Hao, Y., Hao, S., Andersen-Nissen, E., Mauck, W.M., Zheng, S., Butler, A., Lee, M.J., Wilk, A.J., Darby, C., Zagar, M., Hoffman, P., Stoeckius, M., Papalexi, E., Mimitou, E.P., Jain, J., Srivastava, A., Stuart, T., Fleming, L.B., Yeung, B., Rogers, A.J., McElrath, J.M., Blish, C.A., Gottardo, R., Smibert, P., Satija, R., 2020. Integrated analysis of multimodal single-cell data. bioRxiv 2020.10.12.335331. https://doi.org/10.1101/2020.10.12.335331

Hao, Y., Hao, S., Andersen-Nissen, E., Mauck, W.M., Zheng, S., Butler, A., Lee, M.J., Wilk, A.J., Darby, C., Zager, M., Hoffman, P., Stoeckius, M., Papalexi, E., Mimitou, E.P., Jain, J., Srivastava, A., Stuart, T., Fleming, L.M., Yeung, B., Rogers, A.J., McElrath, J.M., Blish, C.A., Gottardo, R., Smibert, P., Satija, R., 2021. Integrated analysis of multimodal single-cell data. Cell 184, 3573-3587.e29. https://doi.org/10.1016/j.cell.2021.04.048

Hao, Y., Stuart, T., Kowalski, M.H., Choudhary, S., Hoffman, P., Hartman, A., Srivastava, A., Molla, G., Madad, S., Fernandez-Granda, C., Satija, R., 2024. Dictionary learning for integrative, multimodal and scalable single-cell analysis. Nat. Biotechnol. 42, 293–304. https://doi.org/10.1038/s41587-023-01767-y

Hara, T., Chanoch-Myers, R., Mathewson, N.D., Myskiw, C., Atta, L., Bussema, L., Eichhorn, S.W., Greenwald, A.C., Kinker, G.S., Rodman, C., Castro, L.N.G., Wakimoto, H., Rozenblatt-Rosen, O., Zhuang, X., Fan, J., Hunter, T., Verma, I.M., Wucherpfennig, K.W., Regev, A., Suvà, M.L., Tirosh, I., 2021. Interactions between cancer cells and immune cells drive transitions to mesenchymal-like states in glioblastoma. Cancer Cell 39, 779-792.e11. https://doi.org/10.1016/j.ccell.2021.05.002

Harper, D.M., Nieminen, P., Donders, G., Einstein, M.H., Garcia, F., Huh, W.K., Stoler, M.H., Glavini, K., Attley, G., Limacher, J.-M., Bastien, B., Calleja, E., 2019. The efficacy and safety of Tipapkinogen Sovacivec therapeutic HPV vaccine in cervical intraepithelial neoplasia grades 2 and 3: Randomized controlled phase II trial with 2.5 years of follow-up. Gynecol. Oncol. 153, 521–529. https://doi.org/10.1016/j.ygyno.2019.03.250

Hartman, A., Satija, R., 2024. Comparative analysis of multiplexed in situ gene expression profiling technologies. BioRxiv Prepr. Serv. Biol. 2024.01.11.575135. https://doi.org/10.1101/2024.01.11.575135

Hashimoto, D., Chow, A., Noizat, C., Teo, P., Beasley, M.B., Leboeuf, M., Becker, C.D., See, P., Price, J., Lucas, D., Greter, M., Mortha, A.,

Boyer, S.W., Forsberg, E.C., Tanaka, M., van Rooijen, N., García-Sastre, A., Stanley, E.R., Ginhoux, F., Frenette, P.S., Merad, M., 2013. Tissue-Resident Macrophages Self-Maintain Locally throughout Adult Life with Minimal Contribution from Circulating Monocytes. Immunity 38, 792–804. https://doi.org/10.1016/j.immuni.2013.04.004

He, S., Bhatt, R., Brown, C., Brown, E.A., Buhr, D.L., Chantranuvatana, K., Danaher, P., Dunaway, D., Garrison, R.G., Geiss, G., Gregory, M.T., Hoang, M.L., Khafizov, R., Killingbeck, E.E., Kim, D., Kim, T.K., Kim, Y., Klock, A., Korukonda, M., Kutchma, A., Lewis, Z.R., Liang, Y., Nelson, J.S., Ong, G.T., Perillo, E.P., Phan, J.C., Phan-Everson, T., Piazza, E., Rane, T., Reitz, Z., Rhodes, M., Rosenbloom, A., Ross, D., Sato, H., Wardhani, A.W., Williams-Wietzikoski, C.A., Wu, L., Beechem, J.M., 2022. High-plex imaging of RNA and proteins at subcellular resolution in fixed tissue by spatial molecular imaging. Nat. Biotechnol. 40, 1794–1806. https://doi.org/10.1038/s41587-022-01483-z

Heger, L., Balk, S., Lühr, J.J., Heidkamp, G.F., Lehmann, C.H.K., Hatscher, L., Purbojo, A., Hartmann, A., Garcia-Martin, F., Nishimura, S.-I., Cesnjevar, R., Nimmerjahn, F., Dudziak, D., 2018. CLEC10A Is a Specific Marker for Human CD1c+ Dendritic Cells and Enhances Their Toll-Like Receptor 7/8-Induced Cytokine Secretion. Front. Immunol. 9. https://doi.org/10.3389/fimmu.2018.00744

Heng, T.S.P., Painter, M.W., Elpek, K., Lukacs-Kornek, V., Mauermann, N., Turley, S.J., Koller, D., Kim, F.S., Wagers, A.J., Asinovski, N., Davis, S., Fassett, M., Feuerer, M., Gray, D.H.D., Haxhinasto, S., Hill, J.A., Hyatt, G., Laplace, C., Leatherbee, K., Mathis, D., Benoist, C., Jianu, R., Laidlaw, D.H., Best, J.A., Knell, J., Goldrath, A.W., Jarjoura, J., Sun, J.C., Zhu, Y., Lanier, L.L., Ergun, A., Li, Z., Collins, J.J., Shinton, S.A., Hardy, R.R., Friedline, R., Sylvia, K., Kang, J., 2008. The Immunological Genome Project: networks of gene expression in immune cells. Nat. Immunol. 9, 1091–1094. https://doi.org/10.1038/ni1008-1091

Hofer, T.P., Zawada, A.M., Frankenberger, M., Skokann, K., Satzl, A.A., Gesierich, W., Schuberth, M., Levin, J., Danek, A., Rotter, B., Heine, G.H., Ziegler-Heitbrock, L., 2015. slan-defined subsets of CD16-positive monocytes: impact of granulomatous inflammation and M-CSF receptor mutation. Blood 126, 2601–2610. https://doi.org/10.1182/blood-2015-06-651331

Hoffmann, D., Sens, J., Brennig, S., Brand, D., Philipp, F., Vollmer Barbosa, P., Kuehle, J., Steinemann, D., Lenz, D., Buchegger, T., Morgan, M., Falk, C.S., Klein, C., Lachmann, N., Schambach, A., 2021. Genetic Correction of IL-10RB Deficiency Reconstitutes

Anti-Inflammatory Regulation in iPSC-Derived Macrophages. J. Pers. Med. 11, 221. https://doi.org/10.3390/jpm11030221
Hoyer, S., Hamman, J., 2017. xarray: N-D labeled Arrays and Datasets in Python. J. Open Res. Softw. 5. https://doi.org/10.5334/jors.148
Ingersoll, M.A., Spanbroek, R., Lottaz, C., Gautier, E.L., Frankenberger, M., Hoffmann, R., Lang, R., Haniffa, M., Collin, M., Tacke, F., Habenicht, A.J.R., Ziegler-Heitbrock, L., Randolph, G.J., 2010. Comparison of gene expression profiles between human and mouse monocyte subsets. Blood 115, e10–e19. https://doi.org/10.1182/blood-2009-07-235028
Iwasaki, A., Medzhitov, R., 2015. Control of adaptive immunity by the innate immune system. Nat. Immunol. 16, 343–353. https://doi.org/10.1038/ni.3123
Jaitin, D.A., Adlung, L., Thaiss, C.A., Weiner, A., Li, B., Descamps, H., Lundgren, P., Bleriot, C., Liu, Z., Deczkowska, A., Keren-Shaul, H., David, E., Zmora, N., Eldar, S.M., Lubezky, N., Shibolet, O., Hill, D.A., Lazar, M.A., Colonna, M., Ginhoux, F., Shapiro, H., Elinav, E., Amit, I., 2019. Lipid-Associated Macrophages Control Metabolic Homeostasis in a Trem2-Dependent Manner. Cell 178, 686-698.e14. https://doi.org/10.1016/j.cell.2019.05.054
Jaitin, D.A., Kenigsberg, E., Keren-Shaul, H., Elefant, N., Paul, F., Zaretsky, I., Mildner, A., Cohen, N., Jung, S., Tanay, A., Amit, I., 2014. Massively parallel single-cell RNA-seq for marker-free decomposition of tissues into cell types. Science 343, 776–9. https://doi.org/10.1126/science.1247651
Jakubzick, C., Gautier, E.L., Gibbings, S.L., Sojka, D.K., Schlitzer, A., Johnson, T.E., Ivanov, S., Duan, Q., Bala, S., Condon, T., van Rooijen, N., Grainger, J.R., Belkaid, Y., Ma'ayan, A., Riches, D.W.H., Yokoyama, W.M., Ginhoux, F., Henson, P.M., Randolph, G.J., 2013. Minimal Differentiation of Classical Monocytes as They Survey Steady-State Tissues and Transport Antigen to Lymph Nodes. Immunity 39, 599–610. https://doi.org/10.1016/j.immuni.2013.08.007
James, K.R., Gomes, T., Elmentaite, R., Kumar, N., Gulliver, E.L., King, H.W., Stares, M.D., Bareham, B.R., Ferdinand, J.R., Petrova, V.N., Polański, K., Forster, S.C., Jarvis, L.B., Suchanek, O., Howlett, S., James, L.K., Jones, J.L., Meyer, K.B., Clatworthy, M.R., Saeb-Parsy, K., Lawley, T.D., Teichmann, S.A., 2020. Distinct microbial and immune niches of the human colon. Nat. Immunol. 21, 343–353. https://doi.org/10.1038/s41590-020-0602-z
Janeway, C.A., 1989. Approaching the asymptote? Evolution and revolution in immunology. Cold Spring Harb. Symp. Quant. Biol. 54 Pt 1, 1–13. https://doi.org/10.1101/sqb.1989.054.01.003

Janeway, C.A., Travers, P., Walport, M., Shlomchik, M., 2001. Immunobiology: The Immune System In Health And Disease. Immuno Biol. 5 892. https://doi.org/10.1111/j.1467-2494.1995.tb00120.x

Jass, J.R., 2007. Classification of colorectal cancer based on correlation of clinical, morphological and molecular features. Histopathology 50, 113–130. https://doi.org/10.1111/j.1365-2559.2006.02549.x

Jefford, M., Schnurr, M., Toy, T., Masterman, K.-A., Shin, A., Beecroft, T., Tai, T.Y., Shortman, K., Shackleton, M., Davis, I.D., Parente, P., Luft, T., Chen, W., Cebon, J., Maraskovsky, E., 2003. Functional comparison of DCs generated in vivo with Flt3 ligand or in vitro from blood monocytes: differential regulation of function by specific classes of physiologic stimuli. Blood 102, 1753–1763. https://doi.org/10.1182/blood-2002-12-3854

Jhaveri, N., Ben Cheikh, B., Nikulina, N., Ma, N., Klymyshyn, D., DeRosa, J., Mihani, R., Pratapa, A., Kassim, Y., Bommakanti, S., Shang, O., Berry, S., Ihley, N., McLane, M., He, Y., Zheng, Y., Monkman, J., Cooper, C., O'Byrne, K., Anand, B., Prater, M., Basu, S., Hughes, B.G.M., Kulasinghe, A., Braubach, O., 2023. Mapping the Spatial Proteome of Head and Neck Tumors: Key Immune Mediators and Metabolic Determinants in the Tumor Microenvironment. GEN Biotechnol. 2, 418–434. https://doi.org/10.1089/genbio.2023.0029

Jin, L., Lloyd, R.V., 1997. In situ hybridization: Methods and applications. J. Clin. Lab. Anal. 11, 2–9. https://doi.org/10.1002/(SICI)1098-2825(1997)11:1<2::AID-JCLA2>3.0.CO;2-F

Jongbloed, S.L., Kassianos, A.J., McDonald, K.J., Clark, G.J., Ju, X., Angel, C.E., Chen, C.-J.J., Dunbar, P.R., Wadley, R.B., Jeet, V., Vulink, A.J.E., Hart, D.N.J., Radford, K.J., 2010. Human CD141+ (BDCA-3)+ dendritic cells (DCs) represent a unique myeloid DC subset that cross-presents necrotic cell antigens. J. Exp. Med. 207, 1247–1260. https://doi.org/10.1084/jem.20092140

Jung, S., Aliberti, J., Graemmel, P., Sunshine, M.J., Kreutzberg, G.W., Sher, A., Littman, D.R., 2000. Analysis of Fractalkine Receptor CX3CR1 Function by Targeted Deletion and Green Fluorescent Protein Reporter Gene Insertion. Mol. Cell. Biol. 20, 4106–4114. https://doi.org/10.1128/MCB.20.11.4106-4114.2000

Kapellos, T.S., Bonaguro, L., Gemünd, I., Reusch, N., Saglam, A., Hinkley, E.R., Schultze, J.L., 2019. Human Monocyte Subsets and Phenotypes in Major Chronic Inflammatory Diseases. Front. Immunol. 10. https://doi.org/10.3389/fimmu.2019.02035

Katzenelenbogen, Y., Sheban, F., Yalin, A., Yofe, I., Svetlichnyy, D., Jaitin, D.A., Bornstein, C., Moshe, A., Keren-Shaul, H., Cohen, M., Wang, S.-Y., Li, B., David, E., Salame, T.-M., Weiner, A., Amit, I., 2020. Coupled scRNA-Seq and Intracellular Protein Activity Reveal an

Immunosuppressive Role of TREM2 in Cancer. Cell 182, 872-885.e19. https://doi.org/10.1016/j.cell.2020.06.032

Kemp, S.B., Steele, N.G., Carpenter, E.S., Donahue, K.L., Bushnell, G.G., Morris, A.H., The, S., Orbach, S.M., Sirihorachai, V.R., Nwosu, Z.C., Espinoza, C., Lima, F., Brown, K., Girgis, A.A., Gunchick, V., Zhang, Y., Lyssiotis, C.A., Frankel, T.L., Bednar, F., Rao, A., Sahai, V., Shea, L.D., Crawford, H.C., Magliano, M.P. di, 2021. Pancreatic cancer is marked by complement-high blood monocytes and tumor-associated macrophages. Life Sci. Alliance 4. https://doi.org/10.26508/lsa.202000935

Kim, N., Kim, H.K., Lee, K., Hong, Y., Cho, J.H., Choi, J.W., Lee, J.-I., Suh, Y.-L., Ku, B.M., Eum, H.H., Choi, S., Choi, Y.-L., Joung, J.-G., Park, W.-Y., Jung, H.A., Sun, J.-M., Lee, S.-H., Ahn, J.S., Park, K., Ahn, M.-J., Lee, H.-O., 2020. Single-cell RNA sequencing demonstrates the molecular and cellular reprogramming of metastatic lung adenocarcinoma. Nat. Commun. 11, 2285. https://doi.org/10.1038/s41467-020-16164-1

Kinkhabwala, A., Herbel, C., Pankratz, J., Yushchenko, D.A., Rüberg, S., Praveen, P., Reiß, S., Rodriguez, F.C., Schäfer, D., Kollet, J., Dittmer, V., Martinez-Osuna, M., Minnerup, L., Reinhard, C., Dzionek, A., Rockel, T.D., Borbe, S., Büscher, M., Krieg, J., Nederlof, M., Jungblut, M., Eckardt, D., Hardt, O., Dose, C., Schumann, E., Peters, R.-P., Miltenyi, S., Schmitz, J., Müller, W., Bosio, A., 2022. MACSima imaging cyclic staining (MICS) technology reveals combinatorial target pairs for CAR T cell treatment of solid tumors. Sci. Rep. 12, 1911. https://doi.org/10.1038/s41598-022-05841-4

Kirschenbaum, D., Xie, K., Ingelfinger, F., Katzenelenbogen, Y., Abadie, K., Look, T., Sheban, F., Phan, T.S., Li, B., Zwicky, P., Yofe, I., David, E., Mazuz, K., Hou, J., Chen, Y., Shaim, H., Shanley, M., Becker, S., Qian, J., Colonna, M., Ginhoux, F., Rezvani, K., Theis, F.J., Yosef, N., Weiss, T., Weiner, A., Amit, I., 2024. Time-resolved single-cell transcriptomics defines immune trajectories in glioblastoma. Cell 187, 149-165.e23. https://doi.org/10.1016/j.cell.2023.11.032

Kissenpfennig, A., Henri, S., Dubois, B., Laplace-Builhé, C., Perrin, P., Romani, N., Tripp, C.H., Douillard, P., Leserman, L., Kaiserlian, D., Saeland, S., Davoust, J., Malissen, B., 2005. Dynamics and Function of Langerhans Cells In Vivo: Dermal Dendritic Cells Colonize Lymph Node AreasDistinct from Slower Migrating Langerhans Cells. Immunity 22, 643–654. https://doi.org/10.1016/j.immuni.2005.04.004

Knab, K., Chambers, D., Krönke, G., 2022. Synovial Macrophage and Fibroblast Heterogeneity in Joint Homeostasis and Inflammation. Front. Med. 9. https://doi.org/10.3389/fmed.2022.862161

Kondo, M., Weissman, I.L., Akashi, K., 1997. Identification of Clonogenic Common Lymphoid Progenitors in Mouse Bone Marrow. Cell 91, 661–672. https://doi.org/10.1016/S0092-8674(00)80453-5

Konecny, A.J., Mage, P.L., Tyznik, A.J., Prlic, M., Mair, F., 2024. OMIP-102: 50-color phenotyping of the human immune system with in-depth assessment of T cells and dendritic cells. Cytom. Part J. Int. Soc. Anal. Cytol. 105, 430–436. https://doi.org/10.1002/cyto.a.24841

Kopp, E.B., Medzhitov, R., 1999. The Toll-receptor family and control of innate immunity. Curr. Opin. Immunol. 11, 13–18. https://doi.org/10.1016/s0952-7915(99)80003-x

Köster, J., Rahmann, S., 2012. Snakemake—a scalable bioinformatics workflow engine. Bioinformatics 28, 2520–2522. https://doi.org/10.1093/bioinformatics/bts480

Krasemann, S., Madore, C., Cialic, R., Baufeld, C., Calcagno, N., El Fatimy, R., Beckers, L., O'Loughlin, E., Xu, Y., Fanek, Z., Greco, D.J., Smith, S.T., Tweet, G., Humulock, Z., Zrzavy, T., Conde-Sanroman, P., Gacias, M., Weng, Z., Chen, H., Tjon, E., Mazaheri, F., Hartmann, K., Madi, A., Ulrich, J.D., Glatzel, M., Worthmann, A., Heeren, J., Budnik, B., Lemere, C., Ikezu, T., Heppner, F.L., Litvak, V., Holtzman, D.M., Lassmann, H., Weiner, H.L., Ochando, J., Haass, C., Butovsky, O., 2017. The TREM2-APOE Pathway Drives the Transcriptional Phenotype of Dysfunctional Microglia in Neurodegenerative Diseases. Immunity 47, 566-581.e9. https://doi.org/10.1016/j.immuni.2017.08.008

Kumar, T., Nee, K., Wei, R., He, S., Nguyen, Q.H., Bai, S., Blake, K., Pein, M., Gong, Y., Sei, E., Hu, M., Casasent, A.K., Thennavan, A., Li, J., Tran, T., Chen, K., Nilges, B., Kashikar, N., Braubach, O., Ben Cheikh, B., Nikulina, N., Chen, H., Teshome, M., Menegaz, B., Javaid, H., Nagi, C., Montalvan, J., Lev, T., Mallya, S., Tifrea, D.F., Edwards, R., Lin, E., Parajuli, R., Hanson, S., Winocour, S., Thompson, A., Lim, B., Lawson, D.A., Kessenbrock, K., Navin, N., 2023. A spatially resolved single-cell genomic atlas of the adult human breast. Nature 620, 181–191. https://doi.org/10.1038/s41586-023-06252-9

Kuo, D., Ding, J., Cohn, I.S., Zhang, F., Wei, K., Rao, D.A., Rozo, C., Sokhi, U.K., Shanaj, S., Oliver, D.J., Echeverria, A.P., DiCarlo, E.F., Brenner, M.B., Bykerk, V.P., Goodman, S.M., Raychaudhuri, S., Rätsch, G., Ivashkiv, L.B., Donlin, L.T., 2019. HBEGF+ macrophages in rheumatoid arthritis induce fibroblast invasiveness. Sci. Transl. Med. 11. https://doi.org/10.1126/scitranslmed.aau8587

Kvedaraite, E., Ginhoux, F., 2022. Human dendritic cells in cancer. Sci. Immunol. 7. https://doi.org/10.1126/SCIIMMUNOL.ABM9409

LaMarche, N.M., Hegde, S., Park, M.D., Maier, B.B., Troncoso, L., Le Berichel, J., Hamon, P., Belabed, M., Mattiuz, R., Hennequin, C., Chin, T., Reid, A.M., Reyes-Torres, I., Nemeth, E., Zhang, R., Olson, O.C., Doroshow, D.B., Rohs, N.C., Gomez, J.E., Veluswamy, R., Hall, N., Venturini, N., Ginhoux, F., Liu, Z., Buckup, M., Figueiredo, I., Roudko, V., Miyake, K., Karasuyama, H., Gonzalez-Kozlova, E., Gnjatic, S., Passegué, E., Kim-Schulze, S., Brown, B.D., Hirsch, F.R., Kim, B.S., Marron, T.U., Merad, M., 2024. An IL-4 signalling axis in bone marrow drives pro-tumorigenic myelopoiesis. Nature 625, 166–174. https://doi.org/10.1038/s41586-023-06797-9

Lamb, J., Crawford, E.D., Peck, D., Modell, J.W., Blat, I.C., Wrobel, M.J., Lerner, J., Brunet, J.-P., Subramanian, A., Ross, K.N., Reich, M., Hieronymus, H., Wei, G., Armstrong, S.A., Haggarty, S.J., Clemons, P.A., Wei, R., Carr, S.A., Lander, E.S., Golub, T.R., 2006. The Connectivity Map: using gene-expression signatures to connect small molecules, genes, and disease. Science 313, 1929–1935. https://doi.org/10.1126/science.1132939

Lánczky, A., Győrffy, B., 2021. Web-Based Survival Analysis Tool Tailored for Medical Research (KMplot): Development and Implementation. J. Med. Internet Res. 23, e27633. https://doi.org/10.2196/27633

Lavin, Y., Kobayashi, S., Leader, A., Amir, E.D., Elefant, N., Bigenwald, C., Remark, R., Sweeney, R., Becker, C.D., Levine, J.H., Meinhof, K., Chow, A., Kim-Shulze, S., Wolf, A., Medaglia, C., Li, H., Rytlewski, J.A., Emerson, R.O., Solovyov, A., Greenbaum, B.D., Sanders, C., Vignali, M., Beasley, M.B., Flores, R., Gnjatic, S., Pe'er, D., Rahman, A., Amit, I., Merad, M., 2017. Innate Immune Landscape in Early Lung Adenocarcinoma by Paired Single-Cell Analyses. Cell 169, 750-765.e17. https://doi.org/10.1016/j.cell.2017.04.014

Lavin, Y., Winter, D., Blecher-Gonen, R., David, E., Keren-Shaul, H., Merad, M., Jung, S., Amit, I., 2014. Tissue-resident macrophage enhancer landscapes are shaped by the local microenvironment. Cell 159, 1312–1326. https://doi.org/10.1016/j.cell.2014.11.018

Leader, A., 2021. Single-cell analysis of human non-small cell lung cancer lesions refines tumor classification and patient stratification. Cancer Cell 39, 1594-1609.e12.

Leader, A.M., Grout, J.A., Maier, B.B., Nabet, B.Y., Park, M.D., Tabachnikova, A., Chang, C., Walker, L., Lansky, A., Le Berichel, J., Troncoso, L., Malissen, N., Davila, M., Martin, J.C., Magri, G., Tuballes, K., Zhao, Z., Petralia, F., Samstein, R., D'Amore, N.R.,

Thurston, G., Kamphorst, A.O., Wolf, A., Flores, R., Wang, P., Müller, S., Mellman, I., Beasley, M.B., Salmon, H., Rahman, A.H., Marron, T.U., Kenigsberg, E., Merad, M., 2021. Single-cell analysis of human non-small cell lung cancer lesions refines tumor classification and patient stratification. Cancer Cell S1535-6108(21)00560–2. https://doi.org/10.1016/j.ccell.2021.10.009

Lee, C.Y.C., Kennedy, B.C., Richoz, N., Dean, I., Tuong, Z.K., Gaspal, F., Li, Z., Willis, C., Hasegawa, T., Whiteside, S.K., Posner, D.A., Carlesso, G., Hammond, S.A., Dovedi, S.J., Roychoudhuri, R., Withers, D.R., Clatworthy, M.R., 2024. Tumour-retained activated CCR7+ dendritic cells are heterogeneous and regulate local anti-tumour cytolytic activity. Nat. Commun. 15, 682. https://doi.org/10.1038/s41467-024-44787-1

Lee, H.-O., Hong, Y., Etlioglu, H.E., Cho, Y.B., Pomella, V., Van den Bosch, B., Vanhecke, J., Verbandt, S., Hong, H., Min, J.-W., Kim, N., Eum, H.H., Qian, J., Boeckx, B., Lambrechts, D., Tsantoulis, P., De Hertogh, G., Chung, W., Lee, T., An, M., Shin, H.-T., Joung, J.-G., Jung, M.-H., Ko, G., Wirapati, P., Kim, S.H., Kim, H.C., Yun, S.H., Tan, I.B.H., Ranjan, B., Lee, W.Y., Kim, T.-Y., Choi, J.K., Kim, Y.-J., Prabhakar, S., Tejpar, S., Park, W.-Y., 2020. Lineage-dependent gene expression programs influence the immune landscape of colorectal cancer. Nat. Genet. 52, 594–603. https://doi.org/10.1038/s41588-020-0636-z

Lee, J., Breton, G., Oliveira, T.Y.K., Zhou, Y.J., Aljoufi, A., Puhr, S., Cameron, M.J., Sékaly, R.-P., Nussenzweig, M.C., Liu, K., 2015. Restricted dendritic cell and monocyte progenitors in human cord blood and bone marrow. J. Exp. Med. 212, 385–399. https://doi.org/10.1084/jem.20141442

Lenz, A., Heine, M., Schuler, G., Romani, N., 1993. Human and murine dermis contain dendritic cells. Isolation by means of a novel method and phenotypical and functional characterization. J. Clin. Invest. 92, 2587–2596.

Levine, J.H., Simonds, E.F., Bendall, S.C., Davis, K.L., Amir el, A.D., Tadmor, M.D., Litvin, O., Fienberg, H.G., Jager, A., Zunder, E.R., Finck, R., Gedman, A.L., Radtke, I., Downing, J.R., Pe'er, D., Nolan, G.P., 2015. Data-Driven Phenotypic Dissection of AML Reveals Progenitor-like Cells that Correlate with Prognosis. Cell 162, 184–97. https://doi.org/10.1016/j.cell.2015.05.047

Lewis, S.M., Asselin-Labat, M.-L., Nguyen, Q., Berthelet, J., Tan, X., Wimmer, V.C., Merino, D., Rogers, K.L., Naik, S.H., 2021. Spatial omics and multiplexed imaging to explore cancer biology. Nat. Methods 18, 997–1012. https://doi.org/10.1038/s41592-021-01203-6

Li, Ziyi, Pai, R., Gupta, S., Currenti, J., Guo, W., Di Bartolomeo, A., Feng, H., Zhang, Z., Li, Zhizhen, Liu, L., Singh, A., Bai, Y., Yang, B.,

Mishra, A., Yang, K., Qiao, L., Wallace, M., Yin, Y., Xia, Q., Chan, J.K.Y., George, J., Chow, P.K.-H., Ginhoux, F., Sharma, A., 2024. Presence of onco-fetal neighborhoods in hepatocellular carcinoma is associated with relapse and response to immunotherapy. Nat. Cancer 5, 167–186. https://doi.org/10.1038/s43018-023-00672-2

Liao, M., Liu, Y., Yuan, J., Wen, Y., Xu, G., Zhao, J., Cheng, L., Li, J., Wang, X., Wang, F., Liu, L., Amit, I., Zhang, S., Zhang, Z., 2020. Single-cell landscape of bronchoalveolar immune cells in patients with COVID-19. Nat. Med. 26, 842–844. https://doi.org/10.1038/s41591-020-0901-9

Lin, C.-C., Gil-Martin, M., Bauer, T.M., Naing, A., Lim, D.W.-T., Sarantopoulos, J., Geva, R., Ando, Y., Fan, L., Choudhury, S., Tu, P.-J., Quadt, C., Santoro, A., 2020. Abstract CT171: Phase I study of BLZ945 alone and with spartalizumab (PDR001) in patients (pts) with advanced solid tumors. Cancer Res. 80, CT171. https://doi.org/10.1158/1538-7445.AM2020-CT171

Liou, G.-Y., Martinez, A.K.F., Döppler, H.R., Bastea, L.I., Storz, P., 2023. Inflammatory and alternatively activated macrophages independently induce metaplasia but cooperatively drive pancreatic precancerous lesion growth. iScience 26. https://doi.org/10.1016/j.isci.2023.106820

Liu, J., Zhang, X., Cheng, Y., Cao, X., 2021. Dendritic cell migration in inflammation and immunity. Cell. Mol. Immunol. 18, 2461–2471. https://doi.org/10.1038/s41423-021-00726-4

Liu, K., Victora, G.D., Schwickert, T.A., Guermonprez, P., Meredith, M.M., Yao, K., Chu, F.-F., Randolph, G.J., Rudensky, A.Y., Nussenzweig, M., 2009. In Vivo Analysis of Dendritic Cell Development and Homeostasis. Science 324, 392–397. https://doi.org/10.1126/science.1170540

Liu, K., Waskow, C., Liu, X., Yao, K., Hoh, J., Nussenzweig, M., 2007. Origin of dendritic cells in peripheral lymphoid organs of mice. Nat. Immunol. 8, 578–583. https://doi.org/10.1038/ni1462

Liu, Y., Zhang, Q., Xing, B., Luo, N., Gao, R., Yu, K., Hu, X., Bu, Z., Peng, J., Ren, X., Zhang, Z., 2022. Immune phenotypic linkage between colorectal cancer and liver metastasis. Cancer Cell 40, 424-437.e5. https://doi.org/10.1016/j.ccell.2022.02.013

Liu, Z., Wang, Haiting, Li, Z., Dress, R.J., Zhu, Y., Zhang, S., De Feo, D., Kong, W.T., Cai, P., Shin, A., Piot, C., Yu, J., Gu, Y., Zhang, M., Gao, C., Chen, L., Wang, Honglin, Vétillard, M., Guermonprez, P., Kwok, I., Ng, L.G., Chakarov, S., Schlitzer, A., Becher, B., Dutertre, C.-A., Su, B., Ginhoux, F., 2023. Dendritic cell type 3 arises from Ly6C+ monocyte-dendritic cell progenitors. Immunity 56, 1761-1777.e6. https://doi.org/10.1016/j.immuni.2023.07.001

Liu, Zhaoyuan, Gu, Y., Chakarov, S., Bleriot, C., Kwok, I., Chen, X., Shin, A., Huang, W., Dress, R.J., Dutertre, C.-A., Schlitzer, A., Chen, J., Ng, L.G., Wang, H., Liu, Zhiduo, Su, B., Ginhoux, F., 2019. Fate Mapping via Ms4a3-Expression History Traces Monocyte-Derived Cells. Cell 178, 1509-1525.e19. https://doi.org/10.1016/J.CELL.2019.08.009

Locati, M., Curtale, G., Mantovani, A., 2020. Diversity, Mechanisms, and Significance of Macrophage Plasticity. Annu. Rev. Pathol. Mech. Dis. 15, 123–147. https://doi.org/10.1146/annurev-pathmechdis-012418-012718

Luber, C.A., Cox, J., Lauterbach, H., Fancke, B., Selbach, M., Tschopp, J., Akira, S., Wiegand, M., Hochrein, H., O'Keeffe, M., Mann, M., 2010. Quantitative Proteomics Reveals Subset-Specific Viral Recognition in Dendritic Cells. Immunity 32, 279–289. https://doi.org/10.1016/j.immuni.2010.01.013

Ma, Y., Adjemian, S., Mattarollo, S.R., Yamazaki, T., Aymeric, L., Yang, H., Portela Catani, J.P., Hannani, D., Duret, H., Steegh, K., Martins, I., Schlemmer, F., Michaud, M., Kepp, O., Sukkurwala, A.Q., Menger, L., Vacchelli, E., Droin, N., Galluzzi, L., Krzysiek, R., Gordon, S., Taylor, P.R., Van Endert, P., Solary, E., Smyth, M.J., Zitvogel, L., Kroemer, G., 2013. Anticancer Chemotherapy-Induced Intratumoral Recruitment and Differentiation of Antigen-Presenting Cells. Immunity 38, 729–741. https://doi.org/10.1016/j.immuni.2013.03.003

Mackay, L.K., Minnich, M., Kragten, N.A.M., Liao, Y., Nota, B., Seillet, C., Zaid, A., Man, K., Preston, S., Freestone, D., Braun, A., Wynne-Jones, E., Behr, F.M., Stark, R., Pellicci, D.G., Godfrey, D.I., Belz, G.T., Pellegrini, M., Gebhardt, T., Busslinger, M., Shi, W., Carbone, F.R., van Lier, R.A.W., Kallies, A., van Gisbergen, K.P.J.M., 2016. Hobit and Blimp1 instruct a universal transcriptional program of tissue residency in lymphocytes. Science 352, 459–463. https://doi.org/10.1126/science.aad2035

MacParland, S.A., Liu, J.C., Ma, X.-Z., Innes, B.T., Bartczak, A.M., Gage, B.K., Manuel, J., Khuu, N., Echeverri, J., Linares, I., Gupta, R., Cheng, M.L., Liu, L.Y., Camat, D., Chung, S.W., Seliga, R.K., Shao, Z., Lee, E., Ogawa, S., Ogawa, M., Wilson, M.D., Fish, J.E., Selzner, M., Ghanekar, A., Grant, D., Greig, P., Sapisochin, G., Selzner, N., Winegarden, N., Adeyi, O., Keller, G., Bader, G.D., McGilvray, I.D., 2018. Single cell RNA sequencing of human liver reveals distinct intrahepatic macrophage populations. Nat. Commun. 9, 4383. https://doi.org/10.1038/s41467-018-06318-7

Magen, A., Hamon, P., Fiaschi, N., Soong, B.Y., Park, M.D., Mattiuz, R., Humblin, E., Troncoso, L., D'souza, D., Dawson, T., Kim, J., Hamel, S., Buckup, M., Chang, C., Tabachnikova, A., Schwartz, H.,

Malissen, N., Lavin, Y., Soares-Schanoski, A., Giotti, B., Hegde, S., Ioannou, G., Gonzalez-Kozlova, E., Hennequin, C., Le Berichel, J., Zhao, Z., Ward, S.C., Fiel, I., Kou, B., Dobosz, M., Li, L., Adler, C., Ni, M., Wei, Y., Wang, W., Atwal, G.S., Kundu, K., Cygan, K.J., Tsankov, A.M., Rahman, A., Price, C., Fernandez, N., He, J., Gupta, N.T., Kim-Schulze, S., Gnjatic, S., Kenigsberg, E., Deering, R.P., Schwartz, M., Marron, T.U., Thurston, G., Kamphorst, A.O., Merad, M., 2023. Intratumoral dendritic cell-CD4+ T helper cell niches enable CD8+ T cell differentiation following PD-1 blockade in hepatocellular carcinoma. Nat. Med. 29, 1389–1399. https://doi.org/10.1038/s41591-023-02345-0

Maier, B., Leader, A.M., Chen, S.T., Tung, N., Chang, C., LeBerichel, J., Chudnovskiy, A., Maskey, S., Walker, L., Finnigan, J.P., Kirkling, M.E., Reizis, B., Ghosh, S., D'Amore, N.R., Bhardwaj, N., Rothlin, C.V., Wolf, A., Flores, R., Marron, T., Rahman, A.H., Kenigsberg, E., Brown, B.D., Merad, M., 2020. A conserved dendritic-cell regulatory program limits antitumour immunity. Nature 580, 257–262. https://doi.org/10.1038/s41586-020-2134-y

Maier, T., Guell, M., Serrano, L., 2009. Correlation of mRNA and protein in complex biological samples. FEBS Lett 583, 3966–3973. https://doi.org/10.1016/j.febslet.2009.10.036

Manji, G.A., Van Tine, B.A., Lee, S.M., Raufi, A.G., Pellicciotta, I., Hirbe, A.C., Pradhan, J., Chen, A., Rabadan, R., Schwartz, G.K., 2021. A Phase I Study of the Combination of Pexidartinib and Sirolimus to Target Tumor-Associated Macrophages in Unresectable Sarcoma and Malignant Peripheral Nerve Sheath Tumors. Clin. Cancer Res. 27, 5519–5527. https://doi.org/10.1158/1078-0432.CCR-21-1779

Mantovani, A., Allavena, P., Marchesi, F., Garlanda, C., 2022. Macrophages as tools and targets in cancer therapy. Nat. Rev. Drug Discov. 21, 799–820. https://doi.org/10.1038/s41573-022-00520-5

Mantovani, A., Marchesi, F., Malesci, A., Laghi, L., Allavena, P., 2017. Tumour-associated macrophages as treatment targets in oncology. Nat. Rev. Clin. Oncol. 14, 399–416. https://doi.org/10.1038/nrclinonc.2016.217

Mantovani, A., Sica, A., Sozzani, S., Allavena, P., Vecchi, A., Locati, M., 2004. The chemokine system in diverse forms of macrophage activation and polarization. Trends Immunol. 25, 677–686. https://doi.org/10.1016/j.it.2004.09.015

Maraskovsky, E., Daro, E., Roux, E., Teepe, M., Maliszewski, C.R., Hoek, J., Caron, D., Lebsack, M.E., McKenna, H.J., 2000. In vivo generation of human dendritic cell subsets by Flt3 ligand. Blood 96, 878–884. https://doi.org/10.1182/blood.V96.3.878

Marconato, L., Palla, G., Yamauchi, K.A., Virshup, I., Heidari, E., Treis, T., Vierdag, W.-M., Toth, M., Stockhaus, S., Shrestha, R.B., Rombaut,

B., Pollaris, L., Lehner, L., Vöhringer, H., Kats, I., Saeys, Y., Saka, S.K., Huber, W., Gerstung, M., Moore, J., Theis, F.J., Stegle, O., 2024. SpatialData: an open and universal data framework for spatial omics. Nat. Methods 1–5. https://doi.org/10.1038/s41592-024-02212-x

Martinek, J., Lin, J., Kim, K.I., Wang, V.G., Wu, T.-C., Chiorazzi, M., Boruchov, H., Gulati, A., Seeniraj, S., Sun, L., Marches, F., Robson, P., Rongvaux, A., Flavell, R.A., George, J., Chuang, J.H., Banchereau, J., Palucka, K., 2022. Transcriptional profiling of macrophages in situ in metastatic melanoma reveals localization-dependent phenotypes and function. Cell Rep. Med. 3, 100621. https://doi.org/10.1016/j.xcrm.2022.100621

Martinez, F.O., Gordon, S., Locati, M., Mantovani, A., 2006. Transcriptional Profiling of the Human Monocyte-to-Macrophage Differentiation and Polarization: New Molecules and Patterns of Gene Expression. J. Immunol. 177, 7303–7311. https://doi.org/10.4049/jimmunol.177.10.7303

Mass, E., Ballesteros, I., Farlik, M., Halbritter, F., Gunther, P., Crozet, L., Jacome-Galarza, C.E., Handler, K., Klughammer, J., Kobayashi, Y., Gomez-Perdiguero, E., Schultze, J.L., Beyer, M., Bock, C., Geissmann, F., 2016. Specification of tissue-resident macrophages during organogenesis. Science 353, aaf4238–aaf4238. https://doi.org/10.1126/science.aaf4238

Mass, E., Nimmerjahn, F., Kierdorf, K., Schlitzer, A., 2023. Tissue-specific macrophages: how they develop and choreograph tissue biology. Nat. Rev. Immunol. 23, 563–579. https://doi.org/10.1038/s41577-023-00848-y

Massalha, H., Bahar Halpern, K., Abu-Gazala, S., Jana, T., Massasa, E.E., Moor, A.E., Buchauer, L., Rozenberg, M., Pikarsky, E., Amit, I., Zamir, G., Itzkovitz, S., 2020. A single cell atlas of the human liver tumor microenvironment. Mol. Syst. Biol. 16, e9682. https://doi.org/10.15252/msb.20209682

Matsui, T., Connolly, J.E., Michnevitz, M., Chaussabel, D., Yu, C.-I., Glaser, C., Tindle, S., Pypaert, M., Freitas, H., Piqueras, B., Banchereau, J., Palucka, A.K., 2009. CD2 Distinguishes Two Subsets of Human Plasmacytoid Dendritic Cells with Distinct Phenotype and Functions1. J. Immunol. 182, 6815–6823. https://doi.org/10.4049/jimmunol.0802008

Matusiak, M., Hickey, J.W., van IJzendoorn, D.G.P., Lu, G., Kidzinski, L., Zhu, S., Colburg, D.R.C., Luca, B., Phillips, D.J., Brubaker, S.W., Charville, G.W., Shen, J., Loh, K.M., Okwan-Duodu, D.K., Nolan, G.P., Newman, A.M., West, R.B., van de Rijn, M., 2024. Spatially Segregated Macrophage Populations Predict Distinct Outcomes In

Colon Cancer. Cancer Discov. https://doi.org/10.1158/2159-8290.CD-23-1300
Maynard, A., McCoach, C.E., Rotow, J.K., Harris, L., Haderk, F., Kerr, D.L., Yu, E.A., Schenk, E.L., Tan, W., Zee, A., Tan, M., Gui, P., Lea, T., Wu, W., Urisman, A., Jones, K., Sit, R., Kolli, P.K., Seeley, E., Gesthalter, Y., Le, D.D., Yamauchi, K.A., Naeger, D.M., Bandyopadhyay, S., Shah, K., Cech, L., Thomas, N.J., Gupta, A., Gonzalez, M., Do, H., Tan, L., Bacaltos, B., Gomez-Sjoberg, R., Gubens, M., Jahan, T., Kratz, J.R., Jablons, D., Neff, N., Doebele, R.C., Weissman, J., Blakely, C.M., Darmanis, S., Bivona, T.G., 2020. Therapy-Induced Evolution of Human Lung Cancer Revealed by Single-Cell RNA Sequencing. Cell 182, 1232-1251.e22. https://doi.org/10.1016/j.cell.2020.07.017
McInnes, L., Healy, J., Melville, J., 2018. UMAP: Uniform Manifold Approximation and Projection for Dimension Reduction. ArXiv180203426 Cs Stat.
McLellan, A.D., Starling, G.C., Williams, L.A., Hock, B.D., Hart, D.N., 1995. Activation of human peripheral blood dendritic cells induces the CD86 co-stimulatory molecule. Eur. J. Immunol. 25, 2064–2068. https://doi.org/10.1002/eji.1830250739
Medvedev, A.E., Sabroe, I., Hasday, J.D., Vogel, S.N., 2006. Tolerance to microbial TLR ligands: molecular mechanisms and relevance to disease. J. Endotoxin Res. 12, 133–150. https://doi.org/10.1179/096805106X102255
Medzhitov, R., Janeway, C., 2000. Innate immune recognition: mechanisms and pathways. Immunol. Rev. 173, 89–97. https://doi.org/10.1034/j.1600-065x.2000.917309.x
Medzhitov, R., Preston-Hurlburt, P., Janeway, C.A., 1997. A human homologue of the Drosophila Toll protein signals activation of adaptive immunity. Nature 388, 394–397. https://doi.org/10.1038/41131
Merad, M., Manz, M.G., Karsunky, H., Wagers, A., Peters, W., Charo, I., Weissman, I.L., Cyster, J.G., Engleman, E.G., 2002. Langerhans cells renew in the skin throughout life under steady-state conditions. Nat. Immunol. 3, 1135–1141. https://doi.org/10.1038/ni852
Merad, M., Sathe, P., Helft, J., Miller, J., Mortha, A., 2013. The Dendritic Cell Lineage: Ontogeny and Function of Dendritic Cells and Their Subsets in the Steady State and the Inflamed Setting. Annu. Rev. Immunol. 31, 10.1146/annurev-immunol-020711–074950. https://doi.org/10.1146/annurev-immunol-020711-074950
Merritt, C.R., Ong, G.T., Church, S.E., Barker, K., Danaher, P., Geiss, G., Hoang, M., Jung, J., Liang, Y., McKay-Fleisch, J., Nguyen, K., Norgaard, Z., Sorg, K., Sprague, I., Warren, C., Warren, S., Webster, P.J., Zhou, Z., Zollinger, D.R., Dunaway, D.L., Mills, G.B.,

Beechem, J.M., 2020. Multiplex digital spatial profiling of proteins and RNA in fixed tissue. Nat. Biotechnol. 38, 586–599. https://doi.org/10.1038/s41587-020-0472-9

Metchnikoff, E., 1892. Leçons sur la pathologie comparée de l'inflammation. Masson.

Meyer, M.A., Baer, J.M., Knolhoff, B.L., Nywening, T.M., Panni, R.Z., Su, X., Weilbaecher, K.N., Hawkins, W.G., Ma, C., Fields, R.C., Linehan, D.C., Challen, G.A., Faccio, R., Aft, R.L., DeNardo, D.G., 2018. Breast and pancreatic cancer interrupt IRF8-dependent dendritic cell development to overcome immune surveillance. Nat. Commun. 9, 1250. https://doi.org/10.1038/s41467-018-03600-6

Michea, P., Noël, F., Zakine, E., Czerwinska, U., Sirven, P., Abouzid, O., Goudot, C., Scholer-Dahirel, A., Vincent-Salomon, A., Reyal, F., Amigorena, S., Guillot-Delost, M., Segura, E., Soumelis, V., 2018. Adjustment of dendritic cells to the breast-cancer microenvironment is subset specific. Nat. Immunol. 19, 885–897. https://doi.org/10.1038/s41590-018-0145-8

Mills, Charles D., Kincaid, K., Alt, J.M., Heilman, M.J., Hill, A.M., 2000. M-1/M-2 Macrophages and the Th1/Th2 Paradigm1. J. Immunol. 164, 6166–6173. https://doi.org/10.4049/jimmunol.164.12.6166

Mills, C. D., Kincaid, K., Alt, J.M., Heilman, M.J., Hill, A.M., 2000. M-1/M-2 macrophages and the Th1/Th2 paradigm. J. Immunol. Baltim. Md 1950 164, 6166–6173. https://doi.org/10.4049/jimmunol.164.12.6166

Minutti, C.M., Piot, C., Pereira da Costa, M., Chakravarty, P., Rogers, N., Huerga Encabo, H., Cardoso, A., Loong, J., Bessou, G., Mionnet, C., Langhorne, J., Bonnet, D., Dalod, M., Tomasello, E., Reis e Sousa, C., 2024. Distinct ontogenetic lineages dictate cDC2 heterogeneity. Nat. Immunol. 25, 448–461. https://doi.org/10.1038/s41590-024-01745-9

Mittag, D., Proietto, A.I., Loudovaris, T., Mannering, S.I., Vremec, D., Shortman, K., Wu, L., Harrison, L.C., 2011. Human Dendritic Cell Subsets from Spleen and Blood Are Similar in Phenotype and Function but Modified by Donor Health Status. J. Immunol. 186, 6207–6217. https://doi.org/10.4049/jimmunol.1002632

Molawi, K., Wolf, Y., Kandalla, P.K., Favret, J., Hagemeyer, N., Frenzel, K., Pinto, A.R., Klapproth, K., Henri, S., Malissen, B., Rodewald, H.-R., Rosenthal, N.A., Bajenoff, M., Prinz, M., Jung, S., Sieweke, M.H., 2014. Progressive replacement of embryo-derived cardiac macrophages with age. J. Exp. Med. 211, 2151–2158. https://doi.org/10.1084/jem.20140639

Molgora, M., Esaulova, E., Vermi, W., Hou, J., Chen, Y., Luo, J., Brioschi, S., Bugatti, M., Omodei, A.S., Ricci, B., Fronick, C., Panda, S.K., Takeuchi, Y., Gubin, M.M., Faccio, R., Cella, M., Gilfillan, S.,

Unanue, E.R., Artyomov, M.N., Schreiber, R.D., Colonna, M., 2020. TREM2 Modulation Remodels the Tumor Myeloid Landscape Enhancing Anti-PD-1 Immunotherapy. Cell 182, 886-900.e17. https://doi.org/10.1016/j.cell.2020.07.013

Momenilandi, M., Lévy, R., Sobrino, S., Li, J., Lagresle-Peyrou, C., Esmaeilzadeh, H., Fayand, A., Le Floc'h, C., Guérin, A., Della Mina, E., Shearer, D., Delmonte, O.M., Yatim, A., Mulder, K., Mancini, M., Rinchai, D., Denis, A., Neehus, A.-L., Balogh, K., Brendle, S., Rokni-Zadeh, H., Changi-Ashtiani, M., Seeleuthner, Y., Deswarte, C., Bessot, B., Cremades, C., Materna, M., Cederholm, A., Ogishi, M., Philippot, Q., Beganovic, O., Ackermann, M., Wuyts, M., Khan, T., Fouéré, S., Herms, F., Chanal, J., Palterer, B., Bruneau, J., Molina, T.J., Leclerc-Mercier, S., Prétet, J.-L., Youssefian, L., Vahidnezhad, H., Parvaneh, N., Claeys, K.G., Schrijvers, R., Luka, M., Pérot, P., Fourgeaud, J., Nourrisson, C., Poirier, P., Jouanguy, E., Boisson-Dupuis, S., Bustamante, J., Notarangelo, L.D., Christensen, N., Landegren, N., Abel, L., Marr, N., Six, E., Langlais, D., Waterboer, T., Ginhoux, F., Ma, C.S., Tangye, S.G., Meyts, I., Lachmann, N., Hu, J., Shahrooei, M., Bossuyt, X., Casanova, J.-L., Béziat, V., 2024. FLT3L governs the development of partially overlapping hematopoietic lineages in humans and mice. Cell 187, 2817-2837.e31. https://doi.org/10.1016/j.cell.2024.04.009

Moses, L., Pachter, L., 2022. Museum of spatial transcriptomics. Nat. Methods 19, 534–546. https://doi.org/10.1038/s41592-022-01409-2

Movassagh, M., Spatz, A., Davoust, J., Lebecque, S., Romero, P., Pittet, M., Rimoldi, D., Liénard, D., Gugerli, O., Ferradini, L., Robert, C., Avril, M.-F., Zitvogel, L., Angevin, E., 2004. Selective Accumulation of Mature DC-Lamp+ Dendritic Cells in Tumor Sites Is Associated with Efficient T-Cell-Mediated Antitumor Response and Control of Metastatic Dissemination in Melanoma. Cancer Res. 64, 2192–2198. https://doi.org/10.1158/0008-5472.CAN-03-2969

Mulder, K., Patel, A.A., Kong, W.T., Piot, C., Halitzki, E., Dunsmore, G., Khalilnezhad, S., Irac, S.E., Dubuisson, A., Chevrier, M., Zhang, X.M., Tam, J.K.C., Lim, T.K.H., Wong, R.M.M., Pai, R., Khalil, A.I.S., Chow, P.K.H., Wu, S.Z., Al-Eryani, G., Roden, D., Swarbrick, A., Chan, J.K.Y., Albani, S., Derosa, L., Zitvogel, L., Sharma, A., Chen, J., Silvin, A., Bertoletti, A., Blériot, C., Dutertre, C.-A., Ginhoux, F., 2021. Cross-tissue single-cell landscape of human monocytes and macrophages in health and disease. Immunity 54, 1883-1900.e5. https://doi.org/10.1016/J.IMMUNI.2021.07.007

Muller, P.A., Koscsó, B., Rajani, G.M., Stevanovic, K., Berres, M.-L., Hashimoto, D., Mortha, A., Leboeuf, M., Li, X.-M., Mucida, D., Stanley, E.R., Dahan, S., Margolis, K.G., Gershon, M.D., Merad,

M., Bogunovic, M., 2014. Crosstalk between Muscularis Macrophages and Enteric Neurons Regulates Gastrointestinal Motility. Cell 158, 300–313. https://doi.org/10.1016/j.cell.2014.04.050

Munn, D.H., Shafizadeh, E., Attwood, J.T., Bondarev, I., Pashine, A., Mellor, A.L., 1999. Inhibition of T Cell Proliferation by Macrophage Tryptophan Catabolism. J. Exp. Med. 189, 1363–1372. https://doi.org/10.1084/jem.189.9.1363

Murray, P.J., Allen, J.E., Biswas, S.K., Fisher, E.A., Gilroy, D.W., Goerdt, S., Gordon, S., Hamilton, J.A., Ivashkiv, L.B., Lawrence, T., Locati, M., Mantovani, A., Martinez, F.O., Mege, J.-L., Mosser, D.M., Natoli, G., Saeij, J.P., Schultze, J.L., Shirey, K.A., Sica, A., Suttles, J., Udalova, I., van Ginderachter, J.A., Vogel, S.N., Wynn, T.A., 2014. Macrophage Activation and Polarization: Nomenclature and Experimental Guidelines. Immunity 41, 14–20. https://doi.org/10.1016/j.immuni.2014.06.008

Naik, S.H., Metcalf, D., van Nieuwenhuijze, A., Wicks, I., Wu, L., O'Keeffe, M., Shortman, K., 2006. Intrasplenic steady-state dendritic cell precursors that are distinct from monocytes. Nat. Immunol. 7, 663–671. https://doi.org/10.1038/ni1340

Naik, S.H., Sathe, P., Park, H.-Y., Metcalf, D., Proietto, A.I., Dakic, A., Carotta, S., O'Keeffe, M., Bahlo, M., Papenfuss, A., Kwak, J.-Y., Wu, L., Shortman, K., 2007. Development of plasmacytoid and conventional dendritic cell subtypes from single precursor cells derived in vitro and in vivo. Nat. Immunol. 8, 1217–1226. https://doi.org/10.1038/ni1522

Nalio Ramos, R., Missolo-Koussou, Y., Gerber-Ferder, Y., Bromley, C.P., Bugatti, M., Núñez, N.G., Tosello Boari, J., Richer, W., Menger, L., Denizeau, J., Sedlik, C., Caudana, P., Kotsias, F., Niborski, L.L., Viel, S., Bohec, M., Lameiras, S., Baulande, S., Lesage, L., Nicolas, A., Meseure, D., Vincent-Salomon, A., Reyal, F., Dutertre, C.-A., Ginhoux, F., Vimeux, L., Donnadieu, E., Buttard, B., Galon, J., Zelenay, S., Vermi, W., Guermonprez, P., Piaggio, E., Helft, J., 2022. Tissue-resident FOLR2+ macrophages associate with CD8+ T cell infiltration in human breast cancer. Cell 185, 1189-1207.e25. https://doi.org/10.1016/j.cell.2022.02.021

Neehus, A.-L., Carey, B., Landekic, M., Panikulam, P., Deutsch, G., Ogishi, M., Arango-Franco, C.A., Philippot, Q., Modaresi, M., Mohammadzadeh, I., Berndt, M.C., Rinchai, D., Voyer, T.L., Rosain, J., Momenilandi, M., Martin-Fernandez, M., Khan, T., Bohlen, J., Han, J.E., Deslys, A., Bernard, M., Gajardo-Carrasco, T., Soudée, C., Floc'h, C.L., Migaud, M., Seeleuthner, Y., Jang, M.-S., Nikolouli, E., Seyedpour, S., Begueret, H., Emile, J.-F., Guen, P.L., Tavazzi, G., Colombo, C.N.J., Marzani, F.C., Angelini, M., Trespidi,

F., Ghirardello, S., Alipour, N., Molitor, A., Carapito, R., Mazloomrezaei, M., Rokni-Zadeh, H., Changi-Ashtiani, M., Brouzes, C., Vargas, P., Borghesi, A., Lachmann, N., Bahram, S., Crestani, B., Fayon, M., Galode, F., Pahari, S., Schlesinger, L.S., Marr, N., Bogunovic, D., Boisson-Dupuis, S., Béziat, V., Abel, L., Borie, R., Young, L.R., Deterding, R., Shahrooei, M., Rezaei, N., Parvaneh, N., Craven, D., Gros, P., Malo, D., Sepulveda, F.E., Nogee, L.M., Aladjidi, N., Trapnell, B.C., Casanova, J.-L., Bustamante, J., 2024. Human inherited CCR2 deficiency underlies progressive polycystic lung disease. Cell 187, 390-408.e23. https://doi.org/10.1016/j.cell.2023.11.036

Nefedova, Y., Cheng, P., Gilkes, D., Blaskovich, M., Beg, A.A., Sebti, S.M., Gabrilovich, D.I., 2005. Activation of dendritic cells via inhibition of Jak2/STAT3 signaling. J. Immunol. Baltim. Md 1950 175, 4338–4346.

Netea, M.G., Domínguez-Andrés, J., Barreiro, L.B., Chavakis, T., Divangahi, M., Fuchs, E., Joosten, L.A.B., van der Meer, J.W.M., Mhlanga, M.M., Mulder, W.J.M., Riksen, N.P., Schlitzer, A., Schultze, J.L., Stabell Benn, C., Sun, J.C., Xavier, R.J., Latz, E., 2020. Defining trained immunity and its role in health and disease. Nat. Rev. Immunol. 20, 375–388. https://doi.org/10.1038/s41577-020-0285-6

Nicolás-Ávila, J.A., Lechuga-Vieco, A.V., Esteban-Martínez, L., Sánchez-Díaz, M., Díaz-García, E., Santiago, D.J., Rubio-Ponce, A., Li, J.L., Balachander, A., Quintana, J.A., Martínez-de-Mena, R., Castejón-Vega, B., Pun-García, A., Través, P.G., Bonzón-Kulichenko, E., García-Marqués, F., Cussó, L., A-González, N., González-Guerra, A., Roche-Molina, M., Martin-Salamanca, S., Crainiciuc, G., Guzmán, G., Larrazabal, J., Herrero-Galán, E., Alegre-Cebollada, J., Lemke, G., Rothlin, C.V., Jimenez-Borreguero, L.J., Reyes, G., Castrillo, A., Desco, M., Muñoz-Cánoves, P., Ibáñez, B., Torres, M., Ng, L.G., Priori, S.G., Bueno, H., Vázquez, J., Cordero, M.D., Bernal, J.A., Enríquez, J.A., Hidalgo, A., 2020. A Network of Macrophages Supports Mitochondrial Homeostasis in the Heart. Cell 183, 94-109.e23. https://doi.org/10.1016/j.cell.2020.08.031

Nizzoli, G., Krietsch, J., Weick, A., Steinfelder, S., Facciotti, F., Gruarin, P., Bianco, A., Steckel, B., Moro, M., Crosti, M., Romagnani, C., Stölzel, K., Torretta, S., Pignataro, L., Scheibenbogen, C., Neddermann, P., De Francesco, R., Abrignani, S., Geginat, J., 2013. Human CD1c+ dendritic cells secrete high levels of IL-12 and potently prime cytotoxic T-cell responses. Blood 122, 932–942. https://doi.org/10.1182/blood-2013-04-495424

Noy, R., Pollard, J.W., 2014. Tumor-Associated Macrophages: From Mechanisms to Therapy. Immunity 41, 49–61. https://doi.org/10.1016/j.immuni.2014.06.010

Nussenzweig, M.C., Steinman, R.M., Gutchinov, B., Cohn, Z.A., 1980. Dendritic cells are accessory cells for the development of anti-trinitrophenyl cytotoxic T lymphocytes. J. Exp. Med. 152, 1070–1084. https://doi.org/10.1084/jem.152.4.1070

Nywening, T.M., Wang-Gillam, A., Sanford, D.E., Belt, B.A., Panni, R.Z., Cusworth, B.M., Toriola, A.T., Nieman, R.K., Worley, L.A., Yano, M., Fowler, K.J., Lockhart, A.C., Suresh, R., Tan, B.R., Lim, K.-H., Fields, R.C., Strasberg, S.M., Hawkins, W.G., DeNardo, D.G., Goedegebuure, S.P., Linehan, D.C., 2016. Targeting tumour-associated macrophages with CCR2 inhibition in combination with FOLFIRINOX in patients with borderline resectable and locally advanced pancreatic cancer: a single-centre, open-label, dose-finding, non-randomised, phase 1b trial. Lancet Oncol. 17, 651–662. https://doi.org/10.1016/S1470-2045(16)00078-4

Obradovic, A., Chowdhury, N., Haake, S.M., Ager, C., Wang, V., Vlahos, L., Guo, X.V., Aggen, D.H., Rathmell, W.K., Jonasch, E., Johnson, J.E., Roth, M., Beckermann, K.E., Rini, B.I., McKiernan, J., Califano, A., Drake, C.G., 2021. Single-cell protein activity analysis identifies recurrence-associated renal tumor macrophages. Cell 184, 2988-3005.e16. https://doi.org/10.1016/j.cell.2021.04.038

Okabe, Y., Medzhitov, R., 2016. Tissue biology perspective on macrophages. Nat. Immunol. 17, 9–17. https://doi.org/10.1038/ni.3320

Okabe, Y., Medzhitov, R., 2014. Tissue-specific signals control reversible program of localization and functional polarization of macrophages. Cell 157, 832–844. https://doi.org/10.1016/j.cell.2014.04.016

Olsson, A., Venkatasubramanian, M., Chaudhri, V.K., Aronow, B.J., Salomonis, N., Singh, H., Grimes, H.L., 2016. Single-cell analysis of mixed-lineage states leading to a binary cell fate choice. Nature 537, 698–702. https://doi.org/10.1038/nature19348

Onai, N., Obata-Onai, A., Schmid, M. a, Ohteki, T., Jarrossay, D., Manz, M.G., 2007. Identification of clonogenic common Flt3+M-CSFR+ plasmacytoid and conventional dendritic cell progenitors in mouse bone marrow. Nat. Immunol. 8, 1207–16. https://doi.org/10.1038/ni1518

Oosterhoff, D., Lougheed, S., van de Ven, R., Lindenberg, J., van Cruijsen, H., Hiddingh, L., Kroon, J., van den Eertwegh, A.J.M., Hangalapura, B., Scheper, R.J., de Gruijl, T.D., 2012. Tumor-mediated inhibition of human dendritic cell differentiation and function is consistently counteracted by combined p38 MAPK and STAT3 inhibition. Oncoimmunology 1, 649–658. https://doi.org/10.4161/onci.20365

O'Sullivan, B., Thomas, R., 2003. CD40 and Dendritic Cell Function. Crit. Rev. Immunol. 23. https://doi.org/10.1615/CritRevImmunol.v23.i12.50
Ott, P.A., Adams, S., 2011. Small Molecule Protein Kinase Inhibitors and their Effects on the Immune System: Implications for Cancer Treatment. Immunotherapy 3, 213–227. https://doi.org/10.2217/imt.10.99
Palframan, R.T., Jung, S., Cheng, G., Weninger, W., Luo, Y., Dorf, M., Littman, D.R., Rollins, B.J., Zweerink, H., Rot, A., von Andrian, U.H., 2001. Inflammatory Chemokine Transport and Presentation in HEV : A Remote Control Mechanism for Monocyte Recruitment to Lymph Nodes in Inflamed Tissues. J. Exp. Med. 194, 1361–1374. https://doi.org/10.1084/jem.194.9.1361
Palla, G., Spitzer, H., Klein, M., Fischer, D., Schaar, A.C., Kuemmerle, L.B., Rybakov, S., Ibarra, I.L., Holmberg, O., Virshup, I., Lotfollahi, M., Richter, S., Theis, F.J., 2022. Squidpy: a scalable framework for spatial omics analysis. Nat. Methods 19, 171–178. https://doi.org/10.1038/s41592-021-01358-2
Parhizkar, S., Arzberger, T., Brendel, M., Kleinberger, G., Deussing, M., Focke, C., Nuscher, B., Xiong, M., Ghasemigharagoz, A., Katzmarski, N., Krasemann, S., Lichtenthaler, S.F., Müller, S.A., Colombo, A., Monasor, L.S., Tahirovic, S., Herms, J., Willem, M., Pettkus, N., Butovsky, O., Bartenstein, P., Edbauer, D., Rominger, A., Ertürk, A., Grathwohl, S.A., Neher, J.J., Holtzman, D.M., Meyer-Luehmann, M., Haass, C., 2019. Loss of TREM2 function increases amyloid seeding but reduces plaque-associated ApoE. Nat. Neurosci. 22, 191–204. https://doi.org/10.1038/s41593-018-0296-9
Park, M.D., Reyes-Torres, I., LeBerichel, J., Hamon, P., LaMarche, N.M., Hegde, S., Belabed, M., Troncoso, L., Grout, J.A., Magen, A., Humblin, E., Nair, A., Molgora, M., Hou, J., Newman, J.H., Farkas, A.M., Leader, A.M., Dawson, T., D'Souza, D., Hamel, S., Sanchez-Paulete, A.R., Maier, B., Bhardwaj, N., Martin, J.C., Kamphorst, A.O., Kenigsberg, E., Casanova-Acebes, M., Horowitz, A., Brown, B.D., De Andrade, L.F., Colonna, M., Marron, T.U., Merad, M., 2023. TREM2 macrophages drive NK cell paucity and dysfunction in lung cancer. Nat. Immunol. 24, 792–801. https://doi.org/10.1038/s41590-023-01475-4
Park, S.L., Gebhardt, T., Mackay, L.K., 2019. Tissue-Resident Memory T Cells in Cancer Immunosurveillance. Trends Immunol. 40, 735–747. https://doi.org/10.1016/j.it.2019.06.002
Passlick, B., Flieger, D., Loms Ziegler-Heitbrock, H.W., 1989. Identification and characterization of a novel monocyte subpopulation in human peripheral blood. Blood 74, 2527–2534. https://doi.org/10.1182/blood.v74.7.2527.bloodjournal7472527

Patel, A.A., Yona, S., 2019. Inherited and Environmental Factors Influence Human Monocyte Heterogeneity. Front. Immunol. 10. https://doi.org/10.3389/fimmu.2019.02581

Patel, A.A., Zhang, Y., Fullerton, J.N., Boelen, L., Rongvaux, A., Maini, A.A., Bigley, V., Flavell, R.A., Gilroy, D.W., Asquith, B., Macallan, D., Yona, S., 2017. The fate and lifespan of human monocyte subsets in steady state and systemic inflammation. J. Exp. Med. 214, 1913–1923. https://doi.org/10.1084/jem.20170355

Patterson, M.T., Firulyova, M.M., Xu, Y., Hillman, H., Bishop, C., Zhu, A., Hickok, G.H., Schrank, P.R., Ronayne, C.E., Caillot, Z., Fredrickson, G., Kennedy, A.E., Acharya, N., Neels, J.G., Chinetti, G., Revelo, X., Stromnes, I.M., Ivanov, S., Bold, T.D., Zaitsev, K., Williams, J.W., 2023. Trem2 promotes foamy macrophage lipid uptake and survival in atherosclerosis. Nat. Cardiovasc. Res. 2, 1015–1031. https://doi.org/10.1038/s44161-023-00354-3

Paul, F., Arkin, Y., Giladi, A., Jaitin, D.A., Kenigsberg, E., Keren-Shaul, H., Winter, D., Lara-Astiaso, D., Gury, M., Weiner, A., David, E., Cohen, N., Lauridsen, F.K.B., Haas, S., Schlitzer, A., Mildner, A., Ginhoux, F., Jung, S., Trumpp, A., Porse, B.T., Tanay, A., Amit, I., 2015. Transcriptional Heterogeneity and Lineage Commitment in Myeloid Progenitors. Cell 163, 1663–1677. https://doi.org/10.1016/j.cell.2015.11.013

Pearson, K., 1901. LIII. On lines and planes of closest fit to systems of points in space. Lond. Edinb. Dublin Philos. Mag. J. Sci. 2, 559–572. https://doi.org/10.1080/14786440109462720

Pellin, D., Loperfido, M., Baricordi, C., Wolock, S.L., Montepeloso, A., Weinberg, O.K., Biffi, A., Klein, A.M., Biasco, L., 2019. A comprehensive single cell transcriptional landscape of human hematopoietic progenitors. Nat. Commun. 10, 2395. https://doi.org/10.1038/s41467-019-10291-0

Perdiguero, E.G., Geissmann, F., 2016. The development and maintenance of resident macrophages. Nat. Immunol. 17, 2–8. https://doi.org/10.1038/ni.3341

Peters, J.M., Blainey, P., Bryson, B.D., 2020. Consensus transcriptional states describe human mononuclear phagocyte diversity in the lung across health and disease | bioRxiv [WWW Document]. URL https://www.biorxiv.org/content/10.1101/2020.08.06.240424v1 (accessed 8.28.20).

Peterson, V.M., Zhang, K.X., Kumar, N., Wong, J., Li, L., Wilson, D.C., Moore, R., McClanahan, T.K., Sadekova, S., Klappenbach, J.A., 2017. Multiplexed quantification of proteins and transcripts in single cells. Nat. Biotechnol. 35, 936–939. https://doi.org/10.1038/nbt.3973

Petukhov, V., Xu, R.J., Soldatov, R.A., Cadinu, P., Khodosevich, K., Moffitt, J.R., Kharchenko, P.V., 2021. Cell segmentation in

imaging-based spatial transcriptomics. Nat. Biotechnol. 2021 1–10. https://doi.org/10.1038/s41587-021-01044-w
Picelli, S., Faridani, O.R., Björklund, A.K., Winberg, G., Sagasser, S., Sandberg, R., 2014. Full-length RNA-seq from single cells using Smart-seq2. Nat. Protoc. 9, 171–181. https://doi.org/10.1038/nprot.2014.006
Pietras, E.M., Reynaud, D., Kang, Y.-A., Carlin, D., Calero-Nieto, F.J., Leavitt, A.D., Stuart, J.M., Göttgens, B., Passegué, E., 2015. Functionally Distinct Subsets of Lineage-Biased Multipotent Progenitors Control Blood Production in Normal and Regenerative Conditions. Cell Stem Cell 17, 35–46. https://doi.org/10.1016/j.stem.2015.05.003
Pittet, M.J., Michielin, O., Migliorini, D., 2022. Clinical relevance of tumour-associated macrophages. Nat. Rev. Clin. Oncol. 19, 402–421. https://doi.org/10.1038/s41571-022-00620-6
Pollard, J.W., 2004. Tumour-educated macrophages promote tumour progression and metastasis. Nat Rev Cancer 4, 71–78. https://doi.org/10.1038/nrc1256
Pombo Antunes, A.R., Scheyltjens, I., Lodi, F., Messiaen, J., Antoranz, A., Duerinck, J., Kancheva, D., Martens, L., De Vlaminck, K., Van Hove, H., Kjølner Hansen, S.S., Bosisio, F.M., Van der Borght, K., De Vleeschouwer, S., Sciot, R., Bouwens, L., Verfaillie, M., Vandamme, N., Vandenbroucke, R.E., De Wever, O., Saeys, Y., Guilliams, M., Gysemans, C., Neyns, B., De Smet, F., Lambrechts, D., Van Ginderachter, J.A., Movahedi, K., 2021. Single-cell profiling of myeloid cells in glioblastoma across species and disease stage reveals macrophage competition and specialization. Nat. Neurosci. 24, 595–610. https://doi.org/10.1038/s41593-020-00789-y
Poulin, L.F., Reyal, Y., Uronen-Hansson, H., Schraml, B.U., Sancho, D., Murphy, K.M., Håkansson, U.K., Ferreira Moita, L., Agace, W.W., Bonnet, D., Reis e Sousa, C., 2012. DNGR-1 is a specific and universal marker of mouse and human Batf3-dependent dendritic cells in lymphoid and nonlymphoid tissues. Blood 119, 6052–6062. https://doi.org/10.1182/blood-2012-01-406967
Poulin, L.F., Salio, M., Griessinger, E., Anjos-Afonso, F., Craciun, L., Chen, J.-L., Keller, A.M., Joffre, O., Zelenay, S., Nye, E., Le Moine, A., Faure, F., Donckier, V., Sancho, D., Cerundolo, V., Bonnet, D., Reis e Sousa, C., 2010. Characterization of human DNGR-1+ BDCA3+ leukocytes as putative equivalents of mouse CD8α+ dendritic cells. J. Exp. Med. 207, 1261–1271. https://doi.org/10.1084/jem.20092618
Proietto, A.I., van Dommelen, S., Zhou, P., Rizzitelli, A., D'Amico, A., Steptoe, R.J., Naik, S.H., Lahoud, M.H., Liu, Y., Zheng, P., Shortman, K., Wu, L., 2008. Dendritic cells in the thymus contribute

to T-regulatory cell induction. Proc. Natl. Acad. Sci. U. S. A. 105, 19869–19874. https://doi.org/10.1073/pnas.0810268105

Qi, J., Sun, H., Zhang, Y., Wang, Z., Xun, Z., Li, Z., Ding, X., Bao, R., Hong, L., Jia, W., Fang, F., Liu, H., Chen, L., Zhong, J., Zou, D., Liu, L., Han, L., Ginhoux, F., Liu, Y., Ye, Y., Su, B., 2022. Single-cell and spatial analysis reveal interaction of FAP+ fibroblasts and SPP1+ macrophages in colorectal cancer. Nat. Commun. 13, 1742. https://doi.org/10.1038/s41467-022-29366-6

Qian, B.-Z., Li, J., Zhang, H., Kitamura, T., Zhang, J., Campion, L.R., Kaiser, E.A., Snyder, L.A., Pollard, J.W., 2011. CCL2 recruits inflammatory monocytes to facilitate breast-tumour metastasis. Nature 475, 222–225. https://doi.org/10.1038/nature10138

Qian, J., Olbrecht, S., Boeckx, B., Vos, H., Laoui, D., Etlioglu, E., Wauters, E., Pomella, V., Verbandt, S., Busschaert, P., Bassez, A., Franken, A., Bempt, M.V., Xiong, J., Weynand, B., van Herck, Y., Antoranz, A., Bosisio, F.M., Thienpont, B., Floris, G., Vergote, I., Smeets, A., Tejpar, S., Lambrechts, D., 2020. A pan-cancer blueprint of the heterogeneous tumor microenvironment revealed by single-cell profiling. Cell Res. 30, 745–762. https://doi.org/10.1038/s41422-020-0355-0

Ramachandran, P., Dobie, R., Wilson-Kanamori, J.R., Dora, E.F., Henderson, B.E.P., Luu, N.T., Portman, J.R., Matchett, K.P., Brice, M., Marwick, J.A., Taylor, R.S., Efremova, M., Vento-Tormo, R., Carragher, N.O., Kendall, T.J., Fallowfield, J.A., Harrison, E.M., Mole, D.J., Wigmore, S.J., Newsome, P.N., Weston, C.J., Iredale, J.P., Tacke, F., Pollard, J.W., Ponting, C.P., Marioni, J.C., Teichmann, S.A., Henderson, N.C., 2019. Resolving the fibrotic niche of human liver cirrhosis at single-cell level. Nature 575, 512–518. https://doi.org/10.1038/s41586-019-1631-3

Ramos, R.N., Missolo-koussou, Y., Gerber-ferder, Y., Bromley, C.P., Lameiras, S., Sedlik, C., Caudana, P., Kotsias, F., Niborski, L.L., Viel, S., Meseure, D., Vincent-salomon, A., Reyal, F., Dutertre, C.A., Ginhoux, F., Vimeux, L., Donnadieu, E., Buttard, B., Galon, J., Zelenay, S., Vermi, W., Guermonprez, P., Piaggio, E., Helft, J., 2022. Tissue-resident FOLR2+ macrophages associate with CD8+ T cell infiltration in human breast cancer. Cell 185, 1–19. https://doi.org/10.1016/J.CELL.2022.02.021

Rao, A., Barkley, D., França, G.S., Yanai, I., 2021. Exploring tissue architecture using spatial transcriptomics. Nature 596, 211–220. https://doi.org/10.1038/s41586-021-03634-9

Reading, J.L., Gálvez-Cancino, F., Swanton, C., Lladser, A., Peggs, K.S., Quezada, S.A., 2018. The function and dysfunction of memory CD8+ T cells in tumor immunity. Immunol. Rev. 283, 194–212. https://doi.org/10.1111/imr.12657

Regev, A., Teichmann, S.A., Lander, E.S., Amit, I., Benoist, C., Birney, E., Bodenmiller, B., Campbell, P., Carninci, P., Clatworthy, M., Clevers, H., Deplancke, B., Dunham, I., Eberwine, J., Eils, R., Enard, W., Farmer, A., Fugger, L., Göttgens, B., Hacohen, N., Haniffa, M., Hemberg, M., Kim, S., Klenerman, P., Kriegstein, A., Lein, E., Linnarsson, S., Lundberg, E., Lundeberg, J., Majumder, P., Marioni, J.C., Merad, M., Mhlanga, M., Nawijn, M., Netea, M., Nolan, G., Pe'er, D., Phillipakis, A., Ponting, C.P., Quake, S., Reik, W., Rozenblatt-Rosen, O., Sanes, J., Satija, R., Schumacher, T.N., Shalek, A., Shapiro, E., Sharma, P., Shin, J.W., Stegle, O., Stratton, M., Stubbington, M.J.T., Theis, F.J., Uhlen, M., van Oudenaarden, A., Wagner, A., Watt, F., Weissman, J., Wold, B., Xavier, R., Yosef, N., Human Cell Atlas Meeting Participants, 2017. The Human Cell Atlas. eLife 6, e27041. https://doi.org/10.7554/eLife.27041

Remmerie, A., Martens, L., Thoné, T., Castoldi, A., Seurinck, R., Pavie, B., Roels, J., Vanneste, B., De Prijck, S., Vanhockerhout, M., Binte Abdul Latib, M., Devisscher, L., Hoorens, A., Bonnardel, J., Vandamme, N., Kremer, A., Borghgraef, P., Van Vlierberghe, H., Lippens, S., Pearce, E., Saeys, Y., Scott, C.L., 2020. Osteopontin Expression Identifies a Subset of Recruited Macrophages Distinct from Kupffer Cells in the Fatty Liver. Immunity 53, 641-657.e14. https://doi.org/10.1016/j.immuni.2020.08.004

Ribas, A., Medina, T., Kummar, S., Amin, A., Kalbasi, A., Drabick, J.J., Barve, M., Daniels, G.A., Wong, D.J., Schmidt, E.V., Candia, A.F., Coffman, R.L., Leung, A.C.F., Janssen, R.S., 2018. SD-101 in Combination with Pembrolizumab in Advanced Melanoma: Results of a Phase Ib, Multicenter Study. Cancer Discov. 8, 1250–1257. https://doi.org/10.1158/2159-8290.CD-18-0280

Robbins, S.H., Walzer, T., Dembélé, D., Thibault, C., Defays, A., Bessou, G., Xu, H., Vivier, E., Sellars, M., Pierre, P., Sharp, F.R., Chan, S., Kastner, P., Dalod, M., 2008. Novel insights into the relationships between dendritic cell subsets in human and mouse revealed by genome-wide expression profiling. Genome Biol. 9, R17. https://doi.org/10.1186/gb-2008-9-1-r17

Rodrigues, P.F., Alberti-Servera, L., Eremin, A., Grajales-Reyes, G.E., Ivanek, R., Tussiwand, R., 2018. Distinct progenitor lineages contribute to the heterogeneity of plasmacytoid dendritic cells. Nat. Immunol. 19, 711–722. https://doi.org/10.1038/s41590-018-0136-9

Rodrigues, P.F., Trsan, T., Cvijetic, G., Khantakova, D., Panda, S.K., Liu, Z., Ginhoux, F., Cella, M., Colonna, M., 2024. Progenitors of distinct lineages shape the diversity of mature type 2 conventional dendritic cells. Immunity 57, 1567-1585.e5. https://doi.org/10.1016/j.immuni.2024.05.007

Roth, M.D., Gitlitz, B.J., Kiertscher, S.M., Park, A.N., Mendenhall, M., Moldawer, N., Figlin, R.A., 2000. Granulocyte Macrophage Colony-stimulating Factor and Interleukin 4 Enhance the Number and Antigen-presenting Activity of Circulating CD14+ and CD83+ Cells in Cancer Patients1. Cancer Res. 60, 1934–1941.

Rozenblatt-Rosen, O., Stubbington, M.J.T., Regev, A., Teichmann, S.A., 2017. The Human Cell Atlas: from vision to reality. Nature 550, 451–453. https://doi.org/10.1038/550451a

Sade-Feldman, M., Yizhak, K., Bjorgaard, S.L., Ray, J.P., de Boer, C.G., Jenkins, R.W., Lieb, D.J., Chen, J.H., Frederick, D.T., Barzily-Rokni, M., Freeman, S.S., Reuben, A., Hoover, P.J., Villani, A.-C., Ivanova, E., Portell, A., Lizotte, P.H., Aref, A.R., Eliane, J.-P., Hammond, M.R., Vitzthum, H., Blackmon, S.M., Li, B., Gopalakrishnan, V., Reddy, S.M., Cooper, Z.A., Paweletz, C.P., Barbie, D.A., Stemmer-Rachamimov, A., Flaherty, K.T., Wargo, J.A., Boland, G.M., Sullivan, R.J., Getz, G., Hacohen, N., 2018. Defining T Cell States Associated with Response to Checkpoint Immunotherapy in Melanoma. Cell 175, 998-1013.e20. https://doi.org/10.1016/j.cell.2018.10.038

Sadik, A., Somarribas Patterson, L.F., Öztürk, S., Mohapatra, S.R., Panitz, V., Secker, P.F., Pfänder, P., Loth, S., Salem, H., Prentzell, M.T., Berdel, B., Iskar, M., Faessler, E., Reuter, F., Kirst, I., Kalter, V., Foerster, K.I., Jäger, E., Guevara, C.R., Sobeh, M., Hielscher, T., Poschet, G., Reinhardt, A., Hassel, J.C., Zapatka, M., Hahn, U., von Deimling, A., Hopf, C., Schlichting, R., Escher, B.I., Burhenne, J., Haefeli, W.E., Ishaque, N., Böhme, A., Schäuble, S., Thedieck, K., Trump, S., Seiffert, M., Opitz, C.A., 2020. IL4I1 Is a Metabolic Immune Checkpoint that Activates the AHR and Promotes Tumor Progression. Cell S0092867420309466. https://doi.org/10.1016/j.cell.2020.07.038

Sakai, M., Troutman, T.D., Seidman, J.S., Ouyang, Z., Spann, N.J., Abe, Y., Ego, K.M., Bruni, C.M., Deng, Z., Schlachetzki, J.C.M., Nott, A., Bennett, H., Chang, J., Vu, B.T., Pasillas, M.P., Link, V.M., Texari, L., Heinz, S., Thompson, B.M., McDonald, J.G., Geissmann, F., Glass, C.K., 2019. Liver-Derived Signals Sequentially Reprogram Myeloid Enhancers to Initiate and Maintain Kupffer Cell Identity. Immunity 51, 655-670.e8. https://doi.org/10.1016/j.immuni.2019.09.002

Salmon, H., Idoyaga, J., Rahman, A., Leboeuf, M., Remark, R., Jordan, S., Casanova-Acebes, M., Khudoynazarova, M., Agudo, J., Tung, N., Chakarov, S., Rivera, C., Hogstad, B., Bosenberg, M., Hashimoto, D., Gnjatic, S., Bhardwaj, N., Palucka, A.K., Brown, B.D., Brody, J., Ginhoux, F., Merad, M., 2016. Expansion and Activation of CD103+ Dendritic Cell Progenitors at the Tumor Site Enhances

Tumor Responses to Therapeutic PD-L1 and BRAF Inhibition. Immunity 44, 924–938. https://doi.org/10.1016/j.immuni.2016.03.012
Sánchez-Paulete, A.R., Cueto, F.J., Martínez-López, M., Labiano, S., Morales-Kastresana, A., Rodríguez-Ruiz, M.E., Jure-Kunkel, M., Azpilikueta, A., Aznar, M.A., Quetglas, J.I., Sancho, D., Melero, I., 2016. Cancer Immunotherapy with Immunomodulatory Anti-CD137 and Anti-PD-1 Monoclonal Antibodies Requires BATF3-Dependent Dendritic Cells. Cancer Discov. 6, 71–79. https://doi.org/10.1158/2159-8290.CD-15-0510
Sánchez-Paulete, A.R., Teijeira, Á., Quetglas, J.I., Rodríguez-Ruiz, M.E., Sánchez-Arráez, Á., Labiano, S., Etxeberria, I., Azpilikueta, A., Bolaños, E., Ballesteros-Briones, M.C., Casares, N., Quezada, S.A., Berraondo, P., Sancho, D., Smerdou, C., Melero, I., 2018. Intratumoral Immunotherapy with XCL1 and sFlt3L Encoded in Recombinant Semliki Forest Virus–Derived Vectors Fosters Dendritic Cell–Mediated T-cell Cross-Priming. Cancer Res. 78, 6643–6654. https://doi.org/10.1158/0008-5472.CAN-18-0933
Sancho, D., Joffre, O.P., Keller, A.M., Rogers, N.C., Martínez, D., Hernanz-Falcón, P., Rosewell, I., Sousa, C.R. e, 2009. Identification of a dendritic cell receptor that couples sensing of necrosis to immunity. Nature 458, 899–903. https://doi.org/10.1038/nature07750
Sautès-Fridman, C., Petitprez, F., Calderaro, J., Fridman, W.H., 2019. Tertiary lymphoid structures in the era of cancer immunotherapy. Nat. Rev. Cancer 19, 307–325. https://doi.org/10.1038/s41568-019-0144-6
Savas, P., Virassamy, B., Ye, C., Salim, A., Mintoff, C.P., Caramia, F., Salgado, R., Byrne, D.J., Teo, Z.L., Dushyanthen, S., Byrne, A., Wein, L., Luen, S.J., Poliness, C., Nightingale, S.S., Skandarajah, A.S., Gyorki, D.E., Thornton, C.M., Beavis, P.A., Fox, S.B., Darcy, P.K., Speed, T.P., Mackay, L.K., Neeson, P.J., Loi, S., 2018. Single-cell profiling of breast cancer T cells reveals a tissue-resident memory subset associated with improved prognosis. Nat. Med. 24, 986–993. https://doi.org/10.1038/s41591-018-0078-7
Scheiblich, H., Dansokho, C., Mercan, D., Schmidt, S.V., Bousset, L., Wischhof, L., Eikens, F., Odainic, A., Spitzer, J., Griep, A., Schwartz, S., Bano, D., Latz, E., Melki, R., Heneka, M.T., 2021. Microglia jointly degrade fibrillar alpha-synuclein cargo by distribution through tunneling nanotubes. Cell 184, 5089-5106.e21. https://doi.org/10.1016/j.cell.2021.09.007
Schlitzer, A., Sivakamasundari, V., Chen, J., Sumatoh, H.R.B., Schreuder, J., Lum, J., Malleret, B., Zhang, S., Larbi, A., Zolezzi, F., Renia, L., Poidinger, M., Naik, S., Newell, E.W., Robson, P., Ginhoux, F., 2015. Identification of cDC1- and cDC2-committed DC progenitors

reveals early lineage priming at the common DC progenitor stage in the bone marrow. Nat Immunol 16, 718–728. https://doi.org/10.1038/ni.3200

Schulz, C., Gomez Perdiguero, E., Chorro, L., Szabo-Rogers, H., Cagnard, N., Kierdorf, K., Prinz, M., Wu, B., Jacobsen, S.E.W., Pollard, J.W., Frampton, J., Liu, K.J., Geissmann, F., 2012. A lineage of myeloid cells independent of Myb and hematopoietic stem cells. Science 336, 86–90. https://doi.org/10.1126/science.1219179

Scott, C.L., T'Jonck, W., Martens, L., Todorov, H., Sichien, D., Soen, B., Bonnardel, J., Prijck, S.D., Vandamme, N., Cannoodt, R., Saelens, W., Vanneste, B., Toussaint, W., Bleser, P.D., Takahashi, N., Vandenabeele, P., Henri, S., Pridans, C., Hume, D.A., Lambrecht, B.N., Baetselier, P.D., Milling, S.W.F., Ginderachter, J.A.V., Malissen, B., Berx, G., Beschin, A., Saeys, Y., Guilliams, M., 2018. The Transcription Factor ZEB2 Is Required to Maintain the Tissue-Specific Identities of Macrophages. Immunity 49, 312-325.e5. https://doi.org/10.1016/j.immuni.2018.07.004

See, P., Dutertre, C.-A., Chen, J., Günther, P., McGovern, N., Irac, S.E., Gunawan, M., Beyer, M., Händler, K., Duan, K., Sumatoh, H.R.B., Ruffin, N., Jouve, M., Gea-Mallorquí, E., Hennekam, R.C.M., Lim, T., Yip, C.C., Wen, M., Malleret, B., Low, I., Shadan, N.B., Fen, C.F.S., Tay, A., Lum, J., Zolezzi, F., Larbi, A., Poidinger, M., Chan, J.K.Y., Chen, Q., Rénia, L., Haniffa, M., Benaroch, P., Schlitzer, A., Schultze, J.L., Newell, E.W., Ginhoux, F., 2017. Mapping the human DC lineage through the integration of high-dimensional techniques. Science 356, eaag3009. https://doi.org/10.1126/science.aag3009

Segura, E., Touzot, M., Bohineust, A., Cappuccio, A., Chiocchia, G., Hosmalin, A., Dalod, M., Soumelis, V., Amigorena, S., 2013. Human Inflammatory Dendritic Cells Induce Th17 Cell Differentiation. Immunity 38, 336–348. https://doi.org/10.1016/j.immuni.2012.10.018

Seidman, J.S., Troutman, T.D., Sakai, M., Gola, A., Spann, N.J., Bennett, H., Bruni, C.M., Ouyang, Z., Li, R.Z., Sun, X., Vu, B.T., Pasillas, M.P., Ego, K.M., Gosselin, D., Link, V.M., Chong, L.-W., Evans, R.M., Thompson, B.M., McDonald, J.G., Hosseini, M., Witztum, J.L., Germain, R.N., Glass, C.K., 2020. Niche-Specific Reprogramming of Epigenetic Landscapes Drives Myeloid Cell Diversity in Nonalcoholic Steatohepatitis. Immunity 52, 1057-1074.e7. https://doi.org/10.1016/j.immuni.2020.04.001

Shalek, A.K., Satija, R., Adiconis, X., Gertner, R.S., Gaublomme, J.T., Raychowdhury, R., Schwartz, S., Yosef, N., Malboeuf, C., Lu, D., Trombetta, J.J., Gennert, D., Gnirke, A., Goren, A., Hacohen, N., Levin, J.Z., Park, H., Regev, A., 2013. Single-cell transcriptomics

reveals bimodality in expression and splicing in immune cells. Nature 498, 236–240. https://doi.org/10.1038/nature12172
Sharma, A., Blériot, C., Currenti, J., Ginhoux, F., 2022. Oncofetal reprogramming in tumour development and progression. Nat. Rev. Cancer 22, 593–602. https://doi.org/10.1038/s41568-022-00497-8
Sharma, A., Seow, J.J.W., Dutertre, C.-A., Pai, R., Blériot, C., Mishra, A., Wong, R.M.M., Singh, G.S.N., Sudhagar, S., Khalilnezhad, S., Erdal, S., Teo, H.M., Khalilnezhad, A., Chakarov, S., Lim, T.K.H., Fui, A.C.Y., Chieh, A.K.W., Chung, C.P., Bonney, G.K., Goh, B.K.-P., Chan, J.K.Y., Chow, P.K.H., Ginhoux, F., DasGupta, R., 2020. Onco-fetal Reprogramming of Endothelial Cells Drives Immunosuppressive Macrophages in Hepatocellular Carcinoma. Cell 183, 377-394.e21. https://doi.org/10.1016/j.cell.2020.08.040
Sharma, S., Sharma, M.C., Sarkar, C., 2005. Morphology of angiogenesis in human cancer: a conceptual overview, histoprognostic perspective and significance of neoangiogenesis. Histopathology 46, 481–489. https://doi.org/10.1111/j.1365-2559.2005.02142.x
Sherwood, E.R., Burelbach, K.R., McBride, M.A., Stothers, C.L., Owen, A.M., Hernandez, A., Patil, N.K., Williams, D.L., Bohannon, J.K., 2022. Innate Immune Memory and the Host Response to Infection. J. Immunol. 208, 785–792. https://doi.org/10.4049/jimmunol.2101058
Shi, C., Pamer, E.G., 2011. Monocyte recruitment during infection and inflammation. Nat. Rev. Immunol. 11, 762–774. https://doi.org/10.1038/nri3070
Silvin, A., Chapuis, N., Dunsmore, G., Goubet, A.-G., Dubuisson, A., Derosa, L., Almire, C., Hénon, C., Kosmider, O., Droin, N., Rameau, P., Catelain, C., Alfaro, A., Dussiau, C., Friedrich, C., Sourdeau, E., Marin, N., Szwebel, T.-A., Cantin, D., Mouthon, L., Borderie, D., Deloger, M., Bredel, D., Mouraud, S., Drubay, D., Andrieu, M., Lhonneur, A.-S., Saada, V., Stoclin, A., Willekens, C., Pommeret, F., Griscelli, F., Ng, L.G., Zhang, Z., Bost, P., Amit, I., Barlesi, F., Marabelle, A., Pène, F., Gachot, B., André, F., Zitvogel, L., Ginhoux, F., Fontenay, M., Solary, E., 2020. Elevated Calprotectin and Abnormal Myeloid Cell Subsets Discriminate Severe from Mild COVID-19. Cell 182, 1401-1418.e18. https://doi.org/10.1016/j.cell.2020.08.002
Smillie, C.S., Biton, M., Ordovas-Montanes, J., Sullivan, K.M., Burgin, G., Graham, D.B., Herbst, R.H., Rogel, N., Slyper, M., Waldman, J., Sud, M., Andrews, E., Velonias, G., Haber, A.L., Jagadeesh, K., Vickovic, S., Yao, J., Stevens, C., Dionne, D., Nguyen, L.T., Villani, A.-C., Hofree, M., Creasey, E.A., Huang, H., Rozenblatt-Rosen, O., Garber, J.J., Khalili, H., Desch, A.N., Daly, M.J., Ananthakrishnan, A.N., Shalek, A.K., Xavier, R.J., Regev, A., 2019. Intra- and Inter-

cellular Rewiring of the Human Colon during Ulcerative Colitis. Cell 178, 714-730.e22. https://doi.org/10.1016/j.cell.2019.06.029
Spranger, S., Dai, D., Horton, B., Gajewski, T.F., 2017. Tumor-Residing Batf3 Dendritic Cells Are Required for Effector T Cell Trafficking and Adoptive T Cell Therapy. Cancer Cell 31, 711-723.e4. https://doi.org/10.1016/j.ccell.2017.04.003
Stein, M., Keshav, S., Harris, N., Gordon, S., 1992. Interleukin 4 potently enhances murine macrophage mannose receptor activity: a marker of alternative immunologic macrophage activation. J. Exp. Med. 176, 287–292. https://doi.org/10.1084/jem.176.1.287
Steinman, R., Gutchinov, B., Witmer, M., Nussenzweig, M., 1983. Dendritic cells are the principal stimulators of the primary mixed leukocyte reaction in mice. J. Exp. Med. 157, 613–627.
Steinman, R.M., Cohn, Z.A., 1973. Identification of a novel cell type in peripheral lymphoid organs of mice: I. Morphology, quantitation, tissue distribution. J. Exp. Med. 137, 1142–1162. https://doi.org/10.1084/jem.137.5.1142
Steinman, R.M., Witmer, M.D., 1978. Lymphoid dendritic cells are potent stimulators of the primary mixed leukocyte reaction in mice. Proc. Natl. Acad. Sci. U. S. A. 75, 5132–5136. https://doi.org/10.1073/pnas.75.10.5132
Stewart, B.J., Ferdinand, J.R., Young, M.D., Mitchell, T.J., Loudon, K.W., Riding, A.M., Richoz, N., Frazer, G.L., Staniforth, J.U.L., Braga, F.A.V., Botting, R.A., Popescu, D.-M., Vento-Tormo, R., Stephenson, E., Cagan, A., Farndon, S.J., Polanski, K., Efremova, M., Green, K., Velasco-Herrera, M.D.C., Guzzo, C., Collord, G., Mamanova, L., Aho, T., Armitage, J.N., Riddick, A.C.P., Mushtaq, I., Farrell, S., Rampling, D., Nicholson, J., Filby, A., Burge, J., Lisgo, S., Lindsay, S., Bajenoff, M., Warren, A.Y., Stewart, G.D., Sebire, N., Coleman, N., Haniffa, M., Teichmann, S.A., Behjati, S., Clatworthy, M.R., 2019. Spatiotemporal immune zonation of the human kidney. Science 365, 1461–1466. https://doi.org/10.1126/science.aat5031
Stoeckius, M., Hafemeister, C., Stephenson, W., Houck-Loomis, B., Chattopadhyay, P.K., Swerdlow, H., Satija, R., Smibert, P., 2017. Simultaneous epitope and transcriptome measurement in single cells. Nat. Methods 14, 865–868. https://doi.org/10.1038/nmeth.4380
Stremmel, C., Schuchert, R., Wagner, F., Thaler, R., Weinberger, T., Pick, R., Mass, E., Ishikawa-Ankerhold, H.C., Margraf, A., Hutter, S., Vagnozzi, R., Klapproth, S., Frampton, J., Yona, S., Scheiermann, C., Molkentin, J.D., Jeschke, U., Moser, M., Sperandio, M., Massberg, S., Geissmann, F., Schulz, C., 2018. Yolk sac macrophage progenitors traffic to the embryo during defined stages

of development. Nat. Commun. 9, 75. https://doi.org/10.1038/s41467-017-02492-2
Stringer, C., Wang, T., Michaelos, M., Pachitariu, M., 2021. Cellpose: a generalist algorithm for cellular segmentation. Nat. Methods 18, 100–106. https://doi.org/10.1038/s41592-020-01018-x
Stuart, T., Butler, A., Hoffman, P., Hafemeister, C., Papalexi, E., Mauck, W.M., Hao, Y., Stoeckius, M., Smibert, P., Satija, R., 2019. Comprehensive Integration of Single-Cell Data. Cell 177, 1888-1902.e21. https://doi.org/10.1016/j.cell.2019.05.031
Stubbington, M.J.T., Rozenblatt-Rosen, O., Regev, A., Teichmann, S.A., 2017. Single-cell transcriptomics to explore the immune system in health and disease. Science 358, 58–63. https://doi.org/10.1126/science.aan6828
Study Details | Dupilumab_Metastatic NSCLC | ClinicalTrials.gov [WWW Document], n.d. URL https://clinicaltrials.gov/study/NCT05013450 (accessed 8.19.24).
Suzuki, S., Honma, K., Matsuyama, T., Suzuki, K., Toriyama, K., Akitoyo, I., Yamamoto, K., Suematsu, T., Nakamura, M., Yui, K., Kumatori, A., 2004. Critical roles of interferon regulatory factor 4 in CD11bhighCD8α– dendritic cell development. Proc. Natl. Acad. Sci. 101, 8981–8986. https://doi.org/10.1073/pnas.0402139101
Suzuki, T., Sakagami, T., Rubin, B.K., Nogee, L.M., Wood, R.E., Zimmerman, S.L., Smolarek, T., Dishop, M.K., Wert, S.E., Whitsett, J.A., Grabowski, G., Carey, B.C., Stevens, C., van der Loo, J.C.M., Trapnell, B.C., 2008. Familial pulmonary alveolar proteinosis caused by mutations in CSF2RA. J. Exp. Med. 205, 2703–2710. https://doi.org/10.1084/jem.20080990
Svensson, V., da Veiga Beltrame, E., Pachter, L., 2019. A curated database reveals trends in single-cell transcriptomics (preprint). Genomics. https://doi.org/10.1101/742304
Swirski, F.K., Nahrendorf, M., Etzrodt, M., Wildgruber, M., Cortez-Retamozo, V., Panizzi, P., Figueiredo, J.-L., Kohler, R.H., Chudnovskiy, A., Waterman, P., Aikawa, E., Mempel, T.R., Libby, P., Weissleder, R., Pittet, M.J., 2009. Identification of Splenic Reservoir Monocytes and Their Deployment to Inflammatory Sites. Science 325, 612–616. https://doi.org/10.1126/science.1175202
Szulzewsky, F., Pelz, A., Feng, X., Synowitz, M., Markovic, D., Langmann, T., Holtman, I.R., Wang, X., Eggen, B.J.L., Boddeke, H.W.G.M., Hambardzumyan, D., Wolf, S.A., Kettenmann, H., 2015. Glioma-Associated Microglia/Macrophages Display an Expression Profile Different from M1 and M2 Polarization and Highly Express Gpnmb and Spp1. PLOS ONE 10, e0116644. https://doi.org/10.1371/journal.pone.0116644

Tamoutounour, S., Guilliams, M., Montanana Sanchis, F., Liu, H., Terhorst, D., Malosse, C., Pollet, E., Ardouin, L., Luche, H., Sanchez, C., Dalod, M., Malissen, B., Henri, S., 2013. Origins and Functional Specialization of Macrophages and of Conventional and Monocyte-Derived Dendritic Cells in Mouse Skin. Immunity 39, 925–938. https://doi.org/10.1016/j.immuni.2013.10.004

Tang, F., Barbacioru, C., Wang, Y., Nordman, E., Lee, C., Xu, N., Wang, X., Bodeau, J., Tuch, B.B., Siddiqui, A., Lao, K., Surani, M.A., 2009. mRNA-Seq whole-transcriptome analysis of a single cell. Nat. Methods 6, 377–382. https://doi.org/10.1038/nmeth.1315

Tan-Garcia, A., Wai, L.-E., Zheng, D., Ceccarello, E., Jo, J., Banu, N., Khakpoor, A., Chia, A., Tham, C.Y.L., Tan, A.T., Hong, M., Keng, C.T., Rivino, L., Tan, K.C., Lee, K.H., Lim, S.G., Newell, E.W., Pavelka, N., Chen, J., Ginhoux, F., Chen, Q., Bertoletti, A., Dutertre, C.-A., 2017. Intrahepatic CD206+ macrophages contribute to inflammation in advanced viral-related liver disease. J. Hepatol. 67, 490–500. https://doi.org/10.1016/j.jhep.2017.04.023

Tekguc, M., Wing, J.B., Osaki, M., Long, J., Sakaguchi, S., 2021. Treg-expressed CTLA-4 depletes CD80/CD86 by trogocytosis, releasing free PD-L1 on antigen-presenting cells. Proc. Natl. Acad. Sci. U. S. A. 118, e2023739118. https://doi.org/10.1073/pnas.2023739118

The Tabula Muris Consortium, Overall coordination, Logistical coordination, Organ collection and processing, Library preparation and sequencing, Computational data analysis, Cell type annotation, Writing group, Supplemental text writing group, Principal investigators, 2018. Single-cell transcriptomics of 20 mouse organs creates a Tabula Muris. Nature 562, 367–372. https://doi.org/10.1038/s41586-018-0590-4

Thomas, R., Al-Khadairi, G., Roelands, J., Hendrickx, W., Dermime, S., Bedognetti, D., Decock, J., 2018. NY-ESO-1 Based Immunotherapy of Cancer: Current Perspectives. Front. Immunol. 9. https://doi.org/10.3389/fimmu.2018.00947

Timperi, E., Gueguen, P., Molgora, M., Magagna, I., Kieffer, Y., Lopez-Lastra, S., Sirven, P., Baudrin, L.G., Baulande, S., Nicolas, A., Champenois, G., Meseure, D., Vincent-Salomon, A., Tardivon, A., Laas, E., Soumelis, V., Colonna, M., Mechta-Grigoriou, F., Amigo-rena, S., Romano, E., 2022. Lipid-Associated Macrophages Are Induced by Cancer-Associated Fibroblasts and Mediate Immune Suppression in Breast Cancer. Cancer Res. 82, 3291–3306. https://doi.org/10.1158/0008-5472.CAN-22-1427

Tirosh, I., Izar, B., Prakadan, S.M., Wadsworth, M.H., Treacy, D., Trombetta, J.J., Rotem, A., Rodman, C., Lian, C., Murphy, G., Fallahi-Sichani, M., Dutton-Regester, K., Lin, J.-R., Cohen, O., Shah, P., Lu, D., Genshaft, A.S., Hughes, T.K., Ziegler, C.G.K.,

Kazer, S.W., Gaillard, A., Kolb, K.E., Villani, A.-C., Johannessen, C.M., Andreev, A.Y., Van Allen, E.M., Bertagnolli, M., Sorger, P.K., Sullivan, R.J., Flaherty, K.T., Frederick, D.T., Jané-Valbuena, J., Yoon, C.H., Rozenblatt-Rosen, O., Shalek, A.K., Regev, A., Garraway, L.A., 2016. Dissecting the multicellular ecosystem of metastatic melanoma by single-cell RNA-seq. Science 352, 189–196. https://doi.org/10.1126/science.aad0501

Trimble, C.L., Morrow, M.P., Kraynyak, K.A., Shen, X., Dallas, M., Yan, J., Edwards, L., Parker, R.L., Denny, L., Giffear, M., Brown, A.S., Marcozzi-Pierce, K., Shah, D., Slager, A.M., Sylvester, A.J., Khan, A., Broderick, K.E., Juba, R.J., Herring, T.A., Boyer, J., Lee, J., Sardesai, N.Y., Weiner, D.B., Bagarazzi, M.L., 2015. Safety, efficacy, and immunogenicity of VGX-3100, a therapeutic synthetic DNA vaccine targeting human papillomavirus 16 and 18 E6 and E7 proteins for cervical intraepithelial neoplasia 2/3: a randomised, double-blind, placebo-controlled phase 2b trial. The Lancet 386, 2078–2088. https://doi.org/10.1016/S0140-6736(15)00239-1

Trouw, L.A., Daha, M.R., 2011. Role of complement in innate immunity and host defense. Immunol. Lett., The role of non-immune tissues in guiding the action of the immune system 138, 35–37. https://doi.org/10.1016/j.imlet.2011.02.014

Trzebanski, S., Kim, J.-S., Larossi, N., Raanan, A., Kancheva, D., Bastos, J., Haddad, M., Solomon, A., Sivan, E., Aizik, D., Kralova, J.S., Gross-Vered, M., Boura-Halfon, S., Lapidot, T., Alon, R., Movahedi, K., Jung, S., 2024. Classical monocyte ontogeny dictates their functions and fates as tissue macrophages. Immunity 57, 1225-1242.e6. https://doi.org/10.1016/j.immuni.2024.04.019

Tsou, C.-L., Peters, W., Si, Y., Slaymaker, S., Aslanian, A.M., Weisberg, S.P., Mack, M., Charo, I.F., 2007. Critical roles for CCR2 and MCP-3 in monocyte mobilization from bone marrow and recruitment to inflammatory sites. J. Clin. Invest. 117, 902–909. https://doi.org/10.1172/JCI29919

Tu, M.M., Abdel-Hafiz, H.A., Jones, R.T., Jean, A., Hoff, K.J., Duex, J.E., Chauca-Diaz, A., Costello, J.C., Dancik, G.M., Tamburini, B.A.J., Czerniak, B., Kaye, J., Theodorescu, D., 2020. Inhibition of the CCL2 receptor, CCR2, enhances tumor response to immune checkpoint therapy. Commun. Biol. 3, 1–12. https://doi.org/10.1038/s42003-020-01441-y

Tze, L.E., Horikawa, K., Domaschenz, H., Howard, D.R., Roots, C.M., Rigby, R.J., Way, D.A., Ohmura-Hoshino, M., Ishido, S., Andoniou, C.E., Degli-Esposti, M.A., Goodnow, C.C., 2011. CD83 increases MHC II and CD86 on dendritic cells by opposing IL-10-driven MARCH1-mediated ubiquitination and degradation. J. Exp. Med. 208, 149–165. https://doi.org/10.1084/jem.20092203

Uderhardt, S., Martins, A.J., Tsang, J.S., Lämmermann, T., Germain, R.N., 2019. Resident Macrophages Cloak Tissue Microlesions to Prevent Neutrophil-Driven Inflammatory Damage. Cell 177, 541-555.e17. https://doi.org/10.1016/j.cell.2019.02.028

Van de Sande, B., Flerin, C., Davie, K., De Waegeneer, M., Hulselmans, G., Aibar, S., Seurinck, R., Saelens, W., Cannoodt, R., Rouchon, Q., Verbeiren, T., De Maeyer, D., Reumers, J., Saeys, Y., Aerts, S., 2020. A scalable SCENIC workflow for single-cell gene regulatory network analysis. Nat. Protoc. 15, 2247–2276. https://doi.org/10.1038/s41596-020-0336-2

van der Vlist, M., Raoof, R., Willemen, H.L.D.M., Prado, J., Versteeg, S., Martin Gil, C., Vos, M., Lokhorst, R.E., Pasterkamp, R.J., Kojima, T., Karasuyama, H., Khoury-Hanold, W., Meyaard, L., Eijkelkamp, N., 2022. Macrophages transfer mitochondria to sensory neurons to resolve inflammatory pain. Neuron 110, 613-626.e9. https://doi.org/10.1016/j.neuron.2021.11.020

van Furth, R., Cohn, Z.A., 1968. The origin and kinetics of mononuclear phagocytes. J. Exp. Med. 128, 415–35.

van Furth, R., Cohn, Z.A., Hirsch, J.G., Humphrey, J.H., Spector, W.G., Langevoort, H.L., 1972. The mononuclear phagocyte system: a new classification of macrophages, monocytes, and their precursor cells. Bull World Health Organ 46, 845–52.

Van Hove, H., Martens, L., Scheyltjens, I., De Vlaminck, K., Pombo Antunes, A.R., De Prijck, S., Vandamme, N., De Schepper, S., Van Isterdael, G., Scott, C.L., Aerts, J., Berx, G., Boeckxstaens, G.E., Vandenbroucke, R.E., Vereecke, L., Moechars, D., Guilliams, M., Van Ginderachter, J.A., Saeys, Y., Movahedi, K., 2019. A single-cell atlas of mouse brain macrophages reveals unique transcriptional identities shaped by ontogeny and tissue environment. Nat. Neurosci. 22, 1021–1035. https://doi.org/10.1038/s41593-019-0393-4

Vandereyken, K., Sifrim, A., Thienpont, B., Voet, T., 2023. Methods and applications for single-cell and spatial multi-omics. Nat. Rev. Genet. 24, 494–515. https://doi.org/10.1038/s41576-023-00580-2

Vieira Braga, F.A., Kar, G., Berg, M., Carpaij, O.A., Polanski, K., Simon, L.M., Brouwer, S., Gomes, T., Hesse, L., Jiang, J., Fasouli, E.S., Efremova, M., Vento-Tormo, R., Talavera-López, C., Jonker, M.R., Affleck, K., Palit, S., Strzelecka, P.M., Firth, H.V., Mahbubani, K.T., Cvejic, A., Meyer, K.B., Saeb-Parsy, K., Luinge, M., Brandsma, C.-A., Timens, W., Angelidis, I., Strunz, M., Koppelman, G.H., van Oosterhout, A.J., Schiller, H.B., Theis, F.J., van den Berge, M., Nawijn, M.C., Teichmann, S.A., 2019. A cellular census of human lungs identifies novel cell states in health and in asthma. Nat. Med. 25, 1153–1163. https://doi.org/10.1038/s41591-019-0468-5

Villani, A.-C., Satija, R., Reynolds, G., Sarkizova, S., Shekhar, K., Fletcher, J., Griesbeck, M., Butler, A., Zheng, S., Lazo, S., Jardine, L., Dixon, D., Stephenson, E., Nilsson, E., Grundberg, I., McDonald, D., Filby, A., Li, W., De Jager, P.L., Rozenblatt-Rosen, O., Lane, A.A., Haniffa, M., Regev, A., Hacohen, N., 2017. Single-cell RNA-seq reveals new types of human blood dendritic cells, monocytes, and progenitors. Science 356, eaah4573. https://doi.org/10.1126/science.aah4573

Villar, J., Cros, A., De Juan, A., Alaoui, L., Bonte, P.-E., Lau, C.M., Tiniakou, I., Reizis, B., Segura, E., 2023. ETV3 and ETV6 enable monocyte differentiation into dendritic cells by repressing macrophage fate commitment. Nat. Immunol. 24, 84–95. https://doi.org/10.1038/s41590-022-01374-0

Virshup, I., Bredikhin, D., Heumos, L., Palla, G., Sturm, G., Gayoso, A., Kats, I., Koutrouli, M., Berger, B., Pe'er, D., Regev, A., Teichmann, S.A., Finotello, F., Wolf, F.A., Yosef, N., Stegle, O., Theis, F.J., 2023. The scverse project provides a computational ecosystem for single-cell omics data analysis. Nat. Biotechnol. 41, 604–606. https://doi.org/10.1038/s41587-023-01733-8

Wang, Y., Szretter, K.J., Vermi, W., Gilfillan, S., Rossini, C., Cella, M., Barrow, A.D., Diamond, M.S., Colonna, M., 2012. IL-34 is a tissue-restricted ligand of CSF1R required for the development of Langerhans cells and microglia. Nat. Immunol. 13, 753–760. https://doi.org/10.1038/ni.2360

Watchmaker, P.B., Lahl, K., Lee, M., Baumjohann, D., Morton, J., Kim, S.J., Zeng, R., Dent, A., Ansel, K.M., Diamond, B., Hadeiba, H., Butcher, E.C., 2014. Comparative transcriptional and functional profiling defines conserved programs of intestinal DC differentiation in humans and mice. Nat. Immunol. 15, 98–108. https://doi.org/10.1038/ni.2768

Wculek, S.K., Cueto, F.J., Mujal, A.M., Melero, I., Krummel, M.F., Sancho, D., 2019. Dendritic cells in cancer immunology and immunotherapy. Nat. Rev. Immunol. https://doi.org/10.1038/s41577-019-0210-z

Wei, T., Zhang, X.-F., Bagante, F., Ratti, F., Marques, H.P., Silva, S., Soubrane, O., Lam, V., Poultsides, G.A., Popescu, I., Grigorie, R., Alexandrescu, S., Martel, G., Workneh, A., Guglielmi, A., Hugh, T., Aldrighetti, L., Endo, I., Pawlik, T.M., 2021. Tumor Necrosis Impacts Prognosis of Patients Undergoing Curative-Intent Hepatocellular Carcinoma. Ann. Surg. Oncol. 28, 797–805. https://doi.org/10.1245/s10434-020-09390-w

Wen, Y., Lambrecht, J., Ju, C., Tacke, F., 2021. Hepatic macrophages in liver homeostasis and diseases-diversity, plasticity and therapeutic opportunities. Cell. Mol. Immunol. 18, 45–56. https://doi.org/10.1038/s41423-020-00558-8

West, E.E., Afzali, B., Kemper, C., 2018. Unexpected Roles for Intracellular Complement in the Regulation of Th1 Responses. Adv. Immunol. 138, 35–70. https://doi.org/10.1016/bs.ai.2018.02.001
West, E.E., Kemper, C., 2023. Complosome — the intracellular complement system. Nat. Rev. Nephrol. 19, 426–439. https://doi.org/10.1038/s41581-023-00704-1
Wilson, C.B., Rowell, E., Sekimata, M., 2009. Epigenetic control of T-helper-cell differentiation. Nat. Rev. Immunol. 9, 91–105. https://doi.org/10.1038/nri2487
Wolf, A.A., Yáñez, A., Barman, P.K., Goodridge, H.S., 2019. The Ontogeny of Monocyte Subsets. Front. Immunol. 10. https://doi.org/10.3389/fimmu.2019.01642
Wolf, Y., Boura-Halfon, S., Cortese, N., Haimon, Z., Sar Shalom, H., Kuperman, Y., Kalchenko, V., Brandis, A., David, E., Segal-Hayoun, Y., Chappell-Maor, L., Yaron, A., Jung, S., 2017. Brown-adipose-tissue macrophages control tissue innervation and homeostatic energy expenditure. Nat. Immunol. 18, 665–674. https://doi.org/10.1038/ni.3746
Wu, S.Z., Al-Eryani, G., Roden, D.L., Junankar, S., Harvey, K., Andersson, A., Thennavan, A., Wang, C., Torpy, J.R., Bartonicek, N., Wang, T., Larsson, L., Kaczorowski, D., Weisenfeld, N.I., Uytingco, C.R., Chew, J.G., Bent, Z.W., Chan, C.-L., Gnanasambandapillai, V., Dutertre, C.-A., Gluch, L., Hui, M.N., Beith, J., Parker, A., Robbins, E., Segara, D., Cooper, C., Mak, C., Chan, B., Warrier, S., Ginhoux, F., Millar, E., Powell, J.E., Williams, S.R., Liu, X.S., O'Toole, S., Lim, E., Lundeberg, J., Perou, C.M., Swarbrick, A., 2021. A single-cell and spatially resolved atlas of human breast cancers. Nat. Genet. 53, 1334–1347. https://doi.org/10.1038/s41588-021-00911-1
Xiong, D., Wang, Y., You, M., 2020. A gene expression signature of TREM2hi macrophages and γδ T cells predicts immunotherapy response. Nat. Commun. 11, 5084. https://doi.org/10.1038/s41467-020-18546-x
Xue, D., Tabib, T., Morse, C., Lafyatis, R., 2019. Single-cell RNA sequencing reveals different subsets of macrophage and dendritic cells in human skin. J. Immunol. 202, 177.8-177.8.
Yáñez, A., Coetzee, S.G., Olsson, A., Muench, D.E., Berman, B.P., Hazelett, D.J., Salomonis, N., Grimes, H.L., Goodridge, H.S., 2017. Granulocyte-Monocyte Progenitors and Monocyte-Dendritic Cell Progenitors Independently Produce Functionally Distinct Monocytes. Immunity 47, 890-902.e4. https://doi.org/10.1016/j.immuni.2017.10.021
Yang, M., McKay, D., Pollard, J.W., Lewis, C.E., 2018. Diverse Functions of Macrophages in Different Tumor Microenvironments. Cancer

Res. 78, 5492–5503. https://doi.org/10.1158/0008-5472.CAN-18-1367

Ye, Z., Hu, W., Wu, B., Zhang, Y., Lei, C., Williams, I., Shouval, D.S., Kanegane, H., Kim, K.M., de Ridder, L., Shah, N., Ling, G., Yerushalmi, B., Kotlarz, D., Snapper, S., Horn, R., Klein, C., Muise, A.M., Huang, Y., Uhlig, H.H., 2021. Predictive Prenatal Diagnosis for Infantile-onset Inflammatory Bowel Disease Because of Interleukin-10 Signalling Defects. J. Pediatr. Gastroenterol. Nutr. 72, 276–281. https://doi.org/10.1097/MPG.0000000000002937

Yona, S., Kim, K.-W., Wolf, Y., Mildner, A., Varol, D., Breker, M., Strauss-Ayali, D., Viukov, S., Guilliams, M., Misharin, A., Hume, D.A., Perlman, H., Malissen, B., Zelzer, E., Jung, S., 2013. Fate mapping reveals origins and dynamics of monocytes and tissue macrophages under homeostasis. Immunity 38, 79–91. https://doi.org/10.1016/j.immuni.2012.12.001

Yoshio, S., Kanto, T., Kuroda, S., Matsubara, T., Higashitani, K., Kakita, N., Ishida, H., Hiramatsu, N., Nagano, H., Sugiyama, M., Murata, K., Fukuhara, T., Matsuura, Y., Hayashi, N., Mizokami, M., Takehara, T., 2013. Human blood dendritic cell antigen 3 (BDCA3)+ dendritic cells are a potent producer of interferon-λ in response to hepatitis C virus. Hepatology 57, 1705–1715. https://doi.org/10.1002/hep.26182

You, S., Li, S., Zeng, L., Song, J., Li, Z., Li, W., Ni, H., Xiao, X., Deng, W., Li, H., Lin, W., Liang, C., Zheng, Y., Cheng, S.-C., Xiao, N., Tong, M., Yu, R., Huang, J., Huang, H., Xu, H., Han, J., Ren, J., Mao, K., 2024. Lymphatic-localized Treg-mregDC crosstalk limits antigen trafficking and restrains anti-tumor immunity. Cancer Cell 42, 1415-1433.e12. https://doi.org/10.1016/j.ccell.2024.06.014

Yu, C.I., Becker, C., Wang, Y., Marches, F., Helft, J., Leboeuf, M., Anguiano, E., Pourpe, S., Goller, K., Pascual, V., Banchereau, J., Merad, M., Palucka, K., 2013. Human CD1c+ Dendritic Cells Drive the Differentiation of CD103+ CD8+ Mucosal Effector T Cells via the Cytokine TGF-β. Immunity 38, 818–830. https://doi.org/10.1016/j.immuni.2013.03.004

Zavidij, O., Haradhvala, N.J., Mouhieddine, T.H., Sklavenitis-Pistofidis, R., Cai, S., Reidy, M., Rahmat, M., Flaifel, A., Ferland, B., Su, N.K., Agius, M.P., Park, J., Manier, S., Bustoros, M., Huynh, D., Capelletti, M., Berrios, B., Liu, C.-J., He, M.X., Braggio, E., Fonseca, R., Maruvka, Y.E., Guerriero, J.L., Goldman, M., Van Allen, E.M., McCarroll, S.A., Azzi, J., Getz, G., Ghobrial, I.M., 2020. Single-cell RNA sequencing reveals compromised immune microenvironment in precursor stages of multiple myeloma. Nat. Cancer 1, 493–506. https://doi.org/10.1038/s43018-020-0053-3

Zeng, Z., Li, Yawei, Li, Yiming, Luo, Y., 2022. Statistical and machine learning methods for spatially resolved transcriptomics data analysis. Genome Biol. 23, 83. https://doi.org/10.1186/s13059-022-02653-7

Zhang, F., Mears, J.R., Shakib, L., Beynor, J.I., Shanaj, S., Korsunsky, I., Nathan, A., Donlin, L.T., Raychaudhuri, S., 2020. IFN-γ and TNF-α drive a CXCL10+ CCL2+ macrophage phenotype expanded in severe COVID-19 and other diseases with tissue inflammation. bioRxiv. https://doi.org/10.1101/2020.08.05.238360

Zhang, H., Liu, Z., Wen, H., Guo, Y., Xu, F., Zhu, Q., Yuan, W., Luo, R., Lu, C., Liu, R., Gu, J., Ge, D., 2022. Immunosuppressive TREM2(+) macrophages are associated with undesirable prognosis and responses to anti-PD-1 immunotherapy in non-small cell lung cancer. Cancer Immunol. Immunother. 71, 2511–2522. https://doi.org/10.1007/s00262-022-03173-w

Zhang, L., Li, Z., Skrzypczynska, K.M., Fang, Q., Zhang, W., O'Brien, S.A., He, Y., Wang, L., Zhang, Q., Kim, A., Gao, R., Orf, J., Wang, T., Sawant, D., Kang, J., Bhatt, D., Lu, D., Li, C.-M., Rapaport, A.S., Perez, K., Ye, Y., Wang, S., Hu, X., Ren, X., Ouyang, W., Shen, Z., Egen, J.G., Zhang, Z., Yu, X., 2020. Single-Cell Analyses Inform Mechanisms of Myeloid-Targeted Therapies in Colon Cancer. Cell 181, 442-459.e29. https://doi.org/10.1016/j.cell.2020.03.048

Zhang, Q., Cheng, S., Wang, Y., Wang, M., Lu, Y., Wen, Z., Ge, Y., Ma, Q., Chen, Y., Zhang, Y., Cao, R., Li, M., Liu, W., Wang, B., Wu, Q., Jia, W., Wang, X., 2021. Interrogation of the microenvironmental landscape in spinal ependymomas reveals dual functions of tumor-associated macrophages. Nat. Commun. 12, 6867. https://doi.org/10.1038/s41467-021-27018-9

Zhang, Q., He, Y., Luo, N., Patel, S.J., Han, Y., Gao, R., Modak, M., Carotta, S., Haslinger, C., Kind, D., Peet, G.W., Zhong, G., Lu, S., Zhu, W., Mao, Y., Xiao, M., Bergmann, M., Hu, X., Kerkar, S.P., Vogt, A.B., Pflanz, S., Liu, K., Peng, J., Ren, X., Zhang, Z., 2019. Landscape and Dynamics of Single Immune Cells in Hepatocellular Carcinoma. Cell 179, 829-845.e20. https://doi.org/10.1016/j.cell.2019.10.003

Zhang, Y., Chen, H., Mo, H., Hu, X., Gao, R., Zhao, Y., Liu, B., Niu, L., Sun, X., Yu, X., Wang, Y., Chang, Q., Gong, T., Guan, X., Hu, T., Qian, T., Xu, B., Ma, F., Zhang, Z., Liu, Z., 2021. Single-cell analyses reveal key immune cell subsets associated with response to PD-L1 blockade in triple-negative breast cancer. Cancer Cell 0. https://doi.org/10.1016/J.CCELL.2021.09.010

Zhao, Q., Kuang, D.-M., Wu, Y., Xiao, X., Li, X.-F., Li, T.-J., Zheng, L., 2012. Activated CD69+ T Cells Foster Immune Privilege by Regulating IDO Expression in Tumor-Associated Macrophages. J.

Immunol. 188, 1117–1124. https://doi.org/10.4049/jimmunol.1100164

Zheng, C., Zheng, L., Yoo, J.-K., Guo, H., Zhang, Y., Guo, X., Kang, B., Hu, R., Huang, J.Y., Zhang, Q., Liu, Z., Dong, M., Hu, X., Ouyang, W., Peng, J., Zhang, Z., 2017. Landscape of Infiltrating T Cells in Liver Cancer Revealed by Single-Cell Sequencing. Cell 169, 1342-1356.e16. https://doi.org/10.1016/j.cell.2017.05.035

Zhou, L., Wang, M., Guo, H., Hou, J., Zhang, Y., Li, M., Wu, X., Chen, X., Wang, L., 2022. Integrated Analysis Highlights the Immunosuppressive Role of TREM2+ Macrophages in Hepatocellular Carcinoma. Front. Immunol. 13. https://doi.org/10.3389/fimmu.2022.848367

Zhou, X., Franklin, R.A., Adler, M., Jacox, J.B., Bailis, W., Shyer, J.A., Flavell, R.A., Mayo, A., Alon, U., Medzhitov, R., 2018. Circuit Design Features of a Stable Two-Cell System. Cell 172, 744-757.e17. https://doi.org/10.1016/j.cell.2018.01.015

Zhou, Yingyue, Song, W.M., Andhey, P.S., Swain, A., Levy, T., Miller, K.R., Poliani, P.L., Cominelli, M., Grover, S., Gilfillan, S., Cella, M., Ulland, T.K., Zaitsev, K., Miyashita, A., Ikeuchi, T., Sainouchi, M., Kakita, A., Bennett, D.A., Schneider, J.A., Nichols, M.R., Beausoleil, S.A., Ulrich, J.D., Holtzman, D.M., Artyomov, M.N., Colonna, M., 2020. Human and mouse single-nucleus transcriptomics reveal TREM2-dependent and TREM2-independent cellular responses in Alzheimer's disease. Nat. Med. 26, 131–142. https://doi.org/10.1038/s41591-019-0695-9

Zhou, Yan, Yang, D., Yang, Q., Lv, X., Huang, W., Zhou, Z., Wang, Yaling, Zhang, Z., Yuan, T., Ding, X., Tang, L., Zhang, J., Yin, J., Huang, Y., Yu, W., Wang, Yonggang, Zhou, C., Su, Y., He, A., Sun, Y., Shen, Z., Qian, B., Meng, W., Fei, J., Yao, Y., Pan, X., Chen, P., Hu, H., 2020. Single-cell RNA landscape of intratumoral heterogeneity and immunosuppressive microenvironment in advanced osteosarcoma. Nat. Commun. 11, 6322. https://doi.org/10.1038/s41467-020-20059-6

Zhu, Y., Herndon, J.M., Sojka, D.K., Kim, K.-W., Knolhoff, B.L., Zuo, C., Cullinan, D.R., Luo, J., Bearden, A.R., Lavine, K.J., Yokoyama, W.M., Hawkins, W.G., Fields, R.C., Randolph, G.J., DeNardo, D.G., 2017. Tissue-Resident Macrophages in Pancreatic Ductal Adenocarcinoma Originate from Embryonic Hematopoiesis and Promote Tumor Progression. Immunity 47, 323-338.e6. https://doi.org/10.1016/j.immuni.2017.07.014

Ziegler-Heitbrock, L., Ancuta, P., Crowe, S., Dalod, M., Grau, V., Hart, D.N., Leenen, P.J.M., Liu, Y.J., MacPherson, G., Randolph, G.J., Scherberich, J., Schmitz, J., Shortman, K., Sozzani, S., Strobl, H., Zembala, M., Austyn, J.M., Lutz, M.B., 2010a. Nomenclature of

monocytes and dendritic cells in blood. Blood 116, e74–e80. https://doi.org/10.1182/blood-2010-02-258558
Ziegler-Heitbrock, L., Ancuta, P., Crowe, S., Dalod, M., Grau, V., Hart, D.N., Leenen, P.J.M., Liu, Y.-J., MacPherson, G., Randolph, G.J., Scherberich, J., Schmitz, J., Shortman, K., Sozzani, S., Strobl, H., Zembala, M., Austyn, J.M., Lutz, M.B., 2010b. Nomenclature of monocytes and dendritic cells in blood. Blood 116, e74-80. https://doi.org/10.1182/blood-2010-02-258558
Zilionis, R., Engblom, C., Pfirschke, C., Savova, V., Zemmour, D., Saatcioglu, H.D., Krishnan, I., Maroni, G., Meyerovitz, C.V., Kerwin, C.M., Choi, S., Richards, W.G., De Rienzo, A., Tenen, D.G., Bueno, R., Levantini, E., Pittet, M.J., Klein, A.M., 2019. Single-Cell Transcriptomics of Human and Mouse Lung Cancers Reveals Conserved Myeloid Populations across Individuals and Species. Immunity. https://doi.org/10.1016/j.immuni.2019.03.009

6 SUPPLEMENTARY